ISBN 978-82-326-1006-8 (printed version)
ISBN 978-82-326-1007-5 (electronic version)
ISSN 1503-8181

Doctoral theses at NTNU, 2015:175

Dhruv Tapasvi

Experimental and Simulation Studies on Biomass Torrefaction and Gasification

NTNU
Norwegian University of Science and Technology
Faculty of Engineering Science and Technology
Department of Energy and Process Engineering

NTNU – Trondheim
Norwegian University of
Science and Technology

NTNU – Trondheim
Norwegian University of
Science and Technology

Doctoral theses at NTNU, 2015:175

NTNU

Dhruv Tapasvi

Experimental and Simulation Studies on Biomass Torrefaction and Gasification

Thesis for the degree of Philosophiae Doctor

Trondheim, June 2015

Norwegian University of Science and Technology

NTNU – Trondheim
Norwegian University of
Science and Technology

NTNU
Norwegian University of Science and Technology

Thesis for the degree of Philosophiae Doctor

ISBN 978-82-326-1006-8 (printed version)
ISBN 978-82-326-1007-5 (electronic version)
ISSN 1503-8181

Doctoral theses at NTNU, 2015:175

Printed by Skipnes Kommunikasjon as

Abstract

The potential for bioenergy in Norway is significant. This potential can be realized by improving the properties of biomass and making it a convenient and competitive alternative to other fuels. Torrefaction is the most promising biomass pretreatment technique to date, improving its effectiveness as a fuel in various thermochemical processes. Torrefaction considerably reduces moisture content but increases the heating value, hydrophobicity and grindability of biomass. Torrefaction is influenced by many parameters, including biomass composition, temperature, holdup time and particle size. To evaluate the feasibility of torrefaction in a particular region, locally available biomass resources should be investigated. This approach forms the basis of the present study. To improve the viability of bioenergy in Norway, I undertook fundamental research on the torrefaction of Norwegian woody biomass and evaluated the behavior of torrefied biomass in thermochemical processes.

Starting with a detailed literature review on the topic, torrefaction behavior of Norwegian Birch and Spruce was experimentally investigated. Torrefaction experiments were performed in a macro-TGA reactor with provisions for continuous measurement of volatiles. Process temperature (225 and 275 °C), holdup time (30 and 60 minutes) and sample size (10 and 40 mm cubes) were varied. Fuel characterization, derivative thermogravimetric (DTG) curves, product yields, hydrophobicity tests, grinding energies and particle size distributions are discussed. Temperature had the strongest effect on the properties of torrefied biomass of all the studied parameters. Overall, considerable improvements in grindability and hydrophobicity were obtained in torrefied biomass from both feedstocks.

To obtain information on the intrinsic kinetics of torrefaction, the pyrolysis kinetics of Norwegian spruce and birch wood was investigated in another study. Micro-TGA was employed with nine different heating programs, including linear, stepwise, modulated and constant reaction rate (CRR) experiments. The 18 experiments on the two feedstocks were evaluated simultaneously using the method of least squares. Part of the kinetic parameters could be assumed common for both woods without a considerable worsening of the fit quality. Three pseudocomponents were assumed. Two of them were described using distributed activation energy models (DAEM), while the decomposition of the cellulose pseudocomponent was described using self-accelerating kinetics. In another approach, all three pseudocomponents were described using *n*-order reactions. A table was calculated to

provide guidance about the extent of devolatilization during torrefaction at various temperatures and residence times.

For understanding torrefied biomass reactivity in oxidative conditions, another micro-TGA study was conducted with four torrefied wood samples and their original feedstocks (birch and spruce) at slow heating rate programs. Particularly low sample masses were employed to avoid self-heating of the samples due to heat of combustion. Linear, modulated and CRR temperature programs were employed in TGA experiments under gas flows of 5 and 20% O_2. The kinetic model consisted of two devolatilization reactions and a subsequent char burn-off reaction. Cellulose decomposition in the presence of oxygen has self-accelerating (autocatalytic) kinetics. Decomposition of the non-cellulosic components of the biomass was described using a distributed activation model. The char burn-off was approximated by power-law (*n*-order) kinetics. Each of these reactions has its own dependence on oxygen concentration, which was also expressed using power-law kinetics. The model contained 15 unknown parameters for a given biomass. Certain of these parameters could be assumed to be identical for the six samples without a substantial worsening of fit.

Lastly, the behavior of torrefied biomass in a gasification process was evaluated. A two-stage biomass gasification model was selected using Aspen Plus as the simulation and modeling tool. The model included minimization of the Gibbs free energy of the produced gas to achieve chemical equilibrium, constrained by mass and energy balances for the system. Air and steam were used as the oxidizing agents with both untreated and torrefied biomass as feedstocks. Three process parameters were studied: equivalence ratio (ER), Gibbs reactor temperature and steam-to-biomass ratio (SBR). A total of 27 cases were included in the analysis, operating the system below the carbon deposition boundary with all carbon in the gaseous form in the product gas. Product gas composition [hydrogen (H_2), carbon monoxide (CO), carbon dioxide (CO_2) and nitrogen (N_2)] was analyzed together with cold gas energy and exergy efficiencies for all cases. Torrefied biomass gave higher H_2 and CO contents in the product gas, as well as higher energy and exergy efficiencies, than untreated biomass. The overall efficiency of an integrated torrefaction-gasification process depends on the mass yield of torrefaction. The results were validated using a C-H-O ternary diagram combined with results from similar studies.

Preface

This work has been carried out at the Norwegian University of Science and Technology (NTNU), the Department of Energy and Process Engineering with Associate Professor Khanh-Quang Tran as main supervisor and Dr. Morten Grønli as co-supervisor. This work was financed by the Research Council of Norway and a number of industrial partners through the Bioenergy Innovation Centre (CenBio).

The thesis is based on the following papers, which are referred to in the text by Roman numerals:

I. **Tapasvi, D.;** Tran, K-Q.; Wang, L.; Skreiberg, Ø.; Khalil, R. Biomass torrefaction – a review. Proceedings of the 9th European Conference on Industrial Furnaces and Boilers, Estoril, Portugal 2011, (ISBN 978-972-99309-6-6)

II. **Tapasvi, D.;** Khalil, R. A.; Skreiberg, Ø.; Tran, K.-Q.; Gronli, M. G. Torrefaction of Norwegian birch and spruce – an experimental study using macro-TGA. Energy Fuels 2012, 26, 5232–5240.

III. **Tapasvi, D.;** Khalil, R.; Várhegyi, G.; Tran, K.-Q.; Grønli, M.; Skreiberg, Ø., Thermal decomposition kinetics of woods with an emphasis on torrefaction. Energy Fuels 2013, 27, (10), 6134-6145.

IV. **Tapasvi, D.;** Khalil, R.; Várhegyi, G.; Skreiberg, Ø.; Tran, K.-Q.; Grønli, M. Kinetic behavior of torrefied biomass in an oxidative environment. Energy Fuels, 2013, 27, 1050-1060.

V. **Tapasvi, D.;** Kempegowda, R.; Tran, K-Q.; Skreiberg, Ø.; Grønli, M. A simulation study on the torrefied biomass gasification. Energy Conversion and Management, 2015, 90, 446-457

Acknowledgments

First of all, I would like to thank my supervisors, Associate Professor Khanh-Quang Tran and Dr. Morten Grønli, for all of their support and encouragement. It was my pleasure to conduct this work under their supervision.

I would also like to thank Dr. Øyvind Skreiberg, Dr. Roger Khalil and Dr. Gabor Várhegyi for providing guidance and sharing their vast knowledge in conducting experimental and kinetic modeling work. I greatly appreciate their contributions of time, ideas, and funding to make my PhD research work meaningful and productive. Thanks also to Dr. Rajesh Kempegowda for his contribution and guidance on Aspen Plus simulations of biomass gasification and to Liang Wang and Willy G. Horrigmo for their contributions to different parts of this thesis.

I thank my colleagues and office-mates from the Department of Energy and Process Engineering; Wenche, Anita, Gerd Randi, Erik, Ehsan, Prashant and Hamid for their help and guidance on numerous administrative and research topics.

Last but not least, I thank God for giving me such a wonderful and caring family. My daughter Aarika, who came to my life while I was conducting this research work, is the best thing that life has given me. I wish to express my special admiration for my wife, Sucheta. I cannot imagine my life without her. Her immense support, encouragement and love is exemplary. I would like to thank my mother and father, who are a source of inspiration to me. They continuously inculcate human values in me, and help me become a better person. I also thank my parents-in-law, my brother Chaitanya and his family, my sister Aarushi, and my brother-in-law Abhishek for their immense love and affection.

Trondheim, Norway

June 2015

Dhruv Tapasvi

Table of contents

List of Figures

List of Tables

Nomenclature

α = reacted fraction of a component or pseudocomponent (dimensionless)

σ = width parameter (variance) of Gaussian distribution (kJ/mol)

A = pre-exponential factor (s^{-1})

E = activation energy (kJ/mol) or the mean of an activation energy distribution (kJ/mol)

f = empirical function expressing the change of reactivity as reactions proceed (dimensionless)

h_k = the height of an experimental curve (s^{-1}) or 5×10^{-4} s^{-1}, whichever is higher

m = the mass of the sample normalized by initial dry sample mass (dimensionless)

n = reaction order (dimensionless)

of = objective function minimized in the least squares evaluation (dimensionless)

N_{exper} = number of experiments evaluated together by the method of least squares

N_k = number of evaluated data points on the kth experimental curve

N_{param} = number of parameters determined in the evaluation of a series of experiments

R = gas constant (8.3143×10^{-3} kJ mol^{-1} K^{-1})

reldev = deviation between observed and calculated value, expressed as percent of the corresponding peak height

$reldev_{18}$ = root mean square of the *reldev* values of 18 experiments

dev = root mean square of deviations between observed and calculated values of a DTG curve (µg/s)

c = the amount of volatiles formed from a unit mass of a pseudocomponent

t = time (s)

T = temperature (°C, K)

z = formal parameter (dimensionless)

ν = reaction order with respect to oxygen concentration

C_{O_2} = V/V concentration of ambient oxygen (dimensionless)

m_{ash}^{anal} = 1/100th of total ash determined by proximate analysis (dimensionless)

y = yield (dimensionless). $y_{cell.char}$ and y_{other_char} represent char yield from cellulose and the rest of the biomass, respectively. y_{ash} denotes ash yield from char.

$\eta_{energy,coldgas}$ = Cold gas energy efficiency of gasification (%)

$E^{'}$ = Total exergy of a material stream (J/sec)

ε_{ph} = Physical exergy of a material stream (J/sec)

ε_{ch} = Chemical exergy of a material stream (J/sec)

h = Material stream enthalpy (J/sec)

h_0 = Material stream ambient enthalpy (J/sec)

T_0 = Ambient temperature (K)

s = Material stream entropy (J/kg-K)

s_0 = Material stream ambient entropy (J/kg-K)

$\varepsilon_{ch,gas}$ = Molar chemical exergy of a gaseous mixture (KJ/K•mol)

φ_{dry} = Ratio of chemical exergy to the lower heating value of dry matter of solid fuel (dimensionless)

ε_{dm} = Chemical exergy of the dry matter of solid fuel (J/sec)

$h_{LHV(dm)}$ = Lower heating value of the dry matter of solid fuel (J/kg)

$\eta_{exergy,coldgas}$ = Exergetic efficiency of gasification (%)

Subscripts

i = digitized point on an experimental curve

j = pseudocomponent

k = experiment

cell = cellulose

other = non-cellulosic organic biomass constituents

ur = unreacted sample

1 Introduction

This chapter provides an introduction to the research presented in this thesis. The chapter begins with an overview of the topics of biomass and bioenergy, further divided into sub-topics: bioenergy use in Norway and the world, biomass as a fuel for energy production, biomass thermochemical conversions and various available pretreatment options. This is followed by the motivation for pursuing this work and the specific objectives. Finally, an outline of the thesis and the list of publications are provided.

1.1 Biomass and Bioenergy

1.1.1 Bioenergy use in Norway and the World

Biomass is biological material derived from living or recently deceased organisms. In the context of bioenergy, biomass often refers to plant-based materials. The heat value of biomass, which is referred to as biomass energy or bioenergy when utilized, is derived from solar energy through the process of photosynthesis. Plants take up carbon dioxide and water from their surroundings and use solar energy to convert them into glucose, which is converted in turn into other sugars, starches, hemicellulose, cellulose, lignin etc. Biomass is widely recognized as a vital renewable energy source to meet current as well as future world energy demands. The increased use of biomass in key sectors, including heat, power, transportation fuel and bio-product production, will gradually replace fossil fuel resources. The extended use of biomass will also help reduce greenhouse gas emissions, as bioenergy is considered CO_2 neutral[1, 2].

Trends for gross global energy consumption from various sources are shown in Figure 1-1. In 2011, the share of total energy consumption was 14% for bioenergy, 4% for other renewable sources such as hydro, solar and wind and 80% for fossil fuels[3]. It can be observed that, similar to other energy sources, bioenergy consumption has gradually increased over the past decade. However, the major contributions to the world bioenergy use came from Asia, followed by Africa, the Americas and Europe. As shown in Figure 1-2, 92% of bioenergy was used in household heating[3]. Bioenergy contributions to the transport and electricity sectors are negligible, with huge potential for future growth. In 2011, 89% of the bioenergy in the world was supplied as solid biomass, 5% as biofuels, 4% as wastes and 2% as biogas[3].

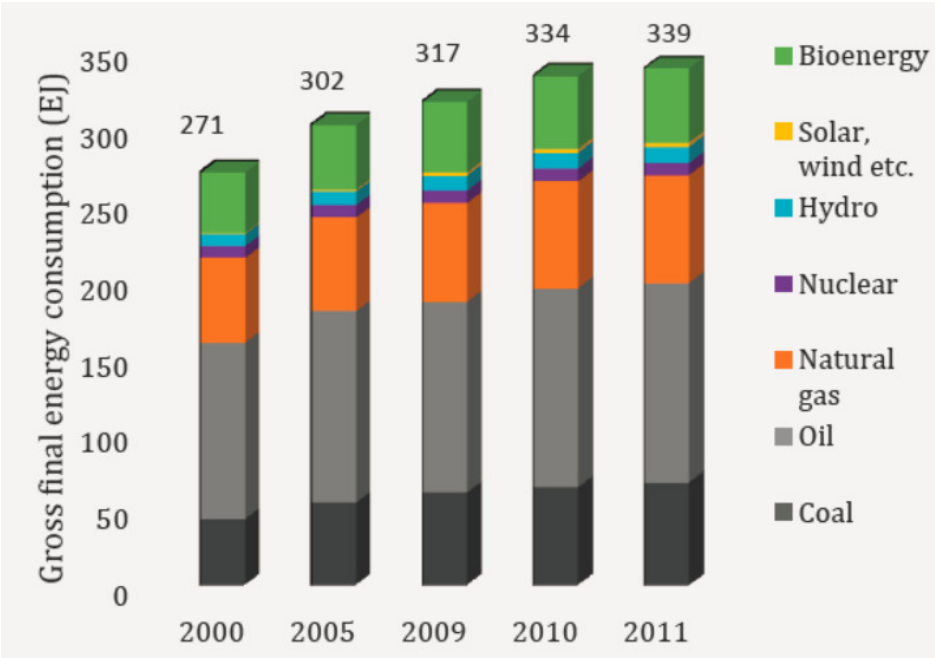

Figure 1-1: Trend of gross final energy consumption by source since 2000[3]

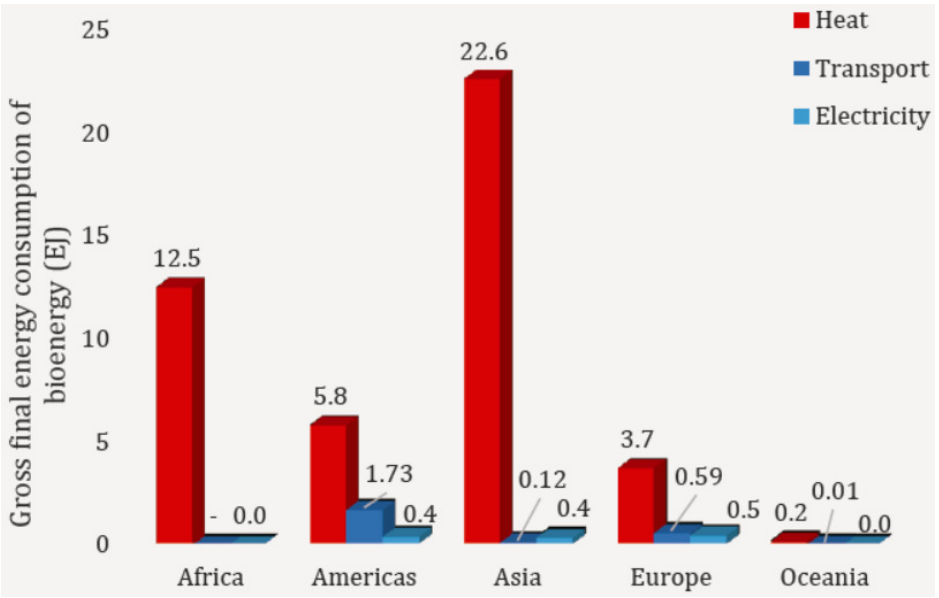

Figure 1-2: Continental distribution of gross consumption of bioenergy for 2011[3]

Nordic countries obtain a significant part of their energy supply from renewable sources, mainly for electricity and heat generation. In Norway, the energy market is characterized by a low electricity price, abundant hydroelectric power (hydro) and large oil and gas reserves. The estimated share of renewable energy in Norway is 58%, of which half is contributed by hydro power[4]. In 2012, bioenergy amounted to 8.5% (0.06 EJ) of total energy consumption in Norway, mainly in households (0.03 EJ)[5] where approximately 50% of the share comes from burning wood in wood stoves. The theoretical bioenergy potential for Norway is approximately 0.11 EJ, excluding aquatic resources[5]. Forests constitute the largest source of bioenergy, with a theoretical potential of 0.07 EJ[4, 5]. The market for bioenergy in several areas such as bio-fuels is fragmented and immature, which leads to under-utilization of the resource. Overall, the resource potential for bioenergy in Norway is significant; this potential can be realized through a variety of technologies and through creating market demand. The greatest challenge lies in technological improvements that can make biomass a convenient and competitive alternative to other fuels. Enhanced incentives, policies and R&D support for bioenergy can increase demand and support the development of a bioenergy market in Norway. According to Bioenergi i Norge[5] and an IEA report[6], Norway has a goal of reducing its greenhouse gas emissions by 30% before 2020 and by 100% before 2050, and an extended use of biomass will certainly help meet this goal.

1.1.2 Biomass as a fuel for energy production

Biomass can come from a wide range of sources, such as wood and agricultural residues, municipal and industry wastes and biological wastes. Biomass contains carbon, hydrogen and oxygen along with small amounts of nitrogen, sulfur, alkali metals, chlorine, and heavy metals. Biomass consists mainly of three polymers: cellulose, hemicellulose and lignin. These are associated with each other in a heteromatrix to different degrees based on the type, species and source of biomass[7]. Cellulose is the main constituent of the plant cell wall, conferring structural support and is a polymer of β-D-glucopyranose moieties linked via β-(1,4) glycosidic bonds[8]. Cellulose chains are grouped together to form microfibrils that bundle together to form cellulose fibers. The structure of cellulose is largely due to the presence of covalent bonds, hydrogen bonding and Van der Waals forces. Hemicelluloses are branched heterogeneous polymers comprised of pentoses, hexoses and acetylated sugars. Their molecular weight is lower than that of cellulose, and branches are easy to hydrolyze, with high thermal and chemical sensitivity. Hemicelluloses differ in composition by biomass type and are thought to ‘coat’ cellulose fibrils. It has been proposed that at least 50% of

hemicelluloses should be removed to increase cellulose digestibility[8]. Lignin is the third most abundant polymer in nature and is present in plant cell walls. It confers rigidity and impermeability to microbial attack and oxidative stress. It is an amorphous heteropolymer network of phenylpropane units held together by different linkages. It is regarded as a 'glue' that binds various biomass components together, making it insoluble in water[8].

The mass balance of a kilogram of biomass is commonly conceptualized in three different ways: biochemical, proximate or ultimate analysis[9]. Biochemical analysis refers to the relative composition of various biopolymers (e.g., hemicellulose, cellulose, lignin, etc.) in biomass, whereas ultimate analysis refers to individual elements (e.g., C, H, O, N, and S). Proximate analysis involves the heating of biomass to quantify the relative proportions of fixed carbon (fC), volatile matter (VM) and ash. Moisture completes the mass balance. Various combinations of these properties result in different bulk properties (intensive properties) such as grindability, density and heating value[9]. The solid fuel most similar to biomass is peat, while coal is quite different. Their heating values are also very different, with averages approximately 28-33 MJ/kg for coal, 20-23 MJ/kg for peat and 17-20 MJ/kg for wood[10, 11]. The variation in energy content is explained by fuel H/C and O/C ratios, as shown in the Van Krevelen diagram in Figure 1-3[12]. As the carbon content of fuel increases, energy content also increases.

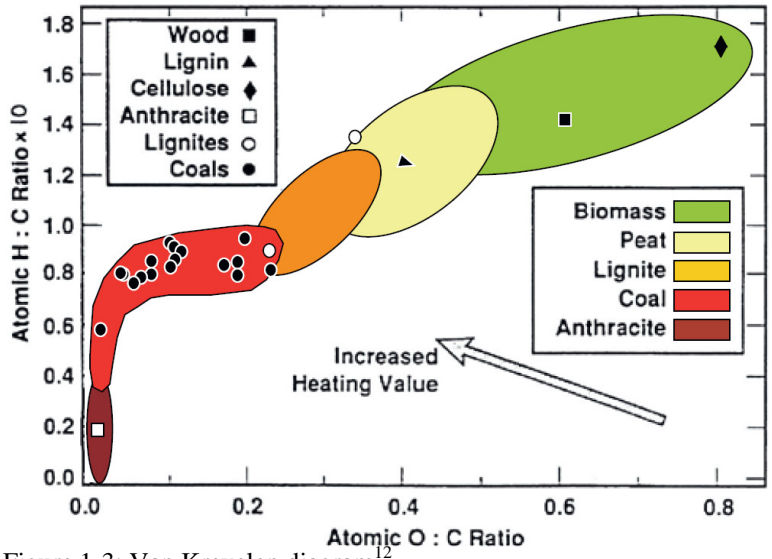

Figure 1-3: Van Krevelen diagram[12]

Three main pathways are used for biomass conversion: thermochemical (heat treatment), biochemical (microbiological action), and physical/chemical processing. However, problems such as low bulk density, high moisture content, poor grindability and relatively low calorific

value make biomass a challenging and expensive fuel to use. These problems have hindered its widespread use[2, 8, 13, 14]. Low bulk density makes transportation and handling more difficult and costly. The heterogeneous nature of biomass results in incomplete reactions and the release of pollutants, such as particulate matter, carbon monoxide and other gases, during combustion or other thermochemical processes[15, 16]. The health impact of air pollution is a significant problem in countries where wood is burnt inefficiently in open fires for domestic cooking and space heating. If these problems are overcome, biomass has the potential to be a major energy source.

1.1.3 Biomass thermochemical conversion

Thermal conversion, or thermochemical conversion, is the most common biomass conversion path. It is the controlled heating and/or oxidation of biomass to produce intermediate energy carriers or heat. It is generally categorized into three groups: pyrolysis, gasification, and combustion (Figure 1-4)[7, 17].

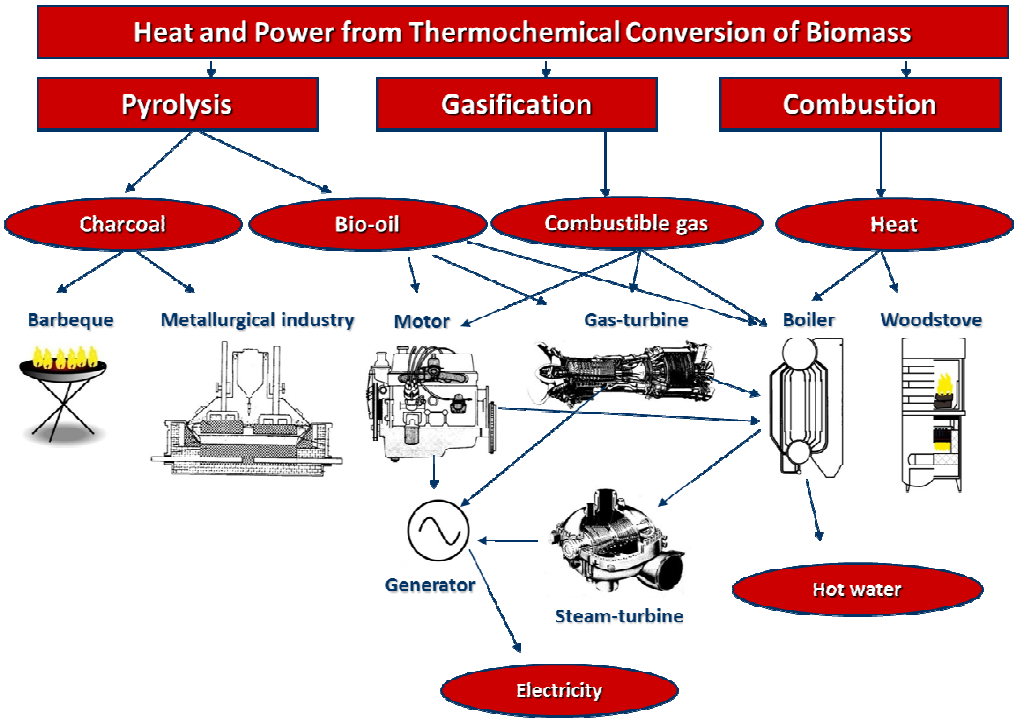

Figure 1-4: Products of thermochemical conversion technologies and their potential end-uses[7, 17]

The primary products are gas, liquid and solid char and/or heat, with yields dependent on the conversion technology applied. The process is mainly regulated by the amount of air

needed in relation to the stoichiometric condition. The characteristics of the products depend on a broad range of factors, such as the chemical and physical characteristics of the feedstock, heating rate, initial and final process temperature, pressure and reactor type[17]. All of these processes are fast compared to other biomass conversion routes, such as biological conversion. Evaluation of the potential utility of thermochemical biomass conversion for the production of power and heat requires extensive qualitative and quantitative analysis of the thermal and chemical behavior of various feedstocks as operating conditions are varied. Generally, the conversion characteristics of biomass can be grouped as follows[18]:

1. Thermochemical parameters: ash and volatile product yields; reactivity of volatile products
2. Intra-particle rate: thermal properties, moisture content, size, kinetics and energetics of chemical processes
3. Extra-particle rate: heat transfer from reactor to particle, residence time and mass transfer conditions

Pyrolysis

Pyrolysis is the thermal degradation of biomass in the absence of an oxidizing agent. . This leads to the formation of a mixture of liquid (tar/bio-oil), gases and char. Parameters that affect the process, which is overall endothermic, include temperature, pressure, gas composition, residence time, heating rate, type of reactor, reaction time and the chemical and physical characteristics of the fuel[18, 19]. Pyrolysis is generally divided into three categories: conventional, fast and flash. The ranges of the main operating parameters, and the product yields for these categories, are given in Table 1-1[18, 19].

Conventional pyrolysis occurs at a slow heating rate and permits the production of solid, liquid, and gaseous pyrolysis products at equal proportions. The first stage of biomass decomposition occurs between 395 and 475 K and results in some internal rearrangement, such as water removal by drying, bond breakage, appearance of free radicals, and formation of carbonyl, carboxyl and hydroperoxide groups. The second stage of solid decomposition occurs at high rates and leads to the formation of liquid and gaseous pyrolysis products. During the third stage, the char decomposes at a very slow rate, resulting in the formation of a carbon-rich residual solid. If the aim is the production of mainly liquid and/or gaseous products, fast pyrolysis is recommended. Fast pyrolysis requires high operating temperatures, very short residence times, and very fine particles. Flash pyrolysis gives mostly gaseous products due to the high heating rate and very small particle size.

Table 1-1: Typical process conditions for different pyrolysis modes[20]

Mode	Temperature (K)	Heating rate (K/s)	Solid residence time (s)	Particle size (mm)	Yield (%)		
					Liquid	Char	Gas
Conventional	550-950	0.1-1.0	450-550	5-50	30	35	35
Fast	850-1250	10-200	0.5-10	<1	50	20	30
Flash	1050-1300	<1000	<0.5	<0.2	75	12	13

Each component of biomass pyrolyzes at different rates and by different mechanisms and pathways. It is believed that as the reaction progresses, the carbon becomes less reactive and forms stable chemical structures. Consequently, activation energy increases as the conversion of biomass proceeds. Cellulose and hemicellulose decompose over a narrow temperature range compared to lignin. The hemicelluloses break down first, at temperatures approximately 470 to 600 K, and cellulose follows in the temperature range 510 to 650 K, with lignin being the last component to pyrolyze, at temperatures of 520 to 770 K[19, 21].

The char produced during pyrolysis can be converted to activated carbon, or used as domestic cooking fuel or for barbecuing[22]. The pyrolysis gas contains mainly hydrogen, carbon dioxide, water vapor, carbon monoxide, methane and light saturated and unsaturated hydrocarbons. The gas can be used for power generation or heat production, or alternatively converted to methanol or ammonia. The liquid product from pyrolysis is a heterogeneous mixture characterized by high oxygen content and alkalinity. It is also called pyrolysis oil or bio-oil, and can be converted to hydrocarbon liquid fuels or chemicals[17, 23].

Gasification

A promising way to use biomass for the production of heat, electricity, and other biofuels is through biomass gasification, in which the biomass is converted through partial oxidation into synthesis gas (CO, H_2, CH_4, and CO_2) and condensable compounds[24]. During gasification the chemical energy of the biomass is transferred into the thermal and chemical energy of the synthesis gas[25]. Figure 1-5 shows a simplified diagram of biomass gasification[17]. Biomass can be gasified in various ways by properly controlling the mix of fuel and oxidant within the gasifier. The oxidizing agents can be air, oxygen, steam, CO_2 or a mixture thereof. The gas can be cleaned and used directly in a gas engine, or converted to liquid fuels or chemical feedstocks through catalytic conversion via e.g., the Fischer-Tropsch process[26].

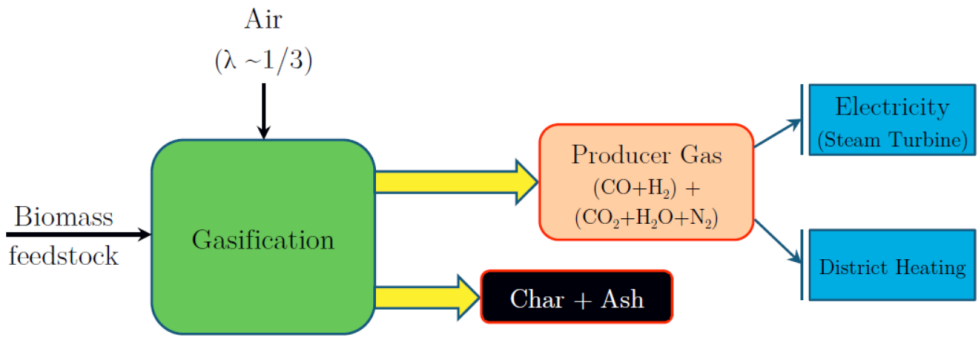

Figure 1-5: Simplified schematic of the gasification process[17]

The process starts with thermal decomposition of biomass particles through pyrolysis into gas species, liquid tar, and solid char. Subsequently, the vapor phase is thermally converted to gas and char. Afterwards, char particles are gasified by means of the gasifying agent. Finally, all three phases (gas, vapor, and char) are partially oxidized to obtain synthesis gas. The liquid fractions (tars) are either cracked further and transformed into gaseous products or cleaned out. The temperature of gasification is usually quite high (800 – 1300 ºC) compared to pyrolysis (400 – 800 ºC)[23]. A high temperature is needed to drive the main gasification reactions forward.

During biomass gasification, several parameters (such as gasifier type, reaction temperature, biomass fuels properties, bed material and gasifying agent) have a substantial influence on product gas composition, carbon conversion efficiency and tar formation[27]. Several decades of reactor design have yielded a number of different reactor technologies[28, 29] including fixed bed, fluidized bed and entrained flow reactors.

Combustion

Combustion consists of complete oxidation of fuel using excess air[30]. For solid fuels, combustion is a complex process that consists of both homogenous and heterogeneous reactions[1]. A combustion process is a set of reactions that is exothermic overall. There are several different zones in a combustion process where drying, pyrolysis, oxidation of char and gas phase reactions occur simultaneously. Several parameters in the combustion zone are crucial to the combustion process; among these are reactor technology, combustion temperature, residence time, air/fuel ratio, particle size and moisture content of the fuel. Although combustion is quite conventional compared to other thermal processes, research and technological improvements are ongoing.

The choice of technology for combustion of solid fuels will depend mainly on plant size and fuel type. The main combustion technologies are fixed bed, fluidized bed and pulverized fuel combustion[31-33]. Most of these technologies are air-staged combustion systems, where a portion of the combustion air is diverted (e.g., from the burners) to 'over-fire' air ports above the burners. The objective is to form a fuel-rich flame zone, followed by a region where the residual char is burned out. After fuel is fed into the reactor, volatiles and char form, each containing fixed nitrogen. Oxygen-rich conditions favor formation of nitrogen oxides (NO_x), while fuel-rich conditions (e.g., staged combustion) enhance conversion to nitrogen (N_2)[34].

1.1.4 Biomass pretreatment

One of the most challenging aspects of bioenergy development is overcoming operational and logistical limitations, i.e., by pretreating or preprocessing the biomass. Pretreatment is often used to modify the size, shape and density of biomass to match the fuel specifications of a particular thermochemical process. Biomass chemical composition, particle shape, size and density differences greatly affect conversion processes and equipment operations. The main goals of biomass pretreatment are as follows[35]:

- Homogenize biomass feedstock
    - Reduce handling difficulties
    - Convert multiple materials into a single feedstock
- Increase biomass energy density
    - Reduce the oxygen content of raw biomass
    - Higher energy density reduces transportation and handling costs
- Improve biomass storage stability
    - Address seasonality of some feedstock
    - Improve suitability for co-firing or co-gasification with coal

Most of these pretreatment options are applicable to production of liquid biofuels such as bioethanol, produced from biomass via fermentation of sugars derived from cellulose and hemicelluloses[8]. Biological methods include the use of fungi whose enzymes can degrade cellulose, lignin, hemicellulose and polyphenol. Chemical methods include the use of acids, alkalis, organic solvents and ionic liquids with significant effects on the native structure of lignocellulosic biomass. Physiochemical pretreatment includes the vast majority of pretreatment technologies, such as steam explosion, hot water treatment, ammonia fiber/freeze explosion, aqueous ammonia pretreatment and organosolv pretreatment[8].

For thermochemical processes, pretreatment options are based on the moisture content of the feedstock and are categorized into wet and dry biomass pretreatment[35].

Wet biomass pretreatment

Generally these options are suitable for biomass feedstock with > 50% moisture content. Two basic technologies are applicable here:

- Anaerobic digestion – a biological process that is well developed and applied in many biogas plants all over the world[35]. The products of the degradation process are biogas (composed mainly of carbon dioxide and methane) and a wet organic fraction called digestate, a high-quality fertilizer.
- Hydrothermal treatment – This method is still in a very preliminary stage of development and many processes are under evaluation. The most promising process so far is wet torrefaction[36, 37]. It occurs under high pressure (up to 50 bar) at relatively low temperatures (approximately 175-260 °C)[36, 37]. Reaction time varies from 5-240 min[36]. Process conditions can be varied to accommodate dry biomass as well. In the process, biomass decomposes in hot compressed water to produce a more energy-dense solid fuel (on both mass and volume basis) after grinding and pelletization, with relatively uniform handling characteristics.

Dry biomass pretreatment

This pretreatment category is applicable to biomass of low moisture content (<50%). The most commonly used options are briefly mentioned here:

- Physical pretreatment – coarse size reduction, chipping, shredding, grinding, and milling are amongst the different mechanical size reduction methods. These methods are used to enhance the subsequent processing/decomposition of lignocellulosic biomass by increasing the available surface area[8, 13, 38].
- Drying – reduction of water content in biomass after drying increases heating value and preservation potential, with less negative impact on the environment and more uniform combustion conditions[39]. Large boilers have often been scaled up for the use of biomass of varying moisture content. However, small scale combustors, gasification units and production of pellets and other processed biofuels demand drier feedstock and more controlled inputs.
- Pelletization – drying and pressing of biomass under high pressure to produce cylinders of compressed, extruded biomass. Pellets are more efficient to store, ship

and convert into energy because of smaller volume and higher volumetric energy density[35]. It not only produces a uniform and stable fuel but also minimizes dust. Production of pellets requires small feedstock particles (3-20 mm) and moisture content below 15%. If the feedstock is too dry or wet, the required pressure increases dramatically. A moisture content of 10-25% is considered optimal. Therefore, the feedstock is first heated to 50-100 °C to obtain a desired moisture level, before performing mechanical densification at approximately 150 °C[40].

- Dry Torrefaction – mild pyrolysis of biomass that is typically conducted at 200–300 °C, under approximately atmospheric pressure and mostly in the absence of oxygen at a relatively low heating rate (<50 °C/min)[41-43]. It is to date the most promising biomass pretreatment technique available for thermochemical processes. Torrefaction retains the benefits of drying, and can be combined with pelletization to produce torrefied pellets[44]. However, industrial technologies are still under development, with ongoing research on several fundamental topics related to the process. Dry torrefaction is the topic of this study. A detailed literature review is provided in Chapter 2, as well as Paper I.

1.2 Motivation

Researchers are looking into solutions to improve the properties of biomass as a fuel, and thus overcome existing operational and logistical limitations. Torrefaction is one potential solution to these problems, and has gained considerable research momentum as a biomass pretreatment process in the last two decades[42, 43]. It is essentially a mild pyrolysis process carried out between 200 and 300 °C, usually under an inert atmosphere. During torrefaction the fuel retains most of its energy content. Torrefaction considerable reduces moisture content, increases heating value, converts hygroscopic raw biomass into a hydrophobic product, and enhances grindability and energy density when compressed. Because of these improved properties, the value of torrefied biomass as a fuel is significantly higher than that of raw biomass. Torrefaction can be dry or wet, depending upon feedstock characteristics and processing conditions. Only dry torrefaction was utilized in this work; therefore, all references to 'torrefaction' should be interpreted as 'dry torrefaction'.

Torrefaction is influenced by many parameters such as biomass composition, processing temperature, holdup time and particle size. Several previous torrefaction studies are available. However, to evaluate the feasibility of torrefaction in a particular region, locally available biomass should be investigated. So far, no study has investigated and compared the torrefaction behavior of Birch (hardwood) and Spruce (softwood), which are the two main wood species in Norway. A few studies[45-47] have compared hardwoods and softwoods for torrefaction. However, only mass and energy yields or individual properties such as grindability were discussed. As mentioned earlier, development of a bioenergy market in Norway is essential to meet CO_2 reduction targets. Therefore, it is important that research is carried out to improve the properties of biomass and make it a competitive fuel option in Norway. Carrying out fundamental research on torrefaction using Norwegian woods will definitely be a step forward in this direction and thus, forms the basis of this work. Additionally, the real test of a torrefaction process is how it affects the behavior of biomass in thermochemical conversion processes. So far, only a few studies have attempted to analyze the reactivity of torrefied biomass in these processes, and only limited information is available. Therefore, the behavior and reactivity of torrefied biomass in thermochemical conversion processes are also covered here.

1.3 Objectives

The present thesis aims to contribute to our fundamental understanding of this topic as follows:

- Review existing literature on biomass torrefaction.
- Compare torrefaction behavior of Norwegian birch and spruce in terms of product yields and characteristics.
- Evaluate decomposition kinetics of Norwegian birch and spruce during torrefaction.
- Evaluate the kinetic behavior of torrefied biomass in an oxidative environment.
- Simulate biomass gasification and quantify the effect of torrefaction on syngas composition and gasification efficiency.

1.4 Thesis organization

An introduction to the subject is provided in Chapter 1. Biomass and bioenergy basics, thermochemical conversion processes, and pretreatment options are briefly described, together with the motivation and objectives for this work. A literature review on biomass torrefaction, chemical reaction kinetics and thermodynamic equilibrium models is included in Chapter 2. Chapter 2 gives brief overviews of torrefied biomass behavior in thermochemical processes, torrefaction technologies and novel techniques, intrinsic kinetic modeling as applied to thermochemical processes and a summary of kinetic modeling studies applied to torrefaction and torrefied biomass reactivity. The experimental section of the thesis in Chapter 3 includes the characterization of fuels, macro- and micro-TGA set-ups, test procedures and assessment methods. In addition, methodologies for evaluation of intrinsic kinetics under oxidative and inert conditions, together with a process modeling approach to study biomass gasification, are also presented in Chapter 3. Major highlights and a short summary of published works are included in Chapter 4. Finally, some recommendations for future work are listed in Chapter 5. Five publications (1 conference paper and 4 journal articles) covering the research performed for this thesis are attached as an appendix.

1.5 List of publications

The thesis is based on the following papers, which are referred to in the text by Roman numerals:

I. **Tapasvi, D.;** Tran, K-Q.; Wang, L.; Skreiberg, Ø.; Khalil, R. Biomass torrefaction – a review. Proceedings of the 9th European Conference on Industrial Furnaces and Boilers, Estoril, Portugal 2011, (ISBN 978-972-99309-6-6)

II. **Tapasvi, D.;** Khalil, R. A.; Skreiberg, Ø.; Tran, K.-Q.; Gronli, M. G. Torrefaction of Norwegian birch and spruce – an experimental study using macro-TGA. Energy Fuels 2012, 26, 5232–5240.

III. **Tapasvi, D.;** Khalil, R.; Várhegyi, G.; Tran, K.-Q.; Grønli, M.; Skreiberg, Ø., Thermal decomposition kinetics of woods with an emphasis on torrefaction. Energy Fuels 2013, 27, (10), 6134-6145.

IV. **Tapasvi, D.;** Khalil, R.; Várhegyi, G.; Skreiberg, Ø.; Tran, K.-Q.; Grønli, M. Kinetic behavior of torrefied biomass in an oxidative environment. Energy Fuels, 2013, 27, 1050-1060.

V. **Tapasvi, D.;** Kempegowda, R.; Tran, K-Q.; Skreiberg, Ø.; Grønli, M. A simulation study on the torrefied biomass gasification. Energy Conversion and Management, 2015, 90, 446-457

2 Literature Review

In this chapter, I present a brief summary of recent published work on biomass torrefaction, product properties and the reactivity of torrefied biomass in thermochemical processes. The reader is referred to Paper I for a detailed literature review on this topic. Brief reviews of intrinsic chemical reaction kinetics, kinetic modeling of biomass thermochemical processes and kinetic modeling of torrefaction are then given. An introduction to the application of thermodynamic equilibrium models to biomass gasification is also provided.

2.1 Biomass torrefaction

During torrefaction, biomass partly decomposes, yielding a solid product (torrefied biomass) as well as condensable liquids and non-condensable gases[46]. The chemistry of torrefaction is influenced by many parameters, such as biomass composition, temperature, holdup time and particle size. The main reactions during torrefaction involve xylan-containing hemicellulose polymers, which are the most reactive polymers in biomass[48]. However, as the temperature is increased, other biomass components such as cellulose, lignin and extractives also decompose, as shown in Figure 2-1[49].

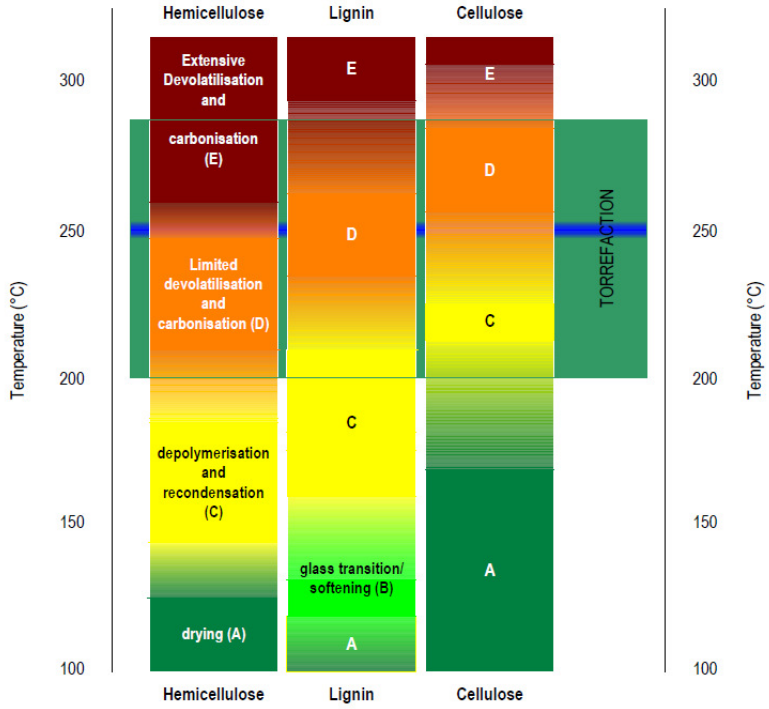

Figure 2-1: The main physicochemical processes during heating of biomass[49]

The following reactions take place in the torrefaction temperature range, at 200-300 °C:

- Devolatilization and carbonization of hemicelluloses.
- Depolymerization and devolatilization/softening of lignin.
- Depolymerization and devolatilization of cellulose.

The decomposition of hemicellulose during torrefaction changes the orientation of cellulose microfibrils in the lignin matrix, thereby improving biomass properties such as grindability, deterioration and fluidization. The ability of torrefaction to improve biomass properties has been investigated in several studies. Most of these studies have focused on compositional changes via proximate and ultimate analyses[50-52] and mass and energy yields[46, 50-55] of woody biomass, agricultural residues and energy crops. Studies have also investigated torrefied biomass properties such as hydrophobicity[56], grindability [47, 53, 54, 57, 58], particle size distribution[54, 59], and reactivity during combustion[56, 60, 61], gasification[62, 63] and pyrolysis[52, 64]. This literature suggests that torrefaction is a promising technique to improve biomass energy utilization. However, despite a number of impressive studies on the topic, many aspects have still not been addressed in sufficient detail. This formed the basis for the studies presented in Papers II-V.

2.1.1 Torrefaction and product properties

Either micro-TGA[45, 61, 65] or laboratory scale reactors[46, 51, 58, 63, 66, 67] have been used in previous studies to perform torrefaction. The kinetically controlled thermal weight loss of biomass can be measured precisely in a micro-TGA, which in this respect makes it preferable to a laboratory or pilot scale reactor for mass loss kinetics studies. Due to the small sample weights used (a few milligrams), negligible heat and mass transfer limitations exist in a micro-TGA, which is not the case in a commercial plant. Therefore, micro-TGA has been used to study the effects of operating parameters on torrefaction products and to obtain data for modeling its kinetics, whereas reactors have been used to study and simulate torrefaction in conditions closer to the industrial environment.

The properties of torrefied biomass obtained using both these methods have been determined using various analytical techniques. Considerable differences were found in the behavior of biomass materials during torrefaction. Solid product mass and energy yield are strongly influenced by raw biomass composition and operating conditions such as temperature and holdup time. Product yields from several types of biomass at different torrefaction temperatures and holdup times are shown in Figure 2-2[46]. Among the product

properties evaluated, grindability is the most studied. Very few studies have attempted to investigate the densification, fluidization, storage and char reactivity of torrefied biomass.

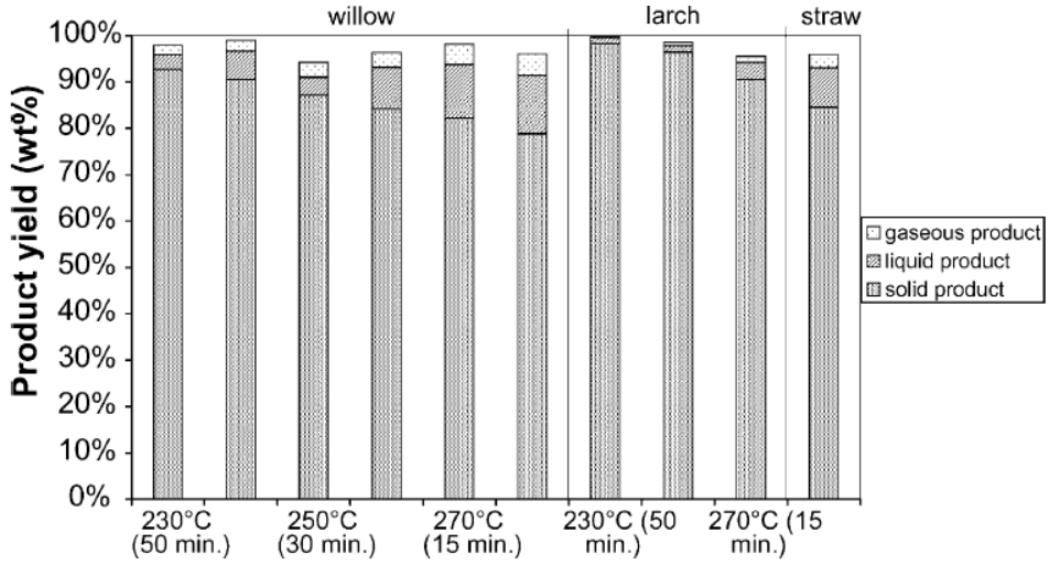

Figure 2-2: Overall mass balance of several torrefaction experiments[46]

Torrefaction results in the following major improvements in biomass properties:

(1) considerable reduction of moisture content due to drying[63, 68, 69]

(2) increased energy density when compressed, and increased heat value due to the reduced O/C ratio[45, 46, 61, 63]

(3) intrinsic conversion of hygroscopic raw biomass into hydrophobic torrefied biomass[58, 70]

(4) enhanced grindability, which reduces energy consumption during milling[53, 54, 57]

A few studies have reported that torrefaction results in reduced biomass density and volume; the extent of this reduction increased with torrefaction severity[71]. However, this can be overcome by pelletizing the torrefied biomass. The compression step during pelletization increases volumetric energy density (GJ/m^3) by a factor of 4-8, leading to significant cost savings in transportation and storage. Table 2-1 shows a comparison between torrefied pellets and other similar fuels[72]. Research is ongoing to reduce energy consumption during pelletization, as it has been reported that torrefied biomass consumes more energy during pelletization than raw biomass[73]. Process conditions during pelletization must be optimized to improve the viability of torrefied biomass during transport, handling and storage[40, 74].

Because of these advantages and high viability, the technique has attracted increasing interest over recent decades. However, Norwegian feedstocks such as spruce and birch have

not previously been tested for torrefaction behavior. This formed the basis for the study presented in Paper II.

Table 2-1: Properties of various solid fuels[72]

Property	Wood	Wood pellets	Torrefied pellets	Charcoal	Coal
Mositure content (% wt)	30 - 45	7 - 10	1 - 5	1 - 5	10 - 15
Lower heating value (MJ/kg)	9 - 12	15 - 18	20 - 24	30 - 32	23 - 28
Volatile matter (% db)	70 - 75	70 - 75	55 - 65	10 - 12	15 - 30
Fixed carbon (% db)	20 - 25	20 - 25	28 - 35	85 - 87	50 - 55
Density (kg/l) (bulk)	0.2 - 0.25	0.55 - 0.75	0.75 - 0.85	~0.20	0.8 - 0.85
Energy density (GJ/m^3) (bulk)	2.0 - 3.0	7.5 - 10.4	15.0 - 18.7	6 - 6.4	18.4 - 23.8
Dust	Average	Limited	Limited	High	Limited
Hydroscopic properties	Hydrophyllic	Hydrophyllic	Hydrophobic	Hydrophobic	Hydrophobic
Biological degradation	Yes	Yes	No	No	No
Grindability	Poor	Poor	Good	Good	Good
Handling	Special	Special	Good	Good	Good
Quality variability	High	Limited	Limited	Limited	Limited

2.1.2 Torrefied biomass behavior in thermochemical processes

Testing the behavior of torrefied biomass in a thermochemical process is an important aspect of improving the viability of torrefaction. A few studies have attempted to do these analyses by simulating combustion and gasification conditions in a laboratory/pilot plant or by evaluating the kinetics of torrefied biomass from thermogravimetric experiments (included in section 2.2.3).

For combustion, being the main process used for biomass, understanding the behavior of torrefied biomass under oxidative conditions should be a priority. A few studies, listed in Paper I, conducted preliminary lab studies using Merker burners or lab-scale combustion simulators to study torrefied biomass behavior during combustion. The results showed decreased combustion time for volatiles in torrefied wood compared to untreated wood. Khalil et al.[75] investigated the combustion of raw and torrefied spruce and spruce tree top and branch (T&B) pellets in a residential pellet stove, and evaluated emissions of gaseous pollutants and particulate matter (PM). Mild torrefaction reduced CO emissions, unburned hydrocarbons, and the organic content of particles smaller than 1 μm (PM1.0). However, these advantages were offset by a substantial increase in the inorganic share of PM1.0 emissions.

Similarly, a few studies investigated the behavior of torrefied biomass during entrained flow gasification (simulated in the lab), as listed in Paper I. Torrefied samples produced more

H_2 and CO, but the reactivity of torrefied char was lower than that of the parent biomass. Recently, Berrueco et al.[76] reported the influence of torrefaction temperature and gasification pressure on syngas yields and composition in lab-scale fluidized bed O_2/steam gasification. The results revealed that syngas yield increased with gasification pressure and torrefaction temperature. However, increasing pressure reduced H_2 and CO levels. Sarkar et al.[77] performed air gasification of torrefied, densified and torrefied/densified biomass in a lab-scale, fixed-bed, externally heated reactor. Densified torrefied biomass gave higher H_2 and CO yields, syngas LHV and process efficiencies at a gasification temperature of 900 °C. The experimental approaches used by these studies are quite different, and it is hard to compare results. Further investigations are needed to confirm these preliminary results on the behavior of torrefied biomass in gasification conditions.

2.1.3 Torrefaction technologies and novel techniques

More than 50 companies are developing torrefaction technologies. Because research is still ongoing into the fundamental understanding of torrefaction, as well as the applications of torrefied biomass, it will take some time to achieve recognition as a feasible biomass pretreatment technology[78]. The advantages of torrefaction are clear for co-firing in pulverized coal power plants, and in co-gasification in entrained-flow gasification plants, due to reduced power consumption in grinding, an attractive C/O ratio and low moisture content[79]. Concepts for reactor technologies are being borrowed from other biomass applications, such as drying, pyrolysis, gasification and combustion. Figure 2-3 shows some of the torrefaction reactor technologies currently in use[72]. Currently, no single technology is clearly superior; all of them have advantages and disadvantages. Proper reactor selection is important, as each design is well suited to specific types of biomass[78]. For commercialization, torrefaction reactors must still be optimized to meet end user requirements economically and to achieve standardization of the solid product.

Reactors can be classified as either directly or indirectly heated[80]. In directly heated reactors, the biomass is in direct contact with hot flue gases, recirculated gases, or superheated steam. Many dryers and gasification technologies are based on direct heating: these include rotary drum, moving bed, fluidized bed, multiple hearth furnace (MHF), oscillating belt, turbodryer, torbed and directly heated screw reactors[72]. The benefits of directly heated reactors include uniform and quick heating of biomass. Reactors such as the microwave type use direct heating, but the heating medium is not hot, flowing gas. In indirectly heated reactors, the biomass is not in direct contact with the heat carrier. Most

carbonization and slow pyrolysis processes are based on this principle, such as rotary kilns and indirectly heated screw reactors. These types of reactors can handle a wide range of biomass types and sizes, but their main flaws include low heat transfer rates and non-uniform heating of feedstock[49].

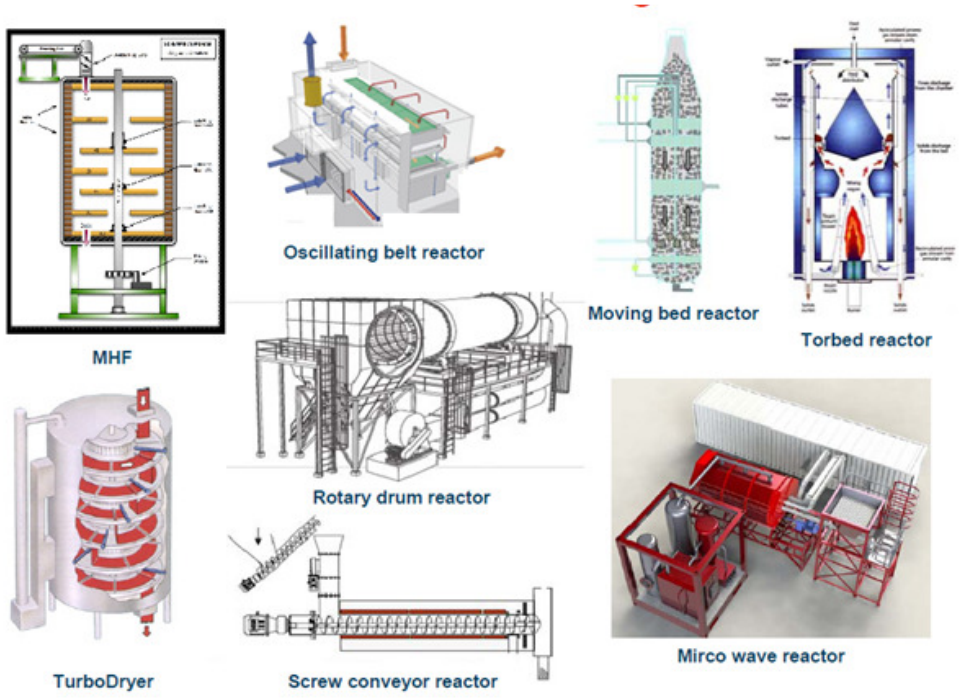

Figure 2-3: Some current torrefaction reactors[72]

Recently, as novel torrefaction methods, a few studies have investigated non-inert environments[81-85]. Air or carbon dioxide were used as substitutes for nitrogen. Except for increased mass loss, biomass fuel properties such as grindability, energy density and heating value were comparable to those achieved in inert environments at the same degree of torrefaction. Increased mass loss under non-inert torrefaction conditions may be due to oxidation and to the catalytic effect of ash components on reactions that occur in the torrefaction temperature range. However, these results are preliminary. Further research is needed to explore the effect of different torrefaction media.

2.2 Chemical reaction kinetics

2.2.1 Overview of modeling intrinsic kinetics

With its high precision and well-controlled experimental conditions, TGA is a useful tool for studying the devolatilization, gasification and combustion of biomass under a kinetic

regime[86-90]. However, TGA can be employed only at relatively low heating rates because the temperature of small samples is unknown at high heating rates. Accordingly, the results of TGA studies cannot be used alone in the modeling of industrial reactors; they serve as basic research to direct further development in the field. Heat and mass transfer limitations must be included in an overall model of industrial reactors. It is assumed that the samples are under kinetic control, meaning that heat and mass transport processes do not generate significant macroscopic heterogeneity in samples. Hence, product formation is governed by chemical reactions[88].

Rate Equations

It is well known that thermogravimetric curves can be analyzed mathematically using the following type of kinetic equation[91]:

$$\frac{d\alpha}{dt} = k(T) f(\alpha) \tag{2-1}$$

where α is the reacted fraction, f(α) is a continuous function representing the reaction model and $k(T)$ is the temperature-dependent rate constant defined by the Arrhenius equation[92]:

$$k(T) = A\mathrm{e}^{-E/RT} \tag{2-2}$$

where A is the pre-exponential factor, E is the activation energy and R is the universal gas constant. Various forms of f(α) and g(α), the integral of 1/f(α), are listed in Table 2-2[92].

Isothermal and non-isothermal kinetics

General expectations for a good kinetic model include: description of the behavior of samples under a wide range of experimental conditions; prediction of behavior outside the domain of the observations; characteristics that can reveal similarities and differences between the samples; and finally a deeper insight into the processes taking place[93].

TGA experiments can be conducted under either isothermal conditions at a particular temperature, or with dynamic/non-isothermal heating programs that involve different heating rates. Non-isothermal heating resolves a major defect of isothermal experiments, which is that a sample requires some time to reach the experimental temperature. During the non-isothermal period of an isothermal experiment, the sample undergoes transformations that are likely to affect the results of the following kinetic analysis. This problem restricts the use of high temperatures in isothermal experiments[92, 94].

It is generally believed that kinetic analysis yields an adequate kinetic description of thermal decomposition in terms of the reaction model and Arrhenius parameters. These three

components ($f(\alpha)$, E and ln A) are also called the 'kinetic triplet'. To determine Arrhenius parameters using equation 2-1, one has to separate the temperature $k(T)$ and conversion dependence $f(\alpha)$ of the reaction rate. The most popular way to do this is by fitting experimental data to different reaction models. This is also referred to as model fitting. Using this method, k(T) is determined by the form of f(α) chosen from Table 2-2[92].

Table 2-2: Alternate reaction models[92]

	Reaction model	$f(\alpha)$	$g(\alpha)$
1	Power law	$4\alpha^{3/4}$	$\alpha^{1/4}$
2	Power law	$3\alpha^{2/3}$	$\alpha^{1/3}$
3	Power law	$2\alpha^{1/2}$	$\alpha^{1/2}$
4	Power law	$2/3\alpha^{-1/2}$	$\alpha^{3/2}$
5	One-dimensional diffusion	$1/2\alpha^{-1}$	α^{2}
6	Mampel (first order)	$1-\alpha$	$-\ln(1-\alpha)$
7	Avrami–Erofeev	$4(1-\alpha)[-\ln(1-\alpha)]^{3/4}$	$[-\ln(1-\alpha)]^{1/4}$
8	Avrami–Erofeev	$3(1-\alpha)[-\ln(1-\alpha)]^{2/3}$	$[-\ln(1-\alpha)]^{1/3}$
9	Avrami–Erofeev	$2(1-\alpha)[-\ln(1-\alpha)]^{1/2}$	$[-\ln(1-\alpha)]^{1/2}$
10	Three-dimensional diffusion	$2(1-\alpha)^{2/3}[1-(1-\alpha)^{1/3}]^{-1}$	$[1-(1-\alpha)^{1/3}]^{2}$
11	Contracting sphere	$3(1-\alpha)^{2/3}$	$1-(1-\alpha)^{1/3}$
12	Contracting cylinder	$2(1-\alpha)^{1/2}$	$1-(1-\alpha)^{1/2}$

In isothermal kinetics, k(T) and f(α) are separated by the conditions of the experiment (k(T) is constant at constant T). The f(α) term is determined by fitting reaction models from Table 2-2 to the experimental data. After the f(α) term has been established for a series of temperatures, k(T) can be evaluated. Note that this procedure involves two sequential constrained fits: the first finds f(α) from data obtained at constant temperature, and the second finds E and A based on a fixed form of f(α)[92].

A single non-isothermal experiment also provides information on both $k(T)$ and $f(\alpha)$, but not separately. The model fitting approach attempts to determine all three members of the kinetic triplet simultaneously. Therefore, almost any $f(\alpha)$ can fit data satisfactorily, at the cost of dramatic variations in the Arrhenius parameters, which compensate for the difference between the assumed form of $f(\alpha)$ and the true but unknown kinetic model. Isothermal experiments include temperature as an experimental variable, whereas non-isothermal experiments allow fits that vary temperature sensitivity (E, ln A) and reaction model $f(\alpha)$ simultaneously. This allows errors in the reaction model to be concealed by other compensating errors[89, 91-93]. To overcome this, one should collect experimental data under a broad range of experimental conditions and evaluate them[21, 90, 93, 95].

For both isothermal and non-isothermal studies, statistical methods are used in most cases to choose a unique kinetic triplet. The method of least squares is the most commonly used to

characterize the goodness of fit; the minimum value of the residual sum of squares is used to choose the unique kinetic triplet[91, 92]. For non-isothermal data, many studies have used Coats-Redfern linearization as follows[92, 93]:

$$\ln\frac{g(\alpha)}{T^2} \cong \ln\frac{AR}{\beta E} - \frac{E}{RT} \tag{2-3}$$

where $g(\alpha)$ is the integral of $1/f(\alpha)$ and β is the heating rate. This method is one of the most frequently used to process non-isothermal data. Inserting various $g(\alpha)$ into the equation results in a set of Arrhenius parameters. The left-hand side can be regarded as an experimental quantity, and this equation can then be used in least squares methods. However, this method is restricted to models containing only one reaction step, and the reaction should obey a variant of equation 2-1[93]. Additionally, the evaluation is restricted to experiments with linear heating programs; $f(\alpha)$ should not contain unknown kinetic parameters, and α should be directly calculated from the experimental data. These criteria are rarely applicable to kinetic models involving wood. Therefore, these linearization techniques or ''model-free'' approaches may help to find initial values for iterations in the method of least squares, but these goals are better fulfilled by a method aiming directly at the description of the experimental data under a wide range of experimental conditions[93]. The least squares method works well for both isothermal and non-isothermal kinetics; there is no need to replace it with methods requiring simpler programming or less computation time. The method of least squares can be applied successfully to models of more than one partial process: competitive, consecutive and parallel reactions. Additionally, simultaneous evaluation of a series of experiments can be achieved[91, 93].

Heterogeneous samples

Biomass is too complex a material to be described by only one chemical reaction. However, as an approximation, we can regard it as composed of pseudocomponents, where a pseudocomponent is a fraction of a reactive species exhibiting similar reactivities. A kinetic equation in the form of equation 2-1 is assumed for each pseudocomponent[21, 90, 93, 95]. Each reaction includes values for E, A and the weighting factors for the pseudocomponents. The resulting mass loss rate curve is the weighted sum of the individual reaction rates[93]:

$$-\frac{dm}{dt} = \sum_{j=1}^{N_{comp}} c_j \frac{d\alpha_j}{dt} \tag{2-4}$$

where m is the normalized sample mass, N_{comp} is the number of pseudocomponents and c_j is the normalized mass of volatiles formed from pseudocomponent j. Obviously one experiment cannot provide enough information for so many parameters. Therefore, one should evaluate a series of experiments. Evaluation can be done in two ways: either the experiments are evaluated simultaneously, looking for a set of kinetic parameters describing all of the experiments, or the thermogravimetric curves are evaluated one by one, independently from each other, and the results are compared after evaluation. The latter approach works well if the information content of an experiment is sufficient for the determination of all unknown parameters, and if it is followed up to verify that the kinetic parameters vary with the experimental conditions[93, 96].

Recently, distributed activation energy models (DAEM) have been applied to the decomposition kinetics of biomass[21, 90, 93, 97, 98]. Several variants of DAEMs are known; usually a Gaussian distribution of activation energy is employed. Due to the complexity of the investigated materials, the model was expanded to simultaneous parallel reactions (pseudocomponents) that were described by separate DAEMs[99-102]. According to this model, the sample is regarded as a sum of *M* pseudocomponents, where *M* is usually between 2 and 4. The reactivity differences between species in a pseudocomponent are described by different activation energy values. On a molecular level, each species in pseudocomponent *j* is assumed to undergo first-order decay. The distribution of the species differing by *E* within a given pseudocomponent is approximated by a Gaussian function, with a mean activation energy value and a width parameter (variation)[97].

2.2.2 Kinetic modeling of thermochemical processes

Pyrolysis, gasification and combustion kinetics, coupled with the description of transport phenomena, produce advanced computational tools for the design and optimization of reactors for the thermochemical conversion of biomass. Weight loss results from the combined activity of numerous reactions. Therefore, TGA curves, measured under isothermal or non-isothermal conditions, are useful for the formulation of global or semi-global mechanisms, which can include the effects of reaction parameters and sample properties[21, 95].

Biomass pyrolysis

Several studies suggest that the primary decomposition rate of biomass can be modeled, taking into account the thermal behavior of the major components (hemicellulose, cellulose, lignin) and their relative contribution to chemical composition[21]. The term “pseudo compo-

nent" is appropriate, as it is impossible to avoid overlap between different components in the measured weight loss curves[21, 90].

A simplified description of primary decomposition processes, usually adopted for isothermal conditions or fast heating rates, is based on a one-component (or one-stage) reaction process. In this case, weight loss curves are often associated with additional measurements of the yields of the three product classes (gases, tar and char), to evaluate formation rates. Both yields and decomposition rate (conversion time) can be predicted if one-component mechanisms are coupled with transport equations. However, the assumption of one-component behavior generates inaccurate decomposition rates due to the heterogeneous nature of biomass[21].

Multi-component (or multi-stage) reaction mechanisms have also been proposed, where each reaction takes into account a pseudocomponent in the measured weight loss curves. Kinetic models make use of Arrhenius dependence on temperature, thus introducing the parameters E and A, and linear or power law dependence on the component mass fraction for each reaction[21, 90]. Several attempts have been made to develop DAEMs[21, 93, 97, 98]. Multicomponent mechanisms describe the devolatilization process, and the final char yields should be known. However, the product distribution cannot be predicted from these mechanisms. Usually, three parallel, first-order reactions are considered, for volatiles released from the pseudocomponents hemicellulose, cellulose and lignin[21]. The analysis of single dynamic (non-isothermal) TGA curves assumes that hemicellulose and cellulose are associated with the shoulder and peak of the rate curves, respectively, whereas lignin decomposes slowly over a very broad temperature range. Activation energies vary between 80–116 kJ/mol for hemicellulose, 195–286 kJ/mol for cellulose, and 18–65 kJ/mol for lignin[21]. Comparison of results between studies is difficult, owing to variations in experimental conditions, mathematical treatment of the data, the nature of the fuel and possible flaws in the measurements. However, it appears that heating rate effects (thermal lag between sample and external temperature), when assuming first-order reactions, result in higher activation energies for the devolatilization of the pseudocomponents hemicellulose and lignin. Therefore, more complex reactions should be used for these two pseudocomponents[21].

Biomass gasification and combustion reactivity

As mentioned earlier, chemistry and transport phenomena should be separated to evaluate intrinsic chemical kinetics. Therefore, reaction conditions, sample characteristics and sample

position in the reaction environment should be carefully chosen for TGA experiments. TGA curves are generally expressed as reactivity versus conversion, and it is widely accepted that the mechanisms of char combustion and gasification proposed for coal chars are also applicable to lignocellulosic fuels[95]. Pyrolysis also plays an important role as the first step in gasification and combustion. In numerous practical applications, solid conversion can be observed as a two-stage process: pyrolysis (or devolatilization) and slow heterogeneous conversion of char[95, 103].

Gasification reactivity

The main reactions responsible for the gasification of solid carbon are the Boudouard reaction and the water-gas reaction, as shown in equations 2-5 and 2-6, respectively. Both reactions are relatively slow and are considered negligible at temperatures below 800 ºC. To predict the rate of the Boudouard reaction, several models have been developed. The common goal for all models is to find a suitable function that will predict the gasification rate of a carbon particle during its conversion to gaseous products[23, 95].

$$C + CO_2 \quad \Leftrightarrow \quad 2CO \tag{2-5}$$

$$C + H_2O \quad \Leftrightarrow \quad CO + H_2 \tag{2-6}$$

The simplest model for the prediction of global reaction rate is the nth order rate equation:

$$r = k \cdot p_x^n \tag{2-7}$$

where r is the intrinsic reaction rate, p_X is the partial pressure of the gasification agent (either p_{CO_2} or p_{H_2O}), n is the true reaction order and k is the intrinsic rate coefficient, which is related to temperature through Arrhenius expression 2-2[23, 95].

More complex expressions have been derived based on active site theory, postulating that chemical reactions occur at favored active sites on the surface of solid particles. Reactions 2-8 and 2-9 are proposed for CO_2 gasification and 2-10 and 2-11 for H_2O gasification.

$$C_f + CO_2 \underset{k_2}{\overset{k_1}{\leftrightarrow}} C(O) + CO \tag{2-8}$$

$$C(O) \overset{k_3}{\rightarrow} CO + C_f \tag{2-9}$$

$$C_f + H_2O \underset{k_2}{\overset{k_1}{\leftrightarrow}} C(O) + H_2 \tag{2-10}$$

$$C(O) \overset{k_3}{\rightarrow} CO \tag{2-11}$$

where C_f represents an active carbon site and $C(O)$ a carbon-oxygen complex. By assuming a pseudo-steady state for the C(O) complex $\left(dC(O)/dt = 0\right)$, the Langmuir-Hinshelwood kinetic equation can be derived[23, 95]:

$$r = \frac{k_1 C_t p_{CO_2}}{1 + \left(k_2/k_3\right) p_{CO} + \left(k_1/k_3\right) p_{CO_2}} \tag{2-12}$$

Here C_t is the total number of active carbon sites. Similar equations exist for steam gasification as well. To calculate A and E for all rate coefficients in equation 2-12, many thermogravimetric experiments are needed. The intrinsic reaction rate of equation 2-12 depends on C_t, a variable likely to change with the particle conversion rate. The number of active carbon sites is difficult to measure, and attempts to relate it to other carbon char properties have been made[95].

When experimental conditions allow the Boudouard reaction to proceed in both directions, the Langmuir-Hinshelwood kinetics is usually employed. If the reaction is far from equilibrium, the kinetics can be well described by *n*th-order equations[104]. Several authors propose a rate of char conversion with a kinetic contribution and a structural term, but simple pure kinetic laws have also been used. In some cases the pre-exponential factor also incorporates partial pressure effects, so that the kinetic parameters have a more limited range of validity[95].

Combustion reactivity

Similar to gasification reactivity, the simplest model for the prediction of a global reaction rate is the nth order intrinsic rate equation[95]:

$$r = k \cdot p_{O_2}^n \tag{2-13}$$

where r is the intrinsic reaction rate, p_{O_2} is the partial pressure of oxygen, n is the true reaction order and k is the intrinsic rate coefficient, which is related to temperature through Arrhenius expression 2-2. This one-step global reaction is used by several authors to describe

the process up to complete conversion. More complex expressions have also been derived from active site theory. Equation 2-14 represents the chemisorption of oxygen on active sites and equation 2-15 the formation of CO through desorption[95].

$$2C_f + O_2 \xrightarrow{k_1} 2C(O) \tag{2-14}$$

$$C(O) \xrightarrow{k_2} CO \tag{2-15}$$

There can be additional reactions involved in the formation of CO_2, but only the above two reactions are modeled in Langmuir-Hinshelwood form[95]:

$$r_c = \frac{k_1 k_2 p_{O_2}}{k_1 p_{O_2} + k_2} \tag{2-16}$$

However, the parameters of the above equation have not yet been evaluated for major biomass materials[95]. Multistep models have also been proposed that include additional steps for low-temperature devolatilization, or both devolatilization and combustion, of char. Several authors incorporate the dependence of reactivity on oxidant partial pressure into the pre-exponential factor[95, 103]. Char combustion experiments have been conducted either or at both isothermal and non-isothermal conditions. Low activation energies are generally obtained when a single-step reaction is assumed. However, the combination of a global one-step reaction for char combustion with a first-order or n-order reaction for the devolatilization stage yields accurate predictions of weight loss curves, and a higher activation energy for the combustion reaction[95]. The most widely used treatment also includes a structural term describing the effects of porosity evolution, and available internal surface area or concentration of active sites, in addition to the kinetic term[95].

2.2.3 Kinetic modeling of torrefaction and torrefied biomass reactivity

Many studies are available on the production and characterization of torrefaction products. However, fewer works address torrefaction kinetics[45, 105-110]. Most of these studies are based on isothermal experiments and first order kinetics. Prins et al.[45], Bates et al.[105], Nocquet et al.[111], Bach et al.[112], Peduzzi et al.[113], Ren et al.[114], employed a one-component, two step successive first-order reaction model based on earlier work by Di Blasi and Lanzetta[115] on xylan kinetics. The same model was used in recent TGA studies by Shang et al.[110, 116]. Peng et al.[109] used a one-component, single step reaction model for torrefaction with long residence times, but a two component, single step model for short residence times. Chen

and Kuo[106] studied the torrefaction of hemicelluloses, cellulose and lignin separately, using a global single step reaction model for each. They described the torrefaction of biomass by superimposing the kinetics of the three components. Klinger et al.[117] employed a one-component, three step successive reaction model, and assumed first-order reactions for all steps. Recently, Sarvaramini et al.[118] applied a DAEM model, but evaluated only isothermal experiments.

Understanding torrefaction reaction mechanisms and kinetics is very important to identify the optimum conditions for this biomass pretreatment technology. Torrefaction kinetics are part of a broader subject: the pyrolysis kinetics of biomass materials. If a kinetic model describes biomass pyrolysis in the torrefaction temperature range well, then the model can also describe the pyrolysis behavior of the torrefied wood. This assumes that the experimental data used for the determination of model parameters include temperature programs where temperature increases are preceded by longer residence times in the torrefaction temperature range. This approach was followed in paper III. Because isothermal experiments involve substantial transient time, which is lost from the evaluation of thermogravimetric experiments, all experiments performed for paper III were evaluated together with the heat-up period.

Few studies have attempted to model the reactivity of torrefied biomass in thermochemical processes. Most of these are combustion reactivity studies, except for the studies by Ren at al.[114] and Vincent et al.[119]. Ren et al.[114] employed a model-free Friedman iso-conversional method and assumed one-step global kinetics for modeling torrefied biomass behavior during pyrolysis. Vincent et al.[119] evaluated the kinetics of torrefied biomass under CO_2 gasification conditions by performing isothermal experiments at temperatures between 750-900 °C. For combustion studies, Bridgeman et al.[61], Arias et al.[53], Jones et al.[120] and Broström et al.[121] utilized TGA to evaluate the combustion reactivity of torrefied samples. No kinetic analysis was performed by Bridgeman et al.[61]. Arias et al.[53] divided TGA experiments into low and high temperature stages (below and above ~400 °C, respectively) and described both stages using first order kinetics. Jones et al.[120] performed TGA experiments on chars prepared from torrefied biomass samples, and applied a first order reaction model to deduce kinetic parameters for char reactivity under oxidizing conditions. They observed that chars from torrefied samples had lower reactivity than those from raw samples, but higher than those from coal. In a later study, Broström et al.[121] provided a detailed kinetic model for the devolatilization and oxidative kinetics of torrefied Norwegian spruce. For devolatilization, measured curves were predicted using three parallel reactions,

corresponding to the three main wood components: hemicellulose, cellulose and lignin. In the presence of oxygen, two additional reactions for char devolatilization and combustion were included. The work presented in paper IV continues the efforts of Broström et al.[121] to establish a detailed model for these oxidation kinetics, using a wider set of experimental conditions, Norwegian feedstocks and a more comprehensive kinetic model. Details of the applied kinetic model are presented in Chapter 3.

2.3 Thermodynamic equilibrium models

Another way to investigate biomass gasification is to use thermodynamic equilibrium models to predict syngas composition[122]. Many studies have evaluated biomass behavior in gasification processes using this approach, and gave reasonable agreement between equilibrium predictions and experimental data[123-129]. Commercial tools such as Aspen Plus have been very useful in applying these thermodynamic equilibrium models to predict biomass gasification behavior as a sub-model with built-in solid properties. Mansaray et al.[130] used Aspen Plus to simulate a dual-distributor-type fluidized-bed rice husk gasifier. Paviet et al.[131] studied thermo-chemical equilibrium modeling of biomass gasification. In a few recent studies, it has been reported that torrefied biomass can significantly affect the efficiency of gasification. Chen et al.[132] employed a process optimization technique, the Taguchi method, for identifying optimal process parameters for co-gasification of torrefied biomass and coal in an entrained-flow gasifier. In another study, Chen et al.[133] simulated an entrained-flow gasifier using oxygen as the gasifying agent. The gasification performance of torrefied bamboo was quite similar to that of coal. Furthermore, Kuo et al.[134] evaluated a two-stage gasification process for raw and torrefied bamboo using a Gibbs minimization approach under isothermal conditions in Aspen Plus simulations. It was reported that carbon conversion and syngas yield were higher for torrefied materials than for raw biomass, whereas the trends for cold gas efficiency were the opposite. Biomass torrefied at 250 °C was found to be the best fuel for gasification considering all process parameters. However, this study did not account for tar formation, and assumed char to be pure carbon. Except for these few studies, there is a lack of information on the behavior of torrefied biomass under gasification conditions. Therefore, better data are needed. This formed the basis of the study conducted in Paper V. This extends the efforts of Kuo et al.[134] to establish a detailed equilibrium model of the effect of torrefaction on syngas composition and efficiency of biomass gasification. The aim was to study a two-stage gasification process using Gibbs free energy minimization in Aspen Plus, giving improved accuracy, together with a

comprehensive thermodynamic analysis. The accuracy of the model was improved by including: tar formation during pyrolysis and further cracking in the gasification reactor; actual experimental decomposition yields as inputs for both untreated and torrefied biomass; the compositions of the chars produced during pyrolysis, as calculated from the elemental balance; and a C-H-O Ternary diagram for validating the results. The model was integrated in an Excel spreadsheet to study energy and exergy efficiencies under different gasifier operating conditions. Exergy analysis of a process is a supplement to energy analysis and is based on the 2nd law of thermodynamics. It is a useful tool to assess the work potential of input and output materials and heat streams and to pinpoint irreversible losses in a system[135-138].

3 Methodology

This chapter includes details on the fuel characterization, the experimental set-up and procedures, the approach followed for the kinetic modeling of the biomass decomposition under inert and oxidative conditions and the process modeling for gasification process with Aspen Plus.

3.1 Fuel characterization

Two primary Norwegian woody biomass materials, namely, birch and spruce, were used as feedstocks for the studies performed in papers II-IV.

Birch (*Betula verrucosa*) is a robust tree that thrives in cold climates. Its adaptive nature makes it easy for it to grow in almost any type of soil; in addition, birch can survive in extreme weather conditions. In Norway, birch is spread across the whole country and is commonly used as firewood. Birch is easy to process, which makes it an attractive material to work with for the manufacture of furniture and other small household articles.

Spruce (*Picea abies*) is one of the most common wood species found in Norway. It is a large, fast-growing, evergreen coniferous tree that grows 35–55 m (115–180 ft) tall and has a trunk diameter of up to 1 to 1.5 m. Norway spruce grows throughout Europe from Norway in the northwest to Poland and eastward, as well as in the mountains of central Europe, southwest to the western end of the Alps, and southeast in the Carpathians and Balkans to the extreme north of Greece.

Norwegian birch and spruce fuel samples were obtained from local sources in Trondheim, Norway. These samples were standardized wood boards that are typically used in buildings. The raw samples were characterized by proximate and ultimate analyses, the results of which are presented in Tables 3-1, including the higher heating values (HHVs).

Table 3-1: Proximate and ultimate analyses of the samples (Paper II-III)

Sample	Proximate analysis[a]			Ultimate analysis[a]					HHV[b]
	VM	fC	Ash	C	H	O	N	S	
Birch	89.4	10.4	0.2	48.62	6.34	44.90	0.09	< 0.05	19.80
Spruce	86.3	13.4	0.2	50.10	6.36	43.52	0.07	< 0.05	20.45

[a] % (m/m), dry basis. [b] Higher heating value, MJ/kg, dry basis.

The proximate analyses of the raw samples were conducted according to ASTM standards ASTM E871, ASTM E872 and ASTM D1102 for the moisture content, volatile matter and ash content, respectively. In addition, the ASTM 1762-84 standard methods, which are

applicable to charcoal powders, were applied to conduct the proximate analyses of the torrefied biomass. The fixed carbon content was calculated by difference to 100 % in both cases. A determination of the C/H/N/S contents by ultimate analysis was conducted by using an "EA 1108 CHNS-O" elemental analyzer by Carlo Erba Instruments. The oxygen content was calculated by difference to 100 % for all samples. The HHV was calculated based on the elemental fuel composition[139].

Before the torrefaction experiments in the macro-TGA (Paper II), the samples were carefully cut to create cubes with sides of either 10 or 40 mm, and the cubes were then dried for 24 hours at 105 °C. The samples were heated at a heating rate of 5 °C/min up to either 225 or 275 °C. For the micro-TGA experiments in Paper III, the samples were cut into smaller pieces and ground in a cutting mill that was equipped with a 1-mm bottom sieve. The samples were sieved afterwards, and particles ranging from 63 to 125 µm were used.

For the micro-TGA experiments in Paper IV, 10-mm cubes from both feedstocks that were torrefied in the macro-TGA were used (only the samples with a 30-min holdup time were not included). A fine grinding of the torrefied samples was performed in a cutting mill equipped with a 1 mm bottom sieve. The powdered samples were sieved afterwards, and particles ranging from 63-125 µm were used. Six samples were prepared for this study in all, with four torrefied samples and two raw fuels. Table 3-2 shows the ultimate and proximate analyses of the samples.

Table 3-2: Proximate and ultimate analyses of the samples (Paper IV)

Sample	Proximate analysis[a]			Ultimate analysis[a]					HHV[b]
	VM	fC	Ash	C	H	O	N	S	
B --	89.4	10.4	0.2	48.62	6.34	44.90	0.09	< 0.05	19.80
B225	86.4	13.2	0.4	49.90	5.98	44.00	0.10	< 0.05	19.90
B275	77.7	21.9	0.4	54.16	5.65	40.00	0.12	< 0.05	21.40
S --	86.3	13.4	0.2	50.10	6.36	43.52	0.07	< 0.05	20.45
S225	84.0	15.8	0.2	50.97	6.15	42.76	0.07	< 0.05	20.62
S275	75.7	24.2	0.2	55.33	5.73	38.81	0.09	< 0.05	22.05

[a] % (m/m), dry basis. [b] MJ/kg, dry basis

The proximate and ultimate analyses data for the feedstocks, which is included in the gasification modeling study (Paper V) and was obtained from Wannapeera et al.[52], is listed in Tables 3-3. Torrefied biomass was produced at 250 °C with 30 minutes of residence time.

Table 3-3: Proximate and ultimate analyses of the samples (Paper V)[52]

Sample	Proximate analysis[a]			Ultimate analysis[a]				HHV[b]
	VM	fC	Ash	C	H	O	N	
Leucaena	86.1	13.1	0.8	50.1	7.4	41.8	0.7	20.3
Torrefied *Leucaena*	82.2	16.9	0.9	53.0	6.4	39.9	0.7	21.2

[a] % (m/m), dry basis. [b] MJ/kg, dry basis

3.2 Experimental set-up and procedures

3.2.1 Micro-TGA

The TGA experiments for the kinetic studies (Papers III and IV) were performed with a Q5000 IR analyzer from TA Instruments, which has a sensitivity of 0.1 µg. With its high precision and well-controlled experimental conditions, the TGA is a useful tool for studying devolatilization and combustion during the kinetic regime[21]. However, TGA can be employed only at relatively low heating rates because the true temperature of the samples is unknown at high heating rates.

For the experiments performed in an inert environment (Paper III), high purity nitrogen was used as the purge gas with a gas flow of 100 mL/min. The initial sample mass was between 3 and 10 mg. The samples from both woods were analyzed with nine different heating programs, as shown in Figure 3-1. The linear T(t) experiments had heating rates of 40, 20, 10 and 5 °C/min. The isothermal experiment with a 30 min residence time at 275 °C mimicked the T(t) of the actual torrefaction experiments used in Paper II. In the modulated experiments, sinus waves with 5 °C amplitudes and a 200 s wavelength were superposed on a slow, 2 °C/min linear T(t). The waves served to increase the rather limited information content of the linear T(t) experiments. In the "constant reaction rate" (CRR) experiments, the equipment regulated the sample heating so that the reaction rate would oscillate around a preset limit[140]. The CRR experiments were aimed at obtaining very low mass loss rates within the whole domain of the reaction. The highest mass loss rate in these experiments was found to be 0.8 µg/s. This value corresponds to 0.8×10^{-4} s^{-1} after normalization by the initial dry sample mass. The T(t) program for a CRR experiment clearly depends on the behavior of the given sample. Two stepwise temperature programs were employed, which also served to increase the amount of experimental information for the kinetic evaluation[86, 97, 100, 141, 142].

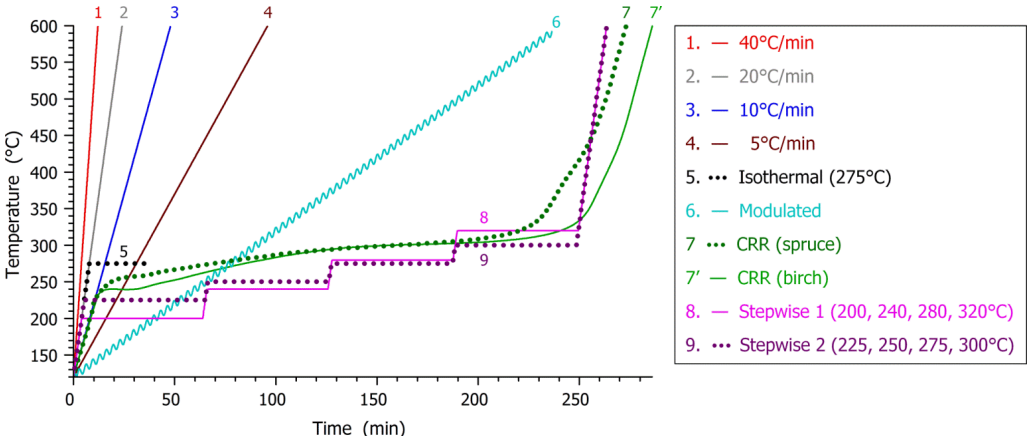

Figure 3-1: The temperature programs used in the TGA experiments for Paper III. Note that the T(t) needed for a nearly constant heating rate in the CRR experiments was determined by the instrument and differed for the two samples.

For the reactivity study under an oxidative environment (Paper IV), 5 % v/v and 20 % v/v oxygen-nitrogen mixtures were used as purge gases with a gas flow of 100 mL/min. Sample masses of 0.5 mg or less were used to avoid self-heating the samples from the high reaction heat. Each sample was analyzed with three different heating programs, as shown in Figure 3-2; (i) 10°C/min linear T(t); (ii) modulated T(t); and (iii) "constant reaction rate" (CRR) T(t). The DTG peak maxima of the CRR experiments varied between 0.04 and 0.07 µg/s. The T(t) program for a CRR experiment obviously depends on the behavior of the given sample.

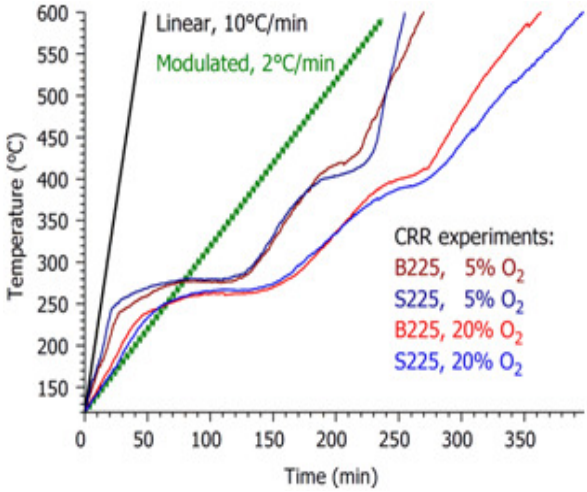

Figure 3-2: The temperature programs used in the TGA experiments for Paper IV. Note that each of the twelve constant heating rate experiments has a different T(t); this figure shows four of them.

3.2.2 Macro-TGA

The biomass torrefaction experiments for Paper II were conducted in the macro-TGA shown in Figure 3-3.

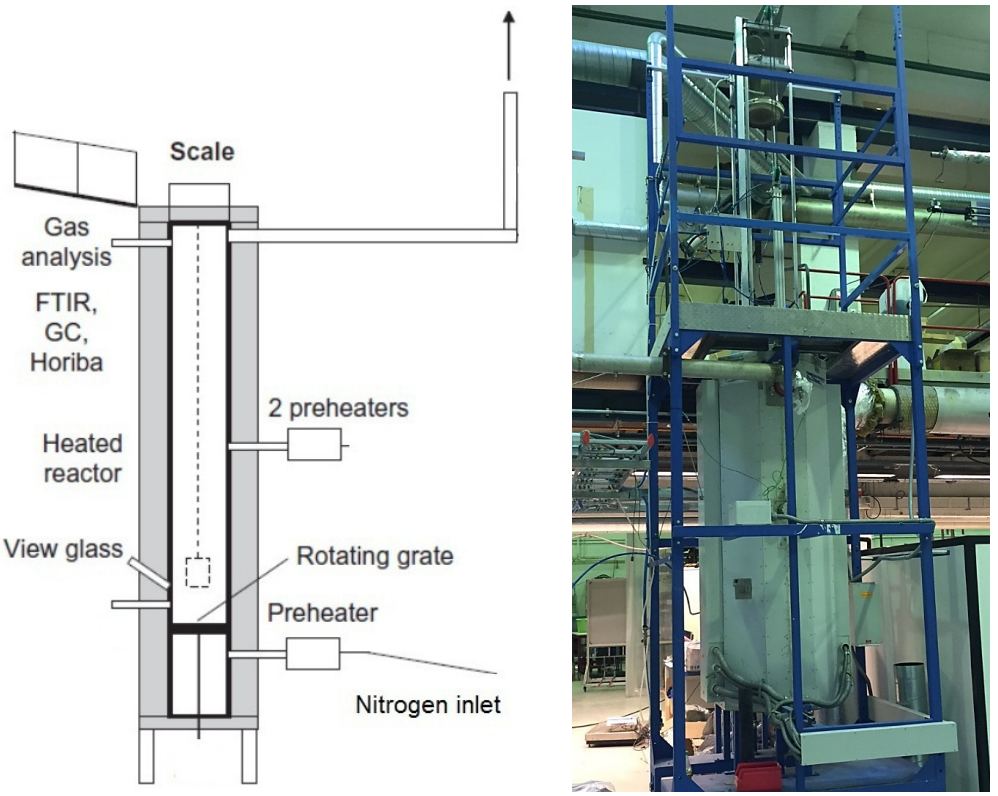

Figure 3-3: The macro-TGA reactor used for torrefaction

This reactor was built by Höker KFT (Hungary) according to design specifications from SINTEF Energy Research. The biomass fuel samples were placed in a rectangular basket that was connected to the balance, and the sample basket was lowered into the reactor prior to heating. The sample basket was composed of several separated layers, and care was taken to provide a small gap between the cubes on each layer to provide uniform heat and mass transfer conditions for all of the cubes. The balance was connected to the reactor top and cooled with nitrogen gas to prevent overheating. The sample weight was 200–300 g, depending on the density and size of the feedstock. A constant flow rate of 100 l/min of nitrogen was used to provide an inert atmosphere inside the reactor. The samples were heated to either 225 or 275 °C at a heating rate of 5 °C/min. The torrefaction start time was measured from the point when the temperature first reached the target torrefaction temperature. The reactor was purged with nitrogen for at least 1 h prior to the start of the

experiment. Before starting the torrefaction experiments, an online oxygen analyzer was used to ensure that the reactor was free of oxygen.

The macro-TGA experiments were focused on studying important parameters such as the fuel type (soft- and hardwood), holdup time in the torrefaction zone (30 and 60 minutes), sample size (10 and 40 mm cubes) and torrefaction temperature (225 and 275 °C). The complete experimental matrix produced 16 different types of torrefied materials. All the reaction products were collected and weighed to determine an overall mass balance. The gas produced in the experiments was measured by FTIR (Fourier transform infrared spectroscopy) and micro-GC (gas chromatography). The outlet tube from the reactor was maintained at an elevated temperature of approximately 200 °C to prevent the condensation of the released volatiles.

Grindability, particle size distribution and hydrophobicity assessments were performed for the torrefied biomass that was obtained from the experiments. The grindability assessment was divided into two stages, namely pre-grinding and fine-grinding. In the pre-grinding stage, the raw and torrefied samples were ground in a cutting mill without a bottom sieve. This stage produced smaller particles that facilitated the feeding step of the fine-grinding stage. The fine-grinding stage was performed by using the same cutting mill equipped with a 1 mm bottom sieve. A numerical wattmeter, a Paladin 256-TWKW from Cromptan Instruments, was employed to record the amount of electricity consumed during grinding at both stages. A computer with a data logger was connected to the wattmeter for data acquisition every 2 seconds. The mill was operated by using the same parameters for all samples. The power consumption for an empty load was logged prior to every grinding step to determine the increase in energy consumption when the mill was under load. The specific energy consumption for grinding was determined by integrating the area under the power consumption curve (watts-seconds) over the total time required to grind a given sample. Given that a known quantity of samples was used in each experiment, the energy consumption is divided by the mass of the ground samples to obtain the final values per unit mass for comparison. The integrated values from both grinding stages were added together to calculate the total grinding requirement for a sample.

The powdered samples produced after the milling step were sieved in a vibrating sieving machine (Fritsch Analysette 3 Pro) that contained a series of sieves with the following mesh sizes: 1 mm, 500 µm, 180 µm, 125 µm and 63 µm. The mass of each sample collected on the different sieves was measured and recorded as a percentage of the initial sample mass to evaluate the particle size distribution as a function of the studied torrefaction parameters.

The hydrophobic characteristics of all raw and torrefied samples were investigated by immersing the samples in distilled water for 2 hours in glass beakers without stirring[56]. The water was drained from the beakers, and the moisture content of the samples was measured as a change in the corresponding initial sample weight.

3.3 Kinetic modeling approach

3.3.1 Method of least squares and the characterization of the fit quality

Because of the complex composition of biomass materials, the conventional linearization techniques for the non-isothermal kinetics are not suitable for evaluating the TGA experiments. Therefore, the TGA experiments on biomass materials are usually evaluated by the non-linear method of least squares, assuming more than one reaction[21, 143, 144]. Fortran 95 and C++ programs were used for numerical calculations and for graphics handling, respectively[141].

The kinetic evaluation was based on the least squares evaluation of the $-dm^{obs}/dt$ curves, where m^{obs} is the sample mass normalized by the initial dry sample mass. The method used for the $-dm^{obs}/dt$ determination does not introduce considerable systematic errors into the least squares kinetic evaluation of the experimental results[98]. The model was solved numerically along the empirical temperature-time functions. The minimization of the least squares sum was performed by direct search method[141]. These values were searched for the unknown model parameters that minimized the objective function (*of*). We looked for:

$$min\ of = \sum_{k=1}^{N_{exper}} \sum_{i=1}^{N_k} \frac{\left[\left(\frac{dm}{dt}\right)_k^{obs}(t_i) - \left(\frac{dm}{dt}\right)_k^{calc}(t_i)\right]^2}{N_k h_k^2} \quad (3\text{-}1)$$

where the minimization was done by all unknown model variables. Here, N_{exper} is the number of experiments evaluated together; its value is 18 in Paper III and 6 or 36 in Paper IV. N_k denotes the number of t_i time points on a given curve, and m is the sample mass normalized by the initial sample dry mass. Dividing by h_k^2 counterbalances the differences of the highest magnitudes. Traditionally, h_k is the highest observed value of the given experiment:

$$h_k = \max\left(\frac{dm}{dt}\right)_k^{obs} \quad (3\text{-}2)$$

The normalization by the highest observed values in the least squares sum implicitly assumes that the relative precision is roughly the same for the different experiments.

The resulting fit quality was characterized separately for each of the experiments that were evaluated together. The relative deviation (*reldev*, %) was used for this purpose. The

root mean square (rms) difference between the observed and calculated values is expressed as the percent of the peak maximum. For experiment *k*, we find the following:

$$reldev\ (\%) = 100\ \left(\sum_{i=1}^{N_k} \frac{\left[\left(\frac{dm}{dt}\right)_k^{obs}(t_i) - \left(\frac{dm}{dt}\right)_k^{calc}(t_i) \right]^2}{N_k h_k^2} \right)^{0.5} \quad (3\text{-}3)$$

The fit quality for a given group of experiments is characterized by the root mean square of the corresponding relative deviations. The relative deviation of the 18 experiments that were evaluated together can be expressed by equations 3-1–3-3 as

$$reldev_{18}\ (\%) = 100\sqrt{of} \quad (3\text{-}4)$$

Clearly, a smaller $reldev_{18}$ value indicates a better fit.

Note on h_k value for Paper IV: The peak maxima of the CRR experiments were scattered around a very low value of 1×10^{-4} s^{-1}, and the peak maxima of the 10 °C/min experiments were approximately 30 times higher. Test calculations showed that it is not possible to assume approximately equal relative precision at high magnitude differences. No information was available on the absolute and relative precision of the -dm/dt values in the CRR experiments; hence, an arbitrary $h_k=5\times10^{-4}$ s^{-1} value was used for the CRR experiments, which is ca. 5 times higher than the peak maximum.

3.3.2 Kinetic models for the inert decomposition of biomass

Three pseudocomponents were assumed, and they signified three simultaneous parallel reactions during the decomposition process. Here, a pseudocomponent is the totality of the decomposing species that can be described by the same reaction kinetic parameters in the given model. A pseudocomponent may involve a large number of different reacting species. The first primarily describes the decomposition of the hemicellulose, the second corresponds to the cellulose decomposition, and the third would be responsible for the long, flat lignin tail that can be observed for nearly all biomasses.

The distributed activation energy model (DAEM)

According to this model, the sample is regarded as a sum of *M* pseudocomponents, where *M* is usually between 2 and 4. The reactivity differences between the species in a pseudocomponent are described by different activation energy values. On a molecular level, each species in pseudocomponent *j* is assumed to undergo first-order decay. The corresponding rate constant (*k*) is thought to depend on the temperature according to an Arrhenius expression. Given $\alpha_j(t,E)$ as the solution of the corresponding first order kinetic equation at a given *E* and *T(t)* with conditions $\alpha_j(0,E)=0$ and $\alpha_j(\infty,E)=1$,

$$d\alpha_j(t,E)/dt = A_j e^{-E/RT} [1-\alpha_j(t,E)] \quad (3\text{-}5)$$

The distribution of the species differing in E within a given pseudocomponent is approximated by a Gaussian function with a mean value $E_{0,j}$ and a width-parameter (variation) σ_j.

$$D_j(E) = (2\pi)^{-1/2} \sigma_j^{-1} \exp[-(E - E_{0,j})^2 / 2\sigma_j^2] \quad (3\text{-}6)$$

From a computational point of view, the approximate solution of a DAEM can simply be calculated from a discrete set of $\alpha_j(t,E)$ functions[145]. The normalized sample mass and its derivative are the linear combinations of $\alpha_j(t)$ and $d\alpha_j/dt$, as follows:

$$-dm/dt = \sum_{j=1}^{M} c_j d\alpha_j/dt \quad \text{and} \quad m(t) = 1 - \sum_{j=1}^{M} c_j \alpha_j(t) \quad (3\text{-}7)$$

where weight factor c_j is equal to the amount of volatiles formed from a unit mass of pseudocomponent j.

N-order reactions

The complex decomposition of the biomass pseudocomponents can be approximated formally by n-order (power-law) kinetics, as well. Manyà et al. demonstrated that third order kinetics provide a better description for the lignin pseudocomponent of the biomass than the simpler first order kinetics[146]. The decomposition of the pseudocomponents can be approximated by n-order reactions as follows:

$$\frac{d\alpha_j}{dt} = A_j \exp\left(-\frac{E_j}{RT}\right) (1-\alpha_j)^{n_j} \quad (j=1, 2, 3) \quad (3\text{-}8)$$

Self-accelerating cellulose decomposition

The self-accelerating reactions can typically be described by an equation of type

$$\frac{d\alpha_2}{dt} = A_2 \exp\left(-\frac{E_2}{RT}\right) f(\alpha_2) \quad (3\text{-}9)$$

where f is a function capable of expressing self-acceleration. The mathematical unambiguity requires a normalization for $f(\alpha_2)$ because f functions differing only in their constant multipliers are equivalent in equation 3-9 (parameter A_2 can compensate any multipliers of f). For a normalization, we require that the maximum of f be 1. $f(\alpha_2)$ is approximated formally by

$$f(\alpha_2) \cong normfactor\ (1-\alpha_2)^{n_2} (\alpha_2 + z_2) \quad (3\text{-}10)$$

where n_2 and z_2 are model parameters, and *normfactor* ensures that max f=1. Parameters n_2 and z_2 do not have separate physical meanings; together, they determine the shape of f, and, in this way, they determine the self-accelerating capabilities of the model.

3.3.3 Kinetic model for the oxidative decomposition of biomass

Four primary reactions that partly overlap with one another are assumed during the oxidative decomposition of raw or torrefied biomass[103] as follows:

(i) the decomposition of the hemicellulose and other thermally labile parts of the sample that dominate the DTG curves between approximately 200 and 300 °C;

(ii) the oxidative decomposition of the cellulose component, which produces a sharper peak with a maximum at approximately 335 °C;

(iii) a flat section; given the high temperature end of the lignin decomposition, the slow carbonization and other reactions of the formed char, these reactions dominate the DTG curves between approximately 360 and 430 °C; and

(iv) the char burn-off, which results in a peak approximately 460 °C.

All of the masses in the treatment are normalized by the initial sample mass. The normalized amounts of the unreacted part of the sample, char and ash are denoted by m_{ur}, m_{char} and m_{ash}, respectively. As the reactions proceed, m_{ur} decreases from 1 to 0 because no unreacted biomass remains at the end. m_{char} is zero at the beginning of an experiment. It reaches a maximum as the char forms and converges to zero again as the char burns off. m^{calc} is the sum of the normalized masses of the solid components as follows:

$$m^{calc}(t) = m_{ur}(t) + m_{char}(t) + m_{ash}(t) \tag{3-11a}$$

$$\frac{dm^{calc}}{dt} = \frac{dm_{ur}}{dt} + \frac{dm_{char}}{dt} + \frac{dm_{ash}}{dt} \tag{3-11b}$$

The unreacted part of the sample, or m_{ur}, is regarded as the sum of the cellulose component and the rest of the sample. The pyrolysis kinetics models are usually written for variables that run from 0 to 1; accordingly, a reacted fraction for cellulose, or $\alpha_{cell}(t)$, and another reacted fraction, or $\alpha_{other}(t)$, is used for the other biomass components. The corresponding boundary conditions are $\alpha_{cell}(0)=0$, $\alpha_{cell}(\infty)=1$, $\alpha_{other}(0)=0$ and $\alpha_{other}(\infty)=1$. $m_{ur}(t)$ is the weighted sum of its two constituents with weight factors c_{cell} and c_{other} as follows:

$$m_{ur}(t) = c_{cell}\,[1-\alpha_{cell}(t)] + c_{other}\,[1-\alpha_{other}(t)] \tag{3-12a}$$

$$-\frac{dm_{ur}}{dt} = c_{cell}\frac{d\alpha_{cell}}{dt} + c_{other}\frac{d\alpha_{other}}{dt} \tag{3-12b}$$

At t=0, eq. 3-12a reduces to

$$1 = c_{cell} + c_{other} \tag{3-12c}$$

Sub model for reactions (i) and (iii)

The oxidative decomposition of the non-cellulosic part of the sample is described by a distributed activation energy model[97, 98, 103]. This pseudocomponent includes the decomposition of the extractives, hemicelluloses, and lignin. There is a high number of different reactive species here. The differences in their reactivity are described by different activation energies. First order reactions are assumed for the parts of the sample that decompose with the various E values as follows:

$$\frac{d\alpha_{other}(t,E)}{dt} = A_{other} C_{O_2}^{\nu_{other}} \, e^{-E/RT} [1-\alpha_{other}(t,E)] \tag{3-13}$$

The oxygen effect is described by a power function, or $C_{O_2}^{\nu_{other}}$, in which C_{O_2} is the dimensionless v/v concentration of the oxygen and ν_{other} is a reaction order parameter. Note that a dimensionless C_{O_2} concentration is needed in the kinetic equations. Otherwise, the dimension of the pre-exponential factor should depend on the ν_{other}.

The activation energies in this pseudocomponent are assumed to have a distribution function. The usual Gaussian distribution function is employed, by using an E_0 mean and σ width, as follows:

$$D(E) = (2\pi)^{-1/2} \sigma^{-1} \exp[-(E-E_0)^2 / 2\sigma^2] \tag{3-14}$$

The overall reacted fraction of this pseudo-component, or α_{other}, is obtained by integration as follows:

$$\alpha_{other}(t) = \int_0^\infty D(E) \alpha_{other}(t,E) dE \tag{3-15}$$

Sub model for reaction (ii)

In the presence of oxygen, the cellulose decomposition was assumed to be a self-accelerating reaction[103] as described by an equation of type

$$\frac{d\alpha_{cell}}{dt} = A_{cell} C_{O_2}^{\nu_{cell}} \exp\left(-\frac{E_{cell}}{RT}\right) f(\alpha_{cell}) \tag{3-16}$$

where f is a function that is capable of expressing self-acceleration. Mathematical unambiguity requires a normalization for $f(\alpha_{cell})$ because f functions differing only in their constant multipliers are equivalent in equation 3-16 (parameter A_{cell} can compensate any multipliers of f). For a normalization, we require that the maximum of f be 1. $f(\alpha_{cell})$ is approximated formally by

$$f(\alpha_{cell}) \cong normfactor\ (1-\alpha_{cell})^{n_{cell}}\ (\alpha_{cell}+z) \quad (3\text{-}17)$$

where n_{cell} and z are model parameters and *normfactor* ensures that max f=1. Parameters n_{cell} and z do not have separate physical meanings; together, they determine the shape of f, and, in this way, they determine the self-accelerating capabilities of the model. A differentiation of equation 3-17 by α_{cell} indicates that $f(\alpha_{cell})$ reaches its maximum at

$$\alpha_{cell} = (1-n_{cell}\,z)/(n_{cell}+1) \quad (3\text{-}18)$$

When equation 3-18 gives a negative value, $f(\alpha_{cell})$ is monotonously decreasing in the [0,1] interval. In the present work, the maximum for $f(\alpha_{cell})$ was approximately 0.4–0.5. The *normfactor* in equation 3-17 is the maximum of $(1-\alpha_{cell})^{n_{cell}}\ (\alpha_{cell}+z)$ in the [0,1] interval; hence, its value can be immediately calculated by substituting the α_{cell} value from equation 3-18.

Sub model for reaction (iv)

The char burn-off was described by power-law kinetics in which the reaction rate is n_{char} order with respect to m_{char} and ν_{char} order with respect to the oxygen concentration, or C_{O_2}. Accordingly, the char burn-off rate is approximated as

$$char\ burn\text{-}off\ rate = A_{char} C_{O_2}^{\nu_{char}} \exp\left(-\frac{E_{char}}{RT}\right) m_{char}^{n_{char}} \quad (3\text{-}19)$$

Both the cellulose and the non-cellulosic parts of the biomass form char. The corresponding char yields are denoted by $y_{cell.char}$ and y_{other_char}, respectively, which are dimensionless quantities. The char is formed from the biomass decomposition and consumed by the burn-off, hence

$$\frac{dm_{char}}{dt} = c_{cell}\frac{d\alpha_{cell}}{dt} y_{cell.char} + c_{other}\frac{d\alpha_{other}}{dt} y_{other\_char} - A_{char} C_{O_2}^{\nu_{char}} \exp\left(-\frac{E_{char}}{RT}\right) m_{char}^{n_{char}} \quad (3\text{-}20)$$

The ash is formed by the char burn-off reaction with a yield of y_{ash} as follows:

$$\frac{dm_{ash}}{dt} = A_{char} C_{O_2}^{\nu_{char}} \exp\left(-\frac{E_{char}}{RT}\right) m_{char}^{n_{char}}\ y_{ash} \quad (3\text{-}21)$$

Parameter y_{ash} expresses the ash yield of the char burn-off. In the present work, y_{ash} is determined from the total ash obtained by proximate analysis. This finding is used as a dimensionless ratio, or m_{ash}^{anal}, which is equal to a hundredth of the corresponding percent value in Table 3-2. The overall ash yield of the model is forced to be equal to m_{ash}^{anal} by equation

$$(c_{cell}\, y_{cell.char} + c_{other}\, y_{other\_char})\, y_{ash} = m_{ash}^{anal} \quad (3\text{-}22)$$

In this way, y_{ash} can be eliminated from the model because it can be expressed as a function of m_{ash}^{anal}, y_{other_char} and c_{cell} by equations 3-22 and 3-12c.

The model outlined above has 16 unknown parameters for each sample, as follows:

A_{cell}, ν_{cell}, E_{cell}, z, n_{cell}, $y_{cell.char}$, and c_{cell} (cellulose decomposition); A_{other}, ν_{other}, E_0, σ, and y_{other_char} (the decomposition of the non-cellulosic parts of the sample; here, c_{other}=1-c_{cell} from equation 3-12c); and A_{char}, ν_{char}, E_{char}, and n_{char} (char burn-off).

These unknown model parameters were determined by the least squares evaluation of the six experiments of a given sample. Eight evaluations were performed based on the number of assumed common parameters for the samples.

3.4 Simulation of biomass gasification

The Gibbs free energy minimization method for the C–H–O–N atom blend of the biomass fuel and oxidant mixture can be applied to predict the thermodynamic equilibrium composition of the major product gas components that include H_2, CO, CH_4, CO_2, H_2O, and N_2, in addition to char[147-150]. A thermodynamic equilibrium model for a biomass gasification system was developed by using the Gibbs minimizing approach in Aspen Plus software as shown in Figure 3-4. Mass and energy balance data were collected from Aspen Plus, and these data were used to calculate the cold gas energy and exergy efficiencies of the process.

3.4.1 Aspen Plus model

In Aspen Plus, streams represent mass or energy flows. Mass streams are divided by Aspen Plus into three categories, that is, mixed, solid, and non-conventional (biomass). Mixed streams contain mixtures of components, which can be in gaseous, liquid and solid phases. The solid phase component in this simulation is solid carbon (C). Thermodynamic properties are defined in the Aspen Plus libraries for chemical components. Non-conventional components (e.g., biomass) are defined in Aspen Plus by supplying the standard enthalpy of formation and the elementary composition (ultimate and proximate analyses) of the components[151].

Sub-systems

The following sub-systems were included in the modeled gasification process:

a) The Aspen Plus heat exchanger, or HEATER, was used to simulate biomass pre-heating to a pyrolyzer temperature of 500 °C

b) The Aspen Plus yield reactor, or RYIELD, was used to simulate the decomposition of biomass into individual elemental components at 500 °C. Actual experimental yield values for volatiles and char, as available in literature[52], were included as inputs to this reactor

c) The Aspen Plus Gibbs reactor, or RGIBBS, was used for the partial combustion of volatiles and char with the addition of air and steam. RGIBBS models chemical equilibrium by minimizing the Gibbs free energy, which is subject to elemental balance constraints. To closely simulate real conditions in a gasifier, an isothermal approach was used in this study

d) The Aspen Plus heat exchanger, or HEATER, was used to simulate syngas cooling from the RGIBBS temperature to the ambient temperature

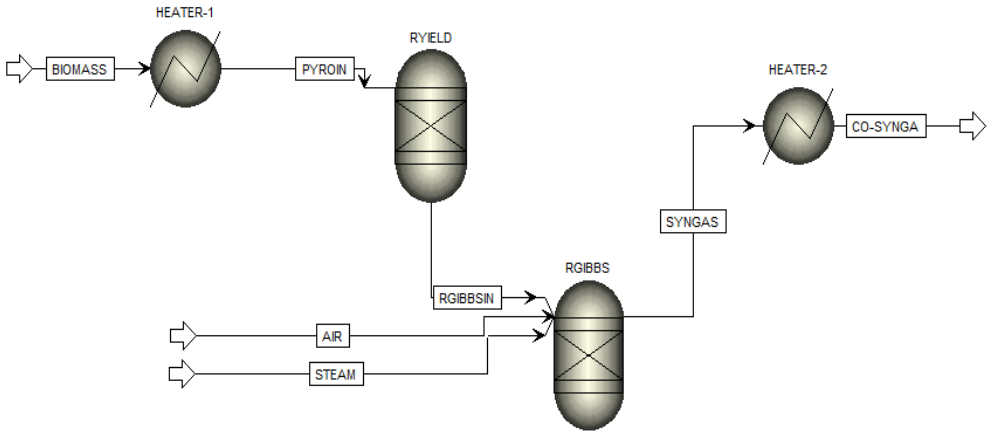

Figure 3-4: The gasification process as modeled in Aspen Plus in this study

Key process variables

The optimal gasification operation reportedly involves operating a gasifier at or below the carbon boundary point, which indicates that all carbon is present in the gaseous phase as carbon monoxide, carbon dioxide or methane[137]. This theory has been applied to this study as well, and all 27 tested cases contain carbon in its gaseous form. This perspective is the basis for selecting the ranges for the three process variables listed in Table 3-4. The ER is defined as the amount of air added relative to the stoichiometric air requirement for combustion, and the SBR is defined as the ratio of steam to biomass molar flow rates. Steam is added to the system to improve the hydrogen production and thus increase the syngas quality[149]. Each of

the 27 cases will be referred to by using these three process variables, that is, SBR-GB-ER, in this study.

Table 3-4: The tested ranges for process variables that resulted in 27 cases

Process variable	Low	Mid	High
SBR	0.2	0.3	0.4
Gibbs (GB) Temperature (°C)	900	1000	1100
ER	0.1	0.2	0.3

Assumptions for the Aspen Plus model

a) All gases behave ideally, the process occurs at steady state, and the residence time was not considered. In addition, all of the biomass feedstocks were completely dry
b) The biomass mass flow rate was calculated for a 10 MW fuel input plant, and atmospheric pressure was assumed for all equipment
c) Air was introduced to RGIBBS at ambient temperature and pressure, and saturated steam was introduced to RGIBBS at 179.9 °C and 10 bar pressure
d) The process was assumed to be autothermal, and the pressure drop and heat losses from the equipment and pipelines were not included
e) Ambient condition data for each stream was collected from Aspen Plus to obtain consistent values for the reference conditions in the physical exergy calculations
f) No physical exergy is associated with the biomass because they were assumed to be at ambient temperature and pressure, and kinetic and potential exergies were ignored in the analysis
g) Minor products such as the sulfur species (e.g., S, COS and H_2S) and nitrogen species (except N_2) were not included in the chemical exergy of the streams because they are present, relatively speaking, in very negligible amounts. Additionally, no work exergy was included in the analysis
h) Tar was considered to be a mixture of 70 % secondary (phenol), 14 % tertiary-alkyl (xylene) and 16 % tertiary-PNA (benzene) components on a mass basis[152, 153]. It was assumed that the tertiary-PNA component is not cracked at all, and the tertiary-alkyl component is 80 % cracked under the temperature conditions used in this study[153]. In addition, untreated biomass is assumed to contain 10 % aqueous phase acid (acetic acid), which remains un-reacted in RGIBBS[154]. For the torrefied biomass, these acids were assumed to be removed during torrefaction. The char composition of the pyrolyzed biomass (from both untreated and torrefied biomass) was calculated from the elemental C, H and O balance based on the assumed tar composition

3.4.2 Methods for cold gas energy and exergy efficiencies

The cold gas efficiency of gasification in an allothermal plant is defined as follows[147]:

$$\eta_{energy,coldgas} = \frac{LHV_{coldgas}}{LHV_{biomass} + Q_{air} + Q_{steam}} \tag{3-23}$$

where $LHV_{coldgas}$ is the heating value of the outgoing (product) heat stream; and $LHV_{biomass}$, Q_{steam} and Q_{air} are the heating value and heat contents of incoming biomass, steam and air streams, respectively. Exergy is the maximum work that can be produced when a heat or material stream is brought to equilibrium relative to a reference environment, which consists of reference components and is characterized by an absence of pressure and temperature gradients. The exergy associated with a material stream is expressed as the sum of its physical and chemical exergies. The total exergy of a material stream is given by the following[147, 155]:

$$E' = N(\varepsilon_{ph} + \varepsilon_{ch}) \tag{3-24}$$

where N is the flow rate. The molar physical exergy of a material stream is expressed in relation to the reference environmental conditions as follows[147, 155]:

$$\varepsilon_{ph} = (h - h_0) - T_0(s - s_0) \tag{3-25}$$

The mole flows, mole fractions, enthalpy and entropy of each material stream were taken from the Aspen Plus flowsheet results. The standard environmental conditions in Aspen Plus (T_0 = 298.15 K, p_0 = 1.013 bar) were adopted as reference conditions in this study. The molar chemical exergy of a gaseous material mixture is given by the following[147, 155]:

$$\varepsilon_{ch,gas} = \sum_i x_i \varepsilon_{0,i} + RT_0 \sum_i x_i \ln x_i \tag{3-26}$$

where x_i is the mole fraction and $\varepsilon_{0,i}$ is the standard molar chemical exergy of each component i, in $Jmol^{-1}$. The latter is available in the literature for the reference atmospheric composition[156].

The chemical exergy of solid fuels (raw biomass and torrefied biomass) was calculated by using the ratio of the chemical exergy to the lower heating value of the dry matter as shown in equation 3-27[157]. This ratio is a function of the elemental composition of the solid fuel.

$$\varphi_{dry} = \frac{\varepsilon_{dm}}{h_{LHV(dm)}} \tag{3-27}$$

For dry solid fuels with a certain oxygen content, the ratio of chemical exergy to the lower heating value for the dry matter is expressed as follows[157]:

$$\varphi_{dry} = \frac{1.0438 + 0.1882\frac{h}{c} - 0.2509\frac{o}{c}\left(1 + 0.7256\frac{h}{c}\right) + 0.0383\frac{n}{c}}{1 - 0.3035\frac{o}{c}} \tag{3-28}$$

Here, h/c is the ratio of hydrogen mass to carbon mass in the fuel, and n/c and o/c correspond to nitrogen and oxygen. This expression is valid for o/c from 0.667 to 2.67, and it is expected to be accurate within +- 1 %. By using Eqs. (3-24)–(3-28), the exergy was calculated for all material streams in the flow sheet. The exergetic efficiency of gasification in an autothermal plant is defined as follows[147]:

$$\eta_{exergy,coldgas} = \frac{E_{coldgas}}{E_{biomass} + E_{air} + E_{steam}} \tag{3-29}$$

where E_{coldgas} is the outgoing (product) exergy stream, and E_{biomass}, E_{steam} and E_{air} are the incoming biomass, steam and air exergies.

4 Summary and Conclusions of Papers

Starting with a detailed literature review on the torrefaction process, the torrefaction of Norwegian birch and spruce was studied in a macro-TGA set-up. This review was followed by detailed kinetic evaluations of the torrefaction of these two feedstocks and the behavior of torrefied biomass under oxidative conditions by using weight loss data obtained from micro-TGA experiments. Lastly, a two-stage gasification process was simulated in Aspen Plus to compare the syngas compositions, cold gas energy and exergy efficiencies from raw and torrefied biomass materials. A summary of all of these studies together with the primary conclusions are included in this chapter.

4.1 Paper I: Biomass torrefaction – a review

Several studies on biomass torrefaction have been documented for heat and power applications. Substantial amounts of data on the technique are available, which had to be reviewed and analyzed for further actions in the area. This analysis was the primary objective of this review paper. First, the review provided an introduction to the biomass torrefaction process. This introduction was followed by a critical analysis of the experimental methods used in the laboratory to perform torrefaction under various process conditions. Later, the tested biomass materials were discussed in terms of the product yields and the evaluated product properties. An overview of the kinetic modeling studies on the topic was also included. A review of the literature suggested that torrefaction is a promising technique to improve the performance of biomass for energy utilization. During torrefaction, the primary thermal decomposition reactions involve the hemicellulose polymers, resulting in improved fuel properties as exhibited by the torrefied samples. Considerable differences were found in the behavior of biomass materials during torrefaction. Mass and energy yields for torrefied biomass are strongly influenced by the raw biomass composition and the operating conditions such as the temperature and residence time. Torrefaction improves the properties of the biomass fuels; it reduces the moisture content, increases the energy density and the heating value per unit mass, changes the hygroscopic behavior of the raw biomass into a hydrophobic behavior, and enhances grindability. However, despite a number of impressive studies on the topic, many aspects were not investigated, especially the torrefaction behavior of Norwegian biomass and the behavior of torrefied biomass in the thermo-chemical processes. This gap formed the basis for the studies conducted in this thesis, Papers II-V.

4.2 Paper II: Torrefaction of Norwegian birch and spruce, an experimental study using macro-TGA

The unique approach of a macro-TGA (thermogravimetric analysis) was used to evaluate the torrefaction behavior of Norwegian birch and spruce. Data obtained from the macro-TGA is an excellent indicator of the relations between the weight loss, process temperature and holdup time for an industrial-scale torrefaction process. Birch and spruce were selected as feedstock because they are typical Norwegian wood species, and because they present an opportunity to compare hardwood (birch) and softwood (spruce) behavior during torrefaction and the qualities of their torrefied versions. Torrefaction experiments were performed in a macro-TGA reactor with provisions for continuous measurements of the biomass weight loss rate and volatiles composition through micro-GC (gas chromatography) and FTIR (Fourier transform infrared spectroscopy). The process temperature (225 and 275 °C), holdup time (30 and 60 minutes) and sample size (10 and 40 mm cubes) were included as variations in the experimental matrix. Fuel characterizations, DTG (derivative thermogravimetric) curves, product yields, hydrophobicity tests, grinding energies and particle size distributions were included as part of study assessment methods. The raw fuels were used as a reference for the comparisons. The raw and torrefied samples were characterized by using proximate and ultimate analyses. The primary conclusions of this work were as follows:

(1) Compared with the raw samples, the composition of the torrefied samples was closer to that of coal, with a higher carbon content and a lower volatile matter content

(2) The birch was found to be more reactive than the spruce, which resulted in a larger percentage increase in its carbon content. The birch exhibited a higher devolatilization rate and a lower solid yield than the spruce at all the tested conditions. These differences may be attributed to the composition of the hemicellulose fractions in these wood types, and it has been reported that the amount of the most reactive hemicellulose component (xylan) is present in lower quantities in softwoods than in hardwoods[45]

(3) Of all of the process parameters, the torrefaction temperature had the strongest effect on the biomass composition, devolatilization rate and solid yield. At 275 °C, the solid yields decreased to 63 % and 75 % for the torrefied birch and spruce, respectively. The proximate and ultimate analyses of the feedstocks showed that the increases in the torrefaction temperature and holdup time result in a higher carbon content, lower hydrogen content and lower oxygen content in the samples. The sample cube size also

affected the solid yield. Higher solid yields were obtained for the larger cubes. However, the differences were not very significant, and they were primarily associated with the size-related limitations in the heat and mass transfer during torrefaction

(4) The hydrophobicity of the torrefied samples was much higher than that of the raw samples. The torrefied samples absorbed approximately 1/3 of the moisture compared with the raw fuels. The percentage decrease in moisture absorbance was similar for both feedstocks. The larger particles were found to be more resistant to moisture absorbance. The amount of water uptake was lower for the 40 mm cubes than for the 10 mm cubes for both feedstocks. However, most of the benefits for this property were achieved after torrefaction at 225 °C with 30 minutes of holdup time, and the improvements were limited when further increasing the temperature or holdup time

(5) Overall, the specific energy consumption for grinding was significantly reduced by torrefaction for both feedstocks. The reduction was higher for the birch than for the spruce, which is likely because of the compositional differences between the birch and spruce. A 40-88 % decrease in the total grinding energy was observed for the torrefied samples of both feedstocks. Among all of the tested process parameters, an increase in the temperature had the largest effect on the grinding energy. The weakening of the biomass cell wall because of the decomposition of hemicellulose along with the depolymerization of cellulose and thermal softening of lignin is the probable reason for its improved grindability after torrefaction[41]

(6) To evaluate the actual effect of torrefaction on the grindability of these two feedstocks, both the grinding energy and particle size distribution should be taken into account. Torrefaction considerably increased the percentage of fine particles (<180 μm) in the particle size distribution after grinding. The torrefied birch samples exhibited up to a 120 % increase in fine particles compared with the raw fuel. For the spruce, an increase of 85 % was obtained. However, it was very interesting to note that these differences in the particle size distributions of the two feedstocks diminished when the torrefaction temperature was increased to 275 °C. A uniform and similar particle size distribution was obtained for the samples from both feedstocks treated at 275 °C

4.3 Paper III: Thermal decomposition kinetics of woods with an emphasis on torrefaction

The pyrolysis kinetics of Norwegian spruce and birch wood was studied to obtain information on the kinetics of torrefaction. Thermogravimetry (TGA) was employed with nine different heating programs, including linear, stepwise, modulated and constant reaction rate (CRR) experiments. The 18 experiments on the two feedstocks were evaluated simultaneously by the method of least squares. Three pseudocomponents were assumed, and several model variants were tested. The best performance was achieved when the cellulose decomposition was described by a submodel that can mimic self-acceleration tendencies. The decomposition of the non-cellulosic parts of the biomass was described by two reactions when assuming a distributed activation energy model in this case. The employed model contains 13 unknown parameters for a given biomass. In another approach, all three pseudocomponents were described by *n*-order reactions. Both approaches resulted in nearly the same fit quality, but the physical meaning of the model based on three *n*-order reactions was found to be problematic. In addition, part of the kinetic parameters could be assumed to be common to both woods without a considerable worsening of the fit quality. The tested model variants and evaluations are listed in Table 4-1.

Table 4-1: Fit qualities[a] and the number of unknown parameters[b] for four model variants assuming various groups of common model parameters[c]

Evaluations	**Common parameters**	**Model variant**			
		I 2 DAEMs + 1st order cellulose	**II** 2 DAEMs + *n*-order cellulose	**III** 2 DAEMs + accelerating cellulose	**IV** 3 *n*-order reactions
1	none	4.78 (22)	2.31 (24)	2.06 (26)	2.19 (24)
2	E_3	4.78 (21)	2.35 (23)	2.10 (25)	2.21 (23)
3	E_3, σ_3 or n_3	4.78 (20)	2.37 (22)	2.14 (24)	2.21 (22)
4	E_3, σ_3 or n_3, E_2, n_2, z_2	4.80 (19)	2.46 (20)	2.25 (21)	2.32 (20)
5	all except the A & c parameters	4.83 (17)	2.61 (18)	2.37 (19)	2.33 (18)

[a] $reldev_{18}$ (%) values are listed (a smaller value indicates a better fit). [b] The total number of determined parameters are listed in parentheses. [c] Refer to the Nomenclature for the meanings of the symbols.

The results were checked by prediction tests. In these tests 10, 20 and 40 °C/min experiments were simulated by the model parameters obtained from the evaluation of 10 experiments with lower reaction rates. Table 4-2 was calculated with preferred model variant III and Evaluation 3, which may provide guidance about the extent of devolatilization at various temperature-residence time values during wood torrefaction.

Table 4-2: Simulated characteristics at various isothermal temperatures[a,b]

	0 min		10 min		30 min		60 min		120 min	
	Birch	Spruce	Birch	Spruce	Birch	Spruce	Birch	Spruce	Birch	Spruce
200°C										
1-$m(t)$	0.00	0.00	0.01	0.01	0.02	0.02	0.03	0.02	0.05	0.03
$c_2\alpha_2(t)$	0.00	0.00	0.00	0.00	0.00	0.00	0.00	0.00	0.00	0.00
$\alpha_2(t)$	0.00	0.00	0.00	0.00	0.00	0.00	0.00	0.00	0.00	0.00
225°C										
1-$m(t)$	0.01	0.01	0.03	0.03	0.07	0.04	0.10	0.06	0.14	0.09
$c_2\alpha_2(t)$	0.00	0.00	0.00	0.00	0.00	0.00	0.00	0.00	0.00	0.00
$\alpha_2(t)$	0.00	0.00	0.00	0.00	0.00	0.00	0.00	0.00	0.00	0.00
250°C										
1-$m(t)$	0.03	0.02	0.10	0.07	0.17	0.11	0.22	0.15	0.27	0.20
$c_2\alpha_2(t)$	0.00	0.00	0.00	0.00	0.00	0.00	0.01	0.01	0.01	0.01
$\alpha_2(t)$	0.00	0.00	0.00	0.00	0.01	0.01	0.01	0.02	0.03	0.03
275°C										
1-$m(t)$	0.08	0.06	0.22	0.16	0.30	0.24	0.35	0.30	0.42	0.38
$c_2\alpha_2(t)$	0	0.00	0.01	0.01	0.02	0.02	0.04	0.04	0.08	0.07
$\alpha_2(t)$	0	0.00	0.02	0.02	0.04	0.05	0.08	0.10	0.17	0.20
300°C										
1-$m(t)$	0.18	0.14	0.35	0.30	0.45	0.42	0.56	0.53	0.71	0.67
$c_2\alpha_2(t)$	0.00	0.00	0.04	0.03	0.10	0.09	0.20	0.17	0.34	0.28
$\alpha_2(t)$	0.01	0.01	0.08	0.10	0.23	0.26	0.44	0.49	0.76	0.83

[a] Isothermal torrefaction was assumed after 10°C/min heating until reaching the desired temperature. The time values in the header line belong to the isothermal section. [b]Three predicted torrefaction characteristics were tabulated at each temperature, that is, the normalized mass loss [1-$m(t)$], the normalized mass loss from cellulose decomposition [$c_2\alpha_2(t)$], and the reacted fraction of the cellulose [$\alpha_2(t)$].

4.4 Paper IV: Kinetic behavior of torrefied biomass in an oxidative environment

The combustion of four torrefied wood samples and their feedstocks (a deciduous and an evergreen species) was studied in slow heating programs, under well-defined conditions. Particularly low sample masses were employed to avoid the self-heating of the samples from the considerable reaction heat of the combustion. Six TGA experiments were performed for each sample with three different temperature programs in 5 and 20 % O_2, respectively. Highly different temperature programs were selected to increase the information content available for the modeling, namely linear, modulated and constant-reaction rate (CRR) temperature programs. The ratio of the highest and lowest peak maxima was approximately 50 in the set of experiments used for the evaluation. In this way, the obtained models described the experiments over a wide range of experimental conditions. A recent combustion model consisting of two devolatilization reactions and a successive char burn-off reaction was employed with a minor modification[103]. The cellulose decomposition in the presence of oxygen was described by a model that had two adjustable parameters to mimic self-acceleration tendencies. The decomposition of the non-cellulosic parts of the biomass was described by a distributed activation model. The char burn-off was approximated by power-law (n-order) kinetics. Each of these reactions had its own dependence on the oxygen concentration that was also expressed by power-law kinetics.

(1) The employed model contains 15 unknown parameters for a given biomass. The relatively wide range of experiments made the determination of so many parameters possible by the method of least squares. If all the parameters are assumed to depend on the sample type, then the 6 samples together have 6×15=90 unknown parameters. The total number of unknown parameters for the six samples is denoted by N_{param}. There were 36 TGA experiments for the determination of the N_{param} unknown parameters. The torrefaction has some impact on the parameters, especially on the ones describing the devolatilization of the hemicellulose and other thermally labile parts of a biomass sample. These parts more or less decompose during the torrefaction, as indicated by the corresponding c_{cell} and c_{other}=1- c_{cell} parameters. The cellulose reactivity was also affected at the highest torrefaction temperature of the study, which was 275 °C

(2) Part of the kinetic parameters could be assumed to be common to the six samples without a substantial worsening of the fit quality. This approach increased the

average experimental information for an unknown parameter and revealed the similarities in the behavior of the different samples. This finding helps to eliminate the usual ill-defined (compensation effect) problems of the non-isothermal kinetics. The compensation effects between A and E or A, E and n are well-known in the literature of the non-isothermal kinetics. Given that more and more parameters are assumed to be common during the evaluation, the objective function of the method of least squares (*of* in eq. 3-1) yields higher and higher values (i.e., the fit worsens); however, the condition of the parameter determination improves[97, 141]. One should find a reasonable compromise between the fit quality and the reliability of the parameter values. This consideration was employed in the present work, as well, as illustrated by Table 4-3. The following kinetic parameters could be assumed to be identical for the six samples with only a slight worsening of the fit quality; the activation energies, the mean and the width of the activation energy distribution in the DAEM part of the model and the dependence of the reactions on the oxygen concentration are given in evaluation 4 of Table 4-3.

Table 4-3: Evaluations with various groups of common model parameters[a]

Evaluation	**Common parameters**	N_{param}	$\frac{N_{param}}{N_{exper}}$	$100\sqrt{of}$
1	none	6×15	2.5	2.30
2	E_{cell}, E_0, E_{char}	75	2.1	2.40
3	E_{cell}, E_0, E_{char}, σ	70	1.9	2.42
4	E_{cell}, E_0, E_{char}, σ, ν_{cell}, ν_{other}, ν_{char}	55	1.5	2.46
5	E_{cell}, E_0, E_{char}, σ, z, n_{cell}, n_{char}	55	1.5	2.64
6	E_{cell}, E_0, E_{char}, σ, A_{cell}, A_{other}, A_{char}	55	1.5	2.71
7	E_{cell}, E_0, E_{char}, σ, y_{other_char}	65	1.8	3.11
8	E_{cell}, E_0, E_{char}, σ, ν_{cell}, ν_{other}, ν_{char}, z, n_{cell}, n_{char}	40	1.1	2.68

[a] See the Nomenclature for the meaning of the symbols in the Table.

4.5 Paper V: A simulation study on the torrefied biomass gasification

Biomass gasification was simulated by using Aspen Plus with a two-stage gasification model based on a Gibbs free energy minimization approach for comparing untreated and torrefied biomasses as feedstocks. The model accuracy was improved by including tar, actual experimental decomposition yields and the compositions of the chars produced during pyrolysis in the evaluations. The model outcomes were validated by using a C-H-O ternary diagram and by comparisons with results from other similar studies. Three process parameters, namely, the steam-to-biomass ratio (SBR), Gibbs reactor temperature (GB Temperature) and equivalence ratio (ER), were varied. The ER is defined as the amount of air added relative to the stoichiometric air requirement for combustion, and the SBR is defined as the ratio of steam to biomass molar flow rates. Twenty-seven cases were selected with all having carbon in the gaseous form for the final syngas product. The syngas composition was found to vary quite a bit based on the process parameters, and the inlet conditions should be selected based on the end requirements for the syngas. The overall efficiencies of an integrated torrefaction-gasification process were also provided by including the mass yield in the torrefaction process. The results obtained from this study can be summarized as follows:

1. Of the three process parameters, the ER had the most significant effect on the syngas composition and energy and exergy efficiencies. Table 4-4 lists the trends for the syngas composition and efficiencies based on an increase in any one of the process variables.

Table 4-4: Trends for syngas composition (mole fractions) and efficiencies

	Increase in SBR	**Increase in GB Temperature**	**Increase in ER**	**Torrefied wood (TW) vs Wood (W)**
H_2	Slightly increases	Slightly decreases	Decreases	TW>W
CO	Decreases	Slightly increases	Decreases	TW>W
CO_2	Slightly Increases	Slightly decreases	Increases	W>TW
N_2	Slightly decreases	Negligible effect	Increases	W>TW
Energy Efficiency	Slightly decreases	Slightly decreases	Decreases	TW>W
Exergy Efficiency	Slightly decreases	Slightly decreases	Decreases	TW>W

2. Maximum energy and exergy efficiencies were achieved by operating the gasifier at or close to the carbon deposition boundary point at that temperature

3. The torrefied biomass gave higher H_2 and CO contents and higher cold gas energy and exergy efficiencies than untreated biomass. Overall, the mole fractions of H_2, CO, CO_2 and N_2 were between 0.23-0.40, 0.22-0.42, 0.01-0.09 and 0.14-0.36 for torrefied wood and 0.21-0.40, 0.17-0.34, 0.03-0.09 and 0.15-0.37 for untreated wood, respectively. Similarly, the cold gas energy and exergy efficiencies were between 76.1-97.9 % and 68.3-85.8 % for torrefied wood and 67.9-91.0 % and 60.7-79.4 % for untreated wood, respectively
4. The overall efficiencies of an integrated torrefaction-gasification process depend on the mass yields of the torrefaction process. Higher mass yields in the torrefaction process will result in improved overall efficiencies for the integrated process. The torrefaction mass yield of 88 % in the present study resulted in better overall energy and exergy efficiencies than untreated biomass. The energy and exergy efficiencies for the torrefaction process itself were 93.3 % and 92.6 %, respectively. The mass yields in a torrefaction process are highly dependent on the choice of the reactor, heat and mass transfer profiles, process control and the production scale
5. The simulation results from this study correlated well with the simulation and experimental results from the Paviet et al.[158] study. Based on the C-H-O ternary diagram analysis, the present study fits very well with the underlying gasification theory
6. Biomass torrefaction did seem to have a positive effect on biomass gasification because of the improved CO and H_2 contents. This effect was primarily related to the increased carbon content of torrefied biomass from the devolatilization, leading to relatively higher oxygen loss during torrefaction. This finding was evident from the increased chemical exergy of torrefied biomass as well, and this higher chemical exergy was used to improve the syngas quality

5 Recommendations for Further Work

The following are some of the potential research areas that can be pursued to improve our understanding of the torrefaction process and its role in improving the biomass fuel properties:

- Evaluate torrefied biomass yields and properties for the biomass materials that are potential fuels for a particular region. The results obtained from this research work form the basis of a torrefaction feasibility study in Norway
- The effects of various torrefaction mediums (inert and non-inert) on the product yields and properties can be studied
- Perform lab and pilot scale studies for understanding torrefied biomass reactivity in combustion and gasification applications by using various biomass feedstocks
- Study the alkali and heavy metal release from the combustion and gasification of torrefied biomass
- Investigate the intrinsic and apparent kinetics of torrefied biomass in different gasification conditions
- The pelletization of torrefied biomass should be evaluated for additional biomass materials
- Combine the heat and mass transfer limitations with the intrinsic torrefaction kinetics data obtained in Paper III for a better simulation of larger industrial scale reactors
- Perform lab- or pilot-scale experiments for the pyrolysis of torrefied biomass that is obtained from Norwegian woods (birch and spruce) and evaluate the overall gasification energy and exergy efficiencies of these feedstocks
- Integrate the torrefaction process model (the drying and torrefaction reactor with energy inputs) with the gasification model presented in Paper V, and evaluate the overall energy and exergy efficiencies
- Reactors used at a laboratory scale may not provide a good simulation for pilot- or industry-scale reactors. Therefore, the overall efficiencies of an integrated torrefaction-gasification industrial process should be evaluated for a specific torrefaction reactor type

6 References

1. Nussbaumer, T., Combustion and co-combustion of biomass: Fundamentals, technologies, and primary measures for emission reduction. *Energy & Fuels* **2003,** 17, 1510-1521
2. Uslu, A.; Faaij, A. P. C.; Bergman, P. C. A., Pre-treatment technologies, and their effect on international bioenergy supply chain logistics. Techno-economic evaluation of torrefaction, fast pyrolysis and pelletisation. *Energy* **2008,** 33, (8), 1206-1223.
3. Venkata, B. K. *WBA Global Bioenergy Statistics 2014*; WBA GBS 2014; World Bioenergy Association: 2014.
4. Scarlat, N.; Dallemand, J.-F.; Skjelhaugen, O. J.; Asplund, D.; Nesheim, L., An overview of the biomass resource potential of Norway for bioenergy use. *Renewable and Sustainable Energy Reviews* **2011,** 15, (7), 3388-3398.
5. Bioenergi i Norge, Rapport 41. In Norges vassdrags- og energidirektorat: Oslo, 2014.
6. *Energy policies of IEA countries - Norway, 2011 Review*; International energy agency (IEA).
7. Grønli, M. G. A theoretical and experimental study of the thermal degradation of biomass. PhD Thesis, Norwegian University of Science and Technology, Trondheim, 1996.
8. Agbor, V. B.; Cicek, N.; Sparling, R.; Berlin, A.; Levin, D. B., Biomass pretreatment: Fundamentals toward application. *Biotechnology Advances* **2011,** 29.
9. Tanger, P.; Field, J. L.; Jahn, C. E.; Defoort, M. W.; Leach, J. E., Biomass for thermochemical conversion: targets and challenges. *Front Plant Sci* **2013,** 4, 218.
10. Jenkins, B. *Properties of Biomass, Appendix to Biomass Energy Fundamentals*; TR-102107; EPRI Report 1993.
11. Andriesse, J. P. *Nature and management of tropical peat soils*; FAO - Food and agriculture organization of the united nations: Rome, 1988.
12. Barrio, M. Experimental investigation of small-scale gasification of woody biomass. PhD Thesis, Norwegian University of Science and Technology, Trondheim, 2002.
13. Kargbo, F. R.; Xing, J.; Zhang, Y., Pretreatment for energy use of rice straw: A review. *African Journal of Agricultural Research* **2009,** 4, (13), 1560-1565.
14. Zwart, R. W. R.; Boerrigter, H.; van der Drift, A., The impact of biomass pretreatment on the feasibility of overseas biomass conversion to fischer-tropsch products. *Energy & Fuels* **2006,** 20, 2192-2197
15. Khan, A. A.; Jong, W. d.; J., J. P.; Spliethoff, H., Biomass combustion in fluidized bed boilers: Potential problems and remedies. *Fuel Processing Technology* **2009,** 90, 21-50
16. Yin, C.; Rosendahl, L. A.; Kær, S. K., Grate-firing of biomass for heat and power production *Progress in Energy and Combustion Science* **2008,** 34, 725-754
17. Houshfar, E. Experimental and numerical studies on two-stage combustion of biomass. PhD Thesis, Norwegian University of Science and Technology, Trondheim, 2012.
18. Babu, B. V., Biomass pyrolysis: a state-of-the-art review. *Biofuels, Bioproducts and Biorefining* **2008,** 2, (5), 393-414.
19. Demirbas, A.; Arin, G., An overview of biomass pyrolysis. *Energy Sources* **2002,** 24, (5), 471-482.
20. Jahirul, M.; Rasul, M.; Chowdhury, A.; Ashwath, N., Biofuels Production through Biomass Pyrolysis —A Technological Review. *Energies* **2012,** 5, (12), 4952-5001.

21. Diblasi, C., Modeling chemical and physical processes of wood and biomass pyrolysis. *Progress in Energy and Combustion Science* **2008,** 34, (1), 47-90.
22. Antal, J. M. J.; Grønli, M., The art, science, and technology of charcoal production. *Ind. Eng. Chem. Res.* **2003,** 42, 1619-1640.
23. Khalil, R. Thermal conversion of biomass with emphasis on product distribution, reaction kinetics and sulfur abatement. PhD Thesis, Norwegian University of Science and Technology, Trondheim, 2009.
24. Rajvanshi, A. K., Biomass gasification In *Alternative enery in agriculture*, D ed.; CRC Press: 1986; Vol. II pp 83-102.
25. Jankes, G.; Trninic, M.; Stamenic, M.; Simonovic, T.; Tanasic, N.; Labus, J., Biomass gasification with CHP production: A review of state of the art technology and near future perspectives. *Thermal Science* **2012,** 16, (suppl. 1), 115-130.
26. Rafiq, M. H. Experimental studies and modeling of synthesis gas production and fischer-tropsch synthesis. PhD Thesis, Norwegian University of Science and Technology, Trondheim, 2012.
27. Fossum, M. Biomass gasification: combustion of gas mixtures. PhD Thesis, Norwegian University of Science and Technology, Trondheim, 2002.
28. Higman, C.; van der Burgt, M., *Gasification*. Second ed.; Gulf Professional Publishing, Elsevier Inc. : MA, USA, 2008.
29. McKendry, P., Energy production from biomass (part 3): gasification technologies. *Bioresour Technol* **2002,** 83, 55-63.
30. Turns, S. R., *An introduction to combustion. Concepts and applications*. Second ed.; McGraw Hill: 2006.
31. *Biomass combined heat and power catalog of technologies*; U. S. Environmental Protection Agency Combined Heat and Power Partnership: 2007.
32. *Pulverised coal combustion (PCC)*; IEA Clean Coal Centre: 2012.
33. Obernberger, I., Decentralized biomass combustion: state of the art and future development. *Biomass and Bioenergy* **1998,** 14, 33-56.
34. Cremer, M.; Wang, D.; Bradley, J.; Thompson, D. *Staged Low NOx Combustion Systems for Coal Fired Boilers and Corrosion*; Praxair Technology, Inc.: 2003.
35. Wellinger, A. *Thermal pre-treatment of biomass for large-scale applications*; ExCo:2011:05; 2011.
36. Chen, W. H.; Ye, S. C.; Sheen, H. K., Hydrothermal carbonization of sugarcane bagasse via wet torrefaction in association with microwave heating. *Bioresour Technol* **2012,** 118, 195-203.
37. Bach, Q.-V.; Tran, K.-Q.; Khalil, R. A.; Skreiberg, Ø.; Seisenbaeva, G., Comparative Assessment of Wet Torrefaction. *Energy & Fuels* **2013,** 27, (11), 6743-6753.
38. Harmsen, P. F. H.; Huijgen, W. J. J.; Lopez, L. M. B.; Bakker, R. R. C. *Literature review of physical and chemical pretreatment processes for lignocellulosic biomass*; ECN-E--10-013; 2010.
39. Rupar-Gadd, K. Biomass pre-treatment for the production of sustainable energy – emissions and self-ignition. Växjö University, Sweden, 2006.
40. Stelte, W. *Guideline: Densification of torrefied biomass*; Danish Technological Institute: Taastrup, Denmark, 2012.
41. Chew, J. J.; Doshi, V., Recent advances in biomass pretreatment – Torrefaction fundamentals and technology. *Renewable and Sustainable Energy Reviews* **2011,** 15, (8), 4212-4222.
42. Tapasvi, D.; Tran, K.-Q.; Wang, L.; Skreiberg, Ø.; Khalil, R., Biomass torrefaction - A review. In *INFUB-9* Estoril, Portugal, 2011.

43. van der Stelt, M. J. C.; Gerhauser, H.; Kiel, J. H. A.; Ptasinski, K. J., Biomass upgrading by torrefaction for the production of biofuels: A review. *Biomass and Bioenergy* **2011**.
44. Bergman, P. C. A. *Combined torrefaction and pelletisation -The TOP process*; ECN-C--05-073; Energy research Centre of the Netherlands (ECN): 2005.
45. Prins, M. J.; Ptasinski, K. J.; Janssen, F. J. J. G., Torrefaction of wood. *Journal of Analytical and Applied Pyrolysis* **2006,** 77, (1), 28-34.
46. Prins, M. J.; Ptasinski, K. J.; Janssen, F. J. J. G., Torrefaction of wood. *Journal of Analytical and Applied Pyrolysis* **2006,** 77, (1), 35-40.
47. Repellin, V.; Govin, A.; Rolland, M.; Guyonnet, R., Energy requirement for fine grinding of torrefied wood. *Biomass and Bioenergy* **2010,** 34, (7), 923-930.
48. Khazraie Shoulaifar, T.; DeMartini, N.; Willför, S.; Pranovich, A.; Smeds, A. I.; Virtanen, T. A. P.; Maunu, S.-L.; Verhoeff, F.; Kiel, J. H. A.; Hupa, M., Impact of Torrefaction on the Chemical Structure of Birch Wood. *Energy & Fuels* **2014,** 28, (6), 3863-3872.
49. Bergman, P. C. A.; Boersma, A. R.; Zwart, R. W. R.; Kiel, J. H. A. *Torrefaction for biomass co-firing in existing coal-fired power stations "BIOCOAL"*; ECN-C--05-013; Energy research Centre of the Netherlands (ECN): 2005.
50. Medic, D.; Darr, M.; Shah, A.; Potter, B.; Zimmerman, J., Effects of torrefaction process parameters on biomass feedstock upgrading. *Fuel* **2012,** 91, (1), 147-154.
51. Uemura, Y.; Omar, W. N.; Tsutsui, T.; Yusup, S. B., Torrefaction of oil palm wastes. *Fuel* **2011,** 90, (8), 2585-2591.
52. Wannapeera, J.; Fungtammasan, B.; Worasuwannarak, N., Effects of temperature and holding time during torrefaction on the pyrolysis behaviors of woody biomass. *Journal of Analytical and Applied Pyrolysis* **2011,** 92, (1), 99-105.
53. Arias, B.; Pevida, C.; Fermoso, J.; Plaza, M. G.; Rubiera, F.; Pis, J. J., Influence of torrefaction on the grindability and reactivity of woody biomass. *Fuel Processing Technology* **2008,** 89, (2), 169-175.
54. Bridgeman, T. G.; Jones, J. M.; Williams, A.; Waldron, D. J., An investigation of the grindability of two torrefied energy crops. *Fuel* **2010,** 89, (12), 3911-3918.
55. Pierre, F.; Almeida, G.; Brito, J. O.; Perré, P., Influence of torrefaction on some chemical and energy properties of maritime pine and pedunculate oak. *BioResources* **2011,** 6, (2), 1204-1218.
56. Pimchuai, A.; Dutta, A.; Basu, P., Torrefaction of Agriculture Residue To Enhance Combustible Properties†. *Energy & Fuels* **2010,** 24, (9), 4638-4645.
57. Phanphanich, M.; Mani, S., Impact of torrefaction on the grindability and fuel characteristics of forest biomass. *Bioresour Technol* **2011,** 102, (2), 1246-53.
58. Deng, J.; Wang, G.-j.; Kuang, J.-h.; Zhang, Y.-l.; Luo, Y.-h., Pretreatment of agricultural residues for co-gasification via torrefaction. *Journal of Analytical and Applied Pyrolysis* **2009,** 86, (2), 331-337.
59. Chen, W.-H.; Cheng, W.-Y.; Lu, K.-M.; Huang, Y.-P., An evaluation on improvement of pulverized biomass property for solid fuel through torrefaction. *Applied Energy* **2011,** 88, (11), 3636-3644.
60. Rousset, P.; Aguiar, C.; Labbe, N.; Commandre, J. M., Enhancing the combustible properties of bamboo by torrefaction. *Bioresour Technol* **2011,** 102, (17), 8225-31.
61. Bridgeman, T. G.; Jones, J. M.; Shield, I.; Williams, P. T., Torrefaction of reed canary grass, wheat straw and willow to enhance solid fuel qualities and combustion properties. *Fuel* **2008,** 87, (6), 844-856.
62. Prins, M. J.; Ptasinski, K. J.; Janssen, F. J. J. G., More efficient biomass gasification via torrefaction. *Energy* **2006,** 31, (15), 3458-3470.

63. Couhert, C.; Salvador, S.; Commandré, J. M., Impact of torrefaction on syngas production from wood. *Fuel* **2009,** 88, (11), 2286-2290.
64. Patel, B.; Gami, B.; Bhimani, H., Improved fuel characteristics of cotton stalk, prosopis and sugarcane bagasse through torrefaction. *Energy for Sustainable Development* **2011**.
65. Chen, W.-H.; Kuo, P.-C., A study on torrefaction of various biomass materials and its impact on lignocellulosic structure simulated by a thermogravimetry. *Energy* **2010,** 35, (6), 2580-2586.
66. Li, H.; Liu, X.; Legros, R.; Bi, X. T.; Lim, C. J.; Sokhansanj, S., Torrefaction of sawdust in a fluidized bed reactor. *Bioresour Technol* **2011**.
67. Chen, W.-H.; Hsu, H.-C.; Lu, K.-M.; Lee, W.-J.; Lin, T.-C., Thermal pretreatment of wood (Lauan) block by torrefaction and its influence on the properties of the biomass. *Energy* **2011,** 36, (5), 3012-3021.
68. Felfli, F. F.; Luengo, C. A.; Suárez, J. A.; Beatón, P. A., Wood briquette torrefaction. *Energy for Sustainable Development* **2005,** IX, (3).
69. Sadaka, S.; Negi, S., Improvements of biomass physical and thermochemical characteristics via torrefaction process. *Environmental Progress & Sustainable Energy* **2009,** 28, (3), 427-434.
70. Chen, Y.; Liu, B.; Yang, H.; Yang, Q.; Chen, H., Evolution of functional groups and pore structure during cotton and corn stalks torrefaction and its correlation with hydrophobicity. *Fuel* **2014,** 137, 41-49.
71. Basu, P.; Rao, S.; Acharya, B.; Dhungana, A., Effect of torrefaction on the density and volume changes of coarse biomass particles. *The Canadian Journal of Chemical Engineering* **2013,** 91, (6), 1040-1044.
72. Koppejan, J.; Sokhansanj, S.; Melin, S.; Madrali, S. *Status overview of torrefaction technologies*; Enschede, 2012.
73. Mišljenović, N.; Bach, Q.-V.; Tran, K.-Q.; Salas-Bringas, C.; Skreiberg, Ø., Torrefaction Influence on Pelletability and Pellet Quality of Norwegian Forest Residues. *Energy & Fuels* **2014,** 28, (4), 2554-2561.
74. Järvinen, T.; Agar, D., Experimentally determined storage and handling properties of fuel pellets made from torrefied whole-tree pine chips, logging residues and beech stem wood. *Fuel* **2014,** 129, 330-339.
75. Khalil, R. A.; Bach, Q.-V.; Skreiberg, Ø.; Tran, K.-Q., Performance of a Residential Pellet Combustor Operating on Raw and Torrefied Spruce and Spruce-Derived Residues. *Energy & Fuels* **2013,** 27, (8), 4760-4769.
76. Berrueco, C.; Recari, J.; Güell, B. M.; Alamo, G. d., Pressurized gasification of torrefied woody biomass in a lab scale fluidized bed. *Energy* **2014,** 70, 68-78.
77. Sarkar, M.; Kumar, A.; Tumuluru, J. S.; Patil, K. N.; Bellmer, D. D., Gasification performance of switchgrass pretreated with torrefaction and densification. *Applied Energy* **2014,** 127, 194-201.
78. Batidzirai, B.; Mignot, A. P. R.; Schakel, W. B.; Junginger, H. M.; Faaij, A. P. C., Biomass torrefaction technology: Techno-economic status and future prospects. *Energy* **2013,** 62, 196-214.
79. Bergman, P. C. A.; Boersma, A. R.; Kiel, J. H. A.; Prins, M. J.; Ptasinski, K. J.; Janssen, F. J. J. G. *Torrefaction for entrained-flow gasification of biomass*; Energy research Centre of the Netherlands (ECN): 2005.
80. Tumuluru, J. S.; Sokhansanj, S.; Wright, C. T.; Boardman, R. D.; Hess, J. R., Review on biomass torrefaction process and product properties and design of moving bed torrefaction system model development. In *ASABE Annual International Meeting*, ASABE: Louisville, Kentucky, 2011.

81. Chen, W.-H.; Lu, K.-M.; Lee, W.-J.; Liu, S.-H.; Lin, T.-C., Non-oxidative and oxidative torrefaction characterization and SEM observations of fibrous and ligneous biomass. *Applied Energy* **2014,** 114, 104-113.
82. Eseltine, D.; Thanapal, S. S.; Annamalai, K.; Ranjan, D., Torrefaction of woody biomass (Juniper and Mesquite) using inert and non-inert gases. *Fuel* **2013,** 113, 379-388.
83. Lu, J.-J.; Chen, W.-H., Product Yields and Characteristics of Corncob Waste under Various Torrefaction Atmospheres. *Energies* **2013,** 7, (1), 13-27.
84. Nhuchhen, D. R.; Basu, P., Experimental Investigation of Mildly Pressurized Torrefaction in Air and Nitrogen. *Energy & Fuels* **2014,** 28, (5), 3110-3121.
85. Thanapal, S. S.; Chen, W.; Annamalai, K.; Carlin, N.; Ansley, R. J.; Ranjan, D., Carbon Dioxide Torrefaction of Woody Biomass. *Energy & Fuels* **2014,** 28, (2), 1147-1157.
86. Becidan, M.; Várhegyi, G.; Hustad, J. E.; Skreiberg, Ø., Thermal decomposition of biomass wastes. A kinetic study. *Ind. Eng. Chem. Res.* **2007,** 46, 2428-2437.
87. Grønli, M. G.; Várhegyi, G.; Blasi, C. D., Thermogravimetric analysis and devolatilization kinetics of wood. *Ind. Eng. Chem. Res.* **2002,** 41, (4201-4208).
88. Tapasvi, D.; Khalil, R.; Várhegyi, G.; Skreiberg, Ø.; Tran, K.-Q.; Grønli, M. G., Kinetic behavior of torrefied biomass in an oxidative environment. *Energy & Fuels* **2013,** 27, (2), 1050-1060.
89. Várhegyi, G., Kinetic evaluation of non-isothermal thermoanalytical curves in the case of independent thermal reactions. *Thermochimica Acta* **1979,** 28, 367-376.
90. Várhegyi, G.; Antal, J. M. J.; Jakab, E.; Szabo, P., Kinetic modeling of biomass pyrolysis. *Journal of Analytical and Applied Pyrolysis* **1997,** 42, 73-87.
91. Várhegyi, G.; Szabo, P.; Jakab, E.; Till, F., Least squares criteria for the kinetic evaluation of thermoanalytical experiments. Examples from a char reactivity study. *Journal of Analytical and Applied Pyrolysis* **2001,** 57, 203-222.
92. Vyazovkin, S.; Wight, C. A., Isothermal and non-isothermal kinetics of thermally stimulated reactions of solids. *International Reviews in Physical Chemistry* **1998,** 17, (3), 407-433.
93. Várhegyi, G., Aims and methods in non-isothermal reaction kinetics. *Journal of Analytical and Applied Pyrolysis* **2007,** 79, (1-2), 278-288.
94. Tapasvi, D.; Khalil, R.; Várhegyi, G.; Tran, K.-Q.; Grønli, M.; Skreiberg, Ø., Thermal decomposition kinetics of Woods with an emphasis on Torrefaction. *Energy & Fuels* **2013,** 27, (10), 6134-6145.
95. Di Blasi, C., Combustion and gasification rates of lignocellulosic chars. *Progress in Energy and Combustion Science* **2009,** 35, (2), 121-140.
96. Várhegyi, G.; Antal, J. M. J.; Szabo, P.; Jakab, E.; Till, F., Application of complex reaction kinetic models in thermal analysis. *Journal of Thermal Analysis* **1996,** 47, 535-542.
97. Várhegyi, G.; Bobály, B.; Jakab, E.; Chen, H., Thermogravimetric study of biomass pyrolysis kinetics. A distributed activation energy model with prediction tests. *Energy & Fuels* **2011,** 25, 24-32.
98. Várhegyi, G.; Chen, H.; Godoy, S., Thermal decomposition of wheat, oat, barley and Brassica carinata straws. A kinetic study. *Energy & Fuels* **2009,** 23, 646-652
99. de Jong, W.; Pirone, A.; Wojtowicz, M. A., Pyrolysis of Miscanthus Giganteus and wood pellets: TG-FTIR analysis and reaction kinetics. *Fuel* **2003,** 82, 1139-1147.
100. Várhegyi, G.; Szabó, P.; Antal, J. M. J., Kinetics of charcoal devolatilization. *Energy & Fuels* **2002,** 16, 724-731.

101. Wójtowicz, M. A.; Bassilakis, R.; Smith, W. W.; Chen, Y.; Carangelo, R. M., Modeling the evolution of volatile species during tobacco pyrolysis. *J. Anal. Appl. Pyrolysis* **2003,** 66, 235-261.
102. Yi, S.-C.; Hajaligol, M. R., Product distribution from the pyrolysis modeling of tobacco particles. *J. Anal. Appl. Pyrolysis* **2003,** 66, 217-234
103. Várhegyi, G.; Sebestyén, Z.; Czégény, Z.; Lezsovits, F.; Könczöl, S., Combustion kinetics of biomass materials in the kinetic regime *Energy & Fuels* **2012,** 26, 1323-1335.
104. Khalil, R.; Varhegyi, G.; Jaschke, S.; Grønli, M.; Hustad, J. E., CO2 gasification of biomass chars: A kinetic study. *Energy & Fuels* **2009,** 23, 94-100.
105. Bates, R. B.; Ghoniem, A. F., Biomass torrefaction: modeling of volatile and solid product evolution kinetics. *Bioresour Technol* **2012,** 124, 460-9.
106. Chen, W.-H.; Kuo, P.-C., Isothermal torrefaction kinetics of hemicellulose, cellulose, lignin and xylan using thermogravimetric analysis. *Energy* **2011,** 36, (11), 6451-6460.
107. Lu, K.-M.; Lee, W.-J.; Chen, W.-H.; Lin, T.-C., Thermogravimetric analysis and kinetics of co-pyrolysis of raw/torrefied wood and coal blends. *Applied Energy* **2013,** 105, 57-65.
108. Park, J.; Meng, J.; Lim, K. H.; Rojas, O. J.; Park, S., Transformation of lignocellulosic biomass during torrefaction. *Journal of Analytical and Applied Pyrolysis* **2013,** 100, 199-206.
109. Peng, J.; Xiaotao, T. B.; Lim, J.; Sokhansanj, S., Development of torrefaction kinetics for british columbia softwoods. *International Journal of Chemical Reactor Engineering* **2012,** 10, (1).
110. Shang, L.; Ahrenfeldt, J.; Holm, J. K.; Barsberg, S.; Zhang, R.-Z.; Luo, Y.-H.; Egsgaard, H.; Henriksen, U. B., Intrinsic kinetics and devolatilization of wheat straw during torrefaction. *Journal of Analytical and Applied Pyrolysis* **2013,** 100, 145-152.
111. Nocquet, T.; Dupont, C.; Commandre, J.-M.; Grateau, M.; Thiery, S.; Salvador, S., Volatile species release during torrefaction of biomass and its macromolecular constituents: Part 2 – Modeling study. *Energy* **2014,** 72, 188-194.
112. Bach, Q.-V.; Khalil, R.; Tran, K.-Q.; Skreiberg, Ø., Torrefaction kinetics of norwegian biomass fuels. *Chemical Engineering Transactions* **2014,** 37.
113. Peduzzi, E.; Boissonnet, G.; Haarlemmer, G.; Dupont, C.; Maréchal, F., Torrefaction modelling for lignocellulosic biomass conversion processes. *Energy* **2014,** 70, 58-67.
114. Ren, S.; Lei, H.; Wang, L.; Bu, Q.; Chen, S.; Wu, J., Thermal behaviour and kinetic study for woody biomass torrefaction and torrefied biomass pyrolysis by TGA. *Biosystems Engineering* **2013,** 116, (4), 420-426.
115. Blasi, C. D.; Lanzetta, M., Intrinsic kinetics of isothermal xylan degradation in inert atmosphere. *Journal of Analytical and Applied Pyroiysis* **1997,** 40-41 (1997), 287-303.
116. Shang, L.; Ahrenfeldt, J.; Holm, J. K.; Bach, L. S.; Stelte, W.; Henriksen, U. B., Kinetic model for torrefaction of wood chips in a pilot-scale continuous reactor. *Journal of Analytical and Applied Pyrolysis* **2014,** 108, 109-116.
117. Klinger, J.; Bar-Ziv, E.; Shonnard, D., Kinetic study of aspen during torrefaction. *Journal of Analytical and Applied Pyrolysis* **2013,** 104, 146-152.
118. Sarvaramini, A.; Assima, G. P.; Larachi, F., Dry torrefaction of biomass – Torrefied products and torrefaction kinetics using the distributed activation energy model. *Chemical Engineering Journal* **2013,** 229, 498-507.
119. Vincent, S. S.; Mahinpey, N.; Aqsha, A., Mass transfer studies during CO2 gasification of torrefied and pyrolyzed chars. *Energy* **2014,** 67, 319-327.

120. Jones, J. M.; Bridgeman, T. G.; Darvell, L. I.; Gudka, B.; Saddawi, A.; Williams, A., Combustion properties of torrefied willow compared with bituminous coals. *Fuel Processing Technology* **2012,** 101, 1-9.
121. Broström, M.; Nordin, A.; Pommer, L.; Branca, C.; Di Blasi, C., Influence of torrefaction on the devolatilization and oxidation kinetics of wood. *Journal of Analytical and Applied Pyrolysis* **2012,** 96, 100-109.
122. Puig-Arnavat, M.; Bruno, J. C.; Coronas, A., Review and analysis of biomass gasification models. *Renewable and Sustainable Energy Reviews* **2010,** 14, (9), 2841-2851.
123. Altafini, C. R.; Wander, P. R.; Barreto, R. M., Prediction of the working parameters of a wood waste gasifier through an equilibrium model. *Energy Conversion and Management* **2003,** 44, (17), 2763-2777.
124. Jarungthammachote, S.; Dutta, A., Thermodynamic equilibrium model and second law analysis of a downdraft waste gasifier. *Energy* **2007,** 32, (9), 1660-1669.
125. Jarungthammachote, S.; Dutta, A., Equilibrium modeling of gasification: Gibbs free energy minimization approach and its application to spouted bed and spout-fluid bed gasifiers. *Energy Conversion and Management* **2008,** 49, (6), 1345-1356.
126. Li, X.; Grace, J. R.; Watkinson, A. P.; Lim, C. J.; Ergüdenler, A., Equilibrium modeling of gasification: a free energy minimization approach and its application to a circulating fluidized bed coal gasifier. *Fuel* **2001,** 80, (2), 195-207.
127. Melgar, A.; Pérez, J. F.; Laget, H.; Horillo, A., Thermochemical equilibrium modelling of a gasifying process. *Energy Conversion and Management* **2007,** 48, (1), 59-67.
128. Schuster, G.; Löffler, G.; Weigl, K.; Hofbauer, H., Biomass steam gasification – an extensive parametric modeling study. *Bioresource Technology* **2001,** 77, (1), 71-79.
129. Yoshida, H.; Kiyono, F. o.; Tajima, H.; Yamasaki, A.; Ogasawara, K.; Masuyama, T., Two-stage equilibrium model for a coal gasifier to predict the accurate carbon conversion in hydrogen production. *Fuel* **2008,** 87, (10–11), 2186-2193.
130. Mansaray, K. G.; Al-Taweel, A. M.; Ghaly, A. E.; Hamdullahpur, F.; Ugursal, V. I., Mathematical modeling of a fluidized bed rice husk gasifier: Part I-model development. *Energy Sources* **2000,** 22, (1), 83-98.
131. Paviet, F.; Chazarenc, F.; Tazerout, M., Thermo chemical equilibrium modelling of a biomass gasifying process using ASPEN PLUS. *International Journal of Chemical Reactor Engineering* **2009,** 7, (1).
132. Chen, W. H.; Chen, C. J.; Hung, C. I., Taguchi approach for co-gasification optimization of torrefied biomass and coal. *Bioresour Technol* **2013,** 144, 615-22.
133. Chen, W.-H.; Chen, C.-J.; Hung, C.-I.; Shen, C.-H.; Hsu, H.-W., A comparison of gasification phenomena among raw biomass, torrefied biomass and coal in an entrained-flow reactor. *Applied Energy* **2013,** 112, 421-430.
134. Kuo, P.-C.; Wu, W.; Chen, W.-H., Gasification performances of raw and torrefied biomass in a downdraft fixed bed gasifier using thermodynamic analysis. *Fuel* **2014,** 117, 1231-1241.
135. Abuadala, A.; Dincer, I.; Naterer, G. F., Exergy analysis of hydrogen production from biomass gasification. *International Journal of Hydrogen Energy* **2010,** 35, (10), 4981-4990.
136. Hosseini, M.; Dincer, I.; Rosen, M. A., Steam and air fed biomass gasification: Comparisons based on energy and exergy. *International Journal of Hydrogen Energy* **2012,** 37, (21), 16446-16452.
137. Ptasinski, K. J., Thermodynamic efficiency of biomass gasification and biofuels conversion. *Biofuels, Bioproducts and Biorefining* **2008,** 2, (3), 239-253.

138. Rao, M. S.; Singh, S. P.; Sodha, M. S.; Dubey, A. K.; Shyam, M., Stoichiometric, mass, energy and exergy balance analysis of countercurrent fixed-bed gasification of post-consumer residues. *Biomass and Bioenergy* **2004,** 27, (2), 155-171.
139. Channiwala, S. A.; Parikh, P. P., A unified correlation for estimating HHV of solid, liquid and gaseous fuels. *Fuel* **2002,** 81, (8), 1051-1063.
140. *High resolution thermogravemetric analysis - A new technique for obtaining superior analytical results*; TA Instruments report TA-023.
141. Várhegyi, G.; Czégény, Z.; Jakab, E.; McAdam, K.; Liu, C., Tobacco pyrolysis. Kinetic evaluation of thermogravimetric – mass spectrometric experiments. *J. Anal. Appl. Pyrolysis* **2009,** 86, 310-322.
142. Trninić, M.; Wang, L.; Várhegyi, G.; Grønli, M.; Skreiberg, Ø., Kinetics of corncob pyrolysis. *Energy & Fuels* **2012,** 26, 2005-2013.
143. Conesa, J. A.; Domene, A., Biomass pyrolysis and combustion kinetics through n-th-order parallel reactions. *Thermochim. Acta* **2011,** 523, 176-181.
144. Várhegyi, G.; Antal, J. M. J., Kinetics of the thermal decomposition of cellulose, hemicellulose, and sugar cane bagasse. *Energy & Fuels* **1989,** 3, 329-335.
145. Donskoi, E.; McElwain, D. L. S., Optimization of coal pyrolysis modeling. *Combust. Flame* **2000,** 122, 359-367.
146. Manyà, J. J.; Velo, E.; Puigjaner, L., Kinetics of biomass pyrolysis: A reformulated three-parallel-reactions model. *Ind. Eng. Chem. Res.* **2003,** 42, 434-441.
147. Fryda, L.; Panopoulos, K. D.; Kakaras, E., Integrated CHP with autothermal biomass gasification and SOFC–MGT. *Energy Conversion and Management* **2008,** 49, (2), 281-290.
148. Karamarkovic, R.; Karamarkovic, V., Energy and exergy analysis of biomass gasification at different temperatures. *Energy* **2010,** 35, (2), 537-549.
149. Kempegowda, R. S.; Assabumrungrat, S.; Laosiripojana, N., Thermodynamic analysis for gasification of thailand rice husk with air, steam, and mixed air/steam for hydrogen-rich gas production. *International Journal of Chemical Reactor Engineering* **2010,** 8.
150. Kempegowda, R. S.; Pannir Selvam, P. V.; Skreiberg, Ø.; Tran, K.-Q., Process synthesis and economics of combined biomethanol and CHP energy production derived from biomass wastes. *Journal of Chemical Technology & Biotechnology* **2012,** 87, (7), 897-902.
151. Nikoo, M. B.; Mahinpey, N., Simulation of biomass gasification in fluidized bed reactor using aspen plus. *Biomass and Bioenergy* **2008,** 32, (12), 1245-1254.
152. Aigner, I.; Wolfesberger, U.; Hofbauer, H. Tar content and composition in producer gas of fluidized bed gasification and low temperature pyrolysis of straw and wood – Influence of temperature. www.bioenergy2020.eu
153. Fjellerup, J.; Ahrenfeldt, J.; Henriksen, U.; Gøbel, B. *Formation, decomposition and cracking of biomass tars in gasification*; MEK-ET-2005-05; Technical University of Denmark: Denmark, 2005; pp 1-60.
154. Chang, S. K.; Sung, P. M., Characterization of pyrolysis tar derived from lignocellulosic biomass. *J. Ind. Eng. Chem.* **2006,** 12, (6), 853-861.
155. Panopoulos, K. D.; Fryda, L.; Karl, J.; Poulou, S.; Kakaras, E., High temperature solid oxide fuel cell integrated with novel allothermal biomass gasification. *Journal of Power Sources* **2006,** 159, (1), 586-594.
156. Kotas, T. J., *The exergy method of thermal plant analysis*. Krieger Publishing Company: 1995.
157. Szargut, V. J.; Styrylska, T., Angenaherte bestimmung der exergie von brennstoffen. . *Brennstoff-Warne-Kraft* **1964,** 16, (12), S.589.

158. Paviet, F.; Chazarenc, F.; Tazerout, M., Thermo chemical equilibrium modelling of a biomass gasifying process using aspen plus. *International Journal of Chemical Reactor Engineering* **2009,** 7.

7 Appendix

I. **Tapasvi, D.;** Tran, K-Q.; Wang, L.; Skreiberg, Ø.; Khalil, R. Biomass torrefaction – a review. Proceedings of the 9th European Conference on Industrial Furnaces and Boilers, Estoril, Portugal 2011, (ISBN 978-972-99309-6-6)

II. **Tapasvi, D.;** Khalil, R. A.; Skreiberg, Ø.; Tran, K.-Q.; Gronli, M. G. Torrefaction of Norwegian birch and spruce – an experimental study using macro-TGA. Energy Fuels 2012, 26, 5232–5240.

III. **Tapasvi, D.;** Khalil, R.; Várhegyi, G.; Tran, K.-Q.; Grønli, M.; Skreiberg, Ø., Thermal decomposition kinetics of woods with an emphasis on torrefaction. Energy Fuels 2013, 27, (10), 6134-6145.

IV. **Tapasvi, D.;** Khalil, R.; Várhegyi, G.; Skreiberg, Ø.; Tran, K.-Q.; Grønli, M. Kinetic behavior of torrefied biomass in an oxidative environment. Energy Fuels, 2013, 27, 1050-1060.

V. **Tapasvi, D.;** Kempegowda, R.; Tran, K-Q.; Skreiberg, Ø.; Grønli, M. A simulation study on the torrefied biomass gasification. Energy Conversion and Management, 2015, 90, 446-457

Paper I

Biomass torrefaction – a review

Tapasvi, D.; Tran, K-Q.; Wang, L.; Skreiberg, Ø.; Khalil, R.

Proceedings of the 9th European Conference on Industrial Furnaces and Boilers, Estoril, Portugal 2011, (ISBN 978-972-99309-6-6)

BIOMASS TORREFACTION – A REVIEW

Dhruv Tapasvi*¤, Khanh-Quang Tran*, Liang Wang, Øyvind Skreiberg** and Roger Khalil****
*Norwegian University of Science and Technology (NTNU), **Sintef Energy Research
¤Corresponding author - Tel.: +4793818918; Fax: +4773593580; E-mail: dhruv.tapasvi@ntnu.no

Abstract: Torrefaction is a mild-pyrolysis (200-300 ^{o}C) process that can be employed as a pre-treatment to improve fuel properties of biomass materials. The treatment can result in not only increased energy density, but also enhanced grindability, and better storage and transport characteristics for biomass fuels. Due to these promising results, torrefaction has attracted increasing research interests in the recent years. Several studies on torrefaction of biomass have been documented for heat and power applications. Substantial amounts of data on the technique are available, which need to be reviewed and analyzed for further actions in the area. This is the primary objective of the present study. Firstly, this review paper provides an introduction to the biomass torrefaction process. This is followed by a critical analysis of the experimental methods used in laboratory to carry out torrefaction under various process conditions. Later, the tested biomass materials are discussed in terms of the product yields and the evaluated product properties. An overview of the kinetic modeling studies on the topic is also included. Finally, the recommendations for future research work are provided. Reviewing the literature suggests that torrefaction is a promising technique to improve the performance of biomass for energy utilization. However, despite a number of impressive studies on the topic, a lot of information still needs to be recognized for improving the viability of the process.
Keywords: Biomass torrefaction; Mild pyrolysis; Biomass pre-treatment

1. Introduction

Wider use of biomass can extend the lifetime of our fossil fuels resources. However, problems such as low bulk density, high moisture content, low grindability and relatively low calorific value, make biomass a challenging fuel to use and hinders its widespread use. Researchers are looking into solutions to overcome these drawbacks and thus, improve the properties of biomass as a fuel. Torrefaction is one of these solutions and is a mild pyrolysis of biomass with typical conditions of 200-300 ^{o}C, near atmospheric pressure, absence of oxygen and relatively low particle heating rates (< 50 ^{o}C/min) [4, 10, 20, 23, 25] . The biomass is partly decomposed and yields a uniform solid product, condensable liquid and non-condensable gases [15, 18, 24]. Main thermal decomposition reactions during torrefaction occur with the xylan-containing hemicelluloses polymers, since these are the most reactive polymeric structures of biomass [6, 13]. The decomposition of hemicelluloses in the torrefaction process changes the orientation of the cellulose microfibrils in the lignin matrix, thereby improving the properties of biomass such as grindability, deterioration and fluidization characteristics [2]. Because of these advantages and the high level of viability, the technique has attracted increasing interests during the last decades. A number of studies have been implemented to investigate the role played by torrefaction in improving the properties of biomass materials. However, the information is quite scattered and covers a broad range of topics related to torrefaction. A critical review is required to avoid duplication of research efforts and to direct them in most important areas required to increase the viability of the process. This is the main objective of this present study. Available information on torrefaction is thoroughly reviewed and recommendations for future work are summarized in this paper. Experimental methods used for carrying out torrefaction are presented in detail along with the information on tested biomass materials and kinetic modeling studies. However, this study only covers the dry torrefaction process and a review of the wet torrefaction process is not part of the scope.

2. Torrefaction Experimental Methods

Studies reported in the literature used two basic experimental approaches to analyze the torrefaction process, (i) thermogravimetric analysis in which biomass weight loss is monitored over the duration of the test and (ii) small-scale reactor methods in which special bench-scale and pilot-scale reactors are designed to investigate torrefaction. Thermogravimetric methods were used to study the effects of operating parameters on the torrefaction products and to obtain data for modeling kinetics of torrefaction. Reactor investigations were used to study and simulate torrefaction in conditions which are closer to the actual industrial environment. Properties of the torrefied products obtained from both these methods were determined by using various analytical techniques.

2.1 Thermogravimetric Studies

Three studies performed thermogravimetric analyses (TGA) to investigate biomass torrefaction. In a recent study by Chen and Kuo [26], biomass materials were first dried in an oven at 60 ^{o}C for 24 hrs. After drying, the materials were grinded and sieved and then kept in a desiccator until the TGA was performed. The temperature during each run was detected and recorded at a frequency of 2 Hz. From the recorded distribution of the weight loss, TGA and derivative thermogravimetric analysis (DTG) was obtained that was used to characterize the biomass components behavior during torrefaction. A similar TGA experimental design was used by Bridgeman et al. [7]. In addition to using the TGA, a Stanton Redcroft simultaneous Analyser STA-780 Series was also integrated in the set-up to simultaneously analyze the volatile products. Instead of drying the biomass separately in an oven before TGA, the temperature program included a 5 min isothermal period at 105 ^{o}C to remove the moisture after the dynamic heating period. After this drying period, a second dynamic heating period was included to heat the sample up to torrefaction temperature. In another TGA study, Prins et al. [14] used the weight loss graphs obtained from the TGA with auto sampler to determine the reaction kinetics of torrefaction. In the temperature program, drying of the biomass samples was achieved only during dynamic heating stage with varying heating rates, which is followed by an isothermal period at torrefaction temperature. This study used the weight loss graphs of the dry biomass to determine the torrefaction reaction kinetics.

Thermogravimetric equipment used by these studies to study torrefaction was similar in design and capability as listed in table 1. However, biomass materials, quantities, particle sizes and the temperature program were different for the conducted experiments. All the TGA systems described above allowed independent temperature control of the biomass materials and the weight loss was constantly measured.

Table 1: Comparisons of torrefaction TGA studies

Study	TGA Type	Biomass Sample	Sample weight	Sample Particle size	Inert Gas type, flow rate	Ramp heating rate C/min	Reaction Temp	Reaction residence time
Chen & Kuo [26]	Perkin Elmer Diamand TG/DTA	bamboo, willow, coconut shell and wood	5 mg	<=0.42 mm	Nitrogen, 200 cc (STP)/ min	20	240, 275 °C	2 hrs
Bridgeman et al [7]	Nicolet Magma IR AEM TGA	wheat straw, reed canary grass and willow	25-35 mg	Not reported	nitrogen at 50 ml/min	10	230-290 °C	30 min
Prins et al [14]	Perkin-Elmer Pyris 6 TGA	beech, willow, larch and wheat straw	2-10 mg	0.7-2.0 mm, < 5.0 mm	nitrogen at 20 ml/min	10 to 100	230-300 °C	0-3 hrs

2.2 Reactor Studies

Many studies designed special small-scale (bench and pilot scale) reactors to carry out torrefaction experiments. Deng et al. [6] designed a vertical corundum tube reactor. Nitrogen was used as a sample heating and was heated at the entrance of the tube. Condensable liquids coming out of the reactor were trapped using a two-necked flask immersed in liquid nitrogen. Non-condensable gases composition and concentration was recorded continuously during the process using infrared gas analysis. Methods used for heating nitrogen and for monitoring temperatures were not reported. Couhert et al. [9] designed a quartz tube reactor surrounded by a 2kW electrical furnace that was used to heat nitrogen entering at the bottom of the reactor. The reactor was sealed at the top by a ceramic wool swab to prevent air from entering the reactor. A thermocouple was placed inside the reactor to measure gas temperature upstream of the sample. The main purpose of designing this reactor was to produce torrefied wood that can be used in a gasification reactor as feedstock; therefore, the gases exiting this torrefaction reactor were not analyzed. Pach et al. [17] used a similar electrically heated reactor consisting of two cylinders. Sample was placed in the inner cylinder of the reactor. The volatiles were cooled in a water cooled condenser for condensing the tar and the water phase. Gas is passed through a cotton filter before being collected in a bag for further analysis by a gas chromatograph. Specifications for the electrical heaters and temperature monitoring instruments were not reported. Prins et al. [15] reported another torrefaction unit consisting of cylindrical reactor placed inside an electrical oven. Instead of nitrogen, as used by other researchers, argon was used as the inert gas. A thermocouple is used to measure sample temperature inside the reactor bed. The inlet and outlet of the reactor were heat-traced to prevent condensation of the products in the tubing. The argon inlet lines were also heat traced for a more stable temperature control. Permanent gases

removed by argon purge gas were collected in a gasbag and analyzed by Micro-GC (offline). Condensable liquids were collected in a cold trap at -15 °C and were analyzed by HPLC. Energy research center (ECN) in Netherlands has developed both batch and continuous pilot scale reactors to carry out torrefaction, as reported by Bergman et al. [18, 19]. The batch reactor was operated as a fixed bed reactor and the sample was heated by direct contact with heated nitrogen acting as the inert gas. Heat losses were minimized by wrapping tracer ribbons around the reactor. For temperature control, the reactor was equipped with thermocouples at several radial and axial positions. Nitrogen was heated in an electric heater at the bottom of the reactor. Specifications for the electric heater were not reported. Permanent gases exiting the reactor were analyzed online using Micro-GC. The condensable fraction of the volatiles were sampled using water filled impinge bottles and then analyzed by GC-FID and GC-MS (offline). The continuous torrefaction reactor designed by ECN was a 25 kW indirectly-heated screw that was originally designed for carrying out biomass pyrolysis. The reactor was heated by independently controlled electrical heating elements wrapped around the reactor. Gas and solid temperatures were registered along the axis of the reactor and gas samples were analyzed. Detailed specifications of the screw reactor, inert gas type and flow rates were not reported.

Experimental approaches followed by these reactor studies are summarized in table 2. As listed, these studies used different design parameters, torrefaction operating conditions, sample types, quantities and particle sizes. The sample sizes used in the bench scale studies were an order of magnitude higher than the TGA studies. Of all the reactors that were reported, the ECN continuous reactor is definitely the most advanced reactor. Temperature monitoring and gas sampling capabilities are considerably higher than for the other reactors.

Table 2: Comparisons of torrefaction reactor studies

Study	Reactor Type	Operation	Biomass Sample	Sample weight	Sample Particle size	Inert Gas type, flow rate (ml/min)	Ramp heating rate C/min	Reaction Temp	Reaction residence time
Deng et al [6]	Vertical corundum tube - 60 mm dia, 500 mm length	Bench	Rice straw, Rape stalk	15 g	2 mm dia, 25 mm length	Nitrogen, 500	30-45	200, 250, 300 C	30 min
Couhert et al [9]	Quartz tube reactor - 60 mm internal diameter	Bench	Beechwood	25 g	80-200 micrometer	Nitrogen, 300	10	240, 260 C	1 hr
Pach et al [17]	Cylindrical Reactor	Bench	Birch, Pine, Bagasse	65 g	1-3.2 mm dia	Nitrogen, 83.33, 166.67	Not reported	230, 250, 280 C	1, 2, 3 hrs
Prins et al [15]	Quartz fixed-bed cylindrical reactor placed inside an oven 1 inch X 10 cm	Bench	Beech, willow, straw, larch	10 g	0.7-2.0 mm, <5 mm	Argon	10-20	220-300 C	10-60 min
ECN [18, 19]	Stainless steel cylindrical batch reactor 0.16 m dia, 100 m length	Batch	Willow, beech, larch, Straw	3-6 kg	<10 mm, 10-30 mm, 30-50 mm	Nitrogen	Not reported	220-300 C	10-60 min
ECN [18, 19]	Indirectly heated screw reactor	Continuous	Willow, wood cuttings, demolition wood	1-10 kg/hr	10 mm dia, 20 mm width, 40 mm length	Not reported	Not reported	250-300 C	7.5 to 30 min

3. Tested Biomass Materials

All biomass materials differ a lot in their compositions and they are commonly divided into four categories: coniferous (softwoods), deciduous (hardwoods), herbaceous species or agricultural residues and mixed woods. Quite often the biomass samples belonging to a particular category or even the same biomass sample from different regions differ substantially in elemental composition and it can be confusing to put them in the same category. However, for ease of comparison, an attempt has been made to include the tested samples from different torrefaction studies into these categories as listed in table 3.

Table 3: Tested biomass materials for torrefaction

Biomass Type	Tested Biomass material
Deciduous woods	Eucalyptus [1,8], Beechwood [9,14,15,19], Willow [3,7,14,15,18,19,26], Birch [17], Bamboo [26]
Coniferous woods	Pine [17], Larch [3,14,15,19]
Herb. species/ agri. residues	Reed canary grass [7], Wheat straw [3,7,14,15,19], Sugarcane bagasse [17], Rice straw [6,24], Rape stalk [6], Verge grass [3], Coconut Shell [26]
Mixed woods	Demolition wood [3,18], Ficus Benjamin L Wood [26], Wood cuttings [3]

3.1 Product Yields

The general result for all the tested feedstock is the decreased mass and energy yield of solid torrefied product as the temperature and residence time for torrefaction is increased. A few studies have reported that the deciduous woods (willow, beech) are more reactive than coniferous woods (larch) under the same torrefaction conditions (temperature and residence time) [15, 19]. Much more volatiles, such as acetic acid and methanol, are formed in the case of deciduous woods, which mainly originate from acetoxy- and methoxy-groups present as side chains in hemicelluloses xylose units, which are not present in the coniferous wood. Thermal behavior of a few herbaceous species/agricultural residues such as wheat straw, rice straw, rape stalk and reed canary grass was also tested and studies have concluded that these species have even lesser mass yield than deciduous woods [6, 7, 15, 19]. A higher percentage of hemicelluloses in these species was noted as the reason for the increased mass loss [6, 7]. However, hemicelluloses structural composition for these species was not reported in any of the studies. Chen at al. [26] compared bamboo, willow, coconut shell and wood each with hemicelluloses content of 33.30 %, 20.06 %, 21.03 % and 25.91 % respectively. It was reported that torrefaction of bamboo and willow was more pronounced than that of coconut shell and wood. Even though, the wood sample had more hemicelluloses percentage than willow and coconut shell, it was less reactive for torrefaction. This indicates that it is more important to investigate the structures of hemicelluloses when comparing the reactivity of two samples rather than just looking at the composition percentages. As the torrefaction conditions become more severe, celluloses and lignin decompositions are also increased. Including celluloses and lignin behavior for predicting torrefaction behavior or for comparing samples seems a logical step. Preliminary structure differences for hemicelluloses and cellulose can be inferred from the DTG analyses, but these provide only qualitative results [26].

Results for energy yield of solid product is very similar to that of its mass yield with coniferous wood having the highest energy yield followed by deciduous and herbaceous species. Again, differences in hemicelluloses structural composition and overall content are the reasons for these variations [6, 7, 15, 19]. Bergman et al. [19] reported that the increase in energy density of the solid product is up to 15% for deciduous wood versus up to 7% for coniferous wood at 270°C and 15 minutes reaction time. Bridgeman et al. [7] reported that for all the samples tested for torrefaction, the energy yield of the solid product was greater than the mass yield, an effect which became more marked for higher temperature treatments. The results from this study are shown in figure 1. Relatively more oxygen and hydrogen are released compared to carbon, in the form of water and CO_2, resulting in increased calorific value of the solid product.

Figure 1: Comparison of mass yield and energy yield of torrefied reed canary grass (RCG), wheat straw (WS) and willow wood (WW) at 250 °C and 270 °C and 30 min residence time [7, 10]

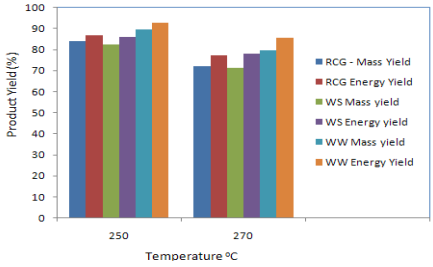

3.2 Effects of Operating Conditions

Studies have used various torrefaction temperature and residence time combinations to evaluate the product yields for the tested samples. Temperatures less than 250 °C have been considered mild for most materials. Bergman et al. [19] reported that for larch, practically all the chemical energy was retained in the solid product up to a temperature of 250 °C and 30 min of residence time. The energy yield of willow, beech and wheat straw was about 95%, 92% and 88% respectively under same torrefaction conditions. Chen et al. [26] reported that at 240 °C and 2 hrs of residence time, 75, 73, 68 and 63 wt% of biomass were remained in wood, coconut shell, willow and bamboo, respectively.

These values were further lowered to 61%, 61%, 48% and 45 % respectively when the temperature was increased to 275 ℃ and residence time kept at 2 hrs. Arias et al. [1] reported that at 280 ℃, even at low residence times, there is large decrease in energy yield for Eucalyptus torrefaction and the mass yield undergoes an important reduction during the first 45min to 1 hr at all three temperatures – 240, 260, 280 ℃. It can be inferred from these results that temperature has more pronounced effect on product yields if a certain minimum residence time is achieved.

Effects of additional variables such as biomass particle sizes, heating rates, inert gas type/flow rates and biomass mineral matter on the torrefaction product yields are scarcely studied topics. Bergman et al. [19] conducted experiments in the batch reactor for different willow size-bins (*viz*., 0-10, 10-30, 30-50 mm). Rather similar solid mass and energy yields were observed despite of the size differences. Minor differences that existed were found to be inconsistent, indicating that particle size do not affect the process. Due to the availability of similar studies from slow pyrolysis investigations, the effects of heating rate variations, during the temperature ramping stage, were not evaluated. Similarly, the effect of inert gases on the torrefaction was not studied in detail. Only the study conducted by Pach et al. [17] reported that there is no strong influence of the role of the inert gas flow on the torrefaction of pine. During the investigations, the nitrogen gas flow was changed from 5 to 10 l/h and the results did show some differences but without any clear trends. The role of biomass mineral matter and metal content during torrefaction has also not been experimentally validated.

3.3 Product Properties

Many studies have evaluated the torrefied product properties to investigate the role played by torrefaction in improving the biomass fuel properties. Grindability, densification, storage, fluidization and char reactivity are the properties that were determined by these studies. This section attempts at discussing the results from these studies based on the tested biomass materials.

3.3.1 Grindability

Biomass feedstock must be dried and ground to particles before using it as a fuel for many combustion and gasification applications. Considerable power consumption is involved in the size reduction operations of raw biomass, thereby, lowering the economic feasibility of these operations. Four studies have attempted to check the size reduction behavior of solid torrefied products to validate the benefits of torrefaction in this regards [1, 6, 18, 19]. Bergman et al. [19] determined grindability by measuring the energy requirements of a heavy duty cutting mill needed to break-up coarse particles to a desired particle size. Considerably lower power consumption was observed for the torrefied biomass in comparison to the untreated biomass as shown in figure 2. Approximately 50% decrease was achieved for willow torrefied at 230 ^{o}C for 30 min. A maximum reduction of 85% was observed for the three willow samples torrefied at 250 ^{o}C, 261 ^{o}C and 271 ^{o}C, each for 30 min. It was reported that neither an increase of temperature in the range of 250 ℃ to 270 ℃ nor a decrease of the reaction time to 8 min at 264 ℃ (willow), reduced the power consumption any further. Similar reduction in power consumption was obtained for all tested biomass samples torrefied above 250 ^{o}C, despite the original differences in shape and polymeric structure. Analysis of dried willow showed that the 65% reduction in power consumtion was due to the chemical changes during torrefaction and the remaining contribution was due to the loss of moisture. Also, the variations in the particle sizes of torrefied willow did not influence the power reduction requirements. Bergman et al. [18] used similar grindability evaluation criteria and observed that the power consumptions of the cutting mill for torrefied biomass are fairly comparable to those of Australian bituminous coal.

Instead of measuring the power consumption of a cutting mill, Arias et al. [1] compared grindability of untreated and torrefied Eucalyptus samples by checking the percentage of ground particles passing through four different size sieves: 425, 425–150, 150–75, and 75 µm. In all cases, the percentage of particles passing to the lower size fractions greatly increased for the torrefied samples. These particle sizes decreased even further with the rise in temperature and residence time for torrefaction. However, torrefaction temperatures greater than 250 ^{o}C were not recommended because the large decrease in mass and energy yields. Deng et al. [6] used similar evaluation criteria with four types of size fractions 450, 450–150, 150– 100 and 100 µm, for sieving ground particles of untreated and torrefied rice straw and rape stalk. It was observed that the ratio of coarse particle size decreased sharply for both kinds of samples after torrefaction. Removal of extra moisture from rice straw was listed as a factor for its better grindability than rape stalk. The percentage of fine particles increased

with the increase of the torrefaction temperature from 200 to 250 °C but the difference was negligible between 250 °C and 300 °C, indicating that grindability benefits were achieved until 250 °C for both the samples.

Figure 2: Relation between power consumption and particle size for willow, beech and larch. Brackets lists the torrefaction temperature (C) and residence time (min). Moisture content (mass basis) values: 10-13% for raw biomass, <1 % for dried willow and 1.2-6.6 % for torrefied biomass [19]

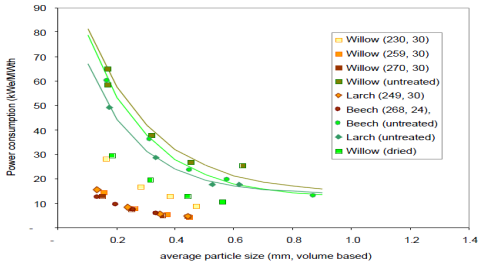

As noted above, studies used different evaluation criteria to determine grindability. Criteria used by Bergman et al. [18, 19] seem to quantify the results with better accuracy in terms of power consumption of the cutting mill. Also, the classification options are less for the studies that used the sieve sizes as the criterion [1, 6]. However, based on the observations from all the grindability studies, it can be concluded that the benefits of grindability is achieved at 250 °C and < 30 min of residence time. These values can form the optimum temperature and residence time conditions if grindability is the main criteria for conducting torrefaction. Effect of operating conditions other than temperature and residence time on the grindability of torrefied biomass was not reported in the literature.

3.3.2 Densification

Studies have reported a decrease in volumetric density of biomass after torrefaction [3, 8, 19]. Bergman et al. [19] reported that the density of torrefied biomass was generally 10-20% lower than the parent feedstock. Rodrigues [8] observed that the increase in temperature resulted in even lower bulk density due to higher mass loss. A couple of studies have investigated the densification of torrefied biomass by pelletisation to form torrefied pellets [3, 21]. The densification process is pre-ceded by the biomass size reduction using a cutting mill. Feedstock involved in these studies include larch, willow, demolition wood, straw and verge grass [3]; and switch grass [21]. Bergman [3] used a piston press to form the pellets and evaluate the densification behavior of torrefied biomass materials produced under different conditions. The press was also operated at different pressures and temperatures and pellets of various diameters were produced. It was reported that the bulk density of torrefied pellets was in the range of 750 to 850 kg/m^3 in comparison to 520 to 640 kg/m^3 range for conventional wood pellets and 230 to 550 kg/m^3 for torrefied biomass. In addition to the increased bulk density, the energy density and mechanical strength of the torrefied pellets were also observed to be higher than the conventional wood pellets and torrefied biomass. Similar study was conducted by Gilbert et al. [21] using a pelletiser that consisted of a hydraulic press capable of providing up to 170 bar (2500 psi) of pressure and operating temperatures up to 300 °C. Torrefied switchgrass was prepared separately at final temperatures of around 250 °C. Tensile strength of the formed pellets was evaluated at varying pressures and temperatures. However, the results were contradictory to those provided by Bergman [3]. The torrefied pellets were observed to be very brittle, uneven and non-homogeneous in shape. The tensile strength of the pellets was reported even lower than that of the shredded grass cases.

These contradictory results for the torrefied pellets can be due to the differences in feedstock used by both studies. The Bergman et al. [3] study had a variety of biomass materials, whereas the Gilbert et al. [21] had only one. Moreover, it is hard to make any conclusions from these studies as some of the key process parameters such as torrefaction temperature, particle sizes after the size reduction process and the pressure-time values actually used in the densification process were not reported. However, both studies included a cooling stage for the torrefied product before starting the size reduction and pelletisation process in order to avoid devolatilization of torrefied product during the operations.

3.3.3 Fluidization

Many combustion and gasification applications require pneumatic transport of raw biomass materials from the feeding systems. Bergman et al. [19] compared the fluidization properties of the untreated willow, torrefied willow and coal using a cold-flow bubbling fluidized bed feeding system with 3 cm x 10 cm x 20 cm particle bed and air as the carrier gas. This is the only study available in the literature that performed these investigations. Smooth fluidization was observed for coal and for wood torrefied at 270 ^{o}C for 30 min with a mean particle size of approximately 100 mm. Additional biomass materials need to be tested to confirm the initial observations from this study.

3.3.4 Deterioration

An important property of torrefied biomass is its hydrophobic nature. It was reported that torrefied biomass loses the capability to form hydrogen bonds with water due to destruction of many OH groups during dehydration reactions [3, 6, 18]. However, very few studies have experimentally verified the hydrophobic nature of torrefied product. Pach et al. [17] observed that the torrefied product (birch, pine and bagasse) has absorbed small amounts of moisture after a period of 30-45 days. But, this moisture content was much less in comparison to the content of moisture of the raw biomass material. In another study, Felfli et al. [11] investigated the hydrophobic characteristics of torrefied briquettes by immersing several torrefied briquettes in water and determining the moisture content by measuring the change in briquette weight. It was determined that the absorbed humidity does not exceed 10 % over the 70-minute retention time and the briquette remains intact, whereas the ordinary briquettes disintegrate in a 10-minute test.

The results from both of these studies are very encouraging in terms of the hydrophobic nature of the torrefied biomass. However, the effects of torrefaction conditions on this property were not reported.

3.3.5 Torrefied Product Reactivity

Testing the behavior of torrefied biomass in the thermo-chemical processes is an important aspect for improving the viability of the torrefaction process. A few studies have attempted to do these analyses by simulating the combustion [1, 7, 16, 18] and [9, 18] gasification conditions in the laboratory. Feedstock tested in these studies include Eucalytus [1]; reed canary grass, wheat straw and willow [7]; wood [16]; wood cuttings and demolition wood [18]; and beechwood [9, 18].

3.3.5.1 Combustion Studies

Thermogravimetric studies [1, 7] and lab-scale burner flames [7, 16, 18] were utilized to study the combustion behavior of torrefied biomass. Arias et al [1] used a non-isothermal TGA for obtaining the differential mass loss (DTG) curves. Approximately 5 mg sample was heated at a constant rate of 15 °C/min under an air flow rate of 50 mL/min. Analysis of the DTG curves for various torrefied samples indicated that the torrefaction only affected the first stage of combustion occurring at temperatures ranging from 235-400 ^{o}C. In this stage, mass losses were lower for the torrefied samples and the values decreased with the increase in torrefaction temperature and residence time. In another study, Bridgeman et al. [7] determined differential temperature measurements (DTA) in addition to the DTG curves. A typical sample mass of 3 mg was heated at 20 ^{o}C/min in a purge of air to a final temperature of 900 ^{o}C. DTG curves showed shorter time period and narrower range of temperatures for the volatile combustion. Most significant changes were observed in wheat straw in comparison to reed canary grass and willow. DTA results indicated higher heats of reactions, lower temperatures for the ignition of the volatile matter and shorter time period for the volatile combustion in comparison to the raw fuel. Bridgeman et al. [7] also used a Meker-burner flame (natural gas) to conduct combustion studies of willow and torrefied willow particles, 2-4 mm in length. A video system was used to record the images of the combusting particles. Reduced volatile combustion times and increased overall char burnout times were observed for the torrefied samples, thus, confirming the results from the TGA studies. Again, these changes were more pronounced for the torrefied willow products of higher torrefaction temperatures and residence times. Pentananunt et al. [16] conducted a similar study and used alcohol flames to investigate combustion behavior of wood. It was observed that the smoking period was much less for torrefied wood than for ordinary wood. At the 50th min when burning was terminated, 15 and 33% of the original combustibles were left in the residues of torrefied wood and wood, respectively. This indicated reduced volatile combustion times for the torrefied wood. In another flame study, Bergman et al. [18] designed a lab-scale combustion simulator (LCS) to simulate a flame/flue gas environment. Conversion behavior of torrefied woodcutting, demolition wood and bituminous coal

was studied after 1000 ms residence time. LCS comprised of a drop tube reactor together with a primary/secondary gas burner. It was observed that the carbon conversion of torrefied biomass is fairly comparable to that of untreated woodcuttings and significantly higher compared to the bituminous coal.

The results from these studies seem logical due to the fact that most of the moisture and volatiles from hemicelluloses decompositions was already released during the torrefaction. This explains the lower mass loss during the first stage of combustion, increased heats of reaction and the shorter time periods for volatile combustion. However, since these studies involved very small samples (few mg), these results can only be regarded as preliminary findings and further investigations should be performed at a higher scale that simulates the industrial combustors more accurately [22]. Also, these observations are very basic and none of the study investigated the effects of torrefaction on the problems of biomass combustion such as alkali and heavy metal releases, ash characteristics, etc.

3.3.5.2 Gasification Studies

A couple of studies evaluated the thermal behavior of the torrefied biomass for gasification applications by simulating entrained flow gasification conditions in the laboratory [9, 18]. A bench-scale high-temperature entrained flow gasification reactor (HT-EFR) was designed by Couhert et al. [9]. Two torrefied beechwood samples produced at 240 ^{o}C and 260 ^{o}C for 1 hour were used as the feedstock. The reactor was electrically heated by an 18 kW three-zone electrical furnace, and was able to reach 1600 ^{o}C in a 1 m long isothermal reaction zone. Constant mass flow rate of 0.5 g/min of torrefied wood particles were fed into the reactor and was swept by a pre-heated atmosphere gas containing 20 volume % of steam in N_2. Gases and particles leaving the reactor were sampled and a then analyzed by a non dispersive IR analyzer and FTIR analyzer. Both the atmosphere gas and the reactor walls were heated to 1200 ^{o}C or 1400 ^{o}C for the experiments. Torrefied samples produced 7% more H_2, 20% more CO and approximately same CO_2 yields in comparison to the parent wood at both gasification temperatures. However, CO_2, CO and H_2 yields were lower at 1200 ^{o}C than at 1400 ^{o}C, indicating that the gasification was not complete at 1200 ^{o}C. Also, proximate analysis performed on solid residues after 1200 ^{o}C gasification showed 66% of ash in the char from the parent wood and only 26% ash from the torrefied wood samples. This showed that the torrefied char is less reactive than the char from the untreated wood. In another study by Bergman et al. [18], the lab-scale combustion simulator (LCS) was used to simulate the entrained flow gasification conditions. Again, beechwood and torrefied beechwood were used as the feedstock. The torrefaction conditions were not reported. It was observed that the carbon conversion of beechwood reached 97-98% after 0.3 s residence time in comparison to 92% for torrefied beechwood. This indicated lower char reactivity for the torrefied samples and thus, achieved similar results as obtained by Couhert et al. [9].

As can be seen from the studies, only torrefied beechwood samples have been tested for gasification application. Since, torrefied biomass can vary a lot due to the differences in the biomass type and the operating conditions, further investigations are needed to confirm these preliminary results. Also, effects of torrefaction on the biomass gasification problems such as alkali and heavy metal release, ash characteristics, etc were not reported.

4. Kinetic Modeling Studies

A few studies have attempted to model the kinetics of torrefaction based on the concepts proposed in the similar studies on pyrolysis kinetics. However, the feedstock, torrefaction methods and the modeling approach used by these studies were quite different. Prins et al. [14] modeled the torrefaction of willow by using the two step mechanism concept of the isothermal degradation of xylan, with parallel reactions for the formation of solids and volatiles [12]. Weight loss curves obtained from the TGA experiments were used for the determination of kinetic parameters. The model with the first order reactions for both the steps was found to be valid and a demarcation time existed between the steps. The model was verified by comparing the values of final char yields as found from the experiments and the ones calculated by the model. It was concluded that the torrefaction kinetics in the temperature range of 230-300 ^{o}C can be accurately described by this model. Hemicellulose and cellulose decompositions can be represented by the first and second steps respectively. However, the weight loss curves did not become completely horizontal and continued to decrease slowly due to the decompositions of less reactive components such as lignin that were not included in the model. Felfli et al. [5] introduced a mathematical model for the torrefaction of wood logs and biomass briquettes.

The model aimed at estimating the operating parameters for torrefaction furnaces such as minimum time of torrefaction, energy consumption and the mass yield. It described both chemical and physical processes that take place in a moist piece of wood heated at temperatures between 230 and 300 ^{o}C. The torrefaction kinetics was based on a three-reaction scheme in which competing primary two-step reaction pyrolyze biomass to gas, tar and charcoal. The primary reaction rates were represented with Arrhenius-type temperature dependence and were first-order with respect to the mass of unreacted biomass. The model was validated by conducting torrefaction experiments on dry sample in an electric furnace at temperatures of 130, 230, 260 and 280 ^{o}C. Experimental and theoretical temperature profiles were then correlated. It was noticed that at 403 K, the data correlation is closer than on other conditions. The agreement between the model and experimental data is good in the temperature range 230 ^{o}C to 260 ^{o}C. However, the model lags experimental data for 280 ^{o}C. These differences were linked to the carbonization reactions for cellulose and lignin, as these were not included in the model. Deng et al. [6] proposed a kinetic model for the generation of gases during torrefaction for rice straw and rape stalk samples. A series of independent first order parallel reactions, each having individual apparent activation energy was assumed. Data was collected from the torrefaction experiments performed in the bench-scale reactor. The rate constant for each gas was found by plotting the change in gas moles with the time at different temperatures. These rate constant values were then used to find the activation energies by using the Arrhenius function. Model did not include any solid char yield determination and verification of the model was also not reported.

The kinetic models presented by these studies are for individual feedstock and may not be valid for a wide range of biomass materials. Only willow [14]; wood logs and briquettes [5]; rice straw and rape stalk [6] have been tested so far. Due to the low temperature range of torrefaction, only hemicelluloses have been included in the kinetic models. However, at temperature higher than 250 ^{o}C, the degradation of cellulose and lignin do become important and this was the reason of deviation of the model results from the experimental values [5, 14]. Further kinetic studies that include steps for cellulose and lignin components should be performed with additional biomass materials. Also, kinetics of torrefied materials in the combustion and gasification processes should be investigated in order to better understand the effects of torrefaction on these processes.

5. Recommendations for Future Work

Thermogravimetric analysis (TGA) and reactor studies were the main experimental methods used to carry out torrefaction. Considerable differences were found in the behavior of biomass materials during torrefaction. Solid product mass and energy yields are strongly influenced by the raw biomass composition and the operating conditions such as temperature and residence time. Among the evaluated product properties, grindability is the most studied topic. Very few studies attempted to investigate the densification, fluidization, storage and char reactivity of torrefied products. Concepts from pyrolysis kinetics were utilized by a few studies to model kinetics of torrefaction, but only hemicelluloses decomposition was included in the analysis. Reviewing the literature suggests that torrefaction is a promising technique to improve the performance of biomass for energy utilization. However, despite a number of impressive studies on the topic, a lot of information is still not recognized in sufficient detail. Following are some of the potential research areas that can be pursued to improve our understanding of the torrefaction process and its role in improving the biomass fuel properties:

1. Evaluate torrefied product yields and properties for the biomass materials that are potential fuels for a particular region
2. Torrefied product reactivity analysis for combustion and gasification applications using other biomass types
3. Study of alkali and heavy metal release from combustion and gasification of torrefied biomass
4. Analyze effects of biomass mineral and metal content, biomass particle sizes, heating rates, inert gases composition and flow rates on the torrefied product yields and properties
5. Verification of kinetic models with the reaction steps for hemicellulose, cellulose and lignin Investigate kinetics of torrefied products in combustion and gasification processes
6. Analyze effects of torrefaction operating conditions on the densification, fluidization and storage properties of torrefied biomass
7. Pelletisation of torrefied products should be evaluated for additional biomass materials

References

(1) Arias, B., C. Pevida, J. Fermoso, M.G. Plaza, F. Rubiera, J.J. Pis. 2008. Influence of torrefaction on the grindability and reactivity of woody biomass. Fuel Processing Technology 89: 169-175
(2) Prins, M.J., K.J. Ptasinski, F. Janssen. 2006. More efficient biomass gasification via torrefaction. Energy 31: 3458-3470
(3) Bergman, P.C.A., 2005. Combined torrefaction and pelletisation – The TOP process. ECN Biomass, ECN-C--05-073
(4) Bergman, P.C.A and J. Kiel. Torrefaction for biomass upgrading. ECN Biomass, ECN-RX-05-180
(5) Felfli, F.F. and C.A. Luengo. Mathematical modeling of wood and briquettes torrefaction. IFGW/DFA/GCA, Universidade Estadual de Campinas, Brasil
(6) Deng, J., G-J. Wang, J-H. Kuang, Y-L. Zhang, Y-H. Luo. 2009. Pretreatment of agricultural residues for co-gasification via torrefaction. J. Anal. Appl. Pyrolysis 86 (2009) 331-337
(7) Bridgeman, T.G., J.M. Jones, I. Shield, P.T. Williams. 2008. Torrefaction of reed canary grass, wheat straw and willow to enhance solid fuel qualities and combustion properties. Fuel 87 (2008) 844-856.
(8) Rodrigues, T. O., P.L.A. Rousset. 2009. Effects of torrefaction on energy properties of Eucalyptus Grandis Wood. Cerne, Lavras, v. 15, n. 4, p. 446-452, out./dez. 2009
(9) Couhert, C., S. Salvador, J-M Commandre. 2009. Impact of torrefaction on syngas production from wood. Fuel 88 (2009) 2286-2290.
(10) Svoboda, K., M. Pohorely, M. Hartman, J. Martinec. 2009. Pretreatment and feeding of biomass for pressurized entrained flow gasification. Fuel Processing Technology 90 (2009) 629-635
(11) Felfli, F.F., G.A. Luengo., J. A. Suarez., P.A. Beaton. 2005. Wood briquette torrefaction. Energy for sustainable development. Volume IX No. 3
(12) Blasi, C.D., and M. Lanzetta. 1997. Intrinsic kinetics of isothermal xylan degradation in inert atmosphere. Journal of Analytical and Applied Pyrolysis 40-41 (1997) 287-303
(13) Lipinsky, E.S., J.R. Arcate, T.B. Reed. 2002. Enhanced wood fuels via torrefaction. Fuel chemistry division preprints. 47 (1). 409
(14) Prins, M.J., K.J. Ptasinski, F.J.J.G. Janssen. 2006. Torrefaction of wood Part 1. Weight loss kinetics. J. Anal. Appl. Pyrolysis 77 (2006) 28-34
(15) Prins, M.J., K.J. Ptasinski, F.J.J.G. Janssen. 2006. Torrefaction of wood Part 2. Analysis of products. J. Anal. Appl. Pyrolysis 77 (2006) 35-40
(16) Pentananunt, R., A.N.M.M. Rahman., S.C. Bhattacharya. 1990. Upgrading of biomass by means of torrefaction. Energy Vol. 15, No. 12, pp 1175-1179
(17) Pach, M., R. Zanzi, E. Bjornbom. 2002. Torrefied biomass a substitute for wood and charcoal. 6th Asia-Pacific International Symposium on Combustion and Energy Utilization. 20 -22 May 2002, Kuala Lumpur
(18) Bergman, P.C.A., A.R. Boersma, R.W.R. Zwart, J.H.A, Kiel. 2005. Torrefaction for biomass co-firing in existing coal-fired power stations “Biocoal”. ECN, Biomass, ECN-C—05-013
(19) Bergman, P.C.A., M.J. Prins, A.R. Boersma, K.J. Ptasinski, J.H.A. Kiel, F.J.J.G. Janssen. Torrefaction for entrained-flow gasification of biomass. ECN Biomass, ECN-C-05-067
(20) Bergman, P.C.A., M.J. Prins, A.R. Boersma, K.J. Ptasinski, J.H.A. Kiel, F.J.J.G. Janssen. Torrefaction for entrained-flow gasification of biomass. ECN Biomass, ECN-RX—04-046
(21) Gilbert, P., C. Ryu, V. Sharifi, J. Swithenbank. 2009. Effect of process parameters on pelletisation of herbaceous crops. Fuel 88 (2009) 1491-1497
(22) TA Instruments Report TA-125. Thermal Analysis Application Brief -Estimation of Polymer Lifetime by TGA Decomposition Kinetics
(23) Arcate, J. R. 2002. Torrefied wood, an enhanced wood fuel. Bioenergy 2002 conference, Biose, Idaho, September 22-26, 2002, paper number 207
(24) Kargbo, F.R., J. Xing, Y. Zhang. 2009. Pretreatment for energy use of rice straw: a review. African Journal of Agricultural Research Vol. 4 (13), pp. 1560-1565
(25) Nimlos, M.N., E. Brooking, M.J. Looker, R.J. Evans. 2003. Biomass Torrefaction studies with a molecular beam mass spectrometer. Prepr. Pap.-Am. Chem. Soc., Div. Fuel Chem. 2003, 48 (2), 590-591
(26) Chen, W-H., and P-C Kuo. 2010. A study on torrefaction of various biomass materials and its impact on lignocellulosic structure simulated by a thermogravimetry. Energy 35 (2010) 2580-2586

Paper II

Torrefaction of Norwegian birch and spruce – an experimental study using macro-TGA

Tapasvi, D.; Khalil, R. A.; Skreiberg, Ø.;

Tran, K.-Q.; Gronli, M. G.

Energy Fuels 2012, 26, 5232–5240.

energy&fuels

Article

pubs.acs.org/EF

Torrefaction of Norwegian Birch and Spruce: An Experimental Study Using Macro-TGA

Dhruv Tapasvi,*[,†] Roger Khalil,[‡] Øyvind Skreiberg,[‡] Khanh-Quang Tran,[†] and Morten Grønli[†]

[†]Department of Energy and Process Engineering, Norwegian University of Science and Technology (NTNU), NO-7491 Trondheim, Norway

[‡]Department of Thermal Energy, SINTEF Energy Research, NO-7465 Trondheim, Norway

ABSTRACT: This work aims to analyze the torrefaction process with Norwegian birch and spruce as feedstocks. Torrefaction experiments were performed in a macro-TGA (thermogravimetric analysis) reactor with provisions for continuous volatile measurements through micro-GC (gas chromatography) and FTIR (Fourier transform infrared spectroscopy). The process temperature (225 and 275 °C), holdup time (30 and 60 min), and sample size (10 and 40 mm cubes) were included as variations in the experimental matrix. Fuel characterizations, DTG (derivative thermogravimetric) curves, product yields, hydrophobicity tests, grinding energies, and particle-size distributions are discussed. The raw fuels were used as a reference for the comparisons. It was found that the birch has a higher devolatilization rate than the spruce under all tested conditions, resulting in a larger percentage increase in its carbon content. An increase in the temperature has the strongest effect on the properties of the torrefied product among all of the studied parameters. At 275 °C, the solid yield decreased to 63% and 75% for the torrefied birch and spruce, respectively. In terms of torrefied product properties, the torrefied samples absorbed approximately one-third of the moisture compared to the raw fuels. The total grinding energy decreased up to 40−88% for the torrefied samples of both feedstocks. An increased percentage of fine particles (<180 μm) was found in the particle-size distributions of most of the torrefied samples. Overall, considerable improvements were observed in the properties of the torrefied products for both feedstocks. Results obtained from this study form the basis of a torrefaction feasibility study in Norway.

1. INTRODUCTION

Biomass is an important renewable energy source and has the potential to play a significant role in the energy future of Norway. The potential of biomass to help meet the world energy demand is widely recognized. The increased use of biomass in key sectors, including heat, power, transportation fuel, and bioproduct production, will also extend the lifetime of fossil fuel resources. A number of thermal conversion processes such as pyrolysis, combustion, and gasification have been applied to develop biomass conversion technologies. In addition, the energy consumption from biomass is considered to be CO_2 neutral. According to *World Energy Outlook 2009*,[1] Norway has a goal of reducing its greenhouse gas emissions by 30% before 2020 and by 100% before 2050, and an extended use of biomass will certainly help meet this goal.

To date, the widespread use of biomass has been hindered by many problems, such as its low bulk density, high moisture content, poor grindability properties, and relatively low calorific value. Solutions for biomass pretreatment to overcome these drawbacks are being studied by researchers.[2,3] Torrefaction has been recognized as one solution. It is basically a mild pyrolysis of the biomass that is typically conducted at 200−300 °C, under nearly atmospheric pressure, in the absence of oxygen and with a relatively low particle heating rate (<50 °C/min).[2−4] During torrefaction, the biomass is partly decomposed, which yields a uniform, solid product as well as condensable liquids and noncondensable gases.[5] The main reactions during torrefaction involve xylan-containing hemicellulose polymers, which are the most reactive polymer structures in biomass.[6−9] Torrefaction results in the following main improvements in the biomass properties: (1) a considerable reduction in the moisture content due to drying;[10−12] (2) an increased energy density and heating value due to a reduction in the O/C ratio;[5,8,11,13] (3) intrinsic conversion of the hygroscopic behavior of the raw biomass into the hydrophobic behavior of the torrefied biomass;[14] (4) enhanced grindability, which results in less energy consumption during milling.[15−17] Because of these altered properties, the value of the torrefied biomass as a fuel is significantly higher than that of the raw biomass. The role of torrefaction in improving the biomass properties has been investigated in several studies. The majority of these studies have focused on examining the compositional changes in the form of proximate and ultimate analyses[18−20] and mass and energy yields[5,13,14,21−23] of the woody biomass materials, agricultural residues, and energy crops. Studies have also attempted to investigate the torrefied product properties such as hydrophobicity,[24] grindability,[14−17,25] particle-size distribution,[16,26] and reactivity in combustion,[13,24,27] gasification,[11,28] or pyrolysis[18,29] processes. As reported in previous studies, the chemistry of torrefaction is influenced by many parameters such as the biomass composition, processing temperature, holdup time, and particle size. This means that, in order to evaluate the feasibility of torrefaction in a particular region, local available biomass resources should be investigated. For Norway, a comparison between hardwood (birch) and softwood (spruce) is very important because these are the two main wood species available. So far, no study is available

Received: February 26, 2012
Published: July 18, 2012

   dx.doi.org/10.1021/ef300993q | *Energy Fuels* 2012, 26, 5232−5240

Table 1. Proximate and Ultimate Analyses of Feedstocks

	proximate analysis			ultimate analysis					
sample	VM[a]	fC[a]	ash[a]	C[a]	H[a]	O[a]	N[a]	S[a]	HHV[b]
birch	89.43	10.35	0.22	48.62	6.34	44.90	0.09	0.05	19.80
spruce	86.34	13.43	0.23	50.10	6.36	43.52	0.07	0.05	20.45

[a]wt %, dry basis. [b]MJ/kg.

that has investigated the torrefaction behavior of these two wood species. This forms the main objective of this study. There are a few studies available[5,8,25] that have compared hardwoods and softwoods for torrefaction; however, only mass and energy yields or individual properties such as grindability are discussed. This study tries to overcome this deficiency and compares hardwood and softwood in terms of product yields as well as product characteristics.

The second objective of this study is to utilize the concept of macro-TGA (thermogravimetric analysis) to study the torrefaction behavior of Norwegian birch and spruce. Either micro-TGA[8,13,21] or laboratory-scale reactors[5,11,14,30−32] were used in previous studies to perform torrefaction, and on the basis of the literature review by the authors, no torrefaction study has utilized macro-TGA so far. The kinetically controlled thermal weight loss characteristics of biomass can be measured precisely in micro-TGA, which in this respect makes it more advantageous than a laboratory-scale reactor for mass loss kinetic studies. Because of the small sample weights used (a few milligrams), negligible heat- and mass-transfer limitations exist in micro-TGA, which is not the case in a commercial plant. This is not the case either in macro-TGA, which can accommodate much larger biomass samples than micro-TGA (in our case, 200−300 g and individual pieces with up to 40 mm sides). It then becomes possible to study thermal processes with heat- and mass-transfer limitations and simultaneously perform weight loss measurements. In another study conducted by one of the authors,[33] the pyrolysis behaviors of biomass materials were compared using both micro-TGA and macro-TGA. It was reported that the pyrolysis of wood occurs faster in micro-TGA than macro-TGA because the heat- and mass-transfer limitations of the larger samples used in macro-TGA cause a lag in the temperature evolution of the wood samples. Therefore, in order to understand the temperature lag in a large-scale industrial torrefaction process, the unique approach of macro-TGA is used in this study. In addition, the DTG (derivative thermogravimetric) curves as collected from macro-TGA can be evaluated further to deduce heat- and mass-transfer limitations.

The focus of the work was to analyze the effects of the torrefaction temperature, holdup time, and sample particle size on the DTG curves, biomass compositions, product yields, and fuel properties of both feedstocks. Proximate and ultimate analyses of both the raw and torrefied products were performed to determine their compositions. The evaluated fuel properties include hydrophobicity, power requirements for grinding, and particle-size distribution after grinding. Torrefaction experiments were also performed in micro-TGA, using the same feedstocks, to confirm the temperature lag in the macro-TGA process.

2. MATERIALS AND METHODS

2.1. Sample Characterization and Preparation. Norwegian birch and spruce fuel samples were obtained from local sources in Trondheim, Norway. These samples were standardized wood boards that are typically used in buildings. The raw samples and torrefied products obtained from macro-TGA experiments were characterized with proximate and ultimate analyses, the results of which are presented in Tables 1 and 3, respectively, including the higher heating values (HHVs).

The proximate analyses of the raw samples were conducted according to the ASTM standards ASTM E871, ASTM E872, and ASTM D1102 for moisture content, volatile matter, and ash content, respectively. In addition, the ASTM 1762-84 standard methods, applicable to charcoal powders, were applied to conduct the proximate analyses of the torrefied products. The fixed carbon content was calculated by difference to 100% in both cases. The determination of the C/H/N/S content in the ultimate analysis was conducted using an "EA 1108 CHNS-O" elemental analyzer by Carlo Erba Instruments. The oxygen content was calculated by difference to 100% for all samples. The HHV was calculated based on the elemental composition of the fuel.[34] Before the torrefaction experiments in macro-TGA, the samples were carefully cut to provide cubes with sides of either 10 or 40 mm and the cubes were then dried for 24 h at 105 °C. For the micro-TGA experiments, raw samples were ground in a cutting mill with a 1 mm bottom sieve.

2.2. Setup and Procedure for Torrefaction Experiments. The biomass torrefaction experiments were conducted in a batch reactor equipped with a macro-thermobalance (macro-TGA), using the experimental setup shown in Figure 1. This unique reactor was built by Höker KFT (Hungary) according to the design specifications from SINTEF Energy Research. The biomass fuel samples were placed in a rectangular basket that was connected to the balance, and the sample basket was lowered into the reactor prior to heating.

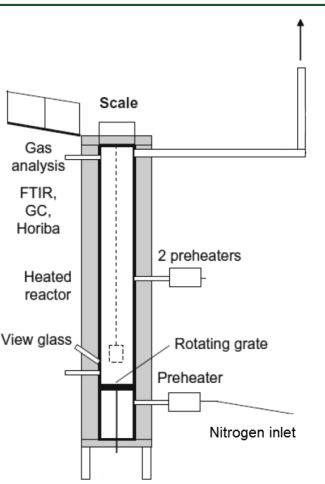

Figure 1. Drawing of the torrefaction macro-TGA reactor.

dx.doi.org/10.1021/ef300993q | Energy Fuels 2012, 26, 5232−5240

The sample basket was composed of several separated layers, and care was taken to provide a small gap between the cubes on each layer to provide uniform heat- and mass-transfer conditions for all cubes. The balance was connected to the reactor top and was cooled with nitrogen gas to prevent overheating. The sample weight was 200−300 g, depending on the density and size of the feedstock used. A constant flow rate of 100 L/min of nitrogen was used to provide an inert atmosphere inside the reactor. The samples were heated to either 225 or 275 °C at a heating rate of 5 °C/min. The torrefaction start time was measured from the point when the temperature first reached the target torrefaction temperature. The reactor was purged with nitrogen for at least 1 h prior to the start of the experiment. Before the torrefaction experiments were started, an online oxygen analyzer was used to ensure that the reactor was free of oxygen.

The macro-TGA experiments focused on the study of important parameters such as the fuel type (softwood and hardwood), holdup time in the torrefaction zone (30 and 60 min), sample size (10 and 40 mm cubes), and torrefaction temperature (225 and 275 °C). The complete experimental matrix produced 16 different types of torrefied materials, as shown in Table 2.

Table 2. Experimental Design

expt no.	sample	final temperature [°C]	sample cubes [mm]	holdup time [min]
1	birch	225	10	30
2	birch	225	40	30
3	birch	225	10	60
4	birch	225	40	60
5	spruce	225	10	30
6	spruce	225	40	30
7	spruce	225	10	60
8	spruce	225	40	60
9	birch	275	10	30
10	birch	275	40	30
11	birch	275	10	60
12	birch	275	40	60
13	spruce	275	10	30
14	spruce	275	40	30
15	spruce	275	10	60
16	spruce	275	40	60

All of the reaction products were collected and weighed to determine an overall mass balance. The gas produced in the experiments was measured using FTIR (Fourier transform infrared spectroscopy) and micro-GC (gas chromatography). The outlet tube from the reactor was maintained at an elevated temperature of approximately 200 °C to prevent condensation of the released volatiles.

In order to show the differences between the micro-TGA and macro-TGA processes, torrefaction experiments were conducted in the micro-TGA Q5000 by TA Instruments. Torrefaction temperatures of 225 and 275 °C with a holdup time of 60 min were selected in the micro-TGA temperature programs, resulting in a total of four experiments, two for each feedstock. A heating rate of 5 °C/min, up to the torrefaction temperatures, was included in the programs to ensure maximum similarity with the macro-TGA experiments. The sample weight was 3−5 mg, and the inert nitrogen gas environment was maintained inside the micro-TGA instrument during all experiments.

2.3. Assessment Methods. Grindability, particle-size distribution, and hydrophobicity assessments were performed for the torrefied products obtained from macro-TGA experiments.

The grindability assessment was divided into two stages: pregrinding and fine grinding. In the pregrinding stage, the raw and torrefied samples were ground in a cutting mill without a bottom sieve. This stage produced smaller particles that facilitated the feeding step of the fine-grinding stage. The fine-grinding stage was performed using the same cutting mill equipped with a 1 mm bottom sieve. A numerical watt meter, Paladin 256-TWKW from Cromptan Instruments, was employed to record the amount of electricity consumed during the grinding in both stages. A computer with a data logger was connected to the watt meter for data acquisition every 2 s. The mill was operated using the same parameters for all samples. The power consumption for an empty load was logged prior to every grinding step to determine the increase in the energy consumption when the mill was under load. The specific energy consumption for grinding was determined by integrating the area under the power consumption curve (watts-seconds) over the total time required to grind a given sample. Because a known quantity of samples was used in each experiment, the energy consumption is divided by the number of samples grinded to obtain the final values per unit mass for comparison. The integrated values from both grinding stages were added together to calculate the total grinding requirement for a sample.

The powder samples produced after the milling step were sieved in a vibrating sieving machine (Fritsch Analysette 3 Pro) that contained a series of sieves with the following mesh sizes: 1 mm, 500 μm, 180 μm, 125 μm, and 63 μm. The mass of each sample collected on the different sieves was measured and recorded as a percentage of the initial sample mass to evaluate the particle-size distribution as a function of the torrefaction parameters studied.

The hydrophobic characteristics of all raw and torrefied samples were investigated by immersing the samples in distilled water for 2 h in glass beakers without stirring.[24] The water was drained from the beakers and the moisture content of the samples was measured as a change in the corresponding initial sample weight.

3. RESULTS AND DISCUSSION

3.1. Fuel Characterization of the Torrefied Solids. As mentioned previously, the proximate and ultimate analyses for the torrefied solids obtained from the macro-TGA experiments were performed according to the ASTM standards 1762-84. Table 3 shows the results from these analyses. As observed in the table, increasing the temperature or holdup time reduced the volatile matter and increased the fixed carbon content of the torrefied solids. In addition, at all tested torrefaction conditions, the torrefied birch exhibited a higher percentage increase in the fixed carbon content (or decrease in volatile matter) compared to the torrefied spruce. The most significant difference between these feedstocks is observed for the 40 mm cube samples that were treated at 275 °C with a 60 min holdup time. The maximum increase in the fixed carbon content of the torrefied birch samples relative to the raw fuel is 176.7%; for the spruce, the increase is 77.9%. Corresponding values for the increase in the fixed carbon content as reported by previous studies for

Table 3. Proximate and Ultimate Analyses of the Torrefied Samples

	proximate analysis			ultimate analysis					
sample	VM[a]	fC[a]	ash[a]	C[a]	H[a]	O[a]	N[a]	S[a]	HHV[b]
birch; 225 °C; 10 mm; 30 min	87.68	12.09	0.23	49.63	6.13	44.09	0.10	0.05	20.00
birch; 225 °C; 40 mm; 30 min	88.24	11.64	0.12	49.93	5.99	43.93	0.10	0.05	19.90
birch; 225 °C; 10 mm; 60 min	86.38	13.23	0.39	49.90	5.98	43.97	0.10	0.05	19.90
birch; 225 °C; 40 mm; 60 min	87.14	12.67	0.19	50.22	5.99	43.64	0.10	0.05	20.10
spruce; 225 °C; 10 mm; 30 min	84.43	15.34	0.23	50.60	6.16	43.13	0.06	0.05	20.46
spruce; 225 °C; 40 mm; 30 min	85.52	14.22	0.26	50.40	6.32	43.17	0.06	0.05	20.58
spruce; 225 °C; 10 mm; 60 min	83.99	15.79	0.22	50.97	6.15	42.76	0.07	0.05	20.62
spruce; 225 °C; 40 mm; 60 min	84.94	14.75	0.31	50.77	6.17	42.94	0.07	0.05	20.55
birch; 275 °C; 10 mm; 30 min	79.98	19.77	0.25	53.71	5.65	40.47	0.12	0.05	21.20
birch; 275 °C; 40 mm; 30 min	77.14	22.64	0.22	55.55	5.77	38.50	0.13	0.05	22.20
birch; 275 °C; 10 mm; 60 min	77.67	21.93	0.40	54.16	5.65	40.02	0.12	0.05	21.40
birch; 275 °C; 40 mm; 60 min	71.02	28.64	0.34	57.21	5.51	37.10	0.13	0.05	22.60
spruce; 275 °C; 10 mm; 30 min	78.13	21.47	0.40	54.38	5.81	39.69	0.07	0.05	21.72
spruce; 275 °C; 40 mm; 30 min	76.68	23.01	0.31	55.01	5.77	39.10	0.07	0.05	21.96
spruce; 275 °C; 10 mm; 60 min	75.65	24.15	0.20	55.33	5.73	38.80	0.09	0.05	22.05
spruce; 275 °C; 40 mm; 60 min	75.77	23.89	0.34	56.04	5.66	38.17	0.08	0.05	22.28

[a]wt%, dry basis. [b]MJ/kg.

other wood materials treated at 275 °C with 30 min of holdup time are 90.1% for leucaena,[18] 66.1% for logging residue chips,[15] and 69% for pine chips.[15]

Among all of the tested process parameters, temperature has the strongest effect on the torrefied biomass composition. As the temperature increases from 225 to 275 °C, the fixed carbon content in the torrefied products rises from approximately 11% to 28% for the birch samples and from 14% to 24% for the spruce samples. For the samples treated at 225 °C, the effect of increasing the holdup time is negligible for both feedstocks. However, when the holdup time is increased at 275 °C, the fixed carbon content increases from approximately 20% to 28% for the birch samples and from 21% to 24% for the spruce samples. These results suggest that most of the changes at 225 °C occur within the first 30 min of the holdup time, whereas these changes occur for 60 min at 275 °C. The proximate analysis results also show noticeable variations due to the increase in the sample size. For both feedstocks, the 10 mm cubes are more reactive than the 40 mm cubes when treated at 225 °C, but there are no clear trends at 275 °C.

The ultimate analyses of the feedstocks showed that increases in the torrefaction temperature and holdup time result in a higher carbon content, lower hydrogen content, and lower oxygen content in the samples. The exceptions are the nitrogen and sulfur contents, which remained nearly constant; this result is in accordance with previous studies.[13] Again, an increase in the temperature has the largest effect on the compositional changes compared to an increase in the holdup time or sample size. In addition, the birch samples exhibited a larger percentage increase in the carbon content and a larger decrease in the hydrogen and oxygen contents than the spruce samples at all tested conditions. Compared to the untreated samples, the increase in the carbon content after torrefaction ranges from 2.1% to 17.7% for the birch samples and from 0.8% to 12.1% for the spruce samples. For the birch samples, the corresponding decreases in the hydrogen and oxygen contents are 3.3% to 13.1% and 1.8% to 17.4%, respectively. For the spruce samples, the decreases in the hydrogen and oxygen contents are 0.6% to 11.0% and 0.8% to 12.3%, respectively. The largest composition changes are exhibited by the 40 mm cube birch and spruce samples that were treated at 275 °C with a holdup time of 60 min.

A consequence of the higher carbon and lower hydrogen and oxygen contents is a decrease in the atomic O/C and H/C ratios for the torrefied samples compared to the raw samples. These results are presented in a Van Krevelen diagram in Figure 2. The O/C and H/C ratios are 0.69 and 1.56 for the raw birch samples and 0.65 and 1.53 for the raw spruce samples, respectively. For both feedstocks, these ratios decrease only marginally at a torrefaction temperature of 225 °C. However, there is a significant decrease when the torrefaction temperature is increased. At 275 °C, the O/C and H/C ratios decrease by up to 30% and 26% for the birch and by up to 21% and 20% for the spruce, respectively.

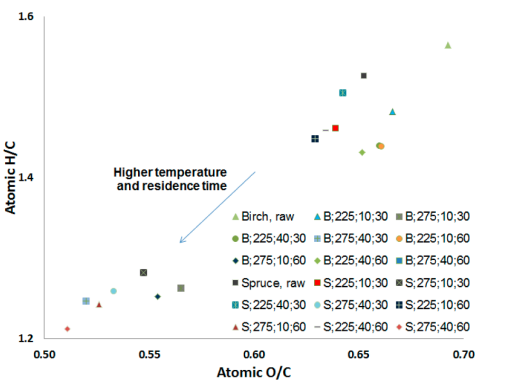

Figure 2. Van Krevelen diagram for the raw and torrefied samples [type; temperature (°C); cube size (mm); holdup time (min)].

These changes in the chemical compositions of the birch and spruce samples are attributed to the extensive removal of hydrogen and oxygen, forming mainly H_2O and CO_2 during torrefaction. The decrease in the relative concentrations of these elements in the solid residue leads to the improvement of these feedstocks as energy sources, which is illustrated by the HHVs shown in Table 3. As expected, the increase in the HHV

dx.doi.org/10.1021/ef300993q | Energy Fuels 2012, 26, 5232−5240

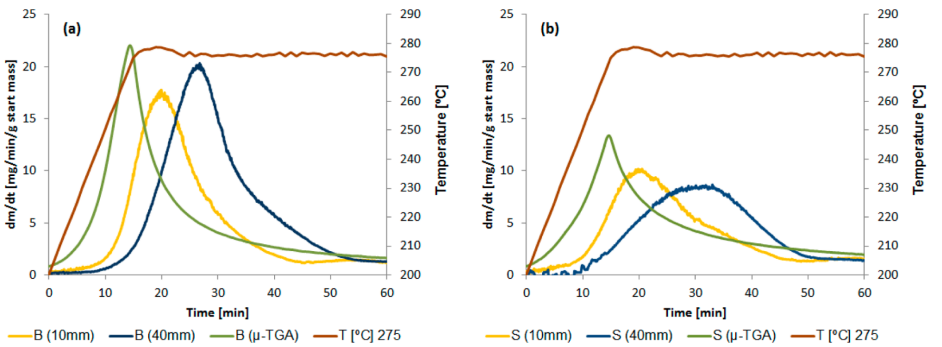

Figure 3. DTG curves (weight loss rate in mg/min relative to the initial weight) for experiments conducted at 275 °C with a holdup time of 60 min (a) for birch and (b) for spruce.

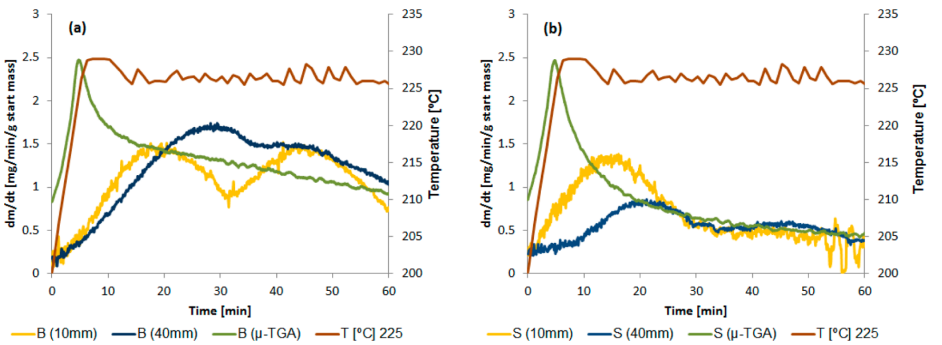

Figure 4. DTG curves (weight loss rate in mg/min relative to the initial weight) for experiments conducted at 225 °C with a holdup time of 60 min (a) for birch and (b) for spruce.

is larger for the birch than for the spruce. The raw birch and spruce have HHVs of 19.8 and 20.45 MJ/kg, respectively. For the samples treated at 225 °C, there is only approximately a 0.5−1% increase in these values. However, at 275 °C, the HHV increase up to 14.3% for the birch samples and 8.9% for the spruce samples. These results reflect the compositional differences between these feedstocks, with the birch being more reactive than the spruce under torrefaction conditions. The percentage increases in HHV as reported by previous studies for other wood samples treated at 225 and 275 °C with 30 min of holdup time are 4.4% and 12.3% for leucaena,[18] 5.3% and 17.2% for logging residue chips,[15] and 5.5% and 18.2% for pine chips,[15] respectively. This indicates that, for the samples treated at 225 °C, a higher increase in HHV is reported in these studies in comparison to this study. This can be attributed to differences in the biomass compositions as well as the torrefaction conditions in macro-TGA in comparison to the reactors used in these studies.

3.2. Macro-TGA. The DTG curves obtained from the macro-TGA experiments are shown in Figures 3a,b and 4a,b for the two torrefaction temperatures (275 and 225 °C). To facilitate interpretation, the experiments with a holdup time of 30 min are not included. From these figures, the following can be observed: (1) the birch has a higher devolatilization rate than the spruce at both temperatures; (2) the peaks for the experiments at 275 °C are 1 order of magnitude higher than those at 225 °C; (3) the weight loss rate flattens out before the holdup time of 60 min is reached for all experiments at 275 °C; (4) the experiments performed at 225 °C exhibit double peaks compared to only one peak at 275 °C; (5) the differences in the maximum and minimum devolatilization rates are much smaller at 225 °C than at 275 °C; (6) for both the birch and spruce samples at both temperatures, the DTG peaks for the 40 mm cubes are shifted slightly to the right compared to the peaks for the 10 mm cubes.

As mentioned previously, birch is a hardwood and spruce is a softwood. Previous studies have shown that softwoods react slower than hardwoods;[5,8] this is confirmed by our results, as shown in Figures 3 and 4. These differences may be attributed to the composition of the hemicellulose fractions in these wood types because it has been reported that the amount of the most reactive hemicellulose component (xylan) is present in less quantities in softwoods than in hardwoods.[8] The higher devolatilization rate at 275 °C compared to 225 °C is due to the higher degradation of the hemicellulose fraction, along with the initial reactions of cellulose decomposition that may occur at temperatures above 250 °C.[8,9,21]

In Figure 4, the appearance of the first peaks may be due to the chemically bound moisture released from the feedstocks, and the second peaks may indicate limited hemicellulose decompositions. The flattening of the weight loss rate before reaching the 60 min holdup time may indicate completion of the hemicellulose decomposition at 275 °C. Because of a lower surface area per unit mass, more time is needed to start the decomposition reactions for the 40 mm cubes than for the 10

dx.doi.org/10.1021/ef300993q | Energy Fuels 2012, 26, 5232−5240

mm cubes. This results in shifting of the peaks of the DTG curves to the right with increased sample cube sizes.

To show the differences between macro-TGA and micro-TGA, DTG curves obtained from the four micro-TGA experiments are also included in Figures 3 and 4. The DTG peaks from these experiments lie to the left of the corresponding peaks from the macro-TGA experiments. This clearly indicates that there is a temperature lag associated with the macro-TGA experiments because of much higher samples weight and heat- and mass-transfer limitations. DTG curves obtained from macro-TGA are much closer to the ones that will be obtained in an actual industrial process.

3.3. Product Yields. During torrefaction of the birch and spruce samples in macro-TGA, volatile compounds were released into the gas phase, leaving solids as the main product (torrefied biomass). The solids were collected and weighed for mass balance calculations and further studies. The color of the solid product varied from light brown for torrefaction at 225 °C to dark brown at 275 °C. The volatiles were composed of permanent (mainly CO_2 and CO) and condensable gases. The release of the gas fraction was quantitatively monitored by FTIR in combination with micro-GC, as presented previously in section 2.2. Figure 5 displays the overall weight distribution

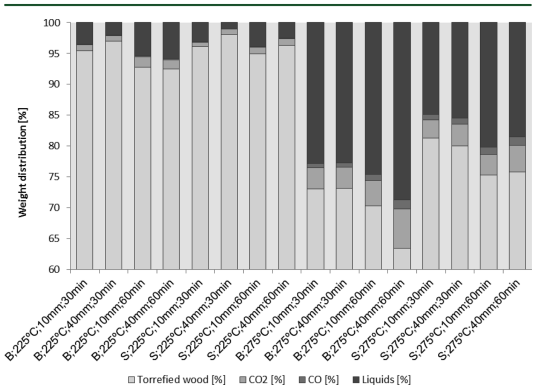

Figure 5. Product distribution for all experiments in weight percent relative to the initial mass.

from all of the torrefaction experiments that were performed in this study. The liquid fraction was calculated as the difference between the weight of the starting material and the sum of the gas and solid fractions.

As observed in Figure 5, there is a general trend toward a decrease in the solid yield and an increase in the volatile yield for both feedstocks as the torrefaction temperature and/or the holdup time is increased. However, the effect of the temperature is more pronounced than that of the holdup time. In addition, the spruce is found to produce higher solid yields and thus be less reactive than the birch at all tested conditions. This observation is in good agreement with the DTG curves and confirms our earlier observation. Furthermore, the most significant difference in the solid yield between the two feedstocks is observed in torrefaction of the 40 mm cubes at 275 °C, with 60 min holdup time. The solid yields amount to 63.5% for the birch and 75.8% for the spruce. The sample cube size also affects the solid yield. For the larger cubes, higher solid yields are obtained. However, the differences are not very significant and are mainly due to the size-related limitations in heat and mass transfer during torrefaction. Solid yield values for wood materials, as investigated by other studies with similar torrefaction parameters of 275 °C and 30 min of holdup time, are 54.5% for leucaena,[18] 70% for logging residue chips,[15] and 73% for pine chips.[15]

More interestingly, Figure 5 shows that the CO/CO_2 ratio increases with the torrefaction temperature and/or holdup time. However, the CO/CO_2 ratio is higher for the spruce at 275 °C compared to the birch. It has been reported in the literature that CO_2 formation from biomass torrefaction may be due to decarboxylation of the acid groups and that CO formation stems from the secondary reaction of CO_2 and steam with porous char.[5] The CO/CO_2 ratio increases with increasing temperature because parts of the cellulose and lignin may also decompose at higher temperatures.[14] The higher lignin and lower cellulose contents of softwoods compared to hardwoods may be a reason for the higher CO/CO_2 ratio of the spruce at 275 °C.[5,14]

3.4. Hydrophobicity. The results from the hydrophobicity tests, presented in Figure 6, show that the torrefied biomass

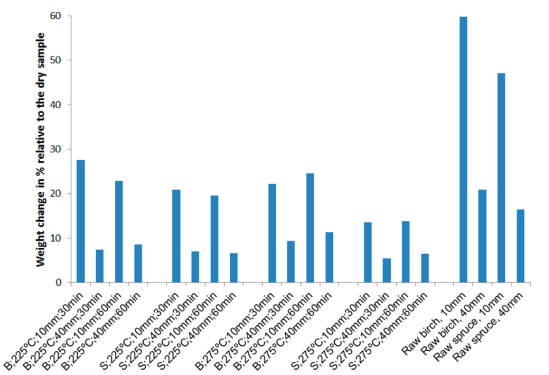

Figure 6. Comparison of the hydrophobicity of the raw and torrefied samples.

samples absorb considerably less water than the untreated samples. The percentage decrease in moisture absorbance is similar for both feedstocks. Because the raw spruce absorbs less moisture than the raw birch, the torrefied spruce also follows the same trend. For example, for the 10 mm cubes treated at 275 °C with 60 min of holdup time, the increase in the moisture content was 24.5% for the birch compared to 13.8% for the spruce. The corresponding values for the increase in the moisture content of the raw birch and spruce are 59.7% and 47.1%, respectively. In another study that used the same immersion test, only a 3.27% moisture increase is reported for torrefied sawdust samples treated at 270 °C with 1 h of holdup time in comparison to a 150.33% increase for the raw sawdust samples.[24]

Interestingly, it is observed that most of the hydrophobicity benefits are achieved at 225 °C with 30 min of holdup time, and the results do not change significantly when the torrefaction temperature or holdup time is increased. For example, the increases in the moisture content exhibited by the 40 mm spruce cubes treated with 60 min of holdup time are 6.7% at 225 °C and 6.4% at 275 °C. The larger particles are found to be more resistant to moisture absorbance. As observed

dx.doi.org/10.1021/ef300993q | Energy Fuels 2012, 26, 5232–5240

in Figure 6, the amount of water uptake is lower for the 40 mm cubes than for the 10 mm cubes for both feedstocks.

The improved hydrophobicity of the torrefied products is mainly due to the loss of organic volatile components and depolymerization of the long polysaccharide chains in the biomass.[14] The breakage of hydroxyls on the cellulose microfibril monomers during torrefaction imparts hydrophobic properties to the torrefied product.[3] The lower moisture absorption by the spruce compared to the birch is related to the different anatomical properties of hardwoods and softwoods. Hardwoods have larger cell cavities, thinner and more permeable cell walls, and larger openings of the pits than softwoods, resulting in their increased moisture absorption capability.[35]

3.5. Grindability. Figure 7 shows the total specific energy required to grind the tested samples, which includes the energy

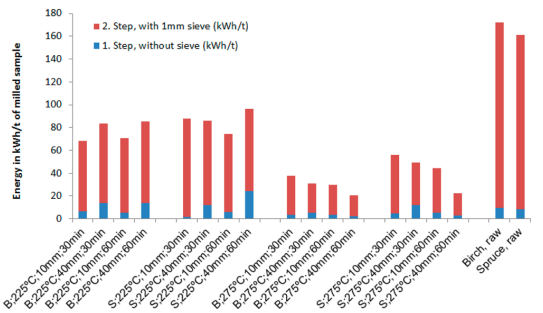

Figure 7. Total grinding energy requirements for the raw and torrefied samples, given in kWh per metric ton.

requirements of both the pregrinding and fine-grinding steps in the procedure described in section 2. Overall, the specific energy consumption for grinding is significantly reduced by torrefaction for both feedstocks. Furthermore, the reduction was higher for the birch (from 171.9 to 20.5−85.1 kWh/t) than for the spruce (from 161.4 to 22.7−96.5 kWh/t), which is likely due to the compositional differences between the birch and spruce. These values are comparable to those reported in the literature for the grinding of torrefied biomass and coal. In a previous study on torrefaction of pine chips,[15] the specific grinding energy consumption was reduced from 237.7 kWh/t for the raw samples to 102.6 kWh/t for the sample treated at 225 °C and to 52.0 kWh/t for the sample treated at 275 °C, both with 30 min of holdup time. The specific grinding energy consumption for coal is 7−36 kWh/t.[15] Weakening of the biomass cell wall due to decomposition of hemicellulose along with depolymerization of cellulose and thermal softening of lignin is the probable reason for improved grindability after torrefaction.[3]

Figure 7 also shows that the energy savings associated with size reduction increased with increasing torrefaction temperatures. The decrease in the energy consumption compared to the raw samples ranged from 45 to 60% at 225 °C to 65−82% at 275 °C for the experiments with a holdup time of 30 min. The increase in the holdup time had a negligible effect on the grinding energy at 225 °C. However, at 275 °C, the total grinding energy decreases by approximately 82−88% for the birch and 73−86% for the spruce with a holdup time of 60 min. In addition, the feedstock size is observed to have an effect on the grinding energy requirements, but the trend is not clear.

To evaluate the actual effect of torrefaction on the grindability of these two feedstocks, both the grinding energy and particle-size distribution should be taken into account. Figures 8a,b and 9a,b show the particle-size distributions of all of the samples tested. Overall, it is observed that there is a noticeable increase in the percentage of fine particles (<180 μm) after torrefaction. This result suggests that the average particle size decreases and the weight distribution shifts toward particle sizes of <180 μm. The torrefied birch samples exhibited up to a 120% increase in fine particles compared to the raw fuel. For the spruce, an increase of 85% is obtained. The only exceptions to this trend are the birch samples, particularly the 40 mm cubes treated at 225 °C. These samples contained more particles in the 500 μm to 1 mm size range than the raw birch samples, with a negligible effect of torrefaction on the fine particle distribution. These observations again point to the structural differences between the birch and spruce samples. However, it is very interesting to note that these differences in the particle-size distributions of the two feedstocks diminish when the torrefaction temperature is increased to 275 °C. As observed in Figures 8 and 9, the particle-size distributions of the samples treated at 275 °C are not influenced by the other parametric variations. This result suggests that, with an increase in the torrefaction temperature, the uniformity of the products is also improved regardless of the biomass type, which supports

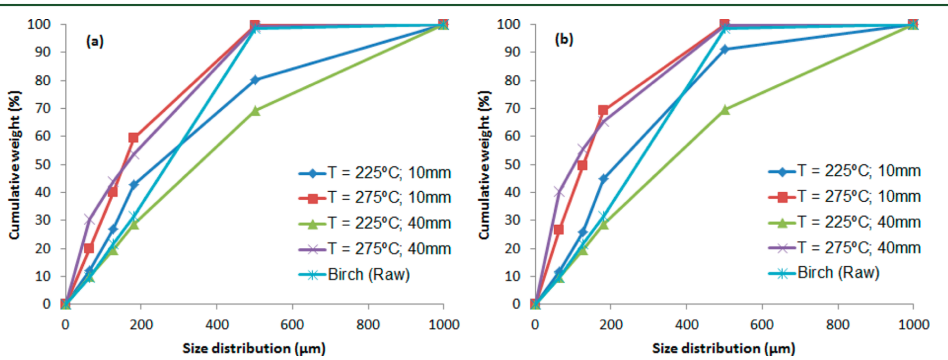

Figure 8. Particle-size distributions for the birch samples as a function of the torrefaction temperature and particle size: (a) 30 min of holdup time; (b) 60 min of holdup time.

dx.doi.org/10.1021/ef300993q | Energy Fuels 2012, 26, 5232−5240

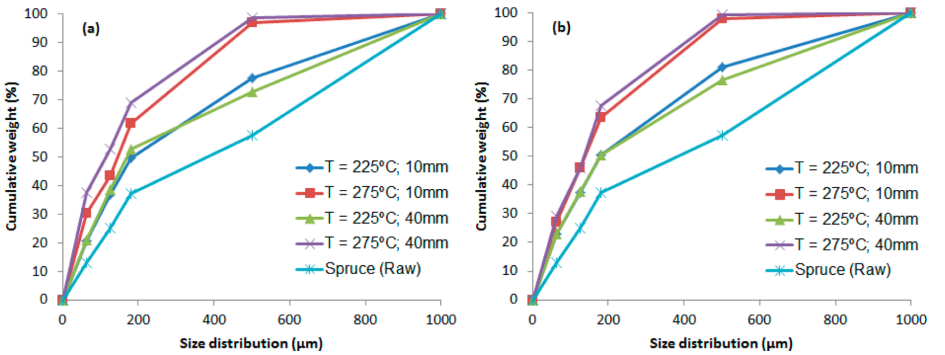

Figure 9. Particle-size distributions for the spruce samples as a function of the torrefaction temperature and particle size: (a) 30 min of holdup time; (b) 60 min of holdup time.

the use of torrefied biomass in applications that require more homogeneous fuels and smaller particles, such as entrained-flow reactors or during cofiring with coal. In addition, among all of the tested process parameters, the temperature has the largest effect on the particle-size distributions of the samples. These results are in agreement with similar studies.[16,17]

4. CONCLUSIONS

The unique approach of macro-TGA was used to evaluate the torrefaction behavior of Norwegian birch and spruce. Data obtained from macro-TGA are excellent indicators of the relationship between the weight loss, process temperature, and holdup time for an industrial-scale torrefaction process, and this is confirmed by comparisons of the DTG curves from macro-TGA and micro-TGA experiments. Birch and spruce were selected as feedstocks because they are typical Norwegian wood species and because they present an opportunity to compare hardwood (birch) and softwood (spruce) behavior during torrefaction and the qualities of their torrefied versions. The biomass weight loss rate and volatile composition were continuously measured in the macro-TGA reactor. The raw and torrefied samples were characterized using proximate and ultimate analyses. The main product distribution between the liquid, gas, and solid fractions is also reported. In addition, the biomass fuel properties such as hydrophobicity, grinding energy requirements, and particle-size distribution were analyzed for all samples. The results suggest that torrefaction is a promising technique for improving the biomass performance for energy utilization. During torrefaction, the main thermal decomposition reactions involve the hemicellulose polymers, resulting in improved fuel properties exhibited by the torrefied samples. The main conclusions of this work are as follows:

(1) Compared to the raw samples, the composition of the torrefied samples is closer to that of coal, with a higher carbon content and a lower volatile matter content.

(2) The birch is found to be more reactive than the spruce. The birch exhibited a higher devolatilization rate and a lower solid yield than the spruce at all of the tested conditions.

(3) Of all of the process parameters, the torrefaction temperature has the strongest effect on the biomass composition, devolatilization rate, and solid yield.

(4) The hydrophobicity of the torrefied samples is much higher than that of the raw samples. However, most of the benefits for this property are achieved after torrefaction at 225 °C with 30 min of holdup time, and the effects from further increasing the temperature or holdup time are limited.

(5) A 40−88% decrease in the total grinding energy is observed for the torrefied samples of both feedstocks. Among all of the tested process parameters, an increase in the temperature had the largest effect on the grinding energy.

(6) Torrefaction considerably increases the percentage of fine particles (<180 μm) in the particle-size distribution after grinding. A uniform and similar particle-size distribution is obtained for the samples treated at 275 °C

AUTHOR INFORMATION

Corresponding Author

*Telephone: +47-93818918. Fax: +47-73593580. E-mail: dhruv.tapasvi@ntnu.no.

Notes

The authors declare no competing financial interest.

ACKNOWLEDGMENTS

This work is financed by the Research Council of Norway and a number of industrial partners through the project STOP ("STable OPerating conditions for biomass combustion plants"). STOP is also a part of the research center CenBio (Bioenergy Innovation Centre).

REFERENCES

(1) International Energy Agency (IEA). *World Energy Outlook 2009*; IEA: Paris, France, 2009.

(2) van der Stelt, M. J. C.; Gerhauser, H.; Kiel, J. H. A.; Ptasinski, K. J. A review. *Biomass Bioenergy* **2011**, *35*, 3748−3762.

(3) Chew, J. J.; Doshi, V. *Renewable Sustainable Energy Rev.* **2011**, *15* (8), 4212−4222.

(4) Tapasvi, D.; Tran, K.-Q.; Wang, L.; Skreiberg, Ø.; Khalil, R. Biomass torrefaction—a review. *Proceedings of the 9th European Conference on Industrial Furnaces and Boilers*, Estoril, Portugal, April 2011; ISBN 978-972-99309-6-6

(5) Prins, M. J.; Ptasinski, K. J.; Janssen, F. J. J. G. *J. Anal. Appl. Pyrolysis* **2006**, *77* (1), 35−40.

(6) Rousset, P.; Davrieux, F.; Macedo, L.; Perré, P. *Biomass Bioenergy* **2011**, *35* (3), 1219−1226.

(7) Melkior, T.; Jacob, S.; Gerbaud, G.; Hediger, S.; Le Pape, L.; Bonnefois, L.; Bardet, M. *Fuel* **2012**, *92* (1), 271−280.

(8) Prins, M. J.; Ptasinski, K. J.; Janssen, F. J. J. G. *J. Anal. Appl. Pyrolysis* **2006**, *77* (1), 28−34.

(9) Chen, W.-H.; Kuo, P.-C. *Energy* **2011**, *36* (2), 803−811.

(10) Sadaka, S.; Negi, S. *Environ. Prog. Sustainable Energy* **2009**, *28* (3), 427−434.
(11) Couhert, C.; Salvador, S.; Commandré, J. M. *Fuel* **2009**, *88* (11), 2286−2290.
(12) Felfli, F. F.; Luengo, C. A.; Suarez, J. A.; Beaton, P. A. *Energy Sustainable Dev.* **2005**, *9* (3), 19−22.
(13) Bridgeman, T. G.; Jones, J. M.; Shield, I.; Williams, P. T. *Fuel* **2008**, *87* (6), 844−856.
(14) Deng, J.; Wang, G.-j.; Kuang, J.-h.; Zhang, Y.-l.; Luo, Y.-h. *J. Anal. Appl. Pyrolysis* **2009**, *86* (2), 331−337.
(15) Phanphanich, M.; Mani, S. *Bioresour. Technol.* **2011**, *102* (2), 1246−53.
(16) Bridgeman, T. G.; Jones, J. M.; Williams, A.; Waldron, D. J. *Fuel* **2010**, *89* (12), 3911−3918.
(17) Arias, B.; Pevida, C.; Fermoso, J.; Plaza, M. G.; Rubiera, F.; Pis, J. J. *Fuel Process. Technol.* **2008**, *89* (2), 169−175.
(18) Wannapeera, J.; Fungtammasan, B.; Worasuwannarak, N. *J. Anal. Appl. Pyrolysis* **2011**, *92* (1), 99−105.
(19) Medic, D.; Darr, M.; Shah, A.; Potter, B.; Zimmerman, J. *Fuel* **2012**, *91* (1), 147−154.
(20) Uemura, Y.; Omar, W.; Tsutsui, T.; Subbarao, D.; Yusup, S. *J. Appl. Sci.* **2010**, *10* (24), 3250−3256.
(21) Chen, W.-H.; Kuo, P.-C. *Energy* **2010**, *35* (6), 2580−2586.
(22) Almeida, G.; Brito, J. O.; Perre, P. *Bioresour. Technol.* **2010**, *101* (24), 9778−84.
(23) Pierre, F.; Almeida, G.; Brito, J. O.; Perre, P. *Bioresources* **2011**, *6* (2), 1204−1218.
(24) Pimchuai, A.; Dutta, A.; Basu, P. *Energy Fuels* **2010**, *24* (9), 4638−4645.
(25) Repellin, V.; Govin, A.; Rolland, M.; Guyonnet, R. *Biomass Bioenergy* **2010**, *34* (7), 923−930.
(26) Chen, W.-H.; Cheng, W.-Y.; Lu, K.-M.; Huang, Y.-P. *Appl. Energy* **2011**, *88* (11), 3636−3644.
(27) Rousset, P.; Aguiar, C.; Labbe, N.; Commandre, J. M. *Bioresour. Technol.* **2011**, *102* (17), 8225−31.
(28) Prins, M. J.; Ptasinski, K. J.; Janssen, F. J. J. G. *Energy* **2006**, *31* (15), 3458−3470.
(29) Patel, B.; Gami, B.; Bhimani, H. *Energy Sustainable Dev.* **2011**, DOI: 10.1016/j.esd.2011.05.002.
(30) Uemura, Y.; Omar, W. N.; Tsutsui, T.; Yusup, S. B. *Fuel* **2011**, *90* (8), 2585−2591.
(31) Li, H.; Liu, X.; Legros, R.; Bi, X. T.; Lim, C. J.; Sokhansanj, S. *Bioresour. Technol.* **2011**.
(32) Chen, W.-H.; Hsu, H.-C.; Lu, K.-M.; Lee, W.-J.; Lin, T.-C. *Energy* **2011**, *36* (5), 3012−3021.
(33) Skreiberg, A.; Skreiberg, Ø.; Sandquist, J.; Sørum, L. *Fuel* **2011**, *90* (6), 2182−2197.
(34) Channiwala, S. A.; Parikh, P. P. *Fuel* **2002**, *81* (8), 1051−1063.
(35) Zabihzadeh, S. M. *Bioresources* **2010**, *5* (1), 316−323.

Paper III

Thermal decomposition kinetics of woods with an emphasis on torrefaction

Tapasvi, D.; Khalil, R.; Várhegyi, G.; Tran, K.-Q.;

Grønli, M.; Skreiberg, Ø,

Energy Fuels 2013, 27, (10), 6134-6145.

energy&fuels

Article

pubs.acs.org/EF

Thermal Decomposition Kinetics of Woods with an Emphasis on Torrefaction

Dhruv Tapasvi,[†] Roger Khalil,[‡] Gábor Várhegyi,*[,§] Khanh-Quang Tran,[†] Morten Grønli,[†] and Øyvind Skreiberg[‡]

[†]Department of Energy and Process Engineering, Norwegian University of Science and Technology (NTNU), NO-7491 Trondheim, Norway

[‡]SINTEF Energy Research, Postboks 4761 Sluppen, NO-7465 Trondheim, Norway

[§]Institute of Materials and Environmental Chemistry, Research Centre for Natural Sciences, Hungarian Academy of Sciences, PO Box 17, Budapest, Hungary 1525

ABSTRACT: The pyrolysis kinetics of Norwegian spruce and birch wood was studied to obtain information on the kinetics of torrefaction. Thermogravimetry (TGA) was employed with nine different heating programs, including linear, stepwise, modulated and constant reaction rate (CRR) experiments. The 18 experiments on the 2 feedstocks were evaluated simultaneously via the method of least-squares. Part of the kinetic parameters could be assumed common for both woods without a considerable worsening of the fit quality. This process results in better defined parameters and emphasizes the similarities between the woods. Three pseudo-components were assumed. Two of them were described by distributed activation energy models (DAEMs), while the decomposition of the cellulose pseudo-component was described by a self-accelerating kinetics. In another approach, the three pseudo-components were described by *n*-order reactions. Both approaches resulted in nearly the same fit quality, but the physical meaning of the model, based on three *n*-order reactions, was found to be problematic. The reliability of the models was tested by checking how well the experiments with higher heating rates can be described by the kinetic parameters obtained from the evaluation of a narrower subset of 10 experiments with slower heating. A table of data was calculated that may provide guidance about the extent of devolatilization at various temperature−residence time values during wood torrefaction.

1. INTRODUCTION

There is a growing interest in lignocellulosic biomass fuels and raw materials, because of climate change problems. However, the widespread use of biomass fuels is frequently hindered by their unfavorable fuel characteristics, such as high moisture content, poor grindability, low calorific value, and low bulk density. Torrefaction is one of the potential solutions to these problems, and it has gained research momentum as a biomass pretreatment process in the last two decades. It results in improved biomass fuel properties, such as reduced moisture content, higher energy density, improved hydrophobic behavior, and less energy consumption during grinding.[1−3] Torrefaction is typically conducted at 200−300 °C, at atmospheric pressure, in the absence of oxygen and with particle heating rates below 50 °C/min.[4] The lignocellulosic biomass is partially decomposed during the torrefaction, releasing condensable liquids and noncondensable gases into the gas phase.[5] Primarily, the xylan-containing hemicellulose polymers decompose because they are the most reactive polymer structures in biomass.[6,7] The extractives of the biomass also decompose while the cellulose and lignin are moderately impacted during torrefaction, depending on the feedstock composition and the torrefaction temperature.[8]

Many studies are available on the production and characterization of torrefaction products. However, fewer works address the torrefaction kinetics.[9−15] Most of these studies are based on isothermal experiments. Prins et al.[9] and Bates et al.[11] employed a one-component, two-step successive reaction model, based on an earlier work of Di Blasi and Lanzetta[16] on xylan kinetics. The same model was used in a recent thermogravimetric analysis−mass spectroscopy (TGA-MS) study by Shang et al.[15] Peng et al.[12] used a one-component, one-step reaction model for torrefaction with long residence time and a two-component, one-step reaction model for torrefaction with short residence time. Chen and Kuo[10] studied the torrefaction of hemicelluloses, cellulose, and lignin separately, using a global one-step reaction model for each. They described the torrefaction process of a biomass material by superimposed kinetics of the three components.

The torrefaction kinetics is part of a broader subject: the pyrolysis kinetics of biomass materials. If a kinetic model describes the biomass pyrolysis well, then it can obviously be used for torrefaction kinetics. Moreover, such a model also can describe the pyrolysis behavior of the torrefied wood, if the experimental data used to determine the model parameters include temperature programs where the heating to higher temperatures is preceded by longer residence times in the temperature domain of the torrefaction. This pathway was followed in the present work. Such kinetic descriptions will be presented which describe both the lower- and the higher-temperature regions of the wood pyrolysis well. The work is based on TGA experiments, because TGA is a high-precision

Received: August 11, 2013
Revised: September 12, 2013
Published: September 13, 2013

dx.doi.org/10.1021/ef4016075 | *Energy Fuels* 2013, 27, 6134−6145

Table 1. Proximate and Ultimate Analyses of the Samples

	Proximate Analysis[a]			Ultimate Analysis[a]					
sample	volatile matter	fixed carbon	ash	C	H	O	N	S	HHV[b]
birch	89.4	10.4	0.2	48.62	6.34	44.90	0.09	<0.05	19.80
spruce	86.3	13.4	0.2	50.10	6.36	43.52	0.07	<0.05	20.45

[a]% (m/m), dry basis. [b]Higher heating value, MJ/kg, dry basis.

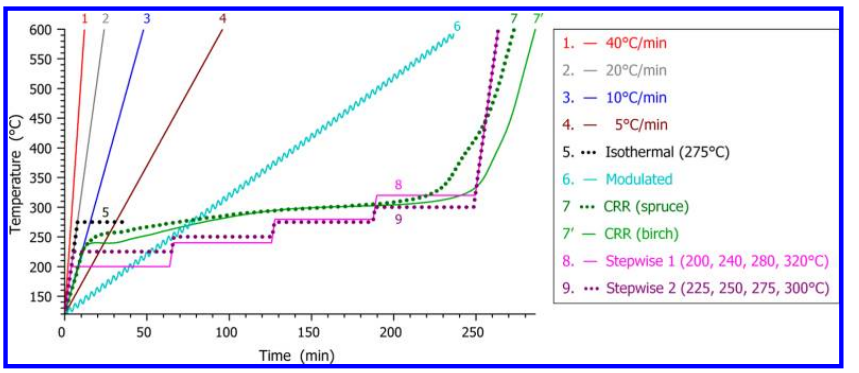

Figure 1. Temperature programs used in the thermogravimetric analysis (TGA) experiments. Note that the $T(t)$ functions in the "constant reaction rate" (CRR) experiments were determined by the instrument and differed for the two samples.

method that provides well-defined conditions in the kinetic regime. The highest heating rate of the study was 40 °C/min, at which the decomposition terminated at ∼600 °C. We did not employ isothermal kinetics, because the "isothermal" concept involves substantial transient time, which is lost from the evaluation of the thermogravimetric experiments. Although an "isothermal" experiment is involved in the study, it is evaluated together with the heat-up period. The information content of an essentially nonisothermal series of experiments was used to draw dependable kinetic information.

Because of the complex composition of biomass materials, the conventional linearization techniques of the nonisothermal kinetics are not suitable for the evaluation of the TGA experiments. Therefore, the TGA experiments of biomass materials are usually evaluated by the nonlinear method of least-squares, assuming more than one reaction.[17−19] Biomass fuels and residues contain a wide variety of reactive species. The assumption of a distribution in the reactivity of the decomposing species frequently helps the kinetic evaluation of the pyrolysis of complex organic samples.[20] The distributed activation energy models (DAEM) have been used for biomass pyrolysis kinetics since 1985, when Avni et al. applied a DAEM for the formation of volatiles from lignin.[21] Several variants of DAEMs are known; usually a Gaussian distribution of the activation energy is employed. The use of DAEM in pyrolysis research was subsequently extended to a wider range of biomasses and materials derived from plants. Because of the complexity of the investigated materials, the model was expanded to simultaneous parallel reactions (pseudo-components) that were described by separate DAEMs.[22−25] The increased number of unknown model parameters required the least-squares evaluation of larger series of experiments with linear and nonlinear temperature programs.[22,26−29] The model parameters obtained in this way allowed accurate prediction outside the domain of the experimental conditions of the given kinetic evaluations.[22,26,28,29] The prediction tests helped to confirm the reliability of the model.

The complex decomposition of the biomass pseudo-components also can be approximated formally by *n*-order (power-law) kinetics. Manyà et al. proved that third-order kinetics gives a better description for the lignin pseudo-component of the biomass than the simpler first-order kinetics.[30] Conesa and Domene showed the applicability of high reaction orders (up to 9.5) for the formal description of the pseudo-components in biomass pyrolysis kinetics.[19] The aims of the present work included a careful comparison of the DAEM and the *n*-order approaches on a particularly wide domain of temperature−time functions.

2. SAMPLES AND METHODS

2.1. Samples. Birch and spruce samples were taken from standard Norwegian construction boards. Table 1 shows the proximate and ultimate analyses, as well as the higher heating values (HHVs) of the samples. A recent work of Tapasvi et al.[3] lists the corresponding data for the torrefied products prepared from the same woods. Before the experiments, the samples were cut into smaller pieces and ground in a cutting mill that was equipped with a 1-mm bottom sieve. The samples were sieved afterward, and the particles in the range of 63−125 μm were used for the kinetic study.

2.2. Experimental Setup and Procedure. The experiments were carried out by a Q5000 IR analyzer from TA Instruments, which has a sensitivity of 0.1 μg. High-purity nitrogen was used as purge gas with a gas flow of 100 mL/min. The initial sample mass was 3−10 mg. The samples of both woods were analyzed with nine different heating programs, as shown in Figure 1. The linear $T(t)$ experiments had heating rates of 40, 20, 10, and 5 °C/min. The isothermal experiment with a residence time of 30 min at 275 °C mimicked the $T(t)$ function of the actual torrefaction experiments used in earlier works.[3,31] In the modulated experiments, sinusoidal waves with

dx.doi.org/10.1021/ef4016075 | Energy Fuels 2013, 27, 6134−6145

amplitudes of 5 °C and a wavelength of 200 s were superposed on a slow, 2 °C/min linear $T(t)$ function. They served to increase the rather limited information content of the linear $T(t)$ experiments. In the "constant reaction rate" (CRR) experiments, the equipment regulated the heating of the samples, so that the reaction rate would oscillate around a preset limit.[32] The CRR experiments aimed at getting very low mass-loss rates in the entire domain of the reaction. The highest mass loss rate was found to be 0.8 μg/s in these experiments. This value corresponds to 0.8×10^{-4} s^{-1} after normalization by the initial dry sample mass. The $T(t)$ program for a CRR experiment obviously depends on the behavior of the given sample. Two stepwise temperature programs were employed, which also served to increase the amount of experimental information for the kinetic evaluation.[22,26−29]

Figure 2 shows a test on the employed sample masses. The comparison of experiments with initial sample masses of 3 and

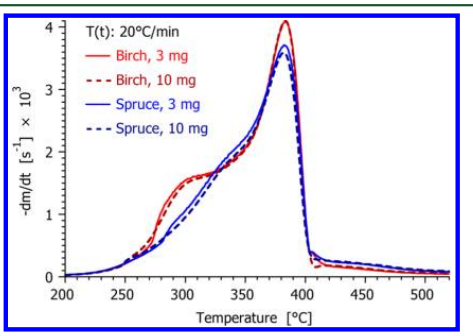

Figure 2. A test on the effect of sample mass and the comparison of the birch and spruce decomposition at a heating rate of 20 °C/min.

10 mg (solid and dashed curves) indicates that the enthalpy change of the decomposition does not result in a considerable thermal lag at the higher sample mass. Figure 2 also compares the decomposition of the birch and spruce samples (red and blue lines). One can see that the low-temperature partial peak, at ∼280−300 °C, is more separated in the case of the birch sample. This is a usual difference between hardwoods (angiosperm trees) and conifers.[33] The main peak, belonging to the cellulose decomposition,[33] is very similar; its peak maximum occurs at ∼383 °C for both samples in Figure 2.

2.3. Kinetic Evaluation by the Method of Least-Squares and Characterization of the Fit Quality. Fortran 95 and C++ programs were used for the numerical calculations and for graphics handling, respectively. The employed numerical methods have been described in detail earlier.[27] The kinetic evaluation was based on the least-squares evaluation of the $-dm^{obs}/dt$ curves, where m^{obs} is the sample mass normalized by the initial dry sample mass. The method used for the determination of $-dm^{obs}/dt$ does not introduce considerable systematic errors into the least-squares kinetic evaluation of experimental results.[34] The model was solved numerically along the empirical temperature−time functions. The minimization of the least-squares sum was carried out by a direct search method, as described earlier.[27] Such values were searched for the unknown model parameters that minimized the following objective function (of):

$$of = \sum_{k=1}^{N_{exper}} \sum_{i=1}^{N_k} \frac{\left[\left(\frac{dm}{dt}\right)_k^{obs}(t_i) - \left(\frac{dm}{dt}\right)_k^{calc}(t_i)\right]^2}{N_k {h_k}^2} \quad (1)$$

Here, N_{exper} is the number of experiments evaluated together; its value is 18 in the present work. N_k denotes the number of t_i time points on a given curve, and m is the sample mass normalized by the initial dry sample mass. The division by ${h_k}^2$ serves to counterbalance the high magnitude differences. Traditionally, h_k is the highest observed value of the given experiment:

$$h_k = \max\left(\frac{dm}{dt}\right)_k^{obs} \quad (2)$$

The normalization by the highest observed values in the least-squares sum implicitly assumes that the relative precision is roughly the same for the different experiments. This assumption has proved to be useful in numerous works on nonisothermal kinetics since 1993.[35] A recent work[31] deviated from this rule, because the extremely low mass loss rates of the CRR experiments (0.04−0.07 μg/s) corresponded to a worse relative precision than the rest of the experiments. In the present work, however, we did not have as low mass loss rates; the peak maxima of the CRR experiments were >10 times higher (0.8 μg/s), while most of the decomposition occurred at mass loss rates of 0.5 μg/s in these experiments.

The obtained fit quality can be characterized separately for each of the experiments evaluated together. For this purpose, the relative deviation (*reldev*, %) will be used. The root-mean-square (rms) difference between the observed and calculated values is expressed as a percentage of the peak maximum. For experiment k, we get

$$reldev\ (\%) = 100\left\{\sum_{i=1}^{N_k} \frac{\left[\left(\frac{dm}{dt}\right)_k^{obs}(t_i) - \left(\frac{dm}{dt}\right)_k^{calc}(t_i)\right]^2}{N_k {h_k}^2}\right\}^{0.5} \quad (3)$$

The fit quality for a given group of experiments is characterized by the rms value of the corresponding relative deviations. The relative deviation of the 18 experiments, evaluated together, can be expressed by eqs 1−3 as

$$reldev_{18}\ (\%) = 100\sqrt{of} \quad (4)$$

Obviously, a smaller $reldev_{18}$ value indicates a better fit.

2.4. Distributed Activation Energy Model (DAEM). As outlined in the Introduction, a model of parallel reactions with Gaussian activation energy distribution was chosen as a starting point, because favorable experience has been obtained by this type of modeling on similarly complex materials.[22−29] According to this model, the sample is regarded as a sum of M pseudo-components, where M is usually between 2 and 4. Here, a pseudo-component is the totality of those decomposing species that can be described by the same reaction kinetic parameters in the given model. A pseudo-component may involve a large number of different reacting species. The reactivity differences are described by different activation energy values. On a molecular level, each species in pseudo-component j is assumed to undergo a first-order decay. The corresponding rate constant (k) is supposed to be dependent

dx.doi.org/10.1021/ef4016075 | Energy Fuels 2013, 27, 6134−6145

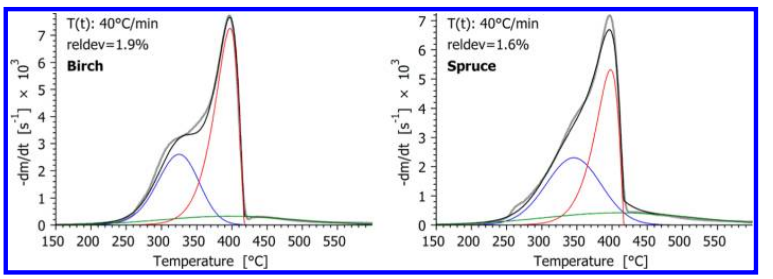

Figure 3. The partial peaks at 40 °C/min obtained by Evaluation **1** and Model Variant **II**. Curves shown in the figure: observed and calculated $-dm/dt$ (gray and black); peaks of pseudo-components 1, 2, and 3 (blue, red, and green).

Table 2. Fit Qualities[a] and Number of Unknown Parameters[b] at Four Model Variants, Assuming Various Groups of Common Model Parameters

		Model Variant			
evaluation	common parameters	**I**, 2 DAEMs +1st order cellulose	**II**, 2 DAEMs + *n*-order cellulose	**III**, 2 DAEMs + accelerating cellulose[c]	**IV**, 3 *n*-order reactions[d]
1	none	4.78 (22)	2.31 (24)	2.06 (26)	2.19 (24)
2	E_3	4.78 (21)	2.35 (23)	2.10 (25)	2.21 (23)
3	E_3, σ_3, or n_3[e]	4.78 (20)	2.37 (22)	2.14 (24)	2.21 (22)
4	E_3, σ_3, or n_3, E_2, n_2, z_2[e]	4.80 (19)	2.46 (20)	2.25 (21)	2.32 (20)
5	all except the A and c parameters	4.83 (17)	2.61 (18)	2.37 (19)	2.33 (18)

[a] $reldev_{18}$ (%) values are listed, which characterize the fit quality of the entire series of experiments, as shown by eqs 1−4. [b] The total number of the parameters determined by the method of least-squares for the two biomasses is indicated in parentheses. [c] See section 3.3. [d] See section 3.6. [e] σ_3 belongs to model variants **I**, **II**, and **III** while n_3 corresponds to model variant **IV**. Parameter z_2 will be introduced in section 3.3 (z_2 occurs only in Model Variant **III**).

on the temperature via an Arrhenius formula. Let $\alpha_j(t,E)$ be the solution of the corresponding first-order kinetic equation at a given E and $T(t)$ with conditions $\alpha_j(0,E) = 0$ and $\alpha_j(\infty,E) = 1$:

$$\frac{d\alpha_j(t, E)}{dt} = A_j \exp\left(-\frac{E}{RT}\right)[1 - \alpha_j(t, E)] \quad (5)$$

The distribution of the species differing by E within a given pseudo-component is approximated by a Gaussian function with a mean value E_j and width parameter (variation) σ_j. From a computational point of view, the approximate solution of a DAEM can simply be calculated from a discrete set of $\alpha_j(t,E)$ functions.[36] The normalized sample mass and its derivative are the linear combinations of $\alpha_j(t)$ and $d\alpha_j/dt$, respectively:

$$-\frac{dm}{dt} = \sum_{j=1}^{M} c_j \frac{d\alpha_j}{dt} \quad \text{and} \quad m(t) = 1 - \sum_{j=1}^{M} c_j \alpha_j(t) \quad (6)$$

where a weight factor c_j is equal to the amount of volatiles formed from a unit mass of pseudo-component j.

This model will be called Model Variant **I** in the later treatment. Its modifications will be denoted by Model Variants **II** and **III**, as outlined in Sections 3.1 and 3.3. Finally, the results were compared to a simpler, but more formal approximation, in which the decomposition of the pseudo-components was described by n-order reactions:

$$\frac{d\alpha_j}{dt} = A_j \exp\left(-\frac{E_j}{RT}\right)(1 - \alpha_j)^{n_j} \qquad (j = 1, 2, 3) \quad (7)$$

This n-order model will be referred as Model Variant **IV** in the treatment.

3. RESULTS AND DISCUSSION

3.1. Evaluation by Assuming Distributed Activation Energy Model for the Pseudo-components. Based on earlier experience with this model,[26,28,29] and keeping in mind the shape of the DTG curves at linear heating programs (as shown by Figure 2), three pseudo-components were assumed. The first mainly describes the decomposition of the hemicelluloses; the second corresponds to the cellulose decomposition, and the third would be responsible for the long, flat tailing that can be observed at linear heating rates for almost all biomasses. The graphical representation of these pseudo-components will be shown in sections 3.4 and 3.5. The width of distribution of the second reaction converged to zero, which means a first-order kinetics. (The Gaussian distribution is a well-known Dirac delta function, hence, a zero width cuts out a single reaction from the multitude of first-order reactions.) Therefore, the results of Model Variant **I** will be referred as "2DAEMs + 1st order cellulose" in the treatment. In Model Variant **II**, the cellulose decomposition was described by an n-order reaction. This approach resulted in much better fit qualities, as shown in section 3.2. The reaction order, n_2, was ∼0.6. Model Variant **II** will be referred as "2DAEMs + n-order cellulose" in the treatment. A further modification of the cellulose decomposition kinetics is presented in section 3.3.

3.2. Evaluation by Assuming Common Parameters. If some of the model parameters are assumed to be common for both samples, two benefits can be achieved:

(i) The common parameters indicate the similarities in the kinetic behavior of the samples; and
(ii) A given parameter value is based on more experimental information; hence, it is less dependent on the various experimental uncertainties.

dx.doi.org/10.1021/ef4016075 | Energy Fuels 2013, 27, 6134−6145

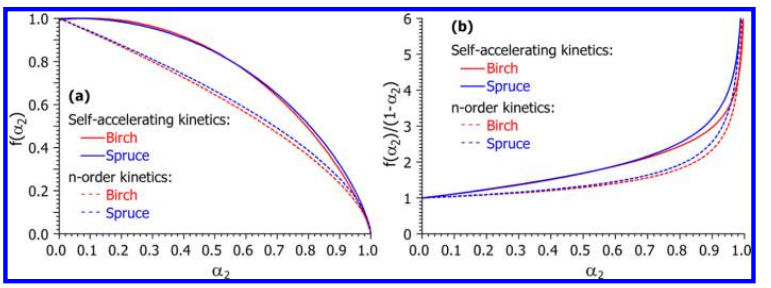

Figure 4. $f(\alpha_2)$ functions (a) and $f(\alpha_2)/(1-\alpha_2)$ ratios (b) obtained in Evaluation **3** by assuming self-accelerating kinetics (Model Variant **III**, solid lines) and *n*-order kinetics (Model Variant **II**, dashed lines) for the decomposition of the cellulose pseudo-component.

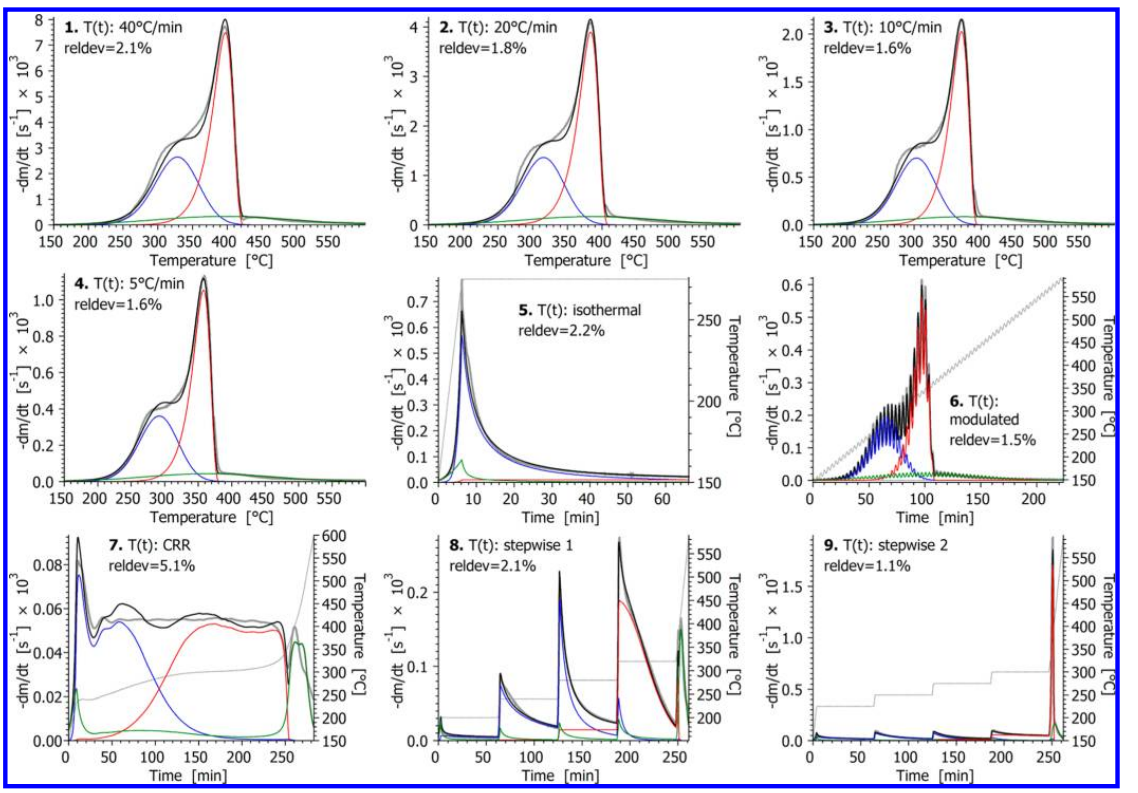

Figure 5. Results obtained for the birch experiments by Evaluation **3** and Model Variant **III**. Curves shown in the figure: observed and calculated $-dm/dt$ (gray and black bold lines); peaks of pseudo-components 1, 2, and 3 (blue, red and green lines). The temperature is indicated by a thin gray line in the experiments with nonlinear $T(t)$.

The basic case is Evaluation **1**, where none of the parameters were assumed to be common. It turned out that the fit quality depends only slightly on the exact choice of the values of E_3 and σ_3; hence, these parameters could be forced to have identical values for both woods with only a slight worsening of the fit qualities. This behavior can be attributed to the ill-defined nature of pseudo-component 3. As the green curve in Figure 3 shows, it is a wide and flat partial peak. A major part of this peak overlaps with the temperature domains of the first and second pseudo-components. A change of the curve in this domain can be compensated by relatively small changes in the parameters of pseudo-components 1 and 2. The situation was similar in two recent works describing biomass pyrolysis by DAEMs.[28,29] The existence of various ill-definition problems (compensation effects) is well-known in nonisothermal reactions. A similar problem was reported by de Jong et al. in 2007 for DAEMs.[37] The assumption of a common E_3 for both woods is denoted as Evaluation **2**, while the assumption of common E_3 and σ_3 for both woods is called Evaluation **3**.

The decomposition of the cellulose component resulted in similar E_2 and n_2 values for both woods. (The cellulose decomposition will be treated in detail in later sections.) Accordingly, these parameters could also be forced to have common values (Evaluation **4**). Finally, we mention that the

dx.doi.org/10.1021/ef4016075 | *Energy Fuels* 2013, 27, 6134−6145

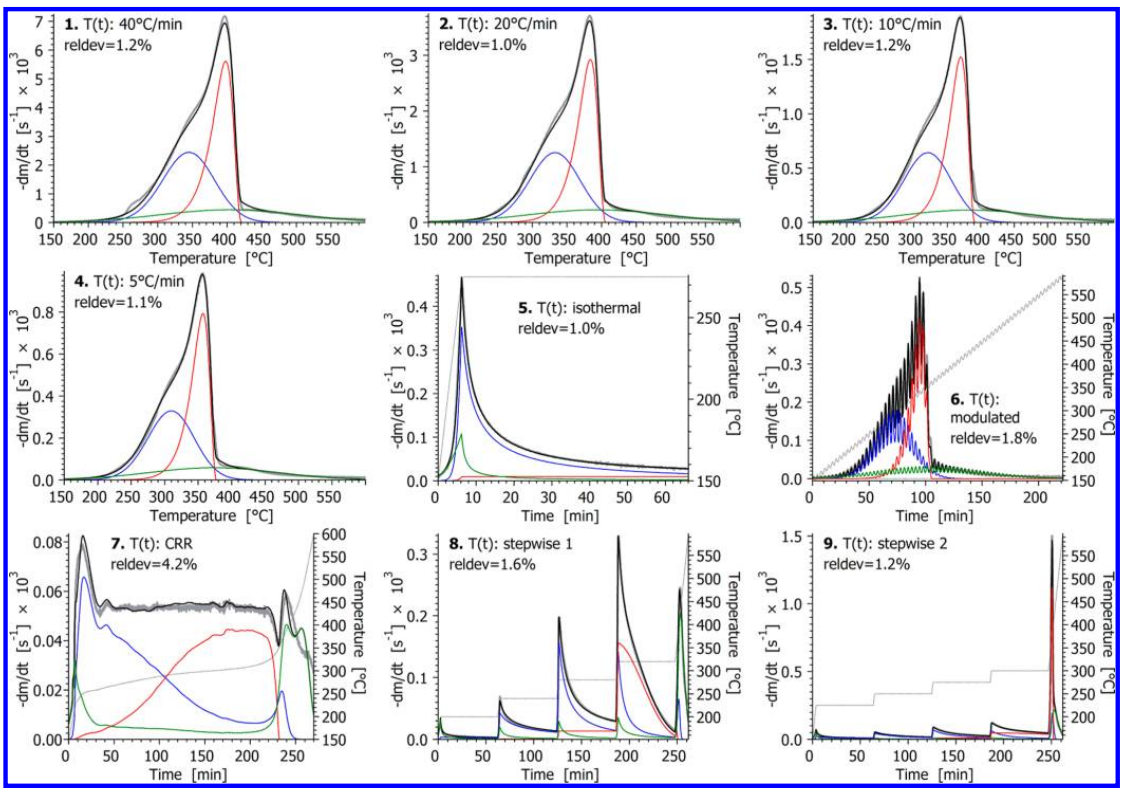

Figure 6. Results obtained for the spruce experiments by Evaluation **3** and Model Variant **III**. (See Figure 5 for the notations.)

kinetics of the hemicellulose pyrolysis could also be described by identical E_1 and σ_1 parameters with some loss in the fit quality (Evaluation **5**). Table 2 shows the fit quality and the number of unknown parameters at the various model variants and evaluation strategies. Model Variants **III** and **IV** will be discussed in later sections.

3.3. Kinetics of the Cellulose Decomposition. In an inert atmosphere, under the conditions of thermal analysis, the cellulose decomposition is usually approximated by first-order kinetics. In the present work, *n*-order kinetics with $n_2 \approx 0.6$ gave considerable better fit quality than the first-order kinetics, as mentioned previously. More-complex models are also employed in the literature. Among others, the use of self-accelerating kinetics has been suggested by Conesa et al.[38] and Capart et al.[39] In the presence of oxygen, the cellulose decomposition was also found to be a self-accelerating reaction in recent studies, based on evaluation strategies similar to the present work.[40,31] The self-accelerating reactions can typically be described by an equation of type

$$\frac{d\alpha_2}{dt} = A_2 \exp\left(-\frac{E_2}{RT}\right) f(\alpha_2) \tag{8}$$

where f is a function capable of expressing self-acceleration. The mathematical unambiguity requires a normalization for $f(\alpha_2)$, because f functions differing only in constant multipliers are equivalent in eq 8 (parameter A_2 can compensate any multipliers of f). As a normalization, we require that the maximum of f be 1. $f(\alpha_2)$ is approximated formally by

$$f(\alpha_2) \cong \text{normfactor}(1 - \alpha_2)^{n_2}(\alpha_2 + z_2) \tag{9}$$

where n_2 and z_2 are model parameters, and normfactor ensures that max $f = 1$. Parameters n_2 and z_2 do not have separate physical meanings; together, however, they determine the shape of f and, in this way, the self-accelerating capabilities of the model. Equation 9 is a slightly simplified version of an earlier approximation that has been applied to different self-accelerating reactions.[40,41] In the present work, $f(\alpha_2)$ reached its maximum at α_2 values in the range of 0.05−0.15. The results obtained by the use of eq 9 are indicated as model variant **III** in the treatment. Table 2 indicates that the use of eq 9 instead of *n*-order kinetics decreases $reldev_{18}$ by 0.21−0.25. This gain in the fit quality is obtained by two extra parameter values in Evaluations **1**−**3** (one z_2 value for birch and another z_2 value for spruce) and one extra parameter value in Evaluations **4** and **5** (a common z_2 for both woods). We cannot determine the statistical significance of this decrease because the experimental errors of the thermal analysis data are neither independent nor random. Nevertheless, the observed changes in $reldev_{18}$ are greater than the other changes in $reldev_{18}$ within Model Variant **II**. Accordingly, the results of Model Variant **III** were selected for a detailed presentation in the next section.

Figure 4a compares the $f(\alpha_2)$ functions obtained by eq 9 (solid lines) to those obtained by *n*-order kinetics [$f(\alpha_2) = (1 - \alpha_2)^{n_2}$, dashed lines].

The amount of the available cellulose is proportional to $1 - \alpha_2$; hence, the reaction rate of a unit mass of cellulose (i.e., the

dx.doi.org/10.1021/ef4016075 | Energy Fuels 2013, 27, 6134−6145

intrinsic reactivity of the sample) is proportional to $f(\alpha_2)/(1-\alpha_2)$. When this quantity increases with α_2, as shown in Figure 4b, the intrinsic reactivity of the sample is increasing at constant T. $f(\alpha_2)/(1-\alpha_2)$ is obviously increasing with α_2 if $f(\alpha_2) = (1-\alpha_2)^{n_2}$ and $n_2 < 1$. When $f(\alpha_2) = (1-\alpha_2)^{n_2}$ is plotted as a function of α_2, the curve has a slight concave curvature, as the dashed lines in Figure 4a show. However, the n-order kinetics has only a limited ability to express kinetics with increasing intrinsic reactivity.

3.4. The Results of Evaluation 3, Assuming Model Variant III. As outlined above, common E_3 and σ_3 values were assumed for both woods in Evaluation **3**, because of the ill-defined nature of these parameters, while the decomposition of the cellulose pseudo-components was described by eq 9 in Model Variant **III**. Figures 5 and 6 illustrate the corresponding results for the birch and spruce experiments, respectively. These figures show the variety of the experiments demonstrating that the present study is based on a wider range of experiments than its predecessors.[28,29] The scaling of the vertical axes is particularly noteworthy. The peak maximum of $-dm/dt$ at $T(t)$ program **1** (40 °C/min) is almost a hundred times higher than at $T(t)$ program 7 (CRR).

Figures 5 and 6 contain the observed and calculated $-dm/dt$ curves (gray and black bold lines); the contributions of the three pseudo-components to the calculated $-dm/dt$ (blue, red, and green lines), and the nonisothermal $T(t)$ functions, too, when appropriate (thin green line). The relative deviation (rms difference between the observed and calculated points) is also displayed. These values are ∼1% and ∼2%, except in the CRR experiments, where the relative deviation is 5.1% and 4.2%. However, the height of the CRR curves is very low; hence, the higher relative deviations correspond to very low deviations between the unnormalized mass loss rate data: 0.04 and 0.03 μg/s for the birch and spruce samples, respectively. It is possible that these low deviations are near the experimental uncertainty of the CRR experiments.

The obtained kinetic parameters are listed in Table 3. For comparison, we have listed the corresponding values from two recent works on agricultural residues that employed similar kinetic models, as well as a least-squares evaluation of experiments with linear and nonlinear $T(t)$.[28,29] In this table, E_1 and E_3 are the means of the corresponding activation energy distributions. The cellulose kinetics in the present work, however, differs from its predecessors: E_2 denotes an activation energy in the columns of "birch" and "spruce", while it is the mean of an activation energy distribution in the columns corresponding to the older works.

The kinetic parameters of the birch and spruce samples are close to each other. The difference between the two E_2 values is only 5 kJ/mol. The differences in the A_j values follow the differences in the E_j values due to the well-known compensation effect between E and A. The n_2 and z_2 values determine similar $f(\alpha_2)$ functions, as shown in Figure 4. This explains why the assumption of common E_2, n_2, and z_2 values resulted only in a slight increase of $reldev_{18}$ in Evaluation **4**.

The E_j, σ_1, and σ_3 values obtained in the present work are comparable to the corresponding values from earlier work on straws and corncobs. The listed differences cannot be regarded as being high if we keep in mind the high ash content of the agricultural residues (1.5%−16%, vs 0.2% in the present wood samples); the well-known differences in the composition of the hemicelluloses and lignin; the different model for the description of the cellulose decomposition; and the much wider range of $T(t)$ functions in the present work.

Table 3. Parameters Obtained in Evaluation 3 for Model Variant III and Their Comparison with Earlier Results[a]

sample	birch	spruce	four agricultural residues[b]	two corncobs[c]
E_1/kJ mol^{-1}	152	169	177	180
E_2/kJ mol^{-1}	174	169	185	187
E_3/kJ mol^{-1}	230	=	194	225
$\log_{10} A_1/s^{-1}$	11.58	12.62	⟨14.43⟩	⟨14.89⟩
$\log_{10} A_2/s^{-1}$	11.98	11.55	⟨13.77⟩	14.11
$\log_{10} A_3/s^{-1}$	16.33	16.11	⟨14.23⟩	16.25
σ_1/kJ mol^{-1}	6.0	8.6	4.3	3.9
σ_2/kJ mol^{-1}	n.a.	n.a.	1.9	0.2
σ_3/kJ mol^{-1}	34.1	=	34.5	31.3
n_2	0.80	0.73	n.a.	n.a.
z_2	1.04	1.26	n.a.	n.a.
c_1	0.32	0.34	⟨0.10⟩	⟨0.22⟩
c_2	0.45	0.34	⟨0.33⟩	⟨0.32⟩
c_3	0.12	0.17	⟨0.29⟩	⟨0.18⟩

[a]Character '=' indicates parameter values that are identical for both woods. Terms shown in angled brackets (⟨·⟩) indicate averages. The term "n.a." denotes "not applicable. [b]Values obtained for corn stalk, rice husk, sorghum straw, and wheat straw were obtained from the work of Várhegyi et al.[28] [c]Values obtained for two corncob samples from different climates by Trninić et al.[29]

3.5. Prediction Tests. A usable model should predict approximately the behavior of the samples outside of the temperature programs at which the model parameters were determined. To test this feature, a narrower subset of the experiments can be evaluated, and, on this basis, predictions can be made for those experiments which were not included into the evaluation.[22,26,28,29] In the present work, the experiments with temperature programs **4**−**9** were selected as a subset and evaluated separately. Figures 5 and 6 show that these experiments produced the lowest decomposition rates in our dataset; the peaks of their $-dm/dt$ curves, $(-dm/dt)_{peak}$, were in the range of $(0.1-1) \times 10^{-3}$ s^{-1}. The evaluation of these 10 slow experiments by Model Variant **III** formed the basis for the prediction of experiments at temperature programs **1**−**3** (heating rates of 10, 20, and 40 °C/min) that had much higher decomposition rates: the peak of their $-dm/dt$ were in the range of $(2-8) \times 10^{-3}$ s^{-1}. It may be interesting to note that Evaluations **1**−**5** provided almost the same fit qualities in the prediction tests. Figure 7 displays the results of these prediction tests by Evaluation **3**. As Figure 3 indicates, the fit quality depends on the range of the extrapolations: it is better at 10 °C [when $(-dm/dt)_{peak} \approx 2 \times 10^{-3}$ s^{-1}] than at 40 °C/min [when $(-dm/dt)_{peak} \approx (7-8) \times 10^{-3}$ s^{-1}]. Nevertheless, the simulated curves approximate reasonably the shape and position of the experimental $-dm/dt$ curves in all cases.

3.6. Modeling by *n*-order Kinetics. The n-order kinetics has the same number of model parameters as the DAEM with Gaussian distribution, while its numerical solution is simpler and faster. Its solution is also easier than that of eqs 8 and 9. To test this approach, all evaluations were carried out by a model

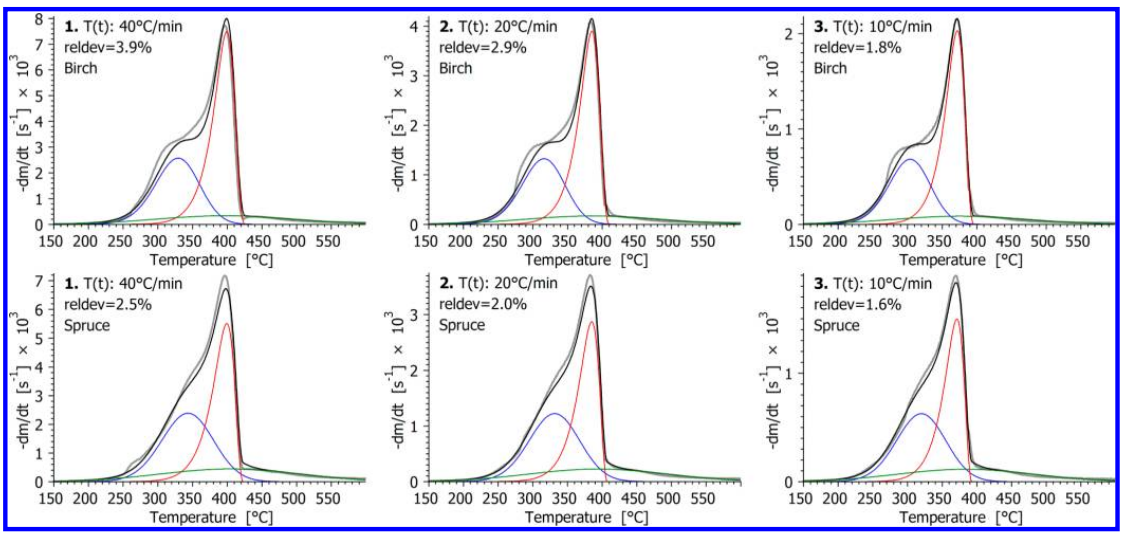

Figure 7. Predicting the faster experiments of the study using parameters obtained from the evaluation of 10 slower experiments in Evaluation **3** by Model Variant **III**. (See Figure 5 for the notations.)

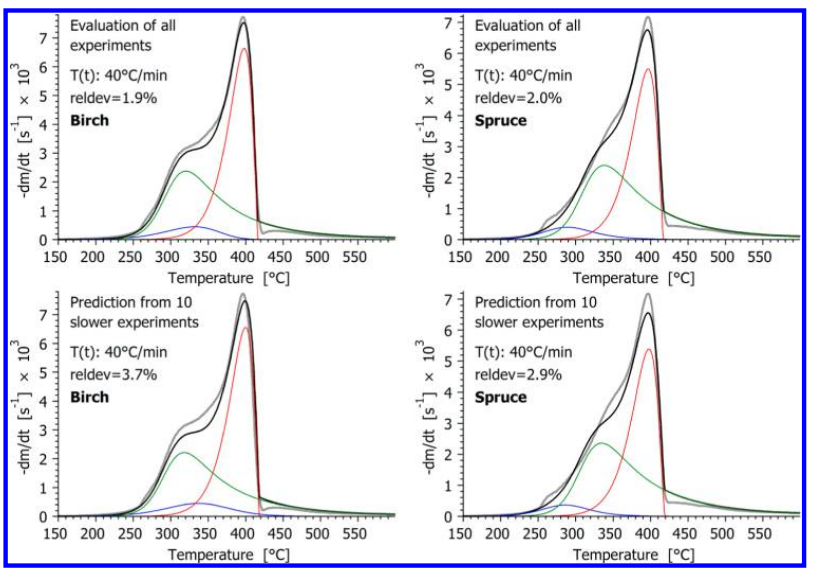

Figure 8. The 40 °C/min experiments in the evaluation and prediction tests by Model Variant **IV** (n-order kinetics) in Evaluation **3**. (See Figure 5 for the notations.)

in which the decomposition of the pseudo-components was described by *n*-order reactions (see eq 7 in section 2.4).

The results are shown as Model Variant **IV** in Table 2. Model Variant **IV** provided fit qualities that were almost as good as those for Model Variant **III**, and the prediction tests outlined in section 3.5 also gave similar relative deviations. Figure 8 shows the results obtained for the 40 °C/min experiments in the evaluation and prediction tests by the model of *n*-order reactions, using the assumptions of Evaluation **3**.

The most striking difference between Figure 8 and the corresponding parts of Figures 5−7 is the peculiar shape of the curve belonging to the third pseudo-component (green line). This problem appeared in all five evaluations with the *n*-order model. In Model Variants **I**−**III**, the third pseudo-component could be associated with the lignin decomposition and, at higher temperatures, with the slow carbonization of the char. In the present case, however, the decomposition of the hemicelluloses is also described mainly by pseudo-component 3, as the peak maxima at ∼320−340 °C of the green curves indicate in Figure 8. Accordingly, pseudo-component 3 describes most of the decomposition of the hemicelluloses plus the lignin pyrolysis plus the slow carbonization of the chars. This is a less

dx.doi.org/10.1021/ef4016075 | *Energy Fuels* 2013, 27, 6134−6145

clear reflection of the processes in the biomass pyrolysis than the ones expressed by the other model variants of the present study. Besides, the *n*-order kinetics describes the complexity of the biomass materials in a rather formal way, while a DAEM gives a simplified, but clear picture on the different reactivities of the different biomass species. The faster numerical calculation of the *n*-order kinetics has little importance nowadays, keeping in mind the low price and high speed of the modern desktop computers.

The corresponding kinetic parameters are listed in Table 4. A recent work on corncobs[29] and the work of Conesa and Domene[19] were used for comparison. The latter work studied five lignocellulosic biomasses: a Mediterranean sort of grass, wheat straw, an oceanic seaweed, and wastes from urban and agricultural pruning. There are several works in the biomass literature that describe the decomposition kinetics of the pseudo-components with *n*-order reactions. The peculiarity of the work of Conesa and Domene was the allowing of high formal reaction order values. This line was followed later by Trninić et al., as well as in the present study. If the reaction order has a lower upper limit, e.g., it is forced to be less than 3, then more pseudo-components are needed for a given fit quality than in the case of DAEM reactions.[26] The improvement is connected to the long tailing of a peak at high *n* that can formally approximate the slow, flat tailing sections of the DTG curves of lignocellulosic materials.

Table 4. Parameters Obtained in Evaluation 3 for Model Variant IV and Their Comparison with Earlier Results[a]

sample	birch	spruce	two corncobs[b]	five biomasses[c]
E_1/kJ mol^{-1}	84	111	173	⟨195⟩
E_2/kJ mol^{-1}	175	170	186	⟨189⟩
E_3/kJ mol^{-1}	172	=	261	⟨157⟩
$\log_{10} A_1/s^{-1}$	5.54	8.70	⟨14.32⟩	⟨21.07⟩
$\log_{10} A_2/s^{-1}$	12.15	11.76	14.00	⟨7.04⟩
$\log_{10} A_3/s^{-1}$	13.63	13.16	19.52	⟨18.27⟩
n_1	1.07	2.07	1.90	⟨3.01⟩
n_2	0.58	0.61	0.94	⟨1.34⟩
n_3	4.71	=	10.38	⟨6.43⟩
c_1	0.06	0.05	0.27	n.a.
c_2	0.42	0.37	0.30	n.a.
c_3	0.41	0.44	0.16	n.a.

[a]The equals sign character (=) indicates parameter values that are identical for both woods. Brackets ⟨·⟩ indicate averages. The term "n.a." means not applicable. [b]Values obtained for two corncob samples from different climates by Trninić et al.[29] [c]Average values calculated from the results of Conesa and Domene on five lignocellulosic biomass materials.[19]

The activation energy values for the cellulose decomposition (E_2) are similar in Tables 3 and 4, as discussed in the next section. The other parameters are rather diverse. The parameters belonging to the birch and spruce samples are not far from each other in Table 4, but differ very much from the values reported for other biomasses as well as for the values in Table 3. The pre-exponential factors follow the activation energies, as usual. The very low pre-exponential factors for the cellulose decomposition in the article of Conesa and Domene appear to be misprints.

3.7. Notes on the Kinetics of the Cellulose Decomposition in the Biomass. The common element in Tables 3 and 4 is the similarities in the activation energy values of the cellulose decomposition (E_2). The E_2 values for the birch and spruce samples differ only by 1 kJ/mol between Tables 3 and 4. The cellulose activation energies taken from earlier works are also similar in Tables 3 and 4, although their range (185−189 kJ/mol) is higher than that obtained in the present study (169−175 kJ/mol). Nevertheless, these differences are not high; the lowest and highest E_2 values in Tables 3 and 4 differ by only 11%. The activation energies reported in the literature are obviously much more diverse, but we selected, for comparison only, such works that employed models and evaluations similar to the present study.

In the present work, 24 E_2 values were obtained in Evaluations **1**−**3** by Model Variants **I**−**IV**: 12 for birch and 12 for spruce. The birch values varied between 174.0 kJ/mol and 175.6 kJ/mol, while the spruce values were between 169.1 kJ/mol and 170.7 kJ/mol. Evaluations **4** and **5** by Model Variants **I**−**IV** yielded 8 E_2 values that were common for the birch and spruce samples; these values fell between 171.6 kJ/mol and 172.7 kJ/mol. Keeping in mind the differences in the modeling and the employed assumptions, the particularly narrow ranges of the E_2 values indicate that the experiments of the present work strongly determine this variable. We believe that this is connected to the particularly wide range of the employed $T(t)$ programs that resulted in the peak maxima of the slowest and fastest experiments differing by a factor of ∼100. The earlier works quoted in Tables 3 and 4 reported E_2 values ca. 10% higher, as noted above. It is possible that this difference is associated with their narrower range of $T(t)$ programs.

3.8. Relevance to Torrefaction. As outlined in the Introduction, the aim of the present model was to describe the thermal decomposition both in the temperature domain of the torrefaction and at higher temperatures. The kinetics of the wood drying was not studied, because most of the drying occurs before the start of the heating in the given apparatus, while the air is flushed out from the furnace.

One can calculate predicted values for characteristics of the torrefaction at any $T(t)$ function by the models presented:

(i) The normalized mass loss after the drying ($1 - m(t)$);
(ii) The normalized mass loss due to the cellulose decomposition ($c_2\alpha_2(t)$);
(iii) The reacted fraction of the cellulose ($0 \le \alpha_2(t) \le 1$);
(iv) The normalized mass loss due to the noncellulosic parts of the sample, which is the difference of $1 - m(t)$ and $c_2\alpha_2(t)$.

The term "normalized" means a division with the mass observed after the drying, as in the other parts of the article. Table 5 lists models (i), (ii), and (iii) from the quantities listed above at various temperature−time values. For this table, a heating rate of 10 °C/min and a subsequent isothermal section was assumed. The calculations were based on Model Variant **III**, using the parameters of Table 3.

The mass loss is higher for birch than for spruce at all temperature−time pairs of Table 5 (although the truncation to two decimals hides this at the lowest values). This can be due to the higher hemicellulose content of the birch wood.[3] As the data indicate, the devolatilization is negligible at 200 °C. One can expect here only the decomposition of a small amount of thermally instable species, which may be enough to hinder the

Table 5. Simulated Characteristics at Various Isothermal Temperatures[a,b,c]

	0 min		10 min		30 min		60 min		120 min	
	birch	spruce	birch	spruce	birch	spruce	birch	spruce	birch	spruce
					200 °C					
$1 - m(t)$	0.00	0.00	0.01	0.01	0.02	0.02	0.03	0.02	0.05	0.03
$c_2\alpha_2(t)$	0.00	0.00	0.00	0.00	0.00	0.00	0.00	0.00	0.00	0.00
$\alpha_2(t)$	0.00	0.00	0.00	0.00	0.00	0.00	0.00	0.00	0.00	0.00
					225 °C					
$1 - m(t)$	0.01	0.01	0.03	0.03	0.07	0.04	0.10	0.06	0.14	0.09
$c_2\alpha_2(t)$	0.00	0.00	0.00	0.00	0.00	0.00	0.00	0.00	0.00	0.00
$\alpha_2(t)$	0.00	0.00	0.00	0.00	0.00	0.00	0.00	0.00	0.00	0.00
					250 °C					
$1 - m(t)$	0.03	0.02	0.10	0.07	0.17	0.11	0.22	0.15	0.27	0.20
$c_2\alpha_2(t)$	0.00	0.00	0.00	0.00	0.00	0.00	0.01	0.01	0.01	0.01
$\alpha_2(t)$	0.00	0.00	0.00	0.00	0.01	0.01	0.01	0.02	0.03	0.03
					275 °C					
$1 - m(t)$	0.08	0.06	0.22	0.16	0.30	0.24	0.35	0.30	0.42	0.38
$c_2\alpha_2(t)$	0	0.00	0.01	0.01	0.02	0.02	0.04	0.04	0.08	0.07
$\alpha_2(t)$	0	0.00	0.02	0.02	0.04	0.05	0.08	0.10	0.17	0.20
					300 °C					
$1 - m(t)$	0.18	0.14	0.35	0.30	0.45	0.42	0.56	0.53	0.71	0.67
$c_2\alpha_2(t)$	0.00	0.00	0.04	0.03	0.10	0.09	0.20	0.17	0.34	0.28
$\alpha_2(t)$	0.01	0.01	0.08	0.10	0.23	0.26	0.44	0.49	0.76	0.83

[a]Model Variant III was used for prediction with the parameters of Table 3. [b]Isothermal torrefaction was assumed after heating at a rate of 10 °C/min until the desired temperature is reached. The time values in the header line belong to the isothermal section. [c]Three predicted torrefaction characteristics were tabulated at each temperature: the normalized mass loss $[1 - m(t)]$; the normalized mass loss due to cellulose decomposition $[c_2\alpha_2(t)]$; and the reacted fraction of the cellulose $[\alpha_2(t)]$.

biological decay (rotting) but cannot increase the energy density of the obtained fuels. It may be interesting to observe that a 60-min decomposition at 250 °C and a 10-min decomposition at 275 °C result in almost the same level of devolatilization for both woods. On the other hand, a prolonged heating at 275 °C leads to a considerable loss of the cellulose component, which is not desired during torrefaction.

The comparison of the values in Table 5 with actual torrefaction data is left for a future work. Note that the temperature values in the present case were much closer to the actual temperatures than in a macro furnace or in an industrial reactor. Accordingly, care is needed for such a comparison.

4. CONCLUSIONS

(1) The thermal decomposition of a deciduous and an evergreen wood species were studied at slow heating programs, under well-defined conditions. Nine TGA experiments were carried out for each sample with different temperature programs. Highly different temperature programs were selected to increase the information content available for the modeling. The ratio of the highest and lowest peak maxima was ∼100 in the set of the experiments used for the evaluation. In this way, the models obtained described the experiments under a wide range of experimental conditions.

(2) Several model variants were tested. The best performance was achieved when the cellulose decomposition was described by a submodel that can mimic self-acceleration tendencies. The decomposition of the noncellulosic parts of the biomass was described by two reactions assuming a distributed activation energy model in this case. The complexity of the applied model reflects the complexity of the studied materials.

(3) The model employed contains 13 unknown parameters for a given biomass. Part of the kinetic parameters could be assumed common for the samples without a substantial worsening of the fit quality. This approach increased the average experimental information for an unknown parameter and revealed the similarities in the behavior of the different samples. In the preferred evaluation strategy of the paper, the number of model parameters was similar to the number of the evaluated differential thermogravimetry (DTG) curves.

(4) When each partial reaction was described by *n*-order kinetics, similar fit qualities were obtained. However, the *n*-order kinetics describes the complexity of the biomass materials in a rather formal way.

(5) The results were checked by prediction tests. In these tests, 10, 20, and 40 °C/min experiments were simulated by the model parameters obtained from the evaluation of 10 experiments with lower reaction rates.

(6) A table was calculated by the preferred model variant that may provide guidance about the extent of devolatilization at various temperature−residence time values during wood torrefaction.

■ AUTHOR INFORMATION

Corresponding Author

*Tel.: +36 1 2461894. Fax: +36 1 4381147. E-mail: varhegyi.gabor@t-online.hu.

Notes

The authors declare no competing financial interest.

■ ACKNOWLEDGMENTS

The authors acknowledge the financial support by the Research Council of Norway and a number of industrial partners through

the project STOP ("STable OPerating conditions for biomass combustion plants"). STOP is also a part of the research center CenBio (Bioenergy Innovation Centre).

NOMENCLATURE

α = reacted fraction of a component or pseudo-component (dimensionless)
σ = width parameter (variance) of Gaussian distribution (kJ/mol)
A = pre-exponential factor (s^{-1})
E = activation energy (kJ/mol) or the mean of an activation energy distribution (kJ/mol)
f = empirical function (eq 9) expressing the change of the reactivity as the reactions proceed (dimensionless)
h_k = height of an experimental $-dm/dt$ curve (s^{-1})
m = mass of the sample normalized by the initial dry sample mass (dimensionless)
n = reaction order (dimensionless)
of = objective function minimized in the least-squares evaluation (dimensionless)
N_{exper} = number of experiments evaluated together by the method of least-squares
N_k = number of evaluated data on the kth experimental curve
R = gas constant; $R = 8.3143 \times 10^{-3}$ kJ mol^{-1} K^{-1}
reldev = deviation between the observed and calculated data, expressed as a percentage of the corresponding peak height
$reldev_{18}$ = root-mean-square of the *reldev* values of 18 experiments
rms = root-mean-square
t = time (s)
T = temperature (°C, K)
z = formal parameter in eq 9 (dimensionless)

Subscripts

i = digitized point on an experimental curve
j = pseudo-component
k = experiment

REFERENCES

(1) van der Stelt, M. J. C.; Gerhauser, H.; Kiel, J. H. A.; Ptasinski, K. J. Biomass upgrading by torrefaction for the production of biofuels: A review. *Biomass Bioenergy* **2011**, *35*, 3748−3762.
(2) Chew, J. J.; Doshi, V. Recent advances in biomass pretreatment—Torrefaction fundamentals and technology. *Renew. Sustain. Energy Rev.* **2011**, *15* (8), 4212−4222.
(3) Tapasvi, D.; Khalil, R. A.; Skreiberg, Ø.; Tran, K.-Q.; Gronli, M. G. Torrefaction of Norwegian birch and spruce − An experimental study using macro-TGA. *Energy Fuels* **2012**, *26*, 5232−5240.
(4) Tapasvi, D. T., K-Q.; Wang, L.; Skreiberg, Ø.; Khalil, R. Biomass torrefaction—A review. In *Proceedings of the 9th European Conference on Industrial Furnaces and Boilers*, Estoril, Portugal, 2011 (ISBN 978-972-99309-6-6).
(5) Prins, M. J.; Ptasinski, K. J.; Janssen, F. J. J. G. Torrefaction of wood. *J. Anal. Appl. Pyrolysis* **2006**, *77*, 35−40.
(6) Rousset, P.; Davrieux, F.; Macedo, L.; Perré, P. Characterisation of the torrefaction of beech wood using NIRS: Combined effects of temperature and duration. *Biomass Bioenergy* **2011**, *35*, 1219−1226.
(7) Melkior, T.; Jacob, S.; Gerbaud, G.; Hediger, S.; Le Pape, L.; Bonnefois, L.; Bardet, M. NMR analysis of the transformation of wood constituents by torrefaction. *Fuel* **2012**, *92* (1), 271−280.
(8) Chen, W.-H.; Kuo, P.-C. Torrefaction and co-torrefaction characterization of hemicellulose, cellulose and lignin as well as torrefaction of some basic constituents in biomass. *Energy* **2011**, *36* (2), 803−811.
(9) Prins, M. J.; Ptasinski, K. J.; Janssen, F. J. J. G. Torrefaction of wood. *J. Anal. Appl. Pyrolysis* **2006**, *77*, 28−34.
(10) Chen, W.-H.; Kuo, P.-C. Isothermal torrefaction kinetics of hemicellulose, cellulose, lignin and xylan using thermogravimetric analysis. *Energy* **2011**, *36* (11), 6451−6460.
(11) Bates, R. B.; Ghoniem, A. F. Biomass torrefaction: Modeling of volatile and solid product evolution kinetics. *Bioresour. Technol.* **2012**, *124*, 460−469.
(12) Peng, J.; Bi, X. T.; Lim, J.; Sokhansanj, S. Development of torrefaction kinetics for British Columbia softwoods. *Int. J. Chem. React. Eng.* **2012**, *10*, DOI:10.1515/1542-6580.2878.
(13) Lu, K.-M.; Lee, W.-J.; Chen, W.-H.; Lin, T.-C. Thermogravimetric analysis and kinetics of co-pyrolysis of raw/torrefied wood and coal blends. *Appl. Energy* **2013**, *105*, 57−65.
(14) Park, J.; Meng, J.; Lim, K. H.; Rojas, O. J.; Park, S. Transformation of lignocellulosic biomass during torrefaction. *J. Anal. Appl. Pyrolysis* **2013**, *100*, 199−206.
(15) Shang, L.; Ahrenfeldt, J.; Holm, J. K.; Barsberg, S.; Zhang, R.-z.; Luo, Y.-h.; Egsgaard, H.; Henriksen, U. B. Intrinsic kinetics and devolatilization of wheat straw during torrefaction. *J. Anal. Appl. Pyrolysis* **2013**, *100*, 145−152.
(16) Blasi, C. D.; Lanzetta, M. Intrinsic kinetics of isothermal xylan degradation in inert atmosphere. *J. Anal. Appl. Pyrolysis* **1997**, *40*−*41*, 287−303.
(17) Várhegyi, G.; Antal, M. J., Jr.; Székely, T.; Szabó, P. Kinetics of the thermal decomposition of cellulose, hemicellulose and sugar cane bagasse. *Energy Fuels* **1989**, *3*, 329−335.
(18) Di Blasi, C. Modeling chemical and physical processes of wood and biomass pyrolysis. *Prog. Energy Combust. Sci.* **2008**, *34*, 47−90.
(19) Conesa, J. A.; Domene, A. Biomass pyrolysis and combustion kinetics through *n*-th-order parallel reactions. *Thermochim. Acta* **2011**, *523*, 176−181.
(20) Burnham, A. K.; Braun, R. L. Global kinetic analysis of complex materials. *Energy Fuels* **1999**, *13*, 1−22.
(21) Avni, E.; Coughlin, R. W.; Solomon, P. R.; King, H. H. Mathematical modelling of lignin pyrolysis. *Fuel* **1985**, *64*, 1495−1501.
(22) Várhegyi, G.; Szabó, P.; Antal, M. J., Jr. Kinetics of charcoal devolatilization. *Energy Fuels* **2002**, *16*, 724−731.
(23) de Jong, W.; Pirone, A.; Wojtowicz, M. A. Pyrolysis of Miscanthus Giganteus and wood pellets: TG-FTIR analysis and reaction kinetics. *Fuel* **2003**, *82*, 1139−1147.
(24) Wójtowicz, M. A.; Bassilakis, R.; Smith, W. W.; Chen, Y.; Carangelo, R. M. Modeling the evolution of volatile species during tobacco pyrolysis. *J. Anal. Appl. Pyrolysis* **2003**, *66*, 235−261.
(25) Yi, S.-C.; Hajaligol, M. R. Product distribution from the pyrolysis modeling of tobacco particles. *J. Anal. Appl. Pyrolysis* **2003**, *66*, 217−234.
(26) Becidan, M.; Várhegyi, G.; Hustad, J. E.; Skreiberg, Ø. Thermal decomposition of biomass wastes. A kinetic study. *Ind. Eng. Chem. Res.* **2007**, *46*, 2428−2437.
(27) Várhegyi, G.; Czégény, Zs.; Jakab, E.; McAdam, K.; Liu, C. Tobacco pyrolysis. Kinetic evaluation of thermogravimetric − mass spectrometric experiments. *J. Anal. Appl. Pyrolysis* **2009**, *86*, 310−322.
(28) Várhegyi, G.; Bobály, B.; Jakab, E.; Chen, H. Thermogravimetric study of biomass pyrolysis kinetics. A distributed activation energy model with prediction tests. *Energy Fuels* **2011**, *25*, 24−32.
(29) Trninić, M.; Wang, L.; Várhegyi, G.; Grønli, M.; Skreiberg, Ø. Kinetics of corncob pyrolysis. *Energy Fuels* **2012**, *26*, 2005−2013.
(30) Manyà, J. J.; Velo, E.; Puigjaner, L. Kinetics of biomass pyrolysis: A reformulated three-parallel-reactions model. *Ind. Eng. Chem. Res.* **2003**, *42*, 434−441.
(31) Tapasvi, D.; Khalil, R.; Várhegyi, G.; Skreiberg, Ø.; Tran, K.-Q.; Grønli, M. Kinetic behavior of torrefied biomass in an oxidative environment. *Energy Fuels* **2013**, *27*, 1050−1060.
(32) *High resolution thermogravemetric analysis—A new technique for obtaining superior analytical results*. Technical Report TA-023, TA Instruments, New Castle, DE. Available via the Internet at http://www.tainstruments.co.jp/application/pdf/Thermal_Library/Applications_Briefs/TA023.PDF.

(33) Grønli, M. G.; Várhegyi, G.; Di Blasi, C. Thermogravimetric analysis and devolatilization kinetics of wood. *Ind. Eng. Chem. Res.* **2002**, *41*, 4201−4208.
(34) Várhegyi, G.; Chen, H.; Godoy, S. Thermal decomposition of wheat, oat, barley and Brassica carinata straws. A kinetic study. *Energy Fuels* **2009**, *23*, 646−652.
(35) Várhegyi, G.; Szabó, P.; Mok, W. S. L.; Antal, M. J., Jr. Kinetics of the thermal decomposition of cellulose in sealed vessels at elevated pressures. Effects of the presence of water on the reaction mechanism. *J. Anal. Appl. Pyrolysis* **1993**, *26*, 159−174.
(36) Donskoi, E.; McElwain, D. L. S. Optimization of coal pyrolysis modeling. *Combust. Flame* **2000**, *122*, 359−367.
(37) de Jong, W.; Di Nola, G.; Venneker, B. C. H.; Spliethoff, H.; Wójtowicz, M. A. TG-FTIR pyrolysis of coal and secondary biomass fuels: Determination of pyrolysis kinetic parameters for main species and NOx precursors. *Fuel* **2007**, *86*, 2367−2376.
(38) Conesa, J. A.; Caballero, J. A.; Marcilla, A.; Font, R. Analysis of different kinetic models in the dynamic pyrolysis of cellulose. *Thermochim. Acta* **1995**, *254*, 175−192.
(39) Capart, R.; Khezami, L.; Burnham, A. K. Assessment of various kinetic models for the pyrolysis of a microgranular cellulose. *Thermochim. Acta* **2004**, *417*, 79−89.
(40) Várhegyi, G.; Sebestyén, Z.; Czégény, Z.; Lezsovits, F.; Könczöl, S. Combustion kinetics of biomass materials in the kinetic regime. *Energy Fuels* **2012**, *26*, 1323−1335.
(41) Várhegyi, G.; Szabó, P.; Jakab, E.; Till, F.; Richard, J.-R. Mathematical modeling of char reactivity in Ar−O_2 and CO_2−O_2 mixtures. *Energy Fuels* **1996**, *10*, 1208−1214.

Paper IV

Kinetic behavior of torrefied biomass in an oxidative environment

Tapasvi, D.; Khalil, R.; Várhegyi, G.; Skreiberg, Ø.;

Tran, K.-Q.; Grønli, M.

Energy Fuels, 2013, 27, 1050-1060.

energy&fuels

Article

pubs.acs.org/EF

Kinetic Behavior of Torrefied Biomass in an Oxidative Environment

Dhruv Tapasvi,[†] Roger Khalil,[‡] Gábor Várhegyi,*[,§] Øyvind Skreiberg,[‡] Khanh-Quang Tran,[†] and Morten Grønli[†]

[†]Department of Energy and Process Engineering, Norwegian University of Science and Technology (NTNU), NO-7491 Trondheim, Norway

[‡]SINTEF Energy Research, Post Office Box 4761, Sluppen, NO-7465 Trondheim, Norway

[§]Institute of Materials and Environmental Chemistry, Research Centre for Natural Sciences, Hungarian Academy of Sciences, Post Office Box 17, Budapest 1525, Hungary

Supporting Information

ABSTRACT: The combustion of four torrefied wood samples and their feedstocks (birch and spruce) was studied at slow heating programs, under well-defined conditions by thermogravimetry (TGA). Particularly low sample masses were employed to avoid the self-heating of the samples because of the huge reaction heat of the combustion. Linear, modulated, and constant reaction rate (CRR) temperature programs were employed in the TGA experiments in gas flows of 5 and 20% O_2. In this way, the kinetics was based on a wide range of experimental conditions. The ratio of the highest and lowest peak maxima was around 50 in the experiments used for the kinetic evaluation. A recent kinetic model by Várhegyi et al. (Várhegyi, G.; Sebestyén, Z.; Czégény, Z.; Lezsovits, F.; Könczöl, S. *Energy Fuels* **2012**, *26*, 1323−1335) was employed with modifications. This model consists of two devolatilization reactions and a successive char burnoff reaction. The cellulose decomposition in the presence of oxygen has a self-accelerating (autocatalytic) kinetics. The decomposition of the non-cellulosic parts of the biomass was described by a distributed activation model. The char burnoff was approximated by power-law (*n*-order) kinetics. Each of these reactions has its own dependence upon the oxygen concentration that was expressed by power-law kinetics too. The complexity of the applied model reflects the complexity of the studied materials. The model contained 15 unknown parameters for a given biomass. Part of these parameters could be assumed common for the six samples without a substantial worsening of the fit quality. This approach increased the average experimental information for an unknown parameter by a factor of 2 and revealed the similarities in the behavior of the different samples.

1. INTRODUCTION

Biomass has been widely recognized as a vital renewable energy source to meet current as well as future energy demands of the world. The extended use of biomass will help to reduce the greenhouse gas emissions and also extend the lifetime of fossil fuel resources. To promote biomass usage, various countries have or are trying to establish promising bioenergy policies. The Scandinavian countries take particular efforts in this direction. Sweden, for example, has set up a goal that 40% of its primary energy supply should come from biomass by 2020.[1] Similarly, Norway formulated a goal of 30% reduction in greenhouse gas emissions before 2020, and certainly, extended biomass usage will help achieve this target.[2]

However, the widespread use of biomass is faced with many challenges linked to the general properties of biomass, such as high moisture content, poor grindability, low calorific value, and low bulk density. Torrefaction is one of the potential solutions to these problems, and it has gained a lot of research momentum as a biomass pretreatment process in the last 2 decades.[3,4] It is essentially a mild pyrolysis process carried out at a temperature between 200 and 300 °C in an inert atmosphere. During torrefaction, the fuel retains most of its energy content. Torrefaction affects mostly the hemicellulose fraction of biomass, but as the process temperature is increased, other biomass components, such as cellulose, lignin, and extractives, are also decomposed. Torrefaction improves the properties of the biomass fuels; among others, it reduces the moisture content, increases the energy density and heating value, changes the hygroscopic behavior of the raw biomass into a hydrophobic behavior, and enhances grindability.[3−5]

Several torrefaction studies are available in the literature. Most of these studies have focused on characterizing torrefied products and evaluating product yields and product properties, such as grindability, particle size distribution, and hydrophobicity, from various biomass materials, such as woods, agricultural residues, and energy crops.[3−5] However, because the eventual use of biomass fuel is use in thermochemical processes, such as combustion, gasification, and pyrolysis, the actual test of torrefaction is how it affects the behavior of biomass in these processes. Thus far, only a few studies have attempted to analyze the reactivity of torrefied products in these processes, and only limited information is available in this field.[6−14] For combustion, being the main process option for the use of biomass, the understanding of the behavior of torrefied biomass under oxidative conditions should be a priority. The present work aims at studying the combustion process under kinetic control and providing a background for future kinetic submodels. Because thermogravimetric analysis (TGA) is a proven method to collect

Received: November 26, 2012
Revised: January 18, 2013
Published: January 18, 2013

dx.doi.org/10.1021/ef3019222 | *Energy Fuels* 2013, 27, 1050−1060

basic information on the partial processes and reaction kinetics of the thermal degradation of biomass materials, it was chosen for this study. With its high precision and well-controlled experimental conditions, TGA is a useful tool for studying devolatilization and combustion in the kinetic regime.[15,16] However, TGA can be employed only at relatively low heating rates because the true temperature of the samples becomes unknown at high heating rates. Accordingly, the results of the TGA studies cannot be used directly in the modeling of industrial combustors; they serve as basic research to direct further development in the field.

Among the previous studies, Bridgeman et al.,[13] Arias et al.,[14] Jones et al.,[10] and Broström et al.[12] have used TGA to evaluate the combustion reactivity of torrefied samples. No kinetic analysis was performed by Bridgeman et al.[13] Arias et al.[14] divided the TGA experiments into low- and high-temperature stages (below and above ca. 400 °C, respectively) and described both stages by first-order kinetics. Jones et al.[10] performed TGA experiments on chars that were prepared from torrefied biomass samples and applied a first-order reaction model to deduce kinetic parameters for the char reactivity under oxidative conditions. They observed that the chars from the torrefied samples had lower reactivity than the chars produced from raw samples, but they had higher reactivity than the chars produced from coal. In a later study, Broström et al.[12] provided a detailed kinetic model for the devolatilization and oxidative kinetics of torrefied Norwegian spruce wood. For the devolatilization, measured curves were predicted by three parallel reaction mechanisms corresponding approximately to the three main wood components: hemicellulose, cellulose, and lignin. In the presence of oxygen, two additional reactions for the char devolatilization and combustion were included.

The present work continues the efforts of Broström et al.[12] to establish a detailed model for the oxidation kinetics with the following extensions: (i) Broström et al.[12] used TGA experiments with heating rates of 2.5, 5, and 10 °C/min at one oxygen concentration on samples prepared from one feedstock (spruce). The TGA experiments of the present work cover a wider set of experimental conditions, as outlined in section 2.2, and the study is based on two feedstocks: a deciduous and an evergreen species (birch and spruce). The presented kinetic model is based on the least-squares evaluation of 36 experiments. (ii) Broström et al.[12] employed a kinetic model built from n-order independent parallel reactions. In the present work, a more complex model is used,[17] which tries to reflect better the real complexity of the biomass combustion. The model itself is outlined in sections 3.2 and 3.3. We believe that the fast development of both software and hardware will make it possible to employ the more complex models too in practical calculations.

2. MATERIALS AND METHODS

2.1. Sample Characterization and Preparation. The samples were composed of two wood types: birch and spruce, which are commonly available in Norway. Sample particle sizes of 10 mm cubes from both feedstocks were torrefied in a batch reactor (macro-TGA). The details of the torrefaction process were presented in a recent work.[5] The samples were heated at a heating rate of 5 °C/min up to either 225 or 275 °C. Samples with a 60 min holdup time at the torrefaction temperature were used in this kinetic study. Fine grinding of the torrefied samples was performed in a cutting mill equipped with 1 mm bottom sieve. The powder samples were sieved afterward with a series of sieves with mesh sizes of 1 mm, 500 μm, 180 μm, 125 μm, and 63 μm in a vibrating sieving machine. The particles belonging to the size 63−125 μm were used for the kinetic study. In all, six samples were prepared for this study, four torrefied samples and two raw fuels. The torrefaction conditions under which the samples were generated, along with the naming convention for these, are presented in Table 1. Table 2 shows the ultimate and proximate analyses of the samples.

Table 1. Samples Used for the Kinetic Modeling

name	sample	torrefaction temperature (°C)
B --	birch	none
B225	birch	225
B275	birch	275
S --	spruce	none
S225	spruce	225
S275	spruce	275

2.2. Experimental Setup and Procedure. The reactivity studies were conducted in a Q5000 IR analyzer from TA Instruments, which has a sensitivity of 0.1 μg. Oxygen−nitrogen mixtures at 5 and 20% (v/v) were used as purge gas with a gas flow of 100 mL/min. Sample masses of 0.5 mg or less were used to avoid self-heating of the samples because of the high reaction heat. Each sample was analyzed with three different heating programs, as shown in Figure 1: (i) 10 °C/min linear $T(t)$, (ii) modulated $T(t)$, where sinus waves with 5 °C amplitudes and 200 s wavelength were superposed on a slow, 2 °C/min linear, and (iii) "constant reaction rate" (CRR) $T(t)$, when the employed equipment regulated the heating of the samples, so that the reaction rate would oscillate around a preset limit.[18] The CRR experiments aimed at getting very low mass-loss rates in the whole domain of the reaction. The differential thermogravimetry (DTG) peak maxima of the CRR experiments varied between 0.04 and 0.07 μg/s. This interval corresponds to rates between 0.8×10^{-4} and 1.3×10^{-4} s^{-1} after normalization by the initial dry sample mass. The $T(t)$ program for a CRR experiment obviously depends upon the behavior of the given sample. Figure 1 shows four of the CRR $T(t)$ programs of the present study.

The modulated and CRR temperature programs were employed to increase the information content of the data, as outlined in earlier work.[19,20] From one point of view, the linear $T(t)$ experiments with different heating rates are rather similar to each other; hence, their information content is limited.[19] On the other hand, an acceptable kinetic model should describe well the experiments at any $T(t)$, including the highly irregular CRR temperature programs too.[20]

2.3. Numerical Methods. Fortran 95 and C++ programs were employed for the numerical calculations and for graphics handling, respectively. The employed numerical methods have been described in details earlier.[21] The kinetic evaluation was based on the least-squares evaluation of the $-dm^{obs}/dt$ curves, where m^{obs} is the sample mass normalized by the initial dry sample mass. The method[22] used for the determination of $-dm^{obs}/dt$ does not introduce considerable systematic errors into the least-squares kinetic evaluation of experimental results.[23] The model was solved numerically along the empirical temperature−time functions. The model parameters were determined by nonlinear least-squares minimization, as outlined in sections 3.1 and 3.4. The calculations were carried out on a desktop computer equipped with a 3.4 GHz Intel Core i7 processor, under Windows. The run times varied between 10 min and 10 h, depending upon the initial guess of the parameters in the nonlinear least-squares minimization. The calculation of one theoretical DTG curve by the model outlined in section 3.3 requires 23 μs on average without parallel computation. With the use of the four cores of the processor, one can calculate one million theoretical curves in 96 min.

3. RESULTS AND DISCUSSION

3.1. Evaluation by the Method of Least Squares and Characterization of the Fit Quality. The kinetic evaluation is carried out by the method of least squares. Such values are searched for the unknown model parameters that minimize the

dx.doi.org/10.1021/ef3019222 | Energy Fuels 2013, 27, 1050−1060

Table 2. Proximate and Ultimate Analyses of the Samples[a]

	proximate analysis			ultimate analysis					
sample	volatile matter	fixed carbon	ash	C	H	O	N	S	HHV[b]
B --	89.4	10.4	0.2	48.62	6.34	44.9	0.09	<0.05	19.80
B22S	86.4	13.2	0.4	49.90	5.98	44.00	0.10	<0.05	19.90
B27S	77.7	21.9	0.4	54.16	5.65	40.00	0.12	<0.05	21.40
S --	86.3	13.4	0.2	50.1	6.36	43.52	0.07	<0.05	20.45
S22S	84.0	15.8	0.2	50.97	6.15	42.76	0.07	<0.05	20.62
S27S	75.7	24.2	0.2	55.33	5.73	38.81	0.09	<0.05	22.05

[a]In units of % (m/m), dry basis. [b]In units of MJ/kg.

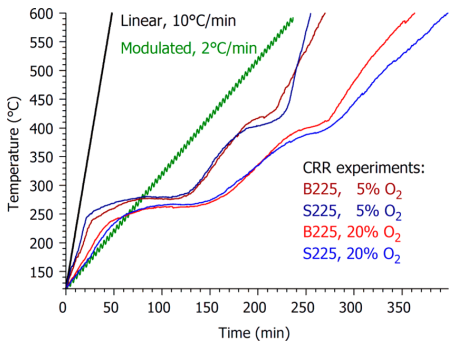

Figure 1. Temperature programs used in the TGA experiments. Note that each of the 12 constant heating rate experiments has different $T(t)$; this figure shows four of them.

following objective function:

$$of = \sum_{k=1}^{N_{exper}} \sum_{i=1}^{N_k} \frac{\left[\left(\frac{dm}{dt}\right)_k^{obs}(t_i) - \left(\frac{dm}{dt}\right)_k^{calc}(t_i)\right]^2}{N_k h_k^{\,2}} \quad (1)$$

Here, N_{exper} is the number of experiments evaluated together; its value in the present work is either 6 or 36, as outlined later. The division by h_k^2 serves to counterbalance the high magnitude differences. Traditionally, h_k is the highest observed value of the given experiment.[24] The normalization by the highest observed values in the least-squares sum assumes implicitly that the relative precision is roughly the same for the different experiments. This assumption has proven to be useful in numerous works on non-isothermal kinetics since 1993.[24] Among others, the antecedents of the present work also used it.[17,20,21] However, the magnitude differences were very high in the present work. The peak maxima of the CRR experiments scattered around a very low value, 1×10^{-4} s^{-1}, while the peak maxima of the 10 °C/min experiments were roughly 30 times higher. The ratio of the highest and lowest peak maxima was around 50 in the given set of the experiments. Test calculations showed that one cannot assume approximately equal relative precisions at such high magnitude differences. No information was available on the absolute and relative precision of the $-dm/dt$ values in the CRR experiments; hence, the choice of the h_k of the CRR experiments could not be based on theoretical considerations. An arbitrary $h_k = 5 \times 10^{-4}$ s^{-1} value was used for the CRR experiments, which is ca. 5 times higher than their peak maxima. The fit qualities obtained in this way will be discussed in section 3.4. The peak maxima of the 10 °C/min linear $T(t)$ experiments and the 2 °C/min modulated experiments were much higher, around 33×10^{-4} and 9×10^{-4} s^{-1}, respectively; hence, their peak maxima could be used as h_k values in the usual way. The fit qualities obtained in this way will be shown in details in section 3.5 and in the Supporting Information.

The obtained fit quality can be characterized separately for each of the experiments evaluated together. The deviation between the observed and calculated DTG values of a given experiment is given as a root mean square (rms).

$$\mathrm{dev}_k\ (\mu g/s) = \left\{ N_k^{-1} \sum_{i=1}^{N_k} \left[\left(\frac{dG}{dt}\right)_k^{obs}(t_i) - \left(\frac{dG}{dt}\right)_k^{calc}(t_i)\right]^2 \right\}^{1/2} \quad (2)$$

Here, subscript k indicates the experiments of the series evaluated; t_i denotes the time values in which the discrete experimental values were taken; N_k is the number of t_i points in a given experiment; and G is the TGA signal without normalization in micrograms.

The deviations defined by eq 2 can also be expressed as percent of the peak maximum, obtaining in this way a sort of relative deviation.

$$\mathrm{rel\ dev}_k\ (\%) = 100\mathrm{dev}_k / \max\left(\frac{dG}{dt}\right)_k^{obs} \quad (3a)$$

The same relative deviations can obviously be calculated from $-dm^{obs}/dt$ values too, because the G and m values differ only by a constant divisor.

$$\mathrm{rel\ dev}_k\ (\%) = 100\left\{ N_k^{-1} \sum_{i=1}^{N_k} \left[\left(\frac{dm}{dt}\right)_k^{obs}(t_i) - \left(\frac{dm}{dt}\right)_k^{calc}(t_i)\right]^2 \right\} / \max\left(\frac{dm}{dt}\right)_k^{obs} \quad (3b)$$

In the tables of the present work, the magnitude of the objective function will be characterized by $100(of)^{1/2}$ because this quantity is related to the relative deviations by eq 3b. If all h_k values were equal to the corresponding peak maxima, $100(of)^{1/2}$ would be equal to the rms formed from the relative deviations of the evaluated experiments.

3.2. Four Main Reactions That Are Described by Three Pseudo-components. Figure 2 compares the behavior of the samples at 10 °C/min heating rate in 20% oxygen. As in a previous work,[17] the DTG curves of the untreated samples (green lines) can be interpreted as the results of four main reactions that partly overlap each other: (i) the decomposition of the hemicellulose and other thermally labile parts of the sample that dominate the DTG approximately between 200 and 300 °C,

dx.doi.org/10.1021/ef3019222 | Energy Fuels 2013, 27, 1050−1060

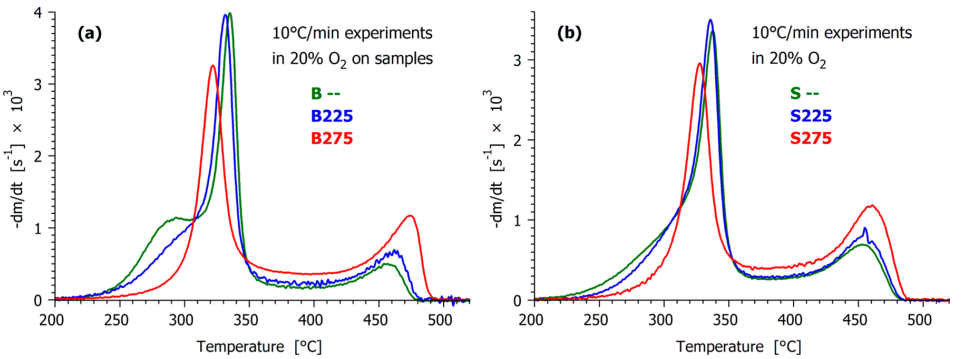

Figure 2. Comparison of the experiments at 10 °C/min heating rate in 20% oxygen.

(ii) the oxidative decomposition of the cellulose component, which produces a sharper peak with a maximum around 335 °C, (iii) a flat section, which, because of the high-temperature end of the lignin decomposition and the slow carbonization and other reactions of the formed char, dominates the DTG approximately between 360 and 430 °C, (iv) and the char burnoff, which results in a peak around 460 °C.

Earlier works have shown that reactions i and iii can be described by the same distributed activation energy model,[17,23,25] as outlined in the next section.

The inorganic components are distributed in various forms in the woody biomass.[26] The ash formation includes chemical reactions as well as the physical agglomeration of the inorganic particles after the burnoff of the organic constituents. The present samples contain only a low amount of mineral matter (0.2−0.4%); hence, it is possible to neglect the ash-formation reactions. However, this would reduce the future applicability potential of the model. As an alternate solution, the parameter connected to the ash formation will be determined from the total ash of the proximate analysis, as outlined in the next section. In this way, the inclusion of a global ash formation reaction will not increase the number of unknown parameters in the least-squares procedure. From a computational point of view, the ash formation rates are proportional to the char burnoff rates; hence, their calculation does not require any extra effort.

3.3. Employed Model. As mentioned in the Introduction, the model of wood combustion is employed from a recent work,[17] except a minor change in the description of the cellulose part of the samples. All masses in the treatment are normalized by the initial sample mass. The normalized amounts of the unreacted part of the sample, char, and ash will be denoted by m_{ur}, m_{char}, and m_{ash}, respectively. As the reactions proceed, m_{ur} decreases from 1 to 0 because no unreacted biomass remains at the end. m_{char} is zero at the beginning of an experiment. It reaches a maximum as the char forms and converges to zero again as the char burns off. m^{calc} is the sum of the normalized masses of the solid components.

$$m^{calc}(t) = m_{ur}(t) + m_{char}(t) + m_{ash}(t) \tag{4a}$$

$$\frac{dm^{calc}}{dt} = \frac{dm_{ur}}{dt} + \frac{dm_{char}}{dt} + \frac{dm_{ash}}{dt} \tag{4b}$$

The unreacted part of the sample, m_{ur}, will be regarded as the sum of the cellulose component and the rest of the sample. The models for pyrolysis kinetics are usually written for variables that run from 0 to 1; accordingly, we shall use a reacted fraction for cellulose, $\alpha_{cell}(t)$, and another reacted fraction, $\alpha_{other}(t)$, for the other components of the biomass. The corresponding boundary conditions are $\alpha_{cell}(0) = 0$, $\alpha_{cell}(\infty) = 1$, $\alpha_{other}(0) = 0$, and $\alpha_{other}(\infty) = 1$. $m_{ur}(t)$ is the weighted sum of its two constituents with weight factors c_{cell} and c_{other}.

$$m_{ur}(t) = c_{cell}[1 - a_{cell}(t)] + c_{other}[1 - a_{other}(t)] \tag{5a}$$

$$-\frac{dm_{ur}}{dt} = c_{cell}\frac{d\alpha_{cell}}{dt} + c_{other}\frac{d\alpha_{other}}{dt} \tag{5b}$$

At $t = 0$, eq 5a reduces to

$$1 = c_{cell} + c_{other} \tag{5c}$$

The char burnoff will be described by power-law kinetics where the reaction rate is n_{char}-order with respect to m_{char} and ν_{char}-order with respect to the oxygen concentration, C_{O_2}. Accordingly, the char burnoff rate is approximated as

$$\text{char burnoff rate} = A_{char}C_{O_2}^{\nu_{char}} \exp\left(-\frac{E_{char}}{RT}\right)m_{char}^{n_{char}} \tag{6}$$

Both the cellulose and non-cellulosic parts of the biomass form char. The corresponding char yields are denoted by $y_{cell.char}$ and y_{other_char}, respectively, which are dimensionless quantities. The char is formed from the biomass decomposition and consumed by the burnoff; hence

$$\frac{dm_{char}}{dt} = c_{cell}\frac{d\alpha_{cell}}{dt}y_{cell.char} + c_{other}\frac{d\alpha_{other}}{dt}y_{other\_char} - A_{char}C_{O_2}^{\nu_{char}} \exp\left(-\frac{E_{char}}{RT}\right)m_{char}^{n_{char}} \tag{7}$$

The ash is formed by the char burnoff reaction with a yield of y_{ash}.

$$\frac{dm_{ash}}{dt} = A_{char}C_{O_2}^{\nu_{char}} \exp\left(-\frac{E_{char}}{RT}\right)m_{char}^{n_{char}}y_{ash} \tag{8}$$

Note that a dimensionless C_{O_2} concentration is needed in the kinetic equations. Otherwise, the dimension of the pre-exponential factor should depend upon ν_{char} to obtain dm_{char}/dt and dm_{ash}/dt in units of s^{-1}.

In an inert atmosphere, under the conditions of thermal analysis, the cellulose decomposition is usually regarded to have

dx.doi.org/10.1021/ef3019222 | Energy Fuels 2013, 27, 1050−1060

approximately first-order kinetics, although more complex models are also employed. Among others, the use of self-accelerating kinetics has been suggested.[27,28] In the presence of oxygen, the cellulose decomposition was found to be a self-accelerating reaction by Várhegyi et al. too.[17] The self-accelerating reactions can typically be described by an equation of type

$$\frac{d\alpha_{cell}}{dt} = A_{cell} C_{O_2}^{\nu_{cell}} \exp\left(-\frac{E_{cell}}{RT}\right) f(\alpha_{cell}) \quad (9)$$

where f is a function capable of expressing self-acceleration. The mathematical unambiguity requires a normalization for $f(\alpha_{cell})$ because f functions differing only in constant multipliers are equivalent in eq 9 (parameter A_{cell} can compensate any multipliers of f). As a normalization, we require that the maximum of f be 1. $f(\alpha_{cell})$ is approximated formally by

$$f(\alpha_{cell}) \cong \text{normfactor}(1 - \alpha_{cell})^{n_{cell}}(\alpha_{cell} + z) \quad (10)$$

where n_{cell} and z are model parameters and normfactor ensures that max $f = 1$. Parameters n_{cell} and z do not have separate physical meaning; together, however, they determine the shape of f and, in this way, the self-accelerating capabilities of the model. Equation 10 is a slightly simplified version of an earlier approximation that has been employed to different self-accelerating reactions.[17,29,30] These earlier works employed an exponent on factor $(\alpha_{cell} + z)$; the omission of this parameter did not affect the fit quality in the present study. A differentiation of eq 10 by α_{cell} yields that $f(\alpha_{cell})$ reaches its maximum at

$$\alpha_{cell} = (1 - n_{cell}z)/(n_{cell} + 1) \quad (11)$$

When eq 11 gives a negative value, $f(\alpha_{cell})$ is monotonously decreasing in the [0,1] interval. In the present work, however, the maximum of $f(\alpha_{cell})$ proved to be around 0.4−0.5. The normfactor in eq 10 is the maximum of $(1 - \alpha_{cell})^{n_{cell}}(\alpha_{cell} + z)$ in the [0,1] interval; hence, its value can be immediately calculated by substituting the α_{cell} value from eq 11.

The oxidative decomposition of the non-cellulosic part of the sample is described by a distributed activation energy model for reasons as follows. This pseudo-component includes the decomposition of the extractives, hemicelluloses, and lignin. There is a high number of different reactive species here. The differences in their reactivity are described by different activation energies. To keep the number of unknown model parameters low, the activation energies in this pseudo-component are assumed to have a distribution function. The usual Gaussian distribution function is employed by an E_0 mean and σ width. The effect of oxygen is described by a power function, $C_{O_2}^{\nu_{other}}$. The reacted fraction of this pseudo-component, α_{other}, is calculated by the same high-precision numerical methods that were used in earlier works.[17,20,21,23,31] Note that the term $A_{other}C_{O_2}^{\nu_{other}}$ is a constant multiplier during the numerical solution for a given experiment.

Parameter y_{ash} expresses the ash yield of the char burnoff. In the present work, y_{ash} is determined from the total ash obtained by proximate analysis. This latter will be used as a dimensionless ratio, m_{ash}^{anal}, which is equal to the hundredth of the corresponding percent value in Table 2. The overall ash yield of the model is forced to be equal to m_{ash}^{anal} by equation

$$(c_{cell}y_{cell.char} + c_{other}y_{other\_char})y_{ash} = m_{ash}^{anal} \quad (12)$$

In this way, y_{ash} can be eliminated from the model because it can be expressed as a function of m_{ash}^{anal}, y_{other_char}, and c_{cell} by eqs 12 and 5c.

3.4. Evaluation by Assuming Common Parameters.

The model outlined above has 16 unknown parameters for each sample, as follows: A_{cell}, ν_{cell}, E_{cell}, z, n_{cell}, $y_{cell.char}$, and c_{cell} (cellulose decomposition); A_{other}, ν_{other}, E_0, σ, and y_{other_char} (the decomposition of the non-cellulosic parts of the sample; here, $c_{other} = 1 - c_{cell}$ because of eq 5c); and A_{char}, ν_{char}, E_{char}, and n_{char} (char burnoff).

It turned out during the evaluation that there is a strong compensation effect between parameters $y_{cell.char}$, c_{cell}, and y_{other_char}. Practically any $y_{cell.char}$ value can be selected between 0 and ca. 0.2 because c_{cell} and y_{other_char} can compensate for its effect, so that neither the fit quality nor the rest of the parameters are affected. Appendix: Compensation Effect between Three Model Parameters at the end of this paper clarifies the problem in detail. As explained there, the physical meaning of the effect is connected to the temperature difference between the devolatilization and char burnoff. As the figures of the next section and the Supporting Information show, the cellulose decomposition terminates before the start of the char burnoff. If the value of $y_{cell.char}$ is altered, c_{cell} and y_{other_char} can be changed, so that the amount of char formed until the start of the char combustion would not change. To overcome this problem, all of the results will be reported at $y_{cell.char} = 0.07$, which was the mean value of the cellulose experiments of eight European laboratories in a round-robin work.[32] It is important to emphasize that this choice affects only c_{cell} and y_{other_char} in the tables. Anything else in the tables and figures is the same as it would be with an assumption of another $y_{cell.char}$ value between 0 and 0.2 (this was carefully checked; all calculations of the present paper were carried out with more than one $y_{cell.char}$ value). In this way, the number of unknown parameters reduces to 15.

The remaining 15 unknown parameters of the model can be determined by the least-squares evaluation of the 6 experiments of a given sample. In this approach, there are 2.5 unknown parameters for one TGA experiment. If all of the parameters are assumed to depend upon the sample type, then the 6 samples together have $6 \times 15 = 90$ unknown parameters. The total number of the unknown parameters for the 6 samples will be denoted by N_{param}. There are 36 TGA experiments for the determination of the N_{param} unknown parameters.

If part of the model parameters is assumed to be common for all samples, two benefits can be achieved: (i) The common parameters will indicate the similarities in the kinetic behavior of the samples. (ii) Less unknown parameters are derived from the given amount of experimental information (i.e., a given parameter value is based on more experimental information). This helps to eliminate the usual ill-definition (compensation effect) problems of the non-isothermal kinetics. The compensation effects between A and E or A, E, and n are well-known in the literature of the non-isothermal kinetics. Many works on non-isothermal kinetics proved that more than one kinetic model of type $d\alpha/dt = A \exp(-E/RT)f(\alpha)$ can describe equally well a given set of non-isothermal experiments. Besides, de Jong et al. have also shown a strong compensation effect between A, E_0, and σ in the distributed activation energy model with Gaussian distribution.[33]

As more and more parameters are assumed to be common during the evaluation, the objective function of the method of least-squares (*of* in eq 1) obtains higher and higher values (i.e., the fit worsens), while, on the other hand, the condition of the parameter determination improves.[25,34] One should find a reasonable compromise between the fit quality and the reliability of the parameter values. This way is followed in the present work too, as illustrated by Table 3. No common parameters

Table 3. Evaluations with Various Groups of Common Model Parameters[a]

evaluation	common parameters	N_{param}	N_{param}/N_{exper}	$100(of)^{1/2}$
1	none	6 × 15	2.5	2.30
2	E_{cell}, E_0, and E_{char}	75	2.1	2.40
3	E_{cell}, E_0, E_{char}, and σ	70	1.9	2.42
4	E_{cell}, E_0, E_{char}, σ, ν_{cell}, ν_{other}, and ν_{char}	55	1.5	2.46
5	E_{cell}, E_0, E_{char}, σ, z, n_{cell}, and n_{char}	55	1.5	2.64
6	E_{cell}, E_0, E_{char}, σ, A_{cell}, A_{other}, and A_{char}	55	1.5	2.71
7	E_{cell}, E_0, E_{char}, σ, and y_{other_char}	65	1.8	3.11
8	E_{cell}, E_0, E_{char}, σ, ν_{cell}, ν_{other}, ν_{char}, z, n_{cell}, and n_{char}	40	1.1	2.68

[a]See the Nomenclature for the meaning of the symbols in the table.

were assumed in evaluation 1; this case corresponds to the separate least-squares evaluation of the six experiments for each sample. In all other evaluations, the whole data set (36 TGA experiments) was evaluated together by the method of least squares.

The assumption of common E_{cell}, E_0, and E_{char} values resulted in a slight worsening in *of*. When σ was also assumed to be common, *of* remained practically the same (cf. evaluations 2 and 3). The assumption of common E_{cell}, E_0, E_{char}, σ, ν_{cell}, ν_{other}, and ν_{char} in evaluation 4 resulted only in a slight worsening of *of* in comparison to evaluations 1−3. Evaluation 4 was found to be the most suitable for the purposes of the present work because its parameters retained the characteristic differences between the samples, while its favorable N_{param}/N_{exper} ratio (1.5) allowed for the reliable determination of its parameters. Its $100(of)^{1/2}$ value, 2.46, is only 7% higher than that of evaluation 1.

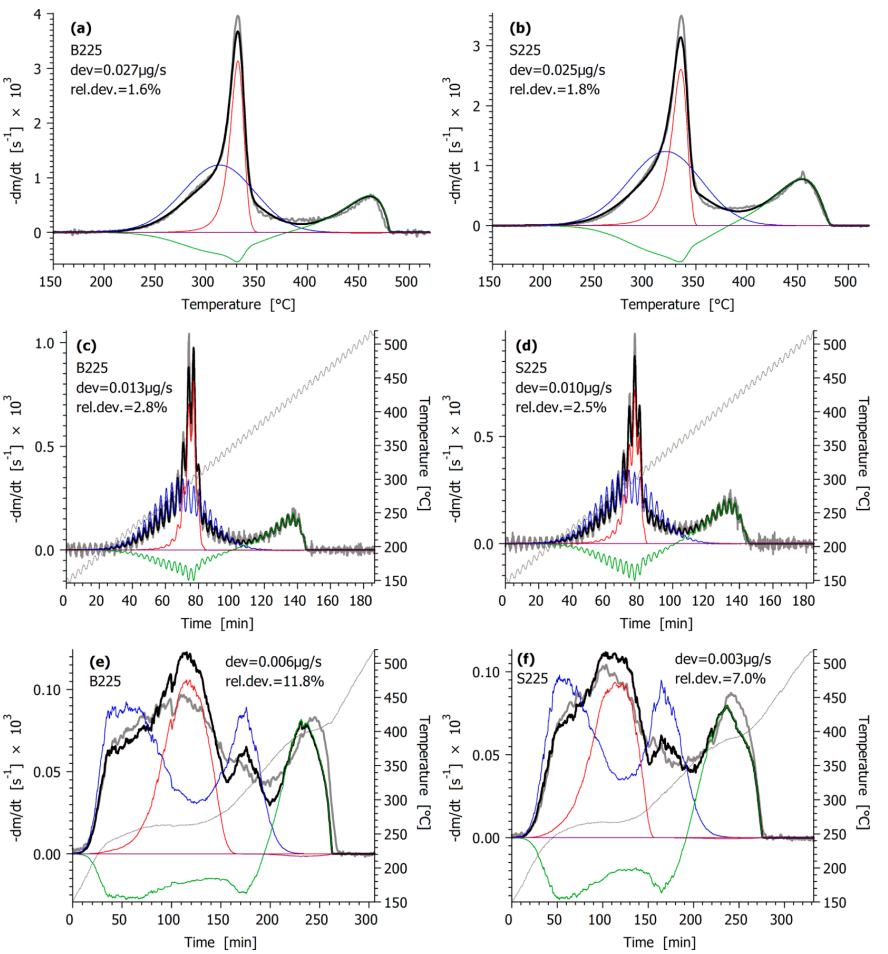

Figure 3. Results of evaluation 4. The experiments with the samples torrefied at 225 °C are shown here at C_{O_2} = 0.20 (the complete figure with 36 experiments is shown in the Supporting Information). Notation: experimental DTG curves normalized by the initial sample mass (gray bold line), their calculated counterpart (black bold line), the simulated partial curves: $-dm_{cell}/dt$ (red line), $-dm_{other}/dt$ (blue line), $-dm_{char}/dt$ (green line), $-dm_{ash}/dt$ (purple line); and the temperature programs of the modulated and CRR experiments (gray line). In this representation, the char formation rate (green line) appears below 0 because mass loss rates ($-dm/dt$) are plotted.

dx.doi.org/10.1021/ef3019222 | *Energy Fuels* 2013, 27, 1050−1060

Table 4. Peak Temperatures at 10 °C/min Heating Rate in 20% O_2 as Obtained by Evaluation 4

	peak temperature (°C)		
	$d\alpha_{cell}/dt$	$d\alpha_{other}/dt$	$-dm_{char}/dt$
B --	335	306	458
S --	338	316	454
difference[a]	3	10	−4
B225	331	313	461
S225	335	321	455
difference[a]	4	8	−6
B275	322	344	473
S275	327	343	460
difference[a]	5	−1	−13

[a]The difference between the peak temperatures of the spruce and birch samples.

Table 5. Dependence of the Deviations and Relative Deviations on the Heating Programs in Evaluation 4[a]

group of experiments	mean DTG peak max[b] (μg/s)	rms dev (μg/s)	rms rel dev (%)
linear $T(t)$ 10 °C/min	1.35	0.03	2.2
modulated 2 °C/min	0.38	0.01	2.8
CRR	0.05	0.06	11.2

[a]The rms of the absolute and relative deviations was calculated for the 10 °C/min, modulated, and CRR experiments. [b]The averages of the observed DTG peak maxima are given in μg/s.

The results obtained by evaluation 4 are shown in details in the next paragraph and in the Supporting Information.

When other parameters were assumed to be common instead of ν_{cell}, ν_{other}, and ν_{char}, worse objective function values were obtained for the same number of the unknown parameters, as evaluations 5−7 show in Table 3. In this latter group, the mildest worsening of *of* was caused by the assumption of common n_{char} and $f(\alpha_{cell})$ parameters (z and n_{cell}) in evaluation 5. Hence, the assumptions of evaluations 4 and 5 were combined to achieve a stronger reduction of the number of parameters in evaluation 8. In this case, 10 model parameters were assumed to be common for all samples: E_{cell}, E_0, E_{char}, σ, ν_{cell}, ν_{other}, ν_{char}, z, n_{cell}, and n_{char}; while 5 parameters have different values for the different samples: A_{cell}, A_{other}, A_{char}, y_{other_char}, and c_{cell}. In this evaluation, $N_{param} = 10 + 6 \times 5 = 40$ parameters were determined from the simultaneous evaluation of 36 experiments; hence, N_{param}/N_{exper} is close to 1. However, evaluation 8 blurs the distinction between the peculiarities of the samples. In this model variant, the differences between the samples are expressed by the height and position of the partial peaks because the parameters determining the shape of these curves (σ, z, n_{cell}, and n_{char}) were kept common for all samples. Such approaches may be useful in cases when the reduced computational time and the smaller number of unknown parameters are important.

3.5. Results of Evaluation 4. The fit quality and partial curves obtained by evaluation 4 are shown for samples B225 and S225 in Figure 3 at $C_{O_2} = 0.20$. The whole version of Figure 3 with all 36 experiments is given in the Supporting Information. Table 4 shows the corresponding peak temperatures at 10 °C/min and $C_{O_2} = 0.20$. The peak temperature differences between the spruce and birch samples are also indicated. These differences are small for $d\alpha_{cell}/dt$. The highest difference was observed for $d\alpha_{other}/dt$ between samples S -- and B --. It reflects the DTG differences in the low-temperature domain, as shown in Figure 2 (see the shoulder of the green-colored curve in Figure 2a). This difference is smaller between samples S225 and B225 and practically disappears between samples S275 and B275, as the amount of hemicelluloses decreases during the 225 °C torrefaction and becomes nearly zero in the 275 °C torrefaction. If the peak temperatures of the $d\alpha_{other}/dt$ curves of the torrefied samples are compared to those of the untreated samples, high differences are observed, because the importance of the thermally labile compounds decreases in this pseudo-component by the torrefaction. The torrefaction at 225 °C has a negligible effect on the peak temperature of $d\alpha_{cell}/dt$ because of the higher thermal stability of the cellulose. The torrefaction at 275 °C, however, markedly

Table 6. Parameters Obtained by Assuming Seven Common Parameters[a]

sample	B --	B225	B275	S --	S225	S275	mean	willow in earlier work[b]
E_{cell} (kJ mol^{-1})	135	=	=	=	=	=	135	145
E_0 (kJ mol^{-1})	160	=	=	=	=	=	160	166
σ (kJ mol^{-1})	8.1	=	=	=	=	=	8.1	11.2
E_{char} (kJ mol^{-1})	153	=	=	=	=	=	153	167
ν_{cell}	0.50	=	=	=	=	=	0.50	0.61
ν_{other}	0.24	=	=	=	=	=	0.24	0.37
ν_{char}	0.47	=	=	=	=	=	0.47	0.62
n_{cell}	0.94	0.93	1.23	0.80	0.81	1.06	0.96	na
z_{cell}	0.01	0.02	0.03	0.04	0.05	0.04	0.03	na
n_{char}	0.58	0.48	0.39	0.64	0.62	0.57	0.55	0.95
$\log_{10} A_{cell}$ (s^{-1})	9.97	9.99	10.09	9.84	9.86	9.98	9.95	10.66
$\log_{10} A_{other}$ (s^{-1})	12.44	12.24	11.47	12.16	12.05	11.51	11.98	13.04
$\log_{10} A_{char}$ (s^{-1})	8.69	8.62	8.50	8.86	8.85	8.80	8.72	10.49
y_{other_char}	0.22	0.30	0.51	0.33	0.38	0.55	0.38	0.23
c_{cell}	0.30	0.35	0.38	0.30	0.33	0.35	0.34	0.30
$c_{other} = 1 - c_{cell}$	0.70	0.65	0.62	0.70	0.67	0.65	0.66	0.70
$y_{cell.char}$[c]	0.07	=	=	=	=	=	0.07	0.21
y_{ash}[c]	0.01	0.02	0.01	0.01	0.01	0.01	0.01	0.20

[a]See evaluation 4 in Table 3. "=" indicates parameter values that are identical in each column. [b]Values obtained in a recent work with a similar model on an untreated willow sample.[17] n_{cell} and z_{cell} are not listed here because the equation for $f(\alpha_{cell})$ was not the same as in the present work. [c]In the present work, $y_{cell.char}$ was fixed, y_{ash} was calculated from the ash yield of the proximate analysis (m_{ash}^{anal}), and y_{other_char} and c_{cell} were calculated from eq 12.

dx.doi.org/10.1021/ef3019222 | Energy Fuels 2013, 27, 1050−1060

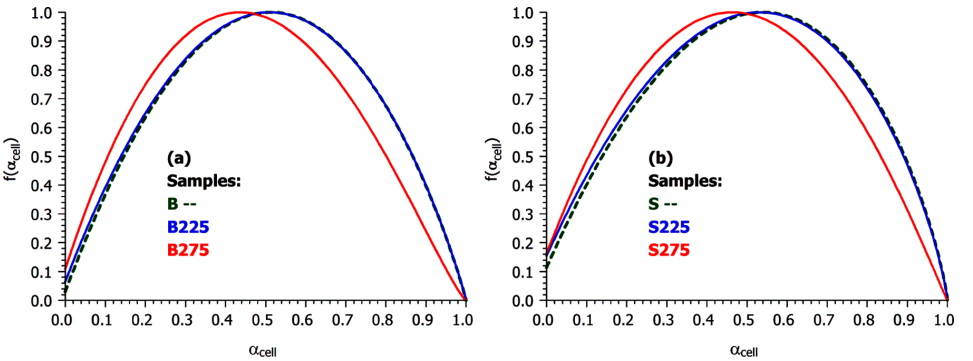

Figure 4. Dependence of the cellulose decomposition rate on the reacted fraction of the cellulose by eqs 9 and 10 in Evaluation 4. $f(\alpha_{cell})$ is plotted as function of α_{cell}. The corresponding parameter values are listed in Table 6.

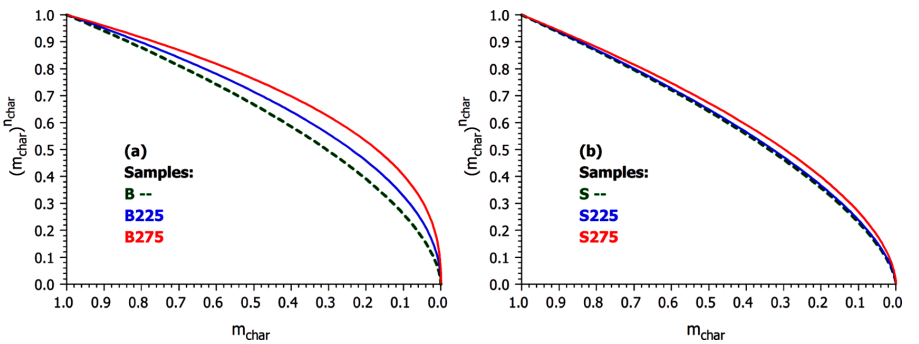

Figure 5. Dependence of the char burn-off rate on the normalized amount of char by eq 6 in Evaluation 4. $m_{char}^{n_{char}}$ is plotted as a function of m_{char}. The corresponding parameter values are listed in Table 6.

decreases the peak temperature of $d\alpha_{cell}/dt$, indicating that the cellulose undergoes some reactions there. The peak temperatures of partial curve $-dm_{char}/dt$ reflect mainly the reactivity differences of the formed char. This value increases with the torrefaction temperature for both samples.

Table 5 shows how the fit quality depends upon the temperature programs of the TGA experiments in evaluations 4. For this purpose, the rms deviation and the rms relative deviation were calculated for the 10 °C/min, modulated, and CRR experiments. The lowest deviation, 0.006 μg/s, was obtained for the CRR experiments. The corresponding values of the 10 °C/min experiments were 5 times higher. On the other hand, the relative deviation of the 10 °C/min experiments were ca. 5 times lower than those of the CRR experiments because of the huge differences in the heights of the corresponding peak maxima, which are also shown in Table 5.

Table 6 lists the parameters obtained in evaluation 4. The parameter values obtained in the present work cannot be compared directly to the parameters of the earlier kinetic works on the combustion of torrefied wood because of the high differences in the assumptions, models, and evaluation. As an example, let us consider an alternative model that contains first-order devolatilization reactions. In first-order kinetics, the sharpness of a peak mainly depends upon the magnitude of the corresponding activation energy. Accordingly, the description of a narrow peak (i.e., the cellulose decomposition) can be described only by high activation energies, while a wide peak can be described by low activation energies. In the present model, however, the width of the cellulose and non-cellulosic parts were influenced mainly by the $f(\alpha_{cell})$ parameters and σ, respectively. Similar basic differences may arise for other sorts of alternative models too. Hence, the work by Várhegyi et al.[17] was selected for comparison, where a similar model was employed on a willow sample. The corresponding values are shown in the last column of Table 6. The differences between the results of the two works are not high. The activation energies show only 4–9% differences, which are less than the activation energy differences reported on pure cellulose in an inert atmosphere in a round-robin TGA study.[32] The reaction order of the char burnoff, however, shows a higher alteration. The n_{char} values were 0.58 and 0.64 for the untreated birch and spruce samples, respectively, while a nearly first-order reaction was observed in the earlier work. This might reflect the differences between the samples. The work by Várhegyi et al.[17] used young willow shoots from a Hungarian energy farm with 1.2% ash content, while the present work was based on Norwegian forest woods with particularly low ash content. On the other hand, c_{cell} and c_{other} are the same for the untreated birch and willow samples of the older work. In the present work, the c_{cell} parameters increase with the torrefaction, reflecting that the partial devolatilization of the hemicellulose increases the cellulose concentration.

$y_{cell.char}$ had a rather unrealistic value, 0.21, in the work by Várhegyi et al.[17] because the ill definition of this parameter had not been recognized yet there. Similarly, the high values of y_{ash} also

dx.doi.org/10.1021/ef3019222 | Energy Fuels 2013, 27, 1050–1060

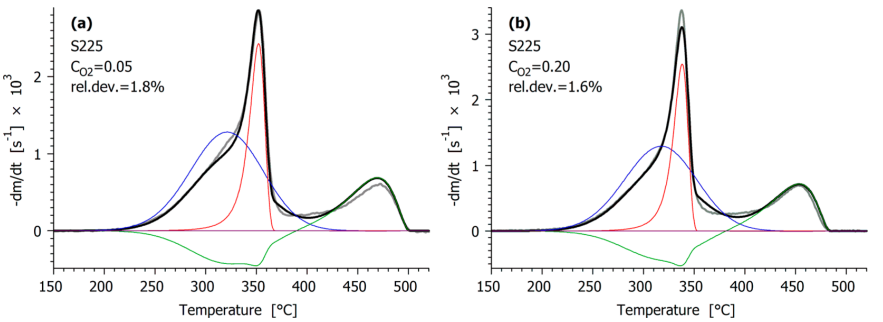

Figure 6. Linear heating rate experiments of the untreated spruce sample in evaluation 1 (see Figure 3 for the notations).

Table 7. Least-Squares Determination of c_{cell} and y_{other_char} at Various Values of $y_{cell.char}$ by the Evaluation of the Untreated Spruce Experiments[a]

$y_{cell.char}$	0	0.1	0.2	0.3	0.4
c_{cell}	0.285	0.316	0.356	0.407	0.475
y_{other_char}	0.346	0.316	0.274	0.212	0.110
$c_{cell}(1 - y_{cell.char})$	0.285	0.285	0.285	0.285	0.285
$(1 - c_{cell})(1 - y_{other\_char})$	0.468	0.468	0.468	0.468	0.468
$c_{cell}y_{cell.char} + (1 - c_{cell})(1 - y_{other\_char})$	0.247	0.247	0.247	0.248	0.248
$100(of)^{1/2}$	2.127	2.127	2.127	2.128	2.129

[a]The values of all other parameters were taken from evaluation 1 and were not changed.

appear problematic in the earlier work, while this parameter was determined from the proximate analysis in the present study.

The n_{cell} and z parameters together determine $f(\alpha_{cell})$ in eqs 9 and 10. Figure 4 shows that the $f(\alpha_{cell})$ curves of the untreated and mildly torrefied samples (green and blue lines) are nearly identical. The torrefaction at 275 °C resulted in different $f(\alpha_{cell})$ functions (denoted by red color), indicating that the 275 °C torrefaction affects the cellulose reactivity too. Note that these samples gave lower peak temperatures for the cellulose decomposition, as mentioned above (see Table 4). All $f(\alpha_{cell})$ functions obtained in the present work revealed a strong self-acceleration, which is shown by the high increase from the starting values of the $f(\alpha_{cell})$ functions until their peak maxima in Figure 4. Mathematically, this is connected to the low values of the z parameters obtained in the least-squares evaluation.

The dependence of the char burnoff rate on the normalized amount of char by eq 6 is shown in Figure 5, where $m_{char}^{n_{char}}$ is plotted as a function of m_{char}. Here, the layout and coloring are the same as in Figure 4. In Figure 5, a first-order kinetics would give a straight line from coordinates 1,1 to 0,0. The alteration of the obtained curves from the linear indicates a moderate self-acceleration because the burnoff rate of a unit mass of char (the ratio of the burnoff rate and m_{char}) is increasing as m_{char} is decreasing. This self-acceleration, however, is much smaller than that of a random-pore kinetics,[35] indicating that the internal pore surfaces have only a limited importance in the char burnoff kinetics of these samples.

4. CONCLUSION

(1) The combustion of four torrefied wood samples and their feedstocks (a deciduous and an evergreen species) was studied at slow heating programs, under well-defined conditions. Particularly low sample masses were employed to avoid the self-heating of the samples because of the huge reaction heat of the combustion. Six TGA experiments were carried out for each sample with three different temperature programs in 5 and 20% O_2, respectively. Strongly different temperature programs were selected to increase the information content available for the modeling: linear, modulated, and CRR temperature programs. The ratio of the highest and lowest peak maxima was around 50 in the set of experiments used for the evaluation. In this way, the obtained models described the experiments in a wide range of experimental conditions. (2) A recent combustion model consisting of two devolatilization reactions and a successive char burnoff reaction was employed with a minor modification. The cellulose decomposition in the presence of oxygen was described by a model that had two adjustable parameters to mimic self-acceleration tendencies. The decomposition of the non-cellulosic parts of the biomass was described by a distributed activation model. The char burnoff was approximated by power-law (n-order) kinetics. Each of these reactions had its own dependence upon the oxygen concentration that was also expressed by power-law kinetics. This model was tested earlier on one wood sample (willow); hence, the present work is a further step to gain experience with its applicability. The reliability of the model and the obtained parameters was improved by decreasing the number of parameters and by clarifying a compensation effect problem. (3) The complexity of the applied model reflects the complexity of the studied materials. The fast developing rate of the computers will allow for the use of complex kinetic submodels in actual industrial simulations too. Presently, a medium-priced desktop computer can calculate one million $-dm/dt$ curves by this model within ca. 1.5 h at the highly irregular $T(t)$ functions of the present study. (4) The employed model contains 15 unknown parameters for a given biomass. The relatively wide range of experiments made possible the determination of so many parameters by the method of least squares. The torrefaction has some impact on the parameters, especially on the parameters describing the devolatilization of the hemicelluloses and other thermally labile parts of a biomass sample. These parts decompose more or less during the torrefaction, as the corresponding c_{cell} and $c_{other} = 1 - c_{cell}$ parameters indicated. The cellulose reactivity was also affected at the higher torrefaction temperature, 275 °C, of the study. (5) Part of the kinetic parameters could be assumed common for the six samples without a substantial worsening of the fit quality. This approach increased the average experimental information for an unknown parameter and revealed the similarities in the behavior of the different samples. The following kinetic parameters could be assumed identical for the six samples with only a slight worsening of the fit quality: the activation energies,

the mean and width of the activation energy distribution in the distributed activation energy model (DAEM) part of the model, and the dependence of the reactions on the oxygen concentration.

APPENDIX: COMPENSATION EFFECT BETWEEN THREE MODEL PARAMETERS

As outlined in section 3.4, there is a strong compensation effect between parameters $y_{cell.char}$, c_{cell}, and y_{other_char}. The problem will be shown here for the behavior of the untreated spruce sample (S --). Figure 6 shows the corresponding linear heating rate experiments from evaluation 1. It is worth observing that the rate of the char burnoff becomes higher than the rate of the char formation between 380 and 390 °C. Note that mass loss rates were plotted; hence, the dominance of the char burnoff is indicated by the positive values of the overall char mass loss rate (green curve). Most of the devolatilization is accomplished until this temperature; only a small portion of the non-cellulosic part of the sample (blue line) decomposes above ca. 380 °C.

The mass loss of the devolatilization depends upon the amount of volatiles formed from the two pseudo-components. Keeping in mind the definitions of the c and y parameters and eq 5c, we obtain

$$\text{normalized mass loss rate of devolatilization} = c_{cell}(1 - y_{cell.char})\frac{d\alpha_{cell}}{dt} + (1 - c_{cell})(1 - y_{other\_char})\frac{d\alpha_{other}}{dt} \quad (13)$$

Any $y_{cell.char}$, c_{cell}, and y_{other_char} combination gives exactly the same mass loss rate in eq 13 as long as the values of the coefficients, $c_{cell}(1 - y_{cell.char})$ and $(1 - c_{cell})(1 - y_{other\_char})$, do not change.

The normalized amount of char formed from the devolatilization is

$$c_{cell}\, y_{cell.char} + (1 - c_{cell})y_{other\_char} \quad (14)$$

Most of the amount defined by eq 14 forms before the start of the char burnoff, while a small portion is produced around ca. 380−420 °C, where the devolatilization of the non-cellulosic part of the sample terminates. The ratio of these amounts, however, has only a limited importance on the overall kinetics because the char burnoff occurs mainly above 420 °C, as the green curves show in Figure 6. If $y_{cell.char}$, c_{cell}, and y_{other_char} vary so that neither the devolatilization kinetics (eq 13) nor the amount of formed char (eq 14) change, then the variation affects only the ratio of the amounts of char formed before the char burnoff and simultaneously with the char burnoff.

As an illustration, the untreated spruce experiments were evaluated so that $y_{cell.char}$ obtained fixed values (0, 0.1, 0.2, 0.3, and 0.4), while c_{cell} and y_{other_char} were determined from the experimental data by the method of least squares. In this test, all other model parameters were kept constant at the values obtained in evaluation 1. The results are shown in Table 7. Note that $100(of)^{1/2}$ was 2.127 for sample S -- in evaluation 1. As the last row of Table 7 indicates, only the third digit of its value changed at higher $y_{cell.char}$. The normalized amount of the formed char, $c_{cell}y_{cell.char} + (1 - c_{cell})(1 - y_{other\_char})$, also shows similarly small changes. On the other hand, c_{cell} and y_{other_char} change markedly to keep the values of the rest of the Table constant or nearly constant.

ASSOCIATED CONTENT

Supporting Information

Results of evaluation 4 shown in figures, including all 36 experiments. This material is available free of charge via the Internet at http://pubs.acs.org.

AUTHOR INFORMATION

Corresponding Author

*Telephone: +36-1-4381148. Fax: +36-1-4381147. E-mail: varhegyi.gabor@ttk.mta.hu.

Notes

The authors declare no competing financial interest.

ACKNOWLEDGMENTS

The authors acknowledge the financial support by the Research Council of Norway and a number of industrial partners through the Project STOP ("Stable Operating Conditions for Biomass Combustion Plants"). STOP is also a part of the research center CenBio (Bioenergy Innovation Centre). Gábor Várhegyi is grateful for the support of the Hungarian National Research Fund (OTKA K72710).

NOMENCLATURE

α = reacted fraction of a component or pseudo-component (dimensionless)
ν = reaction order with respect to the oxygen concentration
σ = width parameter (variance) of Gaussian distribution (kJ/mol)
A = pre-exponential factor (s^{-1})
C_{O_2} = v/v concentration of the ambient oxygen (dimensionless)
dev = rms of the deviations between the observed and calculated values of a DTG curve (μg/s)
E = activation energy (kJ/mol) or mean activation energy in a distributed activation energy model (kJ/mol)
f = empirical function (eq 10) expressing the change of the reactivity as the reactions proceed (dimensionless)
h_k = either the height of an experimental curve (s^{-1}) or 5×10^{-4} s^{-1}, whichever is higher
m = mass of the sample or a component of the sample normalized by the initial sample mass (dimensionless)
m_{ash}^{anal} = $^1/_{100}$ of the total ash determined by proximate analysis (dimensionless)
n = reaction order (dimensionless)
of = objective function minimized in the least-squares evaluation (dimensionless)
N_{exper} = number of experiments evaluated together by the method of least squares
N_k = number of evaluated data on the kth experimental curve
N_{param} = number of parameters determined in the evaluation of a series of experiments
R = gas constant (8.3143×10^{-3} kJ mol^{-1} K^{-1})
rel dev = deviation (dev) expressed as percent of the corresponding peak height
t = time (s)
T = temperature (°C or K)
y = yield (dimensionless)
$y_{cell.char}$ = char yield from the cellulose
y_{other_char} = char yield from the rest of the biomass
y_{ash} = ash yield from char
z = formal parameter in eq 10 (dimensionless)

Subscripts

cell = cellulose

i = digitized point on an experimental curve
k = experiment
other = non-cellulosic organic biomass constituents
ur = unreacted sample

REFERENCES

(1) Faaij, A. P. C. *Energy Policy* **2006**, *34* (3), 322−342.
(2) International Energy Agency (IEA). *World Energy Outlook 2009*; IEA: Paris, France, 2009; http://www.iea.org/publications/freepublications/publication/weo2009.pdf.
(3) van der Stelt, M. J. C.; Gerhauser, H.; Kiel, J. H. A.; Ptasinski, K. J. *Biomass Bioenergy* **2011**, *35*, 3748−3762.
(4) Tapasvi, D.; Tran, K-Q.; Wang, L.; Skreiberg, Ø.; Khalil, R. *Proceedings of the 9th European Conference on Industrial Furnaces and Boilers*; Estoril, Portugal, April 26−29, 2011; ISBN: 978-972-99309-6-6.
(5) Tapasvi, D.; Khalil, R. A.; Skreiberg, Ø.; Tran, K.-Q.; Gronli, M. G. *Energy Fuels* **2012**, *26*, 5232−5240.
(6) Zheng, A.; Zhao, Z.; Chang, S.; Huang, Z.; He, F.; Li, H. *Energy Fuels* **2012**, *26*, 2968−2974.
(7) Wannapeera, J.; Fungtammasan, B.; Worasuwannarak, N. *J. Anal. Appl. Pyrolysis* **2011**, *92*, 99−105.
(8) Prins, M. J.; Ptasinski, K. J.; Janssen, F. J. J. G. *Energy* **2006**, *31*, 3458−3470.
(9) Pimchuai, A.; Dutta, A.; Basu, P. *Energy Fuels* **2010**, *24*, 4638−4645.
(10) Jones, J. M.; Bridgeman, T. G.; Darvell, L. I.; Gudka, B.; Saddawi, A.; Williams, A. *Fuel Proc. Technol.* **2012**, *101*, 1−9.
(11) Couhert, C.; Salvador, S.; Commandré, J. M. *Fuel* **2009**, *88*, 2286−2290.
(12) Broström, M.; Nordin, A.; Pommer, L.; Branca, C.; Di Blasi, C. *J. Anal. Appl. Pyrolysis* **2012**, *96*, 100−109.
(13) Bridgeman, T. G.; Jones, J. M.; Shield, I.; Williams, P. T. *Fuel* **2008**, *87*, 844−856.
(14) Arias, B.; Pevida, C.; Fermoso, J.; Plaza, M. G.; Rubiera, F.; Pis, J. J. *Fuel Proc. Technol.* **2008**, *89*, 169−175.
(15) Di Blasi, C. *Prog. Energy Combust. Sci.* **2008**, *34*, 47−90.
(16) Di Blasi, C. *Prog. Energy Combust. Sci.* **2009**, *35*, 121−140.
(17) Várhegyi, G.; Sebestyén, Z.; Czégény, Z.; Lezsovits, F.; Könczöl, S. *Energy Fuels* **2012**, *26*, 1323−1335.
(18) TA Instruments. *High Resolution Thermogravemetric Analysis—A New Technique for Obtaining Superior Analytical Results*; TA Instruments: New Castle, DE; TA Instruments Report TA-023, http://www.tainstruments.co.jp/application/pdf/Thermal_Library/Applications_Briefs/TA023.PDF.
(19) Várhegyi, G. *J. Anal. Appl. Pyrolysis* **2007**, *79*, 278−288.
(20) Becidan, M.; Várhegyi, G.; Hustad, J. E.; Skreiberg, Ø. *Ind. Eng. Chem. Res.* **2007**, *46*, 2428−2437.
(21) Várhegyi, G.; Czégény, Zs.; Liu, C.; McAdam, K. *Ind. Eng. Chem. Res.* **2010**, *49*, 1591−1599.
(22) Várhegyi, G.; Till, F. *Thermochim. Acta* **1999**, *329*, 141−145.
(23) Várhegyi, G.; Chen, H.; Godoy, S. *Energy Fuels* **2009**, *23*, 646−652.
(24) Várhegyi, G.; Szabó, P.; Mok, W. S. L.; Antal, M. J., Jr. *J. Anal. Appl. Pyrolysis* **1993**, *26*, 159−174.
(25) Várhegyi, G.; Bobály, B.; Jakab, E.; Chen, H. *Energy Fuels* **2011**, *25*, 24−32.
(26) Werkelin, J.; Skrifvars, B.-J.; Zevenhoven, M.; Holmbom, B.; Hupa, M. *Fuel* **2010**, *89*, 481−493.
(27) Conesa, J. A.; Caballero, J. A.; Marcilla, A.; Font, R. *Thermochim. Acta* **1995**, *254*, 175−192.
(28) Capart, R.; Khezami, L.; Burnham, A. K. *Thermochim. Acta* **2004**, *417*, 79−89.
(29) Várhegyi, G.; Szabó, P.; Jakab, E.; Till, F.; Richard, J.-R. *Energy Fuels* **1996**, *10*, 1208−1214.
(30) Várhegyi, G.; Pöppl, L.; Földvári, I. *Thermochim. Acta* **2003**, *399*, 225−239.
(31) Donskoi, E.; McElwain, D. L. S. *Combust. Flame* **2000**, *122*, 359−367.
(32) Grønli, M.; Antal, M. J., Jr.; Várhegyi, G. *Ind. Eng. Chem. Res.* **1999**, *38*, 2238−2244.
(33) de Jong, W.; Di Nola, G.; Venneker, B. C. H.; Spliethoff, H.; Wójtowicz, M. A. *Fuel* **2007**, *86*, 2367−2376.
(34) Várhegyi, G.; Czégény, Zs.; Jakab, E.; McAdam, K.; Liu, C. *J. Anal. Appl. Pyrolysis* **2009**, *86*, 310−322.
(35) Gavalas, G. R. *AIChE J.* **1980**, *26*, 577−585.

Paper V

A simulation study on the torrefied biomass gasification

Tapasvi, D.; Kempegowda, R.; Tran, K-Q.;

Skreiberg, Ø.; Grønli, M.

Energy Conversion and Management, 2015, 90, 446-457

Energy Conversion and Management 90 (2015) 446–457

Contents lists available at ScienceDirect

Energy Conversion and Management

journal homepage: www.elsevier.com/locate/enconman

A simulation study on the torrefied biomass gasification

Dhruv Tapasvi [a,*], Rajesh S. Kempegowda [b], Khanh-Quang Tran [a], Øyvind Skreiberg [b], Morten Grønli [a]

[a] Norwegian University of Science and Technology (NTNU), NO-7491 Trondheim, Norway
[b] SINTEF Energy Research, NO-7465 Trondheim, Norway

ARTICLE INFO

Article history:
Received 1 August 2014
Accepted 16 November 2014

Keywords:
Biomass
Gasification
Torrefaction
Energy efficiency
Exergy efficiency

ABSTRACT

Many studies have evaluated biomass behavior in a gasification process. Similar studies with torrefied biomass are needed to evaluate the improvements in biomass properties with torrefaction. This forms the basis of this study. A two-stage biomass gasification model is presented by using Aspen Plus as the simulation and modeling tool. The model included the minimization of the Gibbs free energy of the produced gas to achieve chemical equilibrium in the process, constrained by mass and energy balances for the system. Air and steam were used as the oxidizing agent in the process that uses both untreated and torrefied biomass as feedstocks. Three process parameters, equivalence ratio (ER), Gibbs reactor temperature and steam-to-biomass ratio (SBR), were studied. 27 cases were included in the analysis by operating the system below the carbon deposition boundary with all carbon in gaseous form in the product gas. Product gas composition in the form of hydrogen (H_2), carbon monoxide (CO), carbon dioxide (CO_2), methane (CH_4) and nitrogen (N_2) was analyzed together with cold gas energy and exergy efficiencies for all the cases. Overall, mole fractions of H_2, CO, CO_2 and N_2 were between 0.23–0.40, 0.22–0.42, 0.01–0.09 and 0.14–0.36 for torrefied wood and 0.21–0.40, 0.17–0.34, 0.03–0.09 and 0.15–0.37 for untreated wood, respectively. Similarly, cold gas energy and exergy efficiencies were between 76.1–97.9% and 68.3–85.8% for torrefied wood and 67.9–91.0% and 60.7–79.4% for untreated wood, respectively. Torrefied biomass has higher H_2 and CO contents in the product gas and higher energy and exergy efficiencies than the untreated biomass. Overall efficiencies of an integrated torrefaction–gasification process depend on the mass yields of the torrefaction process. Results from this study were validated using a C–H–O ternary diagram and with results from other similar studies.

1. Introduction

Biomass is one of the most important renewable energy sources in the near future. Increased use of biomass can extend the lifetime of our fossil fuel resources. The potential of biomass to help meet the world energy demand has been widely recognized. However, problems such as low bulk density, high moisture content and relatively low calorific value, make biomass an expensive fuel to use and hinder its widespread use. Researchers are looking into solutions to overcome these drawbacks and thus, improve the properties of biomass as a fuel. A lot of research is underway to improve the fuel quality of biomass via torrefaction. Torrefaction is a pretreatment method to upgrade raw biomass to a refined fuel with improved properties such as higher heating value and carbon content and improved grindability. Torrefaction is carried out at 200–300 °C for 30–60 min, in an inert environment at atmospheric pressure. Torrefaction results in the following main improvements in the biomass properties [1–14]:

- considerable reduction in the moisture content;
- increased heating value due to reduction in the O/C ratio, and increased energy density when compressed;
- intrinsic conversion of the hygroscopic behavior of raw biomass into the hydrophobic behavior of torrefied biomass;
- enhanced grindability, which results in less energy consumption during milling.

Because of these improved properties, the value of the torrefied biomass as a fuel is significantly higher than that of the raw biomass.

A promising way to use biomass for production of heat, electricity, and other biofuels is through biomass gasification, in which, through a partial oxidation, the biomass is converted into synthesis gas and condensable compounds. During the gasification the chemical energy of the biomass is converted to the thermal and chemical energy of the synthesis gas [15]. Gasification achieves a

* Corresponding author. Tel.: +47 93818918; fax: +47 73593580.
E-mail address: dhruv.tapasvi@ntnu.no (D. Tapasvi).

http://dx.doi.org/10.1016/j.enconman.2014.11.027
0196-8904/

high carbon conversion rate for the formation of syngas [16,17]. Clean synthesis gas (syngas), produced from partial combustion of biomass, can e.g. be burnt in a gas turbine combustion chamber to run a biomass based combined cycle power plant [18]. Biomass can be gasified in various ways by properly controlling the mix of fuel and oxidant within the gasifier. The gasification of coal and biomass began in the 1800s, and by the 1850s, gas light for streets became common. Due to its high efficiency with respect to syngas formation, it is desirable that gasification becomes increasingly applied in the future for biofuels production rather than direct combustion [19].

Many studies have evaluated biomass behavior in a gasification process. Puig-Arnavat et al. [16] reviewed the various gasification models based on thermodynamic equilibrium, kinetics and artificial neural networks. According to Puig-Arnavat et al. [16], thermodynamic equilibrium models have been used widely. For example, Schuster et al. [20] studied the fluidized bed process with main focus on steam gasification; Altafini et al. [21] studied a saw dust gasifier to analyze the operating conditions of an open top stratified downdraft gasifier; Melgar et al. [22] used an equilibrium approach and studied the influence of fuel/air ratio and the moisture content of the biomass on the characteristics of the process and the producer gas composition; Jarungthammachote and Dutta [23,24] used a modified stoichiometric equilibrium approach by accounting for a deviation factor from experiments to three types of gasifiers: a central jet spouted bed, a circular split spouted bed and a spout-fluid bed; Yoshida et al. [25] applied a two-stage equilibrium model for a high temperature gasification process to predict the performance of commercial gasifiers. Similarly, Ghassemi et al. [26], Altafini et al. [21], Bassyouni et al. [27], Ravikiran et al. [28] and Li et al. [29] studied the biomass gasification process by an equilibrium approach based on the minimization of Gibbs free energy. All these authors have shown reasonable agreement between equilibrium predictions and experimental data. Commercial tools such as Aspen Plus are also very useful in predicting the behavior of a biomass gasification process as a sub-model with built-in solids properties. Mansaray et al. [30] used Aspen Plus to simulate a dual-distributor-type fluidised-bed rice husk gasifier. Paviet et al. [31] studied thermo-chemical equilibrium modeling of a biomass gasification process. Based on these studies, it can be concluded that an equilibrium model with Gibbs free energy minimization approach in Aspen Plus is an acknowledged and realistic way of simulating a biomass gasification process.

In a few recent studies, it has been reported that torrefied biomass can significantly affect the efficiency of biomass gasification. Chen et al. [32] employed a process optimization technique, the Taguchi method, for identifying optimum levels for process parameters involved during co-gasification of torrefied biomass and coal in an entrained flow gasifier. In another study, Chen et al. [33] numerically simulated an entrained flow gasifier with oxygen as the gasifying agent and the results indicated that the gasification performance of torrefied bamboo is quite similar to that of coal. Furthermore, Kuo et al. [34] evaluated a two-stage gasification process for raw and torrefied bamboo by using Gibbs minimization approach under isothermal conditions in Aspen Plus simulations. It was reported that the carbon conversion and syngas yield was higher for torrefied materials than the raw biomass, whereas, the trends for cold gas efficiency were opposite. Torrefied biomass produced at 250 °C was found to be the most feasible fuel for gasification when considering all process parameters together. However, this study did not account for tar formation and assumed char as a pure carbon. Except for these few studies, there is a considerable lack of information on the behavior of torrefied biomass under gasification conditions and therefore, better knowledge on the topic is needed. This forms the basis of this present study.

The present work extends the efforts of Kuo et al. [34] to establish a detailed equilibrium model for understanding the effect of torrefaction on the syngas compositions and efficiency of the biomass gasification process. The aim is to study a two-stage gasification process by using Gibbs free energy minimization approach in Aspen Plus with improved accuracy together with a comprehensive thermodynamic analysis. A two-stage process refers to the pyrolysis or decomposition of biomass in the first stage followed by the gasification of the pyrolysis products in the second stage. Accuracy of the model is improved by including tar formation during pyrolysis and its further cracking in the gasification reactor; actual experimental decomposition yields as inputs for both untreated and torrefied biomass; the compositions of the chars produced during pyrolysis, as calculated from the elemental balance; and a C–H–O Ternary diagram for validating the results. The model is integrated with an Excel spreadsheet to study the energy and exergy efficiencies of the process at different operating conditions of the gasifier. Exergy analysis of a process is a supplement to energy analysis and is based on the 2nd law of thermodynamics. It is a very useful tool to assess work potentials of input and output materials and heat streams, and to pinpoint irreversibility losses in a system. Ptasinski [35] studied exergetic efficiency analysis for gasification of biofuels which includes wood, vegetable oil, sludge, and manure. Rao et al. [36] reported results from an investigation of the change in exergy content of the produced gas in gasification for various biomass sources. Pellegreni et al. [37] studied the parametric effect on exergy efficiency by considering the influence of many variables inherent to the model, such as: gasification temperature, moisture content, and air temperature, among others. Abuadala et al. [38] presented an exergy analysis of hydrogen production from gasification. Hosseini et al. [39] also compared energy and exergy for steam fed and air fed gasification systems using sawdust as a fuel. The present study can be regarded as a maiden attempt to carry out a thermodynamic and exergetic efficiency analysis of a gasification process using Gibbs free energy minimization approach in Aspen Plus for comparing untreated and torrefied biomass. Overall efficiencies of an integrated torrefaction–gasification process are also provided by including mass yield in the torrefaction process.

2. Methodology

The Gibbs free energy minimization method for the C–H–O–N atom blend of the biomass fuel and oxidant mixture can be applied for predicting the thermodynamic equilibrium composition of the product gas major components: H_2, CO, CH_4, CO_2, H_2O, N_2 and char [40–43]. A thermodynamic equilibrium model for a biomass gasification system was developed using the Gibbs minimizing approach in the Aspen Plus software as shown in Fig. 1. Material and energy streams data from the Aspen Plus model were used to calculate cold gas energy and exergy efficiencies of the process.

2.1. Aspen Plus model

In Aspen Plus, streams represent mass or energy flows. Mass streams are divided by Aspen Plus into three categories: mixed, solid, and non-conventional (biomass). Mixed streams contain mixtures of components, which can be in gaseous, liquid and solid phases. The solid phase component in this simulation is solid carbon (C). Thermodynamic properties are defined in the Aspen Plus libraries for chemical components. Non-conventional components are defined in Aspen Plus by supplying standard enthalpy of formation and the elementary composition (ultimate and proximate analyses) of the components [44]. Biomass is characterized in this manner in this study.

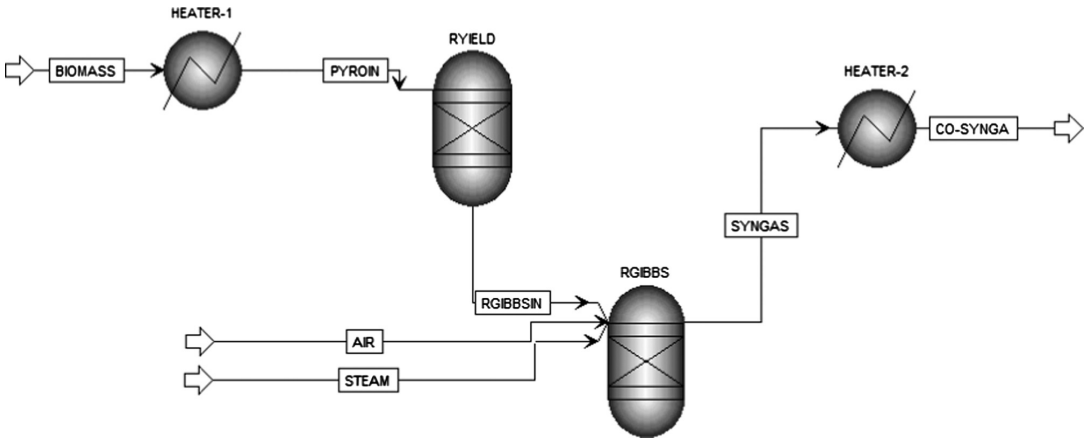

Fig. 1. Gasification process as modeled in Aspen Plus in this study.

2.1.1. Sub-systems

The following sub-systems were included in the modeled gasification process:

(a) Aspen Plus heat exchanger, HEATER, was used to simulate pre-heating of the biomass to a pyrolyzer temperature of 500 °C.
(b) Aspen Plus yield reactor, RYIELD, was used to simulate decomposition of biomass into individual elemental components at 500 °C. This is done by specifying actual experimental yield values for volatiles and char, as available in literature [45].
(c) Aspen Plus Gibbs reactor, RGIBBS, was used for partial combustion of volatiles and char with the addition of air and steam. RGIBBS models chemical equilibrium by minimizing Gibbs free energy, subject to element balance constraints. This model is useful when temperature and pressure are known and reaction stoichiometry is unknown. Both isothermal and adiabatic modeling options are available in the setup of the RGIBBS. Temperature or the heat duty for the RGIBBS unit needs to be specified for these options, respectively. A number of approximations need to be applied for estimating the heat duty for an actual reactor. Therefore, in order to simulate more closely the real conditions in a gasifier, an isothermal approach was used in this study.
(d) Aspen Plus heat exchanger, HEATER, was used to simulate cooling of syngas from RGIBBS temperature to ambient temperature.

2.1.2. Model input data

Based on a recent literature review, only one journal article by Wannapeera et al. [45] listed an experimentally obtained pyrolysis gas composition for both untreated and torrefied biomass. Therefore, the feedstocks used by Wannapeera et al. [45] have been used for this present simulation study. Proximate and ultimate analysis data for the feedstocks and the pyrolysis product yields at 500 °C are listed in Tables 1 and 2, respectively. Torrefied biomass was produced at 250 °C with 30 min of residence time. Starting from the ultimate analysis of biomass and mass fractions of all elements, the biomass formula $C_{a1}H_{a2}O_{a3}N_{a4}$ was calculated by assuming that a_1 is equal to 1.0 by the following Eqs. (1)–(3) [42]:

$$a_2 = \frac{\text{mass fraction(H)} \times \text{Molecular weight(C)}}{\text{mass fraction(C)} \times \text{Molecular weight(H)}} \quad (1)$$

$$a_3 = \frac{\text{mass fraction(O)} \times \text{Molecular weight(C)}}{\text{mass fraction(C)} \times \text{Molecular weight(O)}} \quad (2)$$

$$a_4 = \frac{\text{mass fraction(N)} \times \text{Molecular weight(C)}}{\text{mass fraction(C)} \times \text{Molecular weight(N)}} \quad (3)$$

Based on Eqs. (1)–(3), formulas for the feedstocks are calculated: Biomass $CH_{1.77}O_{0.63}N_{0.012}$; torrefied biomass $CH_{1.45}O_{0.57}N_{0.011}$.

2.1.3. Key process variables

It has been reported that the optimal gasification operation involves operating a gasifier at or below the carbon boundary point, that means that all carbon is present in the gaseous phase as carbon monoxide, carbon dioxide or methane [46]. This theory has been applied for this study as well and all the 27 tested cases have carbon in its gaseous form. This is the basis for selecting the ranges for the three process variables listed in Table 3. ER is defined as the amount of air added relative to the stoichiometric air requirement for combustion and SBR is defined as the ratio of steam to biomass molar flow rates.

Steam is added to the system to improve the hydrogen production and thus increase the syngas quality [42]. Each of the 27 cases will be referred to using these three process variables, as SBR–GB–ER, in this study.

2.1.4. Assumptions made for Aspen Plus simulation and efficiency calculations

(a) All gases behave ideally.
(b) The process occurs at steady state, and residence time was not considered.
(c) Biomass mass flow rate was calculated for a 10 MW fuel input plant.
(d) Air was introduced to RGIBBS at ambient temperature and pressure.
(e) Saturated steam was introduced to RGIBBS at 179.9 °C and 10 bar pressure.
(f) Atmospheric pressure was assumed in all equipment.
(g) The process was assumed to be autothermal and the pressure drop and heat losses from the equipment and pipelines were not included.
(h) Ambient conditions data for each stream was collected from Aspen Plus in order to have consistent values for the reference conditions in the physical exergy calculations.

Table 1
Proximate and ultimate analyses of the samples [45].

Sample	Proximate analysis[a]			Ultimate analysis[a]				HHV[b]
	VM	fC	Ash	C	H	O	N	
Leucaena	86.1	13.1	0.8	50.1	7.4	41.8	0.7	20.3
Torrefied Leucaena	82.2	16.9	0.9	53.0	6.4	39.9	0.7	21.2

[a] % (m/m), dry basis.
[b] MJ/kg, dry basis.

Table 2
Pyrolysis products yield as input to RYIELD [45].

Sample	Pyrolysis product molar yield at 500 °C					
	Char	H_2O	Tar	CO	CH_4	CO_2
Leucaena	0.20	0.20	0.40	0.019	0.001	0.18
Torrefied Leucaena	0.29	0.16	0.34	0.029	0.001	0.18

Table 3
Tested ranges for process variables that resulted in 27 cases.

Process variable	Low	Mid	High
SBR	0.2	0.3	0.4
Gibbs (GB) Temperature (°C)	900	1000	1100
ER	0.1	0.2	0.3

(i) No physical exergy is associated with biomass as these were assumed to be at ambient temperature and pressure.
(j) Minor products such as sulfur species (e.g. S, COS and H_2S) and nitrogen species except N_2 were not included in the chemical exergy of the streams as these are present, relatively speaking, in very negligible amounts.
(k) Kinetic and potential exergies were ignored in the analysis.
(l) No work exergy was included in the exergy analysis.
(m) All biomass feedstocks were completely dry.
(n) Tar was considered as a mixture of 70% secondary (phenol), 14% tertiary-alkyl (xylene) and 16% tertiary-PNA (benzene) components on mass basis [47,48]. Based on the previous studies on tar cracking, it was assumed that tertiary-PNA component is not cracked at all and tertiary-alkyl component is 80% cracked at the temperatures conditions used in this study [48]. In addition to this, untreated biomass is assumed to have 10% aqueous phase acid (acetic acid), which remains un-reacted in RGIBBS [49]. For the torrefied biomass, these acids were assumed to be removed during torrefaction. Char composition of pyrolyzed biomass (from both untreated and torrefied biomass) was calculated from the elemental carbon, hydrogen and oxygen balance based on the assumed tar composition.

2.2. Methods for cold gas energy and exergy efficiencies

The cold gas efficiency of gasification in an allothermal plant is defined in Eq. (4) [40]:

$$\eta_{\text{energy.coldgas}} = \frac{\text{LHV}_{\text{coldgas}}}{\text{LHV}_{\text{biomass}} + Q_{\text{air}} + Q_{\text{steam}}} \tag{4}$$

where $\text{LHV}_{\text{coldgas}}$ is the heating value of the outgoing (product) heat stream; $\text{LHV}_{\text{biomass}}$, Q_{steam} and Q_{air} are the heating value and heat contents of incoming biomass, steam and air streams, respectively. Exergy is the maximum work that can be produced when a heat or material stream is brought to equilibrium relative to a reference environment, which consists of reference components and which is characterized by absence of pressure and temperature gradients. Exergy associated with a material stream is expressed as the sum of its physical and chemical exergies.

The total exergy of a material stream is given by Eq. (5) [40,50]:

$$E = N(\varepsilon_{\text{ph}} + \varepsilon_{\text{ch}}) \tag{5}$$

where N is the flow rate. The molar physical exergy of a material stream is expressed in relation to the reference environmental conditions as shown in Eq. (6) [40,50]:

$$\varepsilon_{\text{ph}} = (h - h_0) - T_0(s - s_0) \tag{6}$$

Mole flows, mole fractions, enthalpy and entropy of each material stream were taken from the Aspen Plus flowsheet results. The standard environmental conditions of Aspen Plus (T_0 = 25 °C, p_0 = 1.013 bar) were adopted as reference conditions in the study. The molar chemical exergy of a gaseous material mixture is given by Eq. (7) [40,50]:

$$\varepsilon_{\text{ch.gas}} = \sum_i x_i \varepsilon_{0,i} + RT_0 \sum_i x_i \ln x_i \tag{7}$$

where x_i is the mole fraction and $\varepsilon_{0,i}$ is the standard molar chemical exergy of each component i, in J mol^{-1}. The latter is available in literature for the reference atmospheric composition [51].

The chemical exergy of solid fuels (biomass and torrefied product) was calculated with the help of the ratio of the chemical exergy to the lower heating value of the dry matter as shown in Eq. (8) [52]. This ratio is a function of the elemental contents of the solid fuel.

$$\varphi_{\text{dry}} = \frac{\varepsilon_{\text{dm}}}{h_{\text{LHV}_{\text{dm}}}} \tag{8}$$

For dry solid fuels with a certain content of oxygen, the ratio of chemical exergy to lower heating value for the dry matter is expressed in Eq. (9) [52]:

$$\varphi_{\text{dry}} = \frac{1.0438 + 0.1882\frac{h}{c} - 0.2509\frac{o}{c}\left(1 + 0.7256\frac{h}{c}\right) + 0.0383\frac{n}{c}}{1 - 0.3035\frac{o}{c}} \tag{9}$$

Here, h/c is the ratio of hydrogen mass to carbon mass in the fuel, and n/c and o/c correspondingly for nitrogen and oxygen. This expression is valid for o/c from 0.667 to 2.67, and is expected to be accurate within ±1%. Using Eqs. (5)–(9), exergy was calculated for all material streams in the flow sheet. The exergetic efficiency of gasification in an autothermal plant is defined in Eq. (10) [40]:

$$\eta_{\text{exergy.coldgas}} = \frac{E_{\text{coldgas}}}{E_{\text{biomass}} + E_{\text{air}} + E_{\text{steam}}} \tag{10}$$

where E_{coldgas} is the outgoing (product) exergy stream, and E_{biomass}, E_{steam} and E_{air} are the incoming biomass (or the torrefied biomass), steam and air exergies.

Table 4 lists the standard chemical exergy and standard lower heating values of the gases that form syngas [53–55].

Table 4
Standard chemical exergy and LHV values of gases.

Reference data	CO (g)	CO_2 (g)	H_2 (g)	N_2 (g)	H_2O (g)
Standard chemical exergy (MJ/kmol)	275.1	19.87	236.1	0.72	9.5
Standard LHV (MJ/kg)	10.112	0	119.96	0	0

3. Results and discussions

3.1. Syngas compositions

Mole fractions of hydrogen (H_2), carbon monoxide (CO), carbon dioxide (CO_2), and nitrogen (N_2) in the syngas generated from all 27 cases are shown in Figs. 2–5. For improved understanding for the readers, the effect of the three process variables SBR, GB Temperature and ER on these mole fractions is shown separately in Figs. 6–8, where two of these variables are fixed and one is varied. In previous studies in the literature, methane production decreases sharply at temperatures above 500 °C [22,56]. Similar trends were observed in this study and negligible amounts of methane is produced (mole fractions close to 1×10^{-5}) since the temperatures tested are close to 1000 °C. Therefore, the methane content is not reported in these results. Table 5 lists the trends for the syngas content based on increase in any one of the process variables.

These trends are explained in terms of common gasification reactions as listed below (Eqs. (11)–(18)) [57]. Heat of reactions are provided in the brackets for these reactions, with minus sign for exothermic and plus sign for endothermic reactions:

Char partial combustion reaction

$$C + 0.5O_2 = CO \quad (-111\ \text{MJ/kmol}) \tag{11}$$

Boudouard reaction

$$C + CO_2 \Longleftrightarrow 2CO \quad (+172\ \text{MJ/kmol}) \tag{12}$$

Water gas reaction

$$C + H_2O \Longleftrightarrow CO + H_2 \quad (+131\ \text{MJ/kmol}) \tag{13}$$

Methanation reaction

$$C + 2H_2 \Longleftrightarrow CH_4 \quad (-75\ \text{MJ/kmol}) \tag{14}$$

CO partial combustion reaction

$$CO + 0.5O_2 = CO_2 \quad (-283\ \text{MJ/kmol}) \tag{15}$$

H_2 partial combustion reaction

$$H_2 + 0.5O_2 = H_2O \quad (-242\ \text{MJ/kmol}) \tag{16}$$

CO shift reaction

$$CO + H_2O \Longleftrightarrow CO_2 + H_2 \quad (-41\ \text{MJ/kmol}) \tag{17}$$

Steam-methane reforming reaction

$$CH_4 + H_2O \Longleftrightarrow CO + 3H_2 \quad (+206\ \text{MJ/kmol}) \tag{18}$$

As reactions (11)–(14) have carbon in solid state, applicability of these reactions is up to the carbon boundary point. These reactions can explain the differences in the gasification behaviors of torrefied wood and untreated wood based on their carbon contents. Since approximately 70–80% devolatilization of biomass has already occurred in RYIELD (experimental values from Wannapeera et al. [45]), the main reactions happening in RGIBBS are the gas phase reactions (15)–(18).

3.1.1. Effect of increase in SBR

The main reaction by an increase in SBR is the CO shift reaction where CO reacts with steam (H_2O) to form CO_2 and H_2. This results in decrease of CO and increase of CO_2 and H_2 production.

3.1.2. Effect of increase in GB Temperature

Increase in Gibbs reactor temperature also involves the CO shift reaction but in the opposite direction. As the CO shift reaction is exothermic (heat of reaction = −41 MJ/kmol), increase in temperature results in the formation of CO and H_2O from CO_2 and H_2.

3.1.3. Effect of increase in ER

Increase in ER results in CO and H_2 partial combustion where these two gases react individually with oxygen to form CO_2 and H_2O, respectively. Also, air increases the nitrogen content of syngas. These two reactions result in increased CO_2 and H_2O production and decreased CO and H_2 contents.

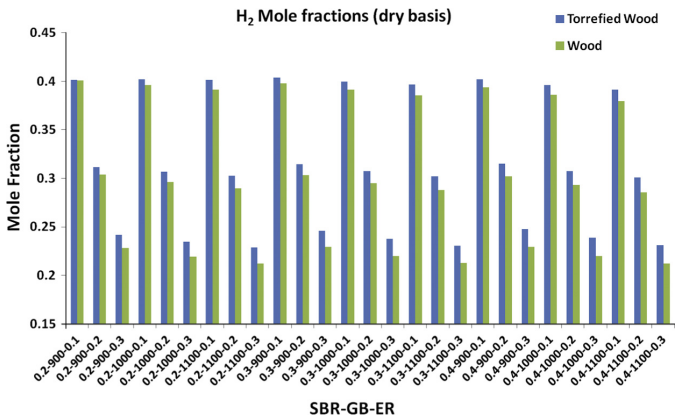

Fig. 2. Hydrogen mole fractions on dry basis for all cases.

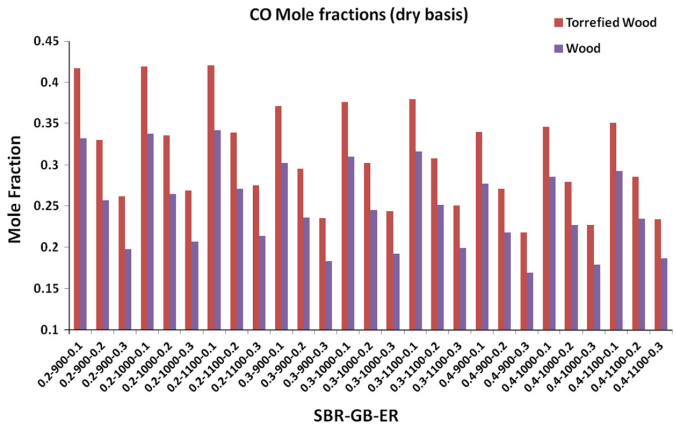

Fig. 3. Carbon monoxide mole fractions on dry basis for all cases.

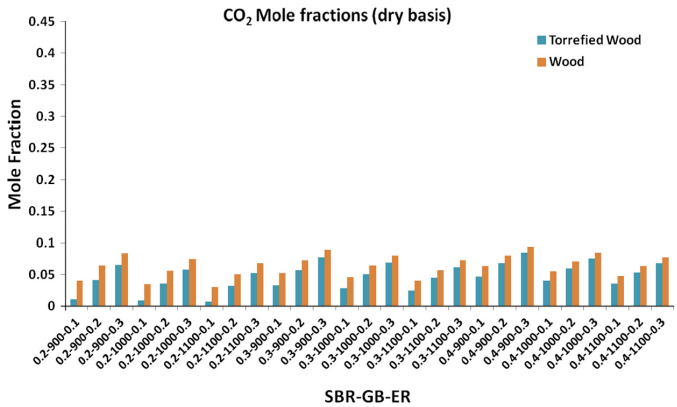

Fig. 4. Carbon dioxide mole fractions on dry basis for all cases.

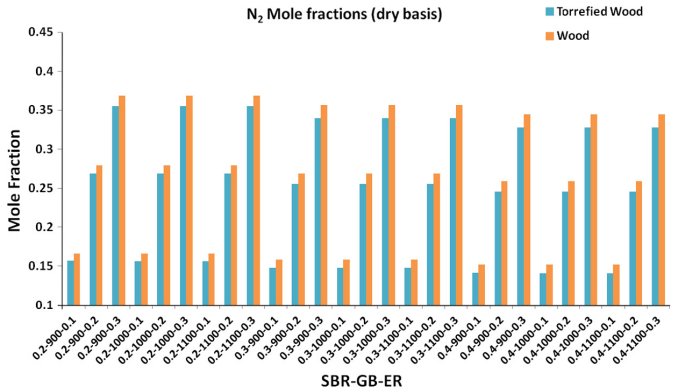

Fig. 5. Nitrogen mole fractions on dry basis for all cases.

3.1.4. Differences between torrefied wood and untreated wood

Torrefied wood results in higher CO and H_2 production in comparison to untreated wood due to higher carbon content. Char partial combustion, Boudouard and water–gas reactions occur with carbon in solid state to form CO and H_2.

3.2. Cold gas energy and exergy efficiencies

Cold gas energy and exergy efficiencies of all the 27 cases are shown in Figs. 9 and 10, respectively. The general trends are listed in Table 6. It can be seen that both energy and exergy efficiencies

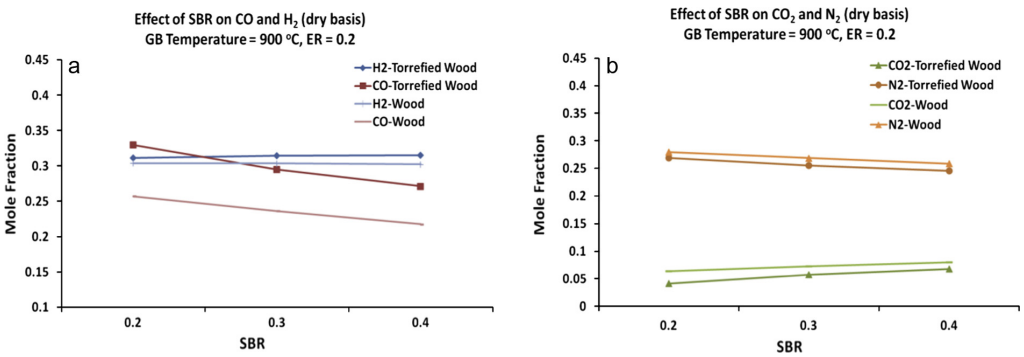

Fig. 6. Effect of SBR on the carbon monoxide and hydrogen (a) and carbon dioxide and nitrogen (b) mole fractions.

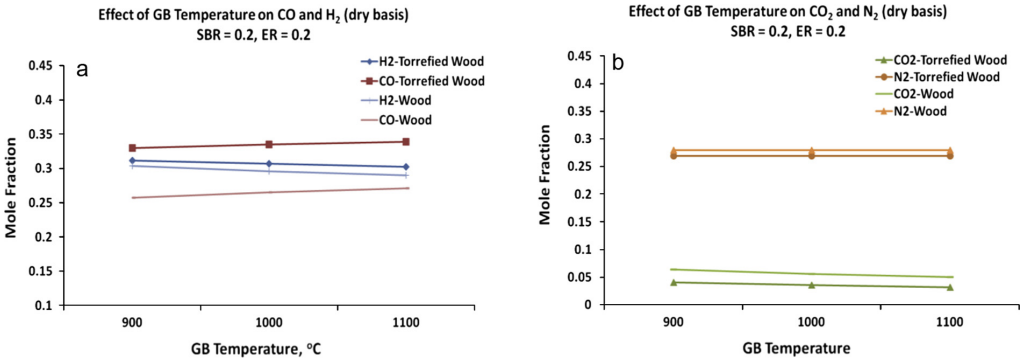

Fig. 7. Effect of GB Temperature on the carbon monoxide and hydrogen (a); carbon dioxide and nitrogen (b) mole fractions.

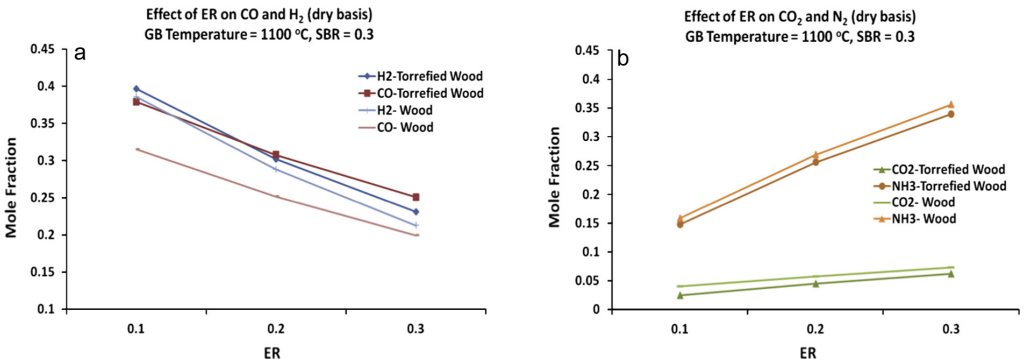

Fig. 8. Effect of ER on the carbon monoxide and hydrogen (a); carbon dioxide and nitrogen (b) mole fractions.

Table 5
Syngas composition trends with changes in SBR, GB Temperature and ER.

Mole fractions	Increase in SBR	Increase in GB Temperature	Increase in ER	Torrefied wood (TW) vs. Wood (W)
H_2	Slightly increases	Slightly decreases	Decreases	TW > W
CO	Decreases	Slightly increases	Decreases	TW > W
CO_2	Slightly increases	Slightly decreases	Increases	W > TW
N_2	Slightly decreases	Negligible effect	Increases	W > TW

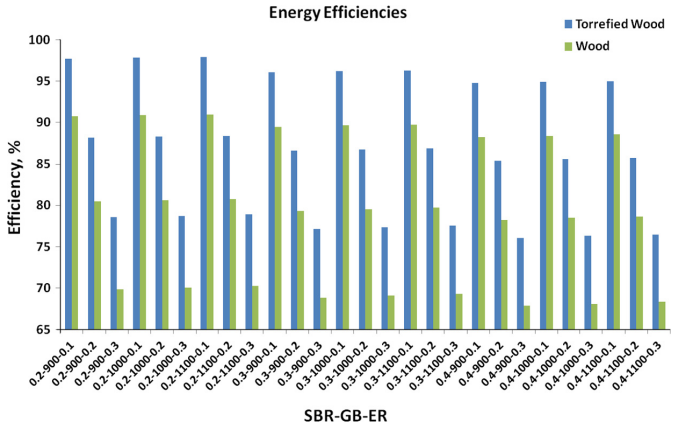

Fig. 9. Cold gas energy efficiencies in percent for all 27 cases.

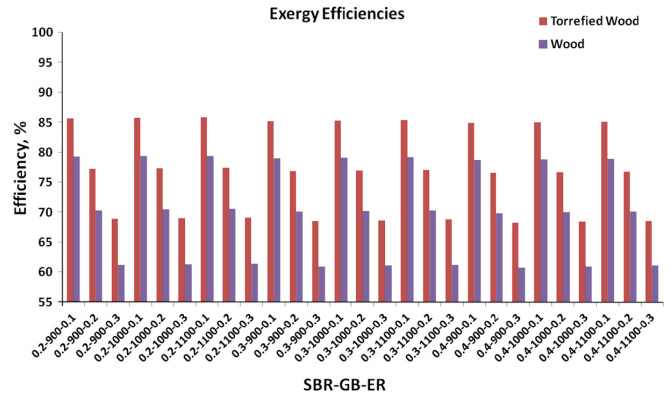

Fig. 10. Exergy efficiencies in percent for all 27 cases.

decrease with increase in SBR, GB Temperature and ER, with ER having the most pronounced effect. Fig. 11(a), (b) and (c) shows the effect of process variables on these efficiencies by varying one of these variables and keeping the other two constant. From Figs. 9–11 it can also be seen that the torrefied wood has higher energy and exergy efficiencies than untreated wood for all cases. Table 7 lists the maximum and minimum values of the energy and exergy efficiencies for all cases.

3.2.1. Effect of increase in SBR

Increase in SBR results in increased CO_2 and H_2 production and decreased CO production. As can be seen from Table 4, standard chemical exergy and standard lower heating values (LHV) for H_2 is lower than for CO and the values for CO_2 are negligible. This results in lower LHV and chemical exergy of the cold syngas and thus, lower energy and exergy efficiencies with increasing SBR.

3.2.2. Effect of increase in GB Temperature

With increasing GB Temperature, CO and H_2O production increases and that of CO_2 and H_2 decreases. Since H_2O and CO_2 have zero LHVs and negligible standard chemical exergies, the increase in CO is compensated by the decrease in H_2. End result is slightly lower (almost constant) energy and exergy efficiencies with the increase in the Gibbs reactor temperature.

3.2.3. Effect of increase in ER

Increase in ER results in increased CO_2, H_2O and N_2 production and decreased CO and H_2 contents. As CO_2, H_2O and N_2 have very low exergy and zero LHV values, reduction in CO and H_2 results in lower syngas chemical exergy and LHV. This results in lower energy and exergy efficiencies with increase in ER.

3.2.4. Differences between torrefied wood and untreated wood

Higher energy and exergy efficiencies for torrefied wood in comparison to untreated wood is mainly attributed to its higher carbon content, which results in higher H_2 and CO contents and thus higher syngas LHV and chemical exergy.

3.2.5. Integrated torrefaction–gasification process

Overall efficiencies of an integrated torrefaction–gasification process can be calculated by including the mass flow rates of the untreated biomass needed for the production of torrefied biomass. Higher mass yields in the torrefaction process will result in improved overall efficiencies of the integrated process. For the current study, torrefied Leucaena has 5.78% higher carbon content than untreated Leucaena in the ultimate analysis with torrefaction at 250 °C for 30 min. For similar torrefaction temperature and residence time and with 8.7% increase in carbon content, mass yields reported in the literature are around 88–90% [2,58]. By using 88%

Table 6
Cold gas energy and exergy efficiency trends.

Efficiency	Increase in SBR	Increase in GB Temperature	Increase in ER	Torrefied wood (TW) vs. Wood (W)
Energy efficiency	Slightly decreases	Slightly decreases	Decreases	TW > W
Exergy efficiency	Slightly decreases	Slightly decreases	Decreases	TW > W

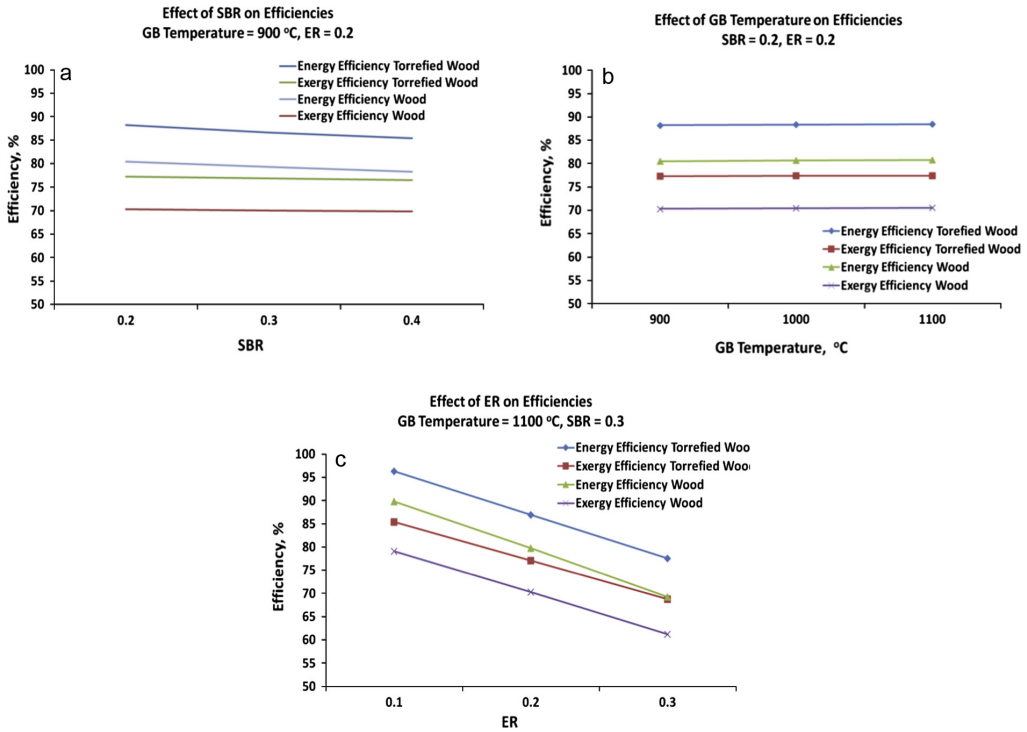

Fig. 11. Effect of SBR (a), GB Temperature (b) and ER (c) on efficiencies.

Table 7
Maximum and minimum efficiencies.

Efficiency		% (TW)	% (W)	SBR	GB Temperature (°C)	ER
Energy efficiency	Maximum	97.9	91.0	0.2	1100	0.1
	Minimum	76.1	67.9	0.4	900	0.3
Exergy efficiency	Maximum	85.8	79.4	0.2	1100	0.1
	Minimum	68.3	60.7	0.4	900	0.3

as torrefaction mass yield for the current study, energy and exergy efficiencies for the integrated process were calculated for a few selected cases. For all of these cases, efficiencies for the integrated process were found to be higher than the stand alone process with untreated biomass as feedstock, as shown in Fig. 12. Effects of the varied process parameters (SBR, GB Temperature and ER) on the efficiencies is similar to the stand alone biomass gasification process.

Efficiencies for the torrefaction process can also be calculated by dividing LHV or the exergy values of torrefied biomass with the corresponding values for untreated biomass. With 88% mass yield and required torrefied biomass production for a 10 MW fuel input plant, energy and exergy efficiencies for the torrefaction process are 93.3% and 92.6%, respectively. Mass yields in a torrefaction process are highly dependent on the choice of the reactor, heat and mass transfer profiles, process control and the production scale. Reactors used at a laboratory scale may not be a good simulation for pilot or industry scale reactors. Therefore, overall efficiencies of an integrated torrefaction–gasification industrial process should be evaluated for a specific reactor type.

3.3. Comparisons of results with other similar studies

For both torrefied and untreated woods, the ranges for the mole fractions of H_2, CO, CO_2 and N_2 in the 27 cases are listed in Table 8.

Based on a literature review, it was found that there is a considerable lack of data for two-stage biomass gasification. The simulation work performed by Paviet et al. [56] is the only one that can be compared to the present work and the results from that study are listed in Table 9. Even though Paviet et al. [56] utilized different

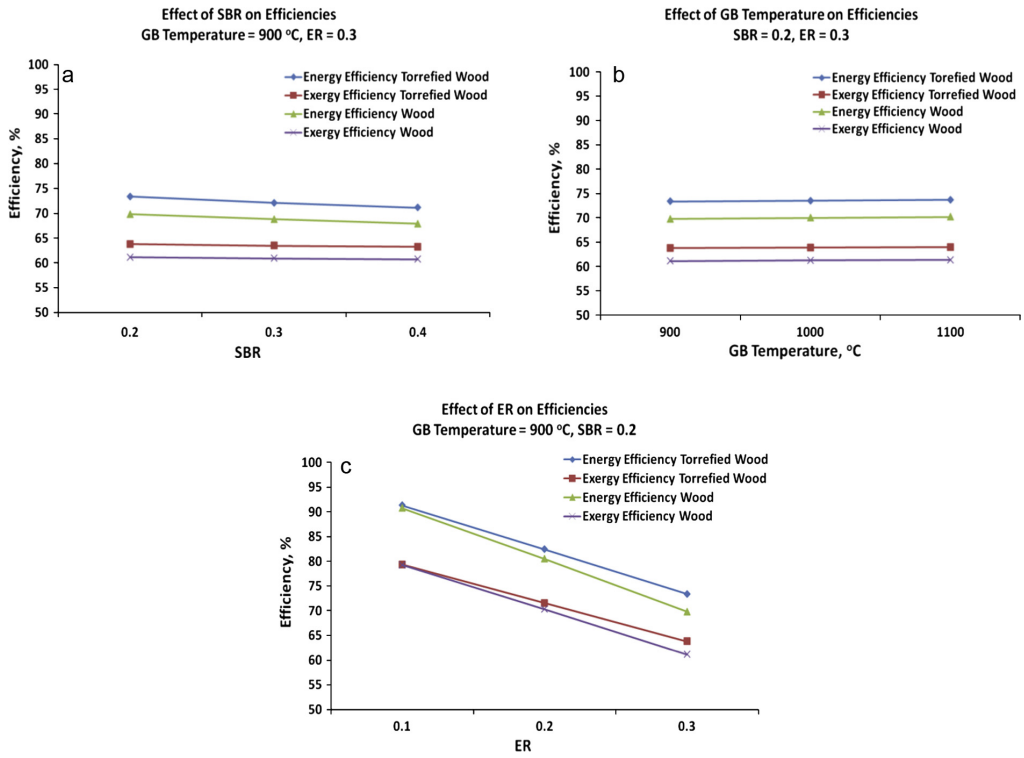

Fig. 12. Effect of SBR (a), GB Temperature (b) and ER (c) on the efficiencies of an integrated torrefaction–gasification process (88% mass yield for torrefaction).

Table 8
Product gas composition.

Syngas components		Mole fraction (TW)	Mole fraction (W)	SBR	GB Temperature (°C)	ER
H_2	Maximum	0.40	0.40	0.3	900	0.1
	Minimum	0.23	0.21	0.3	1100	0.3
CO	Maximum	0.42	0.34	0.2	1100	0.1
	Minimum	0.22	0.17	0.4	900	0.3
CO_2	Maximum	0.09	0.09	0.4	900	0.3
	Minimum	0.01	0.03	0.2	1100	0.1
N_2	Maximum	0.36	0.37	0.2	900	0.3
	Minimum	0.14	0.15	0.4	1100	0.1

operating conditions in the simulation, the two-stage gasification is similar to this present study.

By comparing results from Tables 8 and 9, it can be seen that the syngas contents are quite similar in both studies. The end results for H_2, CO, CO_2 and N_2 are very comparable to both simulation and experimental results from Paviet et al. [56], depending upon the selection of process conditions from the present study. Recently, a few studies have utilized the concept of C–H–O Ternary diagram to show the biomass gasification process with respect to the carbon deposition boundaries [46,59]. Fig. 13 shows the C–H–O ternary diagram for the present study for one case (SBR–GB–ER = 0.3–900–0.2) using the calculation methods mentioned in the literatures [46,59].

In Fig. 13, point A represents untreated biomass, point B represents the syngas produced from RGIBBS. Corresponding points for the torrefied biomass are A′ and B′ respectively. As can be seen,

Table 9
Results from Paviet et al. [56] (dry basis).

Results from Paviet et al.	H_2	CO	CH_4	CO_2	N_2
Simulation results (H: 18.2%, *T*: 1300 K, Ra: 2.53, Rh: 0.40)	0.34	0.26	0.00	0.10	0.30
Experimental results from two-stage gasifier DTU	0.30	0.20	0.01	0.15	0.34

H = Moisture content of fuel; Ra = Air/fuel mass flow ratio; Rh = Steam/fuel mass flow ratio.

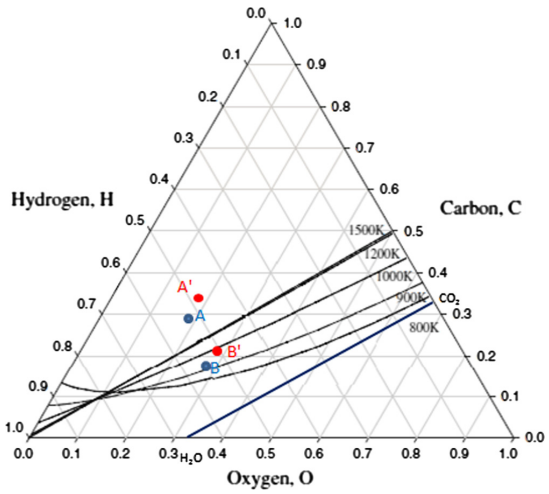

Fig. 13. C–H–O ternary diagram with simulation results from the present study (for one case). Carbon deposition boundary data from literature [59].

point B lies close to the carbon deposition boundaries and this is valid for all 27 cases tested in the present study. The line connecting CO_2 and H_2O represents complete combustion of biomass and in our case point B lies well above this line, thus, indicating a gasification process. If only air is added in the process, the process moves along a line connecting the biomass to the pure oxygen point and the optimum gasification point is where this line intersects the carbon boundary line for a particular temperature. However, with the addition of small amounts of steam, the gasification point moves to point B (or B′) and is slightly below the carbon boundary. This is because the reaction between biomass and steam are endothermic (water gas shift reaction) and those between biomass and air are exothermic (Char partial combustion) [60]. Based on the C–H–O ternary diagram analysis, the present gasification simulation study fits very well with the underlying gasification theory.

4. Conclusions

Biomass gasification was simulated using Aspen Plus with a two-stage gasification model based on Gibbs free energy minimization approach for comparing untreated and torrefied biomass as feedstocks. Model accuracy was improved by including tar, actual experimental decomposition yields and the compositions of the chars produced during pyrolysis in the evaluations. The model outcomes were validated by using a C–H–O Ternary diagram and by comparisons with results from other similar studies. Three process parameters: SBR, GB Temperature and ER were varied. 27 cases were selected with all having carbon in the gaseous form for the final syngas product. It was found that the syngas compositions vary a lot based on the process parameters, and inlet conditions should be selected based on the end requirements for syngas. Here is the summary of results obtained from this study:

1. Out of the three process parameters, ER had the most significant effect on the syngas composition, energy and exergy efficiency.
2. Maximum energy and exergy efficiencies are achieved by operating gasifier at or close to carbon deposition boundary point at that temperature.
3. Torrefied biomass gives higher H_2 and CO contents and higher cold gas energy and exergy efficiencies than untreated biomass.
4. Overall efficiencies of an integrated torrefaction–gasification process depend on the mass yields of the torrefaction process. Torrefaction mass yield of 88% in the present study resulted in better overall energy and exergy efficiencies.
5. Simulation results from this study correlates well with the simulation and experimental results from the Paviet et al. [56] study.

Torrefaction of biomass does seem to have a positive effect on biomass gasification due to improved CO and H_2 contents. This effect is mainly due to the increased carbon content of torrefied biomass due to the devolatilization leading to relatively higher oxygen loss during torrefaction. This is evident from the increased chemical exergy of torrefied biomass as well, and this higher chemical exergy is utilized for improvements in syngas quality. As noted earlier in this study, there is considerable lack of data on the gasification of torrefied biomass and therefore, the authors recommend further studies on additional feedstocks.

Acknowledgements

The authors acknowledge the support of the Bioenergy Innovation Center (CenBio) project team at the Norwegian University of Science and Technology (NTNU) and SINTEF Energy Research for providing financial resources to carry out this study.

References

[1] Sadaka S, Negi S. Improvements of biomass physical and thermochemical characteristics via torrefaction process. Environ Progr Sustain Energy 2009;28:427–34.
[2] van der Stelt MJC, Gerhauser H, Kiel JHA, Ptasinski KJ. Biomass upgrading by torrefaction for the production of biofuels: a review. Biomass Bioenergy 2011;35:3748–62.
[3] Arias B, Pevida C, Fermoso J, Plaza MG, Rubiera F, Pis JJ. Influence of torrefaction on the grindability and reactivity of woody biomass. Fuel Process Technol 2008;89:169–75.
[4] Bridgeman TG, Jones JM, Shield I, Williams PT. Torrefaction of reed canary grass, wheat straw and willow to enhance solid fuel qualities and combustion properties. Fuel 2008;87:844–56.
[5] Bridgeman TG, Jones JM, Williams A, Waldron DJ. An investigation of the grindability of two torrefied energy crops. Fuel 2010;89:3911–8.
[6] Couhert C, Salvador S, Commandré JM. Impact of torrefaction on syngas production from wood. Fuel 2009;88:2286–90.
[7] Deng J, Wang G-J, Kuang J-H, Zhang Y-L, Luo Y-H. Pretreatment of agricultural residues for co-gasification via torrefaction. J Anal Appl Pyrol 2009;86:331–7.
[8] Prins MJ, Ptasinski KJ, Janssen FJJG. Torrefaction of wood. J Anal Appl Pyrol 2006;77:28–34.
[9] Tapasvi D, Khalil R, Skreiberg Ø, Tran K-Q, Grønli M. Torrefaction of Norwegian birch and spruce: an experimental study using macro-TGA. Energy Fuels 2012;26:5232–40.
[10] Tapasvi D, Khalil R, Várhegyi G, Tran K-Q, Grønli M, Skreiberg Ø. Thermal decomposition kinetics of woods with an emphasis on torrefaction. Energy Fuels 2013;27:6134–45.
[11] Tapasvi D, Khalil R, Várhegyi G, Skreiberg Ø, Tran K-Q, Grønli M. Kinetic behavior of torrefied biomass in an oxidative environment. Energy Fuels 2013;27:1050–60.
[12] Tapasvi D, Tran K-Q, Wang L, Skreiberg Ø, Khalil R. Biomass torrefaction – a review. In: INFUB-9 Estoril, Portugal; 2011.
[13] Chen W-H, Kuo P-C. A study on torrefaction of various biomass materials and its impact on lignocellulosic structure simulated by a thermogravimetry. Energy 2010;35:2580–6.
[14] Chen W-H, Kuo P-C. Torrefaction and co-torrefaction characterization of hemicellulose, cellulose and lignin as well as torrefaction of some basic constituents in biomass. Energy 2011;36:803–11.
[15] Jankes G, Trninic M, Stamenic M, Simonovic T, Tanasic N, Labus J. Biomass gasification with CHP production: a review of state of the art technology and near future perspectives. Therm Sci 2012;16:115–30.
[16] Puig-Arnavat M, Bruno JC, Coronas A. Review and analysis of biomass gasification models. Renew Sustain Energy Rev 2010;14:2841–51.
[17] Zhang L, Xu C, Champagne P. Overview of recent advances in thermo-chemical conversion of biomass. Energy Convers Manage 2010;51:969–82.
[18] Balat M, Balat M, Kırtay E, Balat H. Main routes for the thermo-conversion of biomass into fuels and chemicals. Part 2: Gasification systems. Energy Convers Manage 2009;50:3158–68.
[19] Srinivas T, Gupta AVSSKS, Reddy BV. Thermodynamic equilibrium model and exergy analysis of a biomass gasifier. J Energy Res Technol 2009;131.

[20] Schuster G, Löffler G, Weigl K, Hofbauer H. Biomass steam gasification – an extensive parametric modeling study. Bioresour Technol 2001;77:71–9.
[21] Altafini CR, Wander PR, Barreto RM. Prediction of the working parameters of a wood waste gasifier through an equilibrium model. Energy Convers Manage 2003;44:2763–77.
[22] Melgar A, Pérez JF, Laget H, Horillo A. Thermochemical equilibrium modelling of a gasifying process. Energy Convers Manage 2007;48:59–67.
[23] Jarungthammachote S, Dutta A. Thermodynamic equilibrium model and second law analysis of a downdraft waste gasifier. Energy 2007;32:1660–9.
[24] Jarungthammachote S, Dutta A. Equilibrium modeling of gasification: Gibbs free energy minimization approach and its application to spouted bed and spout-fluid bed gasifiers. Energy Convers Manage 2008;49:1345–56.
[25] Yoshida H, Kiyono Fo, Tajima H, Yamasaki A, Ogasawara K, Masuyama T. Two-stage equilibrium model for a coal gasifier to predict the accurate carbon conversion in hydrogen production. Fuel 2008;87:2186–93.
[26] Ghassemi H, Shahsavan-Markadeh R. Effects of various operational parameters on biomass gasification process; a modified equilibrium model. Energy Convers Manage 2014;79:18–24.
[27] Bassyouni M, ul Hasan SW, Abdel-Aziz MH, Abdel-hamid SMS, Naveed S, Hussain A, et al. Date palm waste gasification in downdraft gasifier and simulation using ASPEN HYSYS. Energy Convers Manage 2014;88:693–9.
[28] Ravikiran A, Renganathan T, Pushpavanam S, Voolapalli RK, Cho YS. Generalized analysis of gasifier performance using equilibrium modeling. Ind Eng Chem Res 2012;51:1601–11.
[29] Li X, Grace JR, Watkinson AP, Lim CJ, Ergüdenler A. Equilibrium modeling of gasification: a free energy minimization approach and its application to a circulating fluidized bed coal gasifier. Fuel 2001;80:195–207.
[30] Mansaray KG, Al-Taweel AM, Ghaly AE, Hamdullahpur F, Ugursal VI. Mathematical modeling of a fluidized bed rice husk gasifier: Part I – Model development. Energy Sources 2000;22:83–98.
[31] Paviet F, Chazarenc F, Tazerout M. Thermo chemical equilibrium modelling of a biomass gasifying process using ASPEN PLUS. Int J Chem Reactor Eng 2009;7.
[32] Chen WH, Chen CJ, Hung CI. Taguchi approach for co-gasification optimization of torrefied biomass and coal. Bioresour Technol 2013;144:615–22.
[33] Chen W-H, Chen C-J, Hung C-I, Shen C-H, Hsu H-W. A comparison of gasification phenomena among raw biomass, torrefied biomass and coal in an entrained-flow reactor. Appl Energy 2013;112:421–30.
[34] Kuo P-C, Wu W, Chen W-H. Gasification performances of raw and torrefied biomass in a downdraft fixed bed gasifier using thermodynamic analysis. Fuel 2014;117:1231–41.
[35] Ptasinski KJ, Prins MJ, Pierik A. Exergetic evaluation of biomass gasification. Energy 2007;32:568–74.
[36] Rao MS, Singh SP, Sodha MS, Dubey AK, Shyam M. Stoichiometric, mass, energy and exergy balance analysis of countercurrent fixed-bed gasification of post-consumer residues. Biomass Bioenergy 2004;27:155–71.
[37] Pellegrini L, Deoliveirajr S. Exergy analysis of sugarcane bagasse gasification. Energy 2007;32:314–27.
[38] Abuadala A, Dincer I, Naterer GF. Exergy analysis of hydrogen production from biomass gasification. Int J Hydrogen Energy 2010;35:4981–90.
[39] Hosseini M, Dincer I, Rosen MA. Steam and air fed biomass gasification: comparisons based on energy and exergy. Int J Hydrogen Energy 2012;37:16446–52.
[40] Fryda L, Panopoulos KD, Kakaras E. Integrated CHP with autothermal biomass gasification and SOFC–MGT. Energy Convers Manage 2008;49:281–90.
[41] Karamarkovic R, Karamarkovic V. Energy and exergy analysis of biomass gasification at different temperatures. Energy 2010;35:537–49.
[42] Kempegowda RS, Assabumrungrat S, Laosiripojana N. Thermodynamic analysis for gasification of Thailand rice husk with air, steam, and mixed air/steam for hydrogen-rich gas production. Int J Chem Reactor Eng 2010;8.
[43] Kempegowda RS, Pannir Selvam PV, Skreiberg Ø, Tran K-Q. Process synthesis and economics of combined biomethanol and CHP energy production derived from biomass wastes. J Chem Technol Biotechnol 2012;87:897–902.
[44] Nikoo MB, Mahinpey N. Simulation of biomass gasification in fluidized bed reactor using aspen plus. Biomass Bioenergy 2008;32:1245–54.
[45] Wannapeera J, Fungtammasan B, Worasuwannarak N. Effects of temperature and holding time during torrefaction on the pyrolysis behaviors of woody biomass. J Anal Appl Pyrol 2011;92:99–105.
[46] Ptasinski KJ. Thermodynamic efficiency of biomass gasification and biofuels conversion. Biofuels, Bioprod Biorefin 2008;2:239–53.
[47] Aigner I, Wolfesberger U, Hofbauer H. Tar content and composition in producer gas of fluidized bed gasification and low temperature pyrolysis of straw and wood – influence of temperature; 2009.
[48] Fjellerup J, Ahrenfeldt J, Henriksen U, Gøbel B. Formation, decomposition and cracking of biomass tars in gasification. Denmark: Technical University of Denmark; 2005. p. 1–60.
[49] Chang SK, Sung PM. Characterization of pyrolysis tar derived from lignocellulosic biomass. J Ind Eng Chem 2006;12:853–61.
[50] Panopoulos KD, Fryda L, Karl J, Poulou S, Kakaras E. High temperature solid oxide fuel cell integrated with novel allothermal biomass gasification. J Power Sources 2006;159:586–94.
[51] Kotas TJ. The exergy method of thermal plant analysis. Krieger Publishing Company; 1995.
[52] Szargut VJ, Styrylska T. Angenaherte bestimmung der exergie von brennstoffen. Brennstoff-Warne-Kraft 1964;16:S.589.
[53] Morris DR, Szargut J. Standard chemical exergy of some elements and compounds on the planet earth. Energy 1986;11:733–55.
[54] Wikipedia.org. Heat of combustion. http://en.wikipedia.org/wiki/Heat_of_combustion
[55] Hacker V, Kordesch K. Handbook of fuel cells – fundamentals, technology and applications. In: Ammonia crackers. Chichester: John Wiley & Sons, Ltd.; 2003 [chapter 10].
[56] Paviet F, Chazarenc F, Tazerout M. Thermo chemical equilibrium modelling of a biomass gasifying process using aspen plus. Int J Chem Reactor Eng 2009;7.
[57] Doherty W, Reynolds A, Kennedy D. The effect of air preheating in a biomass CFB gasifier using aspen plus simulation. Biomass Bioenergy 2009;33:1158–67.
[58] Prins MJ, Ptasinski KJ, Janssen FJJG. Torrefaction of wood. J Anal Appl Pyrol 2006;77:35–40.
[59] Tay DHS, Ng DKS, Kheireddine H, El-Halwagi MM. Synthesis of an integrated biorefinery via the C–H–O ternary diagram. Clean Technol Environ Policy 2011;13:567–79.
[60] Prins MJ, Ptasinski KJ, Janssen FJJG. Thermodynamics of gas–char reactions: first and second law analysis. Chem Eng Sci 2003;58:1003–11.